

**Impacts of fuel chemical structure and composition on fundamental  
ignition behavior and autoignition chemistry in a motored engine**

by

Dongil Kang

A dissertation submitted in partial fulfillment  
of the requirements for the degree of  
Doctor of Philosophy  
(Chemical Engineering)  
in the University of Michigan  
2016

Doctoral Committee:

Professor André L. Boehman, Co-chair  
Professor Phillip E. Savage, Co-chair  
Professor Johannes W. Schwank  
Associate Professor Angela Violi

© 2016  
Dongil Kang  
All Rights Reserved

## **Dedication**

To my beloved wife and children, Chanyang, Eliana and Ian..

## **Acknowledgments**

When I look back over the long period of time of my graduate study, only the happy moments remain in my mind. This is not because I was very successful in my graduate study, but because I had and still have many great people around me, which makes me feel very humble and thankful at this moment.

I would like to start by expressing my sincere gratitude to my great advisor, Prof. André Boehman, for his consistent encouragement, research guidance and financial support for 6 years. It may have been a difficult decision for him to embrace me, whose research background is somewhat different from his research vision. However, his direction of the research, his great patience and his belief in my ability encouraged me to explore a new field of knowledge and complete my study. He is the best mentor and advisor; he sincerely cares about his students in all aspects. “Thanks a million, Prof. Boehman.”

I would like to extend my sincere gratitude to my other advisor, Prof. Phillip Savage for his research guidance and encouragement during my masters and even Ph.D. study periods. I also appreciated his warm welcome when I came back from PSU. He kindly agreed to accept a request to serve as one of the committee members and to act as co-chair and my academic advisor. Also, I would like to thank the other committee

members, Prof. Johannes Schwank and Prof. Angela Violi, for their valuable comments on my research and their excellent review of my thesis.

I want to thank my former group members in the Diesel Combustion and Emission Lab at PSU. I have acquired many skills in operating engines, managing fuels and utilizing various devices from them; Dr. Greg Lilik, Dr. Bhaskar Prabhakar, Dr. Peng Ye, Dr. Eduardo Barrientos and Dr. Vickey Kalaskar. Special thanks go to Dr. Vickey Kalaskar for his excellent collaborations and valuable discussions of the work we have conducted together at both universities, PSU and UM. I also appreciate senior group members, Dr. Yi Yang and Dr. Yu Zhang, for their guidance on utilizing the exhaust species collection system of the CFR engine, and Dr. Kuen Yehliu and Dr. Hee Je Seong for their great mentorship and friendship. During a short period of time at PSU, I had a chance to work with two passionate and brilliant visiting professors, Prof. John Agudelo and Prof. Magin Lapuerta, who must be gratefully acknowledged for their valuable advice and discussion on various research projects.

I would also like to thank my current group members for their friendship and help on many occasions. Special thanks must go to Kwang Hee Yoo and Taehoon Han, who greatly helped me building up the engine test cell and resolving several technical problems that I ran into. Also, I thank Chenxi Sun and Dr. Stani Bohac for sharing their knowledge and discussing valuable results of our PCCI work. Also, I have worked with many undergraduate students. Among many, I must thank two people, John Fuerst and Iljin Eum, for their great assistance.

I am thankful to former and current Savage group members for their friendship and sharing the gas chromatography equipment. In particular, many thanks must be

delivered to Dr. Natalie Rebacz for her great advice on the research project, and Dr. Chad Huelsman for his friendship. I am also thankful to Violi group members, Tyler Dillstrom and Dr. Doohyun Kim, for being great collaborators who improve my work to the next level.

Perhaps my biggest accomplishment that I have made is the friendships while staying in Ann Arbor. There are too many people to name here, but in particular I thank my former roommates, Dr. Kyunghoon Lee and Dr. Sangjo Choi, and my friends in the Department of Chemical Engineering, Jae Sung Lee, Yoonseob Kim, Chang Yup Seo and Dr. Youngri Kim for their encouragement and great friendship. In addition, I would like to express my sincere gratitude to the Korean Presbyterian Church of Ann Arbor members for their prayers.

I would like to give my special thanks to my parents, parents-in-law and all family members for their endless love, continuous support and prayers. Finally and most importantly, I would like to thank my beloved wife, Chanyang Bae, for her constant love, sacrifice, encouragement, patience and belief along this journey. I consider myself greatly blessed to share this moment with my wife and children, Eliana and Ian, who were born in the middle of this journey. Of course, I would like to thank my children as well, since they have been bringing great joy and happiness to my family.

The financial support from Automotive Research Center (ARC) and King Abdullah University of Science & Technology (KAUST) is gratefully acknowledged.

## Table of Contents

<b>Dedication .....</b>	<b>ii</b>
<b>Acknowledgments .....</b>	<b>iii</b>
<b>List of Figures.....</b>	<b>xii</b>
<b>List of Tables .....</b>	<b>xxvii</b>
<b>List of Appendices.....</b>	<b>xxix</b>
<b>Abstract.....</b>	<b>xxx</b>
<b>Chapter 1 Introduction.....</b>	<b>1</b>
<b>Chapter 2 Literature Review .....</b>	<b>6</b>
2.1 Chain Reactions of Hydrocarbon Oxidation Mechanism.....	6
2.2 Temperature Regimes of Hydrocarbon Oxidation .....	8
2.3 Ignition Behaviors in HCCI Engine .....	11
2.4 Autoignition Phenomenon.....	12
2.4.1 Chemical kinetic modeling of autoignition.....	12
2.4.2 Ignition delay .....	13
2.4.3 Empirical approaches to defining autoignition quality.....	16
2.5 Overview of Hydrocarbon Oxidation.....	20

2.5.1	Formation of alkylperoxy radicals .....	23
2.5.2	Isomerization in the transition state theory .....	24
2.5.3	Major chain propagation reaction channels .....	26
2.6	Reactors for Hydrocarbon Oxidation and Combustion Research .....	27
2.6.1	Shock tube.....	28
2.6.2	Rapid compression machine .....	29
2.6.3	Flow reactors.....	31
2.6.4	Motored engine .....	33
2.6.5	Constant volume combustion chamber .....	35
2.7	Surrogate Development .....	37
<b>Chapter 3</b>	<b>Experimental .....</b>	<b>42</b>
3.1	Cooperative Fuel Research (CFR) Motored Engine .....	43
3.1.1	Motored engine setup.....	43
3.1.2	Method of heat release calculation .....	45
3.1.3	Measurement of engine parameters .....	47
3.1.4	Descriptions of autoignition characteristics.....	48
3.1.5	Intermediate species analysis methodology.....	49
3.2	Cetane Ignition Delay (CID) 510 unit .....	53
3.2.1	Constant volume combustion chamber modification .....	53
3.2.2	Chemiluminescence detection system (CDS).....	55
3.2.3	Ignition delay from PMT data analysis.....	56
3.2.4	Thermodynamic calculations from pressure data .....	59



<b>Chapter 4</b>	<b>Impact of Branched Structure on Cycloalkane Ignition in a Motored Engine: Detailed Product and Conformational Analyses .....</b>	<b>61</b>
4.1	Introduction .....	61
4.2	Research Objectives .....	64
4.3	Test Fuels.....	64
4.4	Test Conditions.....	66
4.5	Results and Discussion.....	66
4.5.1	Low temperature heat release analysis .....	66
4.5.2	CO and CO <sub>2</sub> emissions from low temperature oxidation.....	68
4.5.3	Intermediate product analysis .....	70
4.5.4	Conformational analysis .....	92
4.6	Conclusions .....	103
<b>Chapter 5</b>	<b>Autoignition Studies of C<sub>5</sub> Isomers in a Motored Engine .....</b>	<b>106</b>
5.1	Introduction .....	106
5.2	Research Objectives .....	109
5.3	Test Fuels.....	109
5.4	Test Conditions.....	110
5.5	Results and Discussion.....	110
5.5.1	Autoignition characteristics of pentane isomers .....	110
5.5.2	Intermediate condensed species analysis .....	117
5.6	Conclusions .....	128

<b>Chapter 6</b>	<b>Combined Impact of Branched and Unsaturation on the Autoignition of Binary Blends in a Motored Engine.....</b>	<b>130</b>
6.1	Introduction .....	130
6.2	Research Objectives .....	135
6.3	Test Fuels.....	135
6.4	Test Conditions.....	137
6.5	Results and Discussion.....	138
6.5.1	Heat release analysis .....	138
6.5.2	CO emission analysis .....	144
6.5.3	Structural impact on ignition characteristics.....	146
6.5.4	Condensed intermediate hydrocarbon species .....	147
6.6	Conclusions .....	161
<b>Chapter 7</b>	<b>Experimental Investigation of Autoignition Behavior of Surrogates for Conventional and Synthetic Alternative Jet Fuels and their Validation in a Motored Engine and a Constant Volume Combustion Chamber .....</b>	<b>163</b>
7.1	Introduction .....	163
7.2	Research Objectives .....	169
7.3	Test Conditions.....	170
7.3.1	Modified CFR engine .....	170
7.3.2	Constant volume spray combustion chamber .....	171
7.4	Conventional and Alternative Synthetic Jet Fuels.....	172
7.4.1	Test fuels.....	172

7.4.2	Results and discussion .....	176
7.5	UM I and UM II Surrogates for Jet-A (POSF 4658).....	194
7.5.1	Test Fuels .....	194
7.5.2	Result and discussion .....	198
7.6	UM Surrogates for Alternative Jet Fuels (S8, and IPK).....	222
7.6.1	Test Fuels .....	222
7.6.2	Results and Discussion .....	225
7.7	Summary and Conclusions .....	228
<b>Chapter 8</b>	<b>Conclusions and Recommendations for Future Works .....</b>	<b>233</b>
8.1	Conclusions .....	233
8.1.1	Conclusion from Chapter 4; Impact of Branched Structure on Cycloalkane Ignition in a Motored Engine .....	234
8.1.2	Conclusion from Chapter 5; Autoignition Studies of C5 Isomers in a Motored Engine .....	235
8.1.3	Conclusion from Chapter 6; Combined Impact of Branching and Unsaturation on the Autoignition of Binary Blends in a Motored Engine .....	236
8.1.4	Conclusion from Chapter 7; Experimental Investigation of Autoignition Behaviors of Conventional and Synthetic Alternative Jet Surrogates and their Validation in a Motored Engine and a Constant Volume Combustion Chamber.....	237
8.2	Recommendations for Future Work .....	240
<b>Appendices</b> .....		<b>242</b>

**Bibliography ..... 254**

## List of Figures

Figure 2-1 Chain reactions of hydrocarbon oxidation proposed by Semenov [6], reproduced from [7] .....	8
Figure 2-2 Conceptual classification of hydrocarbon oxidation temperature regimes. The lines delineate the main kinetic chain-branching process. The upper line connects points where the overall $H + O_2$ reaction is neutral: above the line it is net branching; below it is net terminating. The lower lines are where the peroxy chemistry is neutral: above these lines there is net termination and below net branching. The regime between the two lines is the region of negative temperature coefficient. The “low”-, “intermediate”- and “high”- temperature regions are broadly characterized by the types of chemistry included [8]. .....	9
Figure 2-3: Negative temperature coefficient (NTC) and cool flame behaviors in hydrocarbons oxidation [7] .....	10
Figure 2-4 Typical two stage heat release curve of HCCI combustion of a reactive fuel such as n-heptane [3] .....	12
Figure 2-5 Ignition delay time plotted against $1000/T$ for different fuels at 40 bar [16,19] adapted from [20]. .....	15

Figure 2-6 A correlation between cetane number measured by ASTM D613 [24] against research octane number measure by [22] for primary reference fuel (PRF) and toluene blended PRF .....	18
Figure 2-7 Ignition delay (ID) measured by ignition quality tester [25] against cetane number [24] or research octane number [22].....	19
Figure 2-8. Schematic mechanism for low-temperature hydrocarbon oxidation and auto-ignition chemistry [12].....	21
Figure 2-9. Variation of the number of the internal rotors during the isomerization of a 3-peroxyheptyl radical.....	25
Figure 2-10 Decomposition of 2-hydroperoxyheptyl radicals through chain propagation channels.....	27
Figure 2-11 Illustration of a single pulse shock tube [49] .....	29
Figure 2-12 Illustration of a basic rapid compression machine (RCM) [66] adapted from [67].....	31
Figure 2-13 Simplified sketch of a jet-stirred reactor of volume $V$ at constant temperature (T) and pressure (P). $F_j^i$ and $F_j^o$ are the mole flow rates of the species $j$ at the inlet and at the outlet of the reactor. $Q^i$ and $Q^o$ are the volume flow rates of the gas at the inlet and at the outlet of the reactor ( $Q^o$ is symbolized under the conditions of pressure and temperature inside the reactor) [35].....	32
Figure 2-14 Schematic of a basic plug flow reactor [35].....	33
Figure 2-15 Constant volume combustion chamber and design of optical diagnostics at Sandia National Laboratory [89] .....	36

Figure 2-16 Surrogate species pallet used to emulate distillation and physical properties of diesel and jet fuels as originally extracted from [96], regenerated by [97] .....	39
Figure 2-17 Schematic diagram of real fuel oxidation and concept of distinct chemical functionality as it applies to high temperature combustion kinetic phenomena [46]. .....	39
Figure 2-18 Typical distillation range and organic class distribution of species found in gasoline, diesel and jet fuels [101].....	41
Figure 3-1 Schematic of modified CFR motored engine.....	44
Figure 3-2. Schematic of light pathway in the chemiluminescence detection system (CDS) [67].....	56
Figure 3-3. Three PMT signals from one of the fifteen ignitions of POSF 4658 at 600°C and 20 atm; (a) Actual observed raw PMT signals passed for three different wavelength filters observed in Labview house-code; (b) Reduced scale view of raw 307±5nm PMT signal used to derive $\tau_{tot}$ and (c) Reduced scale view of raw 430±5nm PMT signal used to derive $\tau_{phys}$ .....	58
Figure 4-1 Apparent heat release and maximum bulk cylinder temperature for three different substituted cycloalkanes and <i>n</i> -heptane: (a) apparent heat release profiles of three different cycloalkanes at a CR of 6 and <i>n</i> -heptane at a CR of 4.88 as a function of crank angle. Crank angle 0 deg indicates piston top dead center; (b) Calculated maximum bulk gas in-cylinder temperature profile at various CRs for oxidation of four different pure fuels.....	68

- Figure 4-2 Gaseous emissions as functions of compression ratio (CR) from the oxidation of four different neat fuels: (a) mole percent of CO; and (b) mole percent of CO<sub>2</sub>. Error bars indicate the 95% confidence interval..... 70
- Figure 4-3 Condensed gaseous species from ethylcyclohexane oxidation: (a) small olefins; (b) small oxygenates; (c) cycloalkanes and ethylbenzene; (d) conjugate olefins; (e) oxygenated species; and (f) fuel and cyclohexene. Line represents the onset of autoignition. .... 75
- Figure 4-4 Proposed reaction pathways to (A) cyclohexene and oxygenated species; (B) octahydrobenzofuran and (C) cyclohexanone during low temperature oxidation of ethylcyclohexane..... 77
- Figure 4-5 A proposed reaction pathway to 2-cyclohexen-1-one during low temperature oxidation of ethylcyclohexane ..... 78
- Figure 4-6 Condensed gaseous species from 1,3-dimethylcyclohexane oxidation: (a) Small olefins and acids; (b) Small oxygenated species; (c) Cyclohexenes, benzenes and norbornane; (d) Conjugate olefins; (e) Large oxygenated species; and (f) Fuels and cyclohexene. Line represents the onset of autoignition..... 81
- Figure 4-7 A proposed reaction pathway to observed oxygenated species from low temperature oxidation of 1,3-dimethylcyclohexane: (A) 1,5-dimethyl-7-oxabicyclo[4,1,0]heptane; (B) 6-methylhept-6-en-2-one; and (C) 3-methyl-2-cyclohexen-1-one;..... 84
- Figure 4-8 Condensed gaseous species from 1,2-dimethylcyclohexane: (a) Small olefins and Acetic acid; (b) Small oxygenated species; (c) 1-methylcyclohexene and 1,2-



dimethylbenzene; (d) Conjugate olefins; (e) Large oxygenated species; and (f) Test fuel and cyclohexene. Line represents the onset of autoignition. ....	87
Figure 4-9 Proposed reaction pathways of oxygenated species from the low temperature oxidation of 1,2-dimethylcyclohexane: (A) 2-methylcyclohexanone; (B) octahydro-2-benzofuran ; and (C) 6-octen-2-one; .....	90
Figure 4-10 Chair conformation of (a) Methylcyclohexane and (b) Ethylcyclohexane. There are 11 and 16 hydrogens available for (1,5) H-shift of peroxy groups in MCH and ECH, respectively. ....	96
Figure 4-11 Chair conformation of <i>cis</i> -1,3-dimethylcyclohexane. The most stable conformation with both equatorial methyl groups is favored over the conformation with both axial methyl groups in the two chair conformations of <i>cis</i> -1,3-dimethylcyclohexane. ....	98
Figure 4-12 Chair conformation of <i>trans</i> -1,3-dimethylcyclohexane. The two chair conformations are equal in steric strain energy because each has one axial methyl group and one equatorial methyl group. ....	99
Figure 4-13 Chair conformation of <i>trans</i> -1,2-dimethylcyclohexane and the most stable conformation with both equatorial methyl groups is favored over the conformation with both axial methyl groups in the two chair conformations of <i>trans</i> -1,2-dimethylcyclohexane. ....	100
Figure 4-14 Chair conformation of <i>cis</i> -1,2-dimethylcyclohexane. The two chair conformations are equal in steric strain energy because each has one axial methyl group and one equatorial methyl group. ....	101
Figure 5-1 Chemical structure of pentane isomers .....	109

Figure 5-2 Autoignition characteristic of neo-pentane at $\phi$ of 0.25 in a respect of measured CO formation and calculated in-cylinder gas $T_{\max}$ (calculated from measured in-cylinder pressure).....	111
Figure 5-3 Apparent heat release rates (AHRR) in a wide range of CRs of neo-pentane at equivalence ratio of 0.25, as corresponded to Figure 5-2; Apparent heat release rate at (a) CR of 4.0 in region (I), (b) CR of 5.8 in region (II), (c) CR of 7.0 in region (III), (d) CR of 9.5 in region (IV) and (e) CR of 10.1 in region (V) .....	112
Figure 5-4 Autoignition behaviors of pentane isomers in comparison with primary reference fuels (PRF); (a) Fuel conversions of pentane isomers at equivalence ratio of 0.25; (b) CO emission comparisons at equivalence ratio of 0.25; and (c) CO emission comparisons at equivalence ratio of 0.5.....	114
Figure 5-5 Comparisons of apparent heat release rates (AHRR) for pentane isomers in equivalence ratio of 0.25 at (a) compression ratio of 8.5 and at (b) critical compression ratios (CCRs) of 8.5 for <i>n</i> -pentane, 10.1 for neo-pentane and 13.2 for <i>iso</i> -pentane .....	116
Figure 5-6 Autoignition characteristics of pentane isomers; (a) critical compression ratios (open symbols) and critical equivalence ratios (closed symbols), (b) percentages of low temperature heat release (% LTHR) at high temperature heat releases (open symbols for critical compression ratio and closed symbols for critical equivalence ratio).....	117
Figure 5-7 Intermediate species of <i>n</i> -pentane oxidation (a) alkenes (b) aldehydes (c) ketones and (d) cyclic ethers.....	120

Figure 5-8 A proposed reaction path forming 2-methyltetrahydrofuran in low temperature oxidation of <i>n</i> -pentane .....	121
Figure 5-9 Possible reaction pathways of a competitive formation of acetone and <i>iso</i> -butene from <i>i</i> -C <sub>4</sub> H <sub>8</sub> OH radical in low temperature regime .....	122
Figure 5-10 Possible reaction pathway forming <i>iso</i> -butene and formaldehyde in negative temperature coefficient (NTC) regime during neo-pentane oxidation .....	123
Figure 5-11 Intermediate species of <i>neo</i> -pentane oxidation (a) small alkenes (b) aldehydes and 2-methyl-2-propen-ol (c) other oxygenates .....	124
Figure 5-12 Intermediate species from <i>iso</i> -pentane oxidation (a) alkenes (b) conjugate alkenes (c) aldehydes (d) ketones and cyclic ethers .....	127
Figure 6-1 Chemical structure parameter of test fuels.....	132
Figure 6-2 Test molecule structures (A) <i>n</i> -heptane (B) isooctane (C) 2,4,4-trimethyl-1-pentene, and (D) 2,4,4-trimethyl-2-pentene.....	136
Figure 6-3 High temperature heat release as a function of crank angle for (a) 0, 10 and 20 wt % v/v diisobutylene (DIB) blended in <i>n</i> -heptane (HEP) and (b) 0, 5 and 10 wt % v/v diisobutylene (DIB) blended in <i>iso</i> -octane (ISO) ; (c) Low temperature heat release for 0, 5, 10, 15 and 20 wt % v/v diisobutylene in <i>n</i> -heptane (HEP) at CRs ; (d) Apparent heat release for 0, 5, 10 and 15 wt % v/v diisobutylene in isooctane (ISO) at CR of 14.....	142
Figure 6-4 Maximum in-cylinder temperature for (a) diisobutylene / <i>n</i> -heptane blends and (b) diisobutylene/ isooctane blends.....	144
Figure 6-5 CO emissions from the oxidation of (a) <i>n</i> -heptane and blends with diisobutylene and (b) isooctane and blends with diisobutylene.....	146

Figure 6-6 Ignition characteristics of the fuel blends, (a) Critical compression ratios of test binary blends at different volume percent substitutions (b) % LTHR and Max LTHR at different % HEP in binary blends. No evidence of LTHR was found in ISO and DIB blend.....	147
Figure 6-7 Mole fractions of intermediates species from the oxidation of blends with <i>n</i> -heptane and different volume % of diisobutylene at selected compression ratios at test conditions as per Table 8.....	150
Figure 6-8. A reaction pathway leading to the formation of 4,4-dimethyl-2-pentanone derived from 2,4,4-trimethyl-1-pentene during low temperature oxidation of <i>n</i> -heptane blends.....	151
Figure 6-9 Possible reaction pathways leading to the formation of various intermediate species derived from radical attack on beta-carbon of <i>n</i> -heptane in low temperature oxidation of <i>n</i> -heptane blends: (A) 2-heptanone; (B) 3-hepten-2-one; (C) 2-butyl-3-methyl-oxirane; (D) 2-heptene; (E) 1-heptene; and (F) 2-methyltetrahydropyran .....	153
Figure 6-10 Possible reaction pathways leading to the formations of various intermediate species derived from radical attack on gamma-carbon of <i>n</i> -heptane in low temperature oxidation of <i>n</i> -heptane blends. (A) 3-heptanone; (B) 2-ethyl-3-propyl-oxirane; and (C) 3-heptene.....	153
Figure 6-11 A possible reaction pathway leading to the formation of 4-heptanone derived from radical attack on sigma-carbon of <i>n</i> -heptane in low temperature oxidation of <i>n</i> -heptane blends. ....	154

Figure 6-12 A possible reaction pathway leading to the formation of heptanal derived from radical attack on alpha-carbon of <i>n</i> -heptane in low temperature oxidation of <i>n</i> -heptane blends. ....	154
Figure 6-13 Possible reaction pathways leading to the formation of diisobutylene from the low temperature oxidation of 2,4,4-trimethylpentane: (A) 2,4,4-trimethyl-2-pentene; and (B) 2,4,4-trimethyl-1-pentene.....	155
Figure 6-14 Mole fractions of intermediates species from the oxidation of blends with isooctane and different volume % of diisobutylene at compression ratios before the actual auto-ignition is occurred.....	157
Figure 6-15 Possible reaction pathways leading to the formation of (A) 2,4-dimethyl-2-pentene (B) 2,4-dimethyl-1-pentene (C) 4,4-dimethyl-1-pentene and (D) 4,4-dimethyl-2-pentene in low temperature oxidation of isooctane blends.....	159
Figure 6-16 Possible reaction pathways leading to the formation of (A) 2,2,4,4-tetramethyl-tetrahydrofuran and (B) 4,4-dimethyl-2-pentanone during the oxidation of the isooctane blends.....	160
Figure 7-1 Physical and chemical properties affecting diesel engine combustion processes, inspired by [148].....	168
Figure 7-2 Gas chromatography/mass spectrometry scan of conventional and alternative Jet fuels tested. ....	174
Figure 7-3 Apparent heat release rates (AHRR) of conventional jet fuels of JP-8, Jet-A and JP-5 at equivalence ratios of 0.25 and 0.5.....	182
Figure 7-4 Apparent heat release rates (AHRR) of synthetic alternative jet fuels and blends with JP-8 in a wide range of CRs at equivalence ratio of 0.25 .....	183

Figure 7-5 Apparent heat release rates (AHRR) of synthetic alternative jet fuels and blends with JP-8 in a wide range of CRs at equivalence ratio of 0.5 .....	184
Figure 7-6 (a) – (e); Maximum in-cylinder temperatures and (f) – (j); CO emissions of alternative jet fuels and 50 v/v % of JP-8 in alternative jet fuels in a wide range of compression ratios at equivalence ratio of 0.25 .....	185
Figure 7-7 (a) – (e); Maximum in-cylinder temperatures and (f) – (j); CO emissions of alternative jet fuels and 50v/v % of JP-8 in alternative jet fuels in a wide range of compression ratios at equivalence ratio of 0.5 .....	186
Figure 7-8 The percentage of low temperature heat release (% LTHR) and critical compression ratio (CCR) in respect of derived cetane number (DCN) of jet fuels tested at equivalence ratio of 0.25; Error bar indicates 95 % confidential interval. ....	187
Figure 7-9 The percentage of low temperature heat release (% LTHR) and critical compression ratio (CCR) in respect of derived cetane number (DCN) of jet fuels tested at equivalence ratio of 0.5; Error bar indicates 95 % confidential interval. ....	188
Figure 7-10 Critical equivalence ratio of jet fuels tested at different compression ratios .....	189
Figure 7-11 Comparisons of physical, chemical and total ignition delays of a conventional jet fuel (JP-8), synthetic alternative jet fuels including (a) S8, (b) SPK and (c) HRJ8, and 50 volume percent of JP-8 in alternative jet fuel blends in a range of temperature (540 to 640°C) at 20 bar in a constant volume spray combustion chamber .....	191

Figure 7-12 Comparisons of physical, chemical and total ignition delays of a conventional jet fuel (JP-8), synthetic alternative jet fuels, IPK and ATJ, and 50 volume percent of JP-8 in alternative jet fuel blends in a range of temperature (540 to 640°C) at 20 bar in a constant volume spray combustion chamber.....	193
Figure 7-13 Distribution of classes of hydrocarbons as volume fraction for the UM surrogates and POSF 4658 measured in [143];.....	197
Figure 7-14 Low temperature oxidation reactivity comparisons of five pure individual hydrocarbons at equivalence ratio of 0.25 at intake temperature of 260°C; (a) Maximum bulk in-cylinder temperatures as CR increases; and (b) apparent heat release rates for each individual component at ~1120 K of the maximum bulk in-cylinder temperatures, which are marked as black circles in (a) .....	200
Figure 7-15 Low temperature oxidation reactivity comparisons of five pure individual hydrocarbons at equivalence ratio of 0.25 at intake temperature of 260°C; (a) CO emission for each individual compound in a wide range of compression ratio, representing a good indication of critical compression ratio (CCR) (b) Zoom-in on the dash-square shown in (a). The error bars indicate 95 % confidence interval. ....	202
Figure 7-16 Low temperature oxidation reactivity comparison in critical equivalence ratios of each individual component and a target Jet-A over a wide range of compression ratios .....	203
Figure 7-17 The maximum mass-averaged bulk in-cylinder temperature of the target Jet-A (POSF 4658) and the two UM surrogates during a CR sweep; (a) $\phi=0.25$ (b) $\phi=0.5$ .....	206

Figure 7-18 CO emissions of the target Jet-A (POSF 4658) and the two UM surrogates in a wide range of CR; (a) $\phi=0.25$ and (b) $\phi=0.5$ . The error bar indicates a 95% confidence interval.....	206
Figure 7-19 Comparisons of LTHR of the practical Jet-A (POSF 4658) and two UM surrogate mixtures; (a) $\phi=0.25$ and (b) $\phi=0.5$ .....	209
Figure 7-20 Comparisons of HRR of the target Jet-A (POSF4658) and two UM surrogate mixtures; (a) $\phi=0.25$ and (b) $\phi=0.5$ .....	209
Figure 7-21 Comparisons of critical equivalence ratios of the target Jet-A (POSF4658) and two UM surrogate mixtures at different CRs. The error bar indicates 95% confidence interval.....	211
Figure 7-22 Comparisons of critical compression ratios and AHRR of a practical jet fuel and two UM surrogate mixtures with intake air boosting.....	212
Figure 7-23 Ignition delays against air temperature for individual components and the target Jet-A (POSF 4658); (a) Physical ignition delay (b) Chemical ignition delay and (c) Total ignition delay. The error bar indicates 95% confidence interval. .	215
Figure 7-24 Ignition delays against air temperature for UM surrogate mixtures and the target Jet-A (POSF 4658); (a) Physical ignition delay (b) Chemical ignition delay and (c) Total ignition delay. The error bar indicates 95% confidence interval. .	217
Figure 7-25 Apparent heat release rate profile at various chamber temperatures for the UM surrogate mixtures and the target Jet-A (POSF 4658).....	219
Figure 7-26 The percentage of low temperature heat release in a sweep of chamber temperature for the target Jet-A (POSF 4658) and the UM surrogate mixtures. .	219



Figure 7-27 Ignition delays against simulated exhaust gas recirculation (EGR) for UM surrogate mixtures, the target Jet-A (POSF 4658), <i>n</i> -dodecane and decalin; (a) Physical ignition delay (b) Chemical ignition delay and (c) Total ignition delay. The error bar indicates 95% confidence interval. ....	221
Figure 7-28 Mass fractions of newly developed UM surrogates; (a) S8 and its UM surrogate and (b) IPK and its UM surrogate (black, red and blue colors indicate <i>n</i> -alkanes, <i>iso</i> -alkanes and cycloalkanes, respectively).....	223
Figure 7-29 CO emissions in a respect of increasing CRs in a modified CFR motored engine at intake temperature of 260°C; (a) S8 and its UM surrogate (b) IPK and its UM surrogate .....	227
Figure 7-30 Measurements of physical, chemical and total ignition delays in a constant volume combustion chamber in a range of temperature between 540-640°C at 20 bar; (a) S8 and its surrogate and (b) IPK and its surrogate.....	227
Figure B-1 (a) In-cylinder gas maximum temperatures and (b) cylinder wall maximum temperatures of pentane isomers and primary reference fuels in wide range of compression ratio at $\phi$ of 0.25 ( $\square$ ; <i>n</i> -heptane, $\circ$ ; <i>n</i> -pentane, $\triangle$ ; neo-pentane, $\nabla$ ; <i>iso</i> -pentane, $\diamond$ ; <i>iso</i> -octane) .....	245
Figure B-2 (a) In-cylinder gas maximum temperatures and (b) cylinder wall maximum temperatures of pentane isomers and primary reference fuels in wide range of compression ratio at $\phi$ of 0.5 ( $\square$ ; <i>n</i> -heptane, $\circ$ ; <i>n</i> -pentane, $\triangle$ ; neo-pentane, $\nabla$ ; <i>iso</i> -pentane, $\diamond$ ; <i>iso</i> -octane) .....	246

Figure C-1 CO emissions from the oxidation of <i>n</i> -heptane at intake temperature of 120°C and the engine speed of 600 rpm in the CFR motored engine at the University of Melbourne, Australia. (a) $\phi=0.5$ and (b) $\phi=0.25$ .....	249
Figure C-2 CO emissions from the oxidation of <i>n</i> -heptane at intake temperature of 120°C and the engine speed of 600 rpm in the modified CFR motored engine at the University of Michigan, United States. (a) $\phi=0.5$ and (b) $\phi=0.25$ .....	249
Figure D-1 Product distribution in the oxidation of <i>n</i> -pentane at a compression ratio of 8: oxygenated species analyzed in an Agilent 6890 GC-FID with an HP-5 column .....	250
Figure D-2 Product distribution in the oxidation of <i>n</i> -pentane at a compression ratio of 8: gas sample was diluted with N <sub>2</sub> and 9.3 ppmC <sub>1</sub> propane (internal standard) at 10:1, and alkanes were analyzed in a Shimadzu GC-17A with a Restek Rtx-1 column .....	251
Figure D-3 Product distribution in the oxidation of neo-pentane at a compression ratio of 8.5: oxygenated species analyzed in an Agilent 6890 GC-FID with an HP-5 column.....	252
Figure D-4 Product distribution in the oxidation of neo-pentane at a compression ratio of 8.5: gas sample was diluted with N <sub>2</sub> and 9.3 ppmC <sub>1</sub> propane (internal standard) at 10:1, and alkanes were analyzed in a Shimadzu GC-17A with a Restek Rtx-1 column.....	252
Figure D-5 Product distribution in the oxidation of <i>iso</i> -pentane at a compression ratio of 11: oxygenated species analyzed in an Agilent 6890 GC-FID with an HP-5 column.....	253

Figure D-6 Product distribution in the oxidation of *iso*-pentane at a compression ratio of 11: gas sample was diluted with N<sub>2</sub> and 9.3 ppmC<sub>1</sub> propane (internal standard) at 10:1, and alkanes were analyzed in a Shimadzu GC-17A with a Restek Rtx-1 column..... 253

## List of Tables

Table 1 CFR motored engine specifications .....	44
Table 2 Molecular structure of branched cycloalkanes and their properties tested .....	65
Table 3 Classified groups of intermediate products from low temperature oxidation of ECH, 13DMCH and 12DMCH.....	72
Table 4 Energy barriers of mono- and di-substituted cyclohexane .....	95
Table 5 Hydrogen availability of cyclic hydrocarbon isomers .....	103
Table 6 Previous oxidation and ignition studies of pentane isomers .....	107
Table 7 Properties of pure test fuels .....	137
Table 8 Compression ratios (CR) where the intermediates are sampled and analyzed, and critical compression ratios (CCR) where the actual ignition occurred. ....	148
Table 9 Physical and chemical properties of conventional and alternative Jet fuels .....	175
Table 10 Properties of conventional and synthetic alternative jet fuels, and 50 volume percent of JP-8 blended with alternative jet fuels tested in this study .....	177
Table 11 Properties of individual surrogate components consisting surrogate mixtures formulated by a surrogate optimizer developed by Kim <i>et al.</i> [100].....	195

Table 12 Properties (except TSI) of a target fuel measured [44] and the UM surrogates mixtures estimated by the surrogate optimizer [100] .....	197
Table 13 Temperature-independent properties of the target fuels and their surrogates [150] .....	224
Table 14. Experimental conditions of the CFR motored engines at two different places .....	248

## List of Appendices

A. Appendix A. Algorithm for Combustion Phase	242
A.1 Filter and Smoothing	242
A.2 Start of Combustion	243
A.3 End of Combustion	244
B. Appendix B. Measurements of the CFR Wall Cylinder Temperature	245
C. Appendix C. Cross Reference Check for the CFR Motored Engines	247
D. Appendix D. Product Distribution in the Low Temperature Oxidation of pentane isomers	250
D.1 The FID signals of low temperature oxidation of <i>n</i> -pentane	250
D.2 The FID signals of low temperature oxidation of neo-pentane	252
D.3 The FID signals of low temperature oxidation of <i>iso</i> -pentane	253

## Abstract

Recognizing the significance of chemical kinetics development for model compounds, that can contribute to reliable predictions of various combustion properties (i.e., ignition behavior, burning velocity, viscosity, vaporization and pollutant emissions) for practical fuels, the current research investigates the fundamental understanding of the combustion chemistry for various chemical structures and compositions during the ignition process, which is of great importance for next generation engine designs that employ low temperature combustion strategies.

The first part of this dissertation discusses autoignition data on ethyl-cyclohexane (ECH) and its two isomers (1,3-dimethyl-cyclohexane (13DMCH) and 1,2-dimethyl-cyclohexane (12DMCH)), three pentane isomers (*n*-pentane, neo-pentane and *iso*-pentane), and lastly diisobutylene mixed with individual hydrocarbons (*n*-heptane and *iso*-octane) in binary blends. The low and intermediate temperature regimes of autoignition were explored using a motored variable compression ratio engine, developed from a Cooperative Fuel Research (CFR) Octane Rating engine. Analyses of the stable intermediates in the CFR engine exhaust at various end of compression pressures and temperatures can help to identify reaction pathways through which different compounds

prefer to autoignite. The approach of those studies is to conduct a systematic investigation of the autoignition process, which can provide useful input for qualitative and semi-quantitative validation of kinetic mechanisms for oxidation of target chemical compounds.

It is found that the molecular structures of various fuel compounds play a critical role in determining their autoignition characteristics. In particular, the C<sub>5</sub> alkane isomers possess unique chemical structures (n-alkane (*n*-pentane), one methyl-branched alkane (*iso*-pentane) and two methyl-branched alkane (*neo*-pentane)). The differences in molecular structure result in distinct ignition characteristics and formation of chemical intermediates, with *n*-pentane showing the strongest ignition reactivity, followed by *neo*- and *iso*-pentane.

Furthermore, the impact on autoignition characteristics of the position of alkyl-substituents in the cycloalkane ring was demonstrated using ECH and its two isomers, 13DMCH and 12DMCH. Ethylcyclohexane, possessing longer alkyl chain substituent, has stronger ignition reactivity than the other test fuels, methylcyclohexane (MCH), 13DMCH and 12DMCH. The impact on autoignition reactivity of the position of the methyl substituent on the cycloalkane ring can be explained by comparing the total number of hydrogen atoms that are available for (1,5) hydrogen shift isomerization. This hydrogen shift isomerization is a key reaction step in the low temperature oxidation. This comparison is consistent with the experimentally observed ranking of the order of ignition reactivity, which is ECH > 13DMCH > 12DMCH (> MCH).



The addition of branched and unsaturated fuel structures (diisobutylene) shows a linear retarding effect on oxidation reactivity, resulting in a longer negative temperature coefficient (NTC) behavior with gradual addition to primary reference fuels.

The second part of this dissertation investigates chemical composition effects on autoignition behavior of practical and synthetic alternative jet fuels (18 different fuel/fuel mixtures) by using an optically accessible constant volume spray combustion chamber and the modified CFR motored engine. Furthermore, the study is extended to experimental validation of jet aviation fuel surrogates for a conventional jet fuel (Jet-A, POSF 4658) and two synthetic jet fuels (S8, POSF 5018 and *Iso*-Paraffinic Kerosene (IPK), POSF 7629). The work explored surrogate compounds mixtures (referred to as UM I and UM II) intended to emulate the series of physical and chemical ignition processes occurring in diesel engines. The present work demonstrates the need for detailed measurements of auto-ignition characteristics of various individual hydrocarbon species.

This study shows that chemical composition of alternative jet fuels greatly influences their ignition reactivity, demonstrating that S8, SPK and HRJ8, which are composed mostly of n-alkanes and lightly branched alkanes, possess stronger ignition reactivity than conventional jet fuels. In contrast, IPK and ATJ, whose compositions mostly consist of highly branched alkanes, possess weaker ignition reactivity, as compared to conventional jet fuels.

From the validation experiments comparing UM surrogate fuel mixtures with their target jet fuels, UM II surrogate showed delayed critical compression ratio (CCR), relative to the target Jet-A. In contrast, the ignition characteristics of UM I reasonably

well match that of a target Jet-A even under a boosted intake condition. The ignition behavior of a S8 UM surrogate and the actual S8 fuel were perfectly matched in the motored engine experiment and matched very closely in terms of physical and chemical ignition delays when compared in terms of spray ignition behavior in a constant volume combustion chamber. The physical ignition delay of IPK UM surrogate agreed well with that of neat IPK in the constant volume combustion chamber, however, the trend of chemical ignition delay was partially matched with that of neat IPK up to a chamber temperature of 580°C. At higher chamber temperatures, the trends of chemical ignition delay diverged for the IPK surrogate and neat IPK fuel.

This study suggests that the individual hydrocarbon components included in surrogate mixtures should be drawn from a broader range of chemical structures to better emulate the chemical and physical processes during diesel engine combustion. Starting with a broader palette of surrogate compounds can lead to higher quality emulation of the target fuels. Better surrogate representations of practical fuels can enable optimization of engine simulation and thereby future engine design.

# **Chapter 1**

## **Introduction**

The continuous usage of fossil fuels in the internal combustion engine contributes to not only severe global climate change, but also a rise in cost of these finite resources. Therefore, a need for increased efficiency from the internal combustion engine has placed the diesel engine in the spotlight, due to its high efficiency as compared to other engines. Moreover, recent stringent emission regulations of internal combustion engines and vehicles have led to research and development of advanced engine combustion strategies, which offer the potential for low NO<sub>x</sub> and soot emissions and improved efficiency. In contrast to conventional compression ignition combustion, advanced combustion strategies typically rely on increased premixing of fuel and air prior to combustion [1–3]. Therefore, ignition of various single component and multi-component surrogates in the low- and intermediate temperature region has been widely studied to better understand the autoignition process and to provide validation of predictions of autoignition related to advanced engine combustion strategies, such as low temperature combustion (LTC), premixed charged compression ignition (PCCI), reactivity controlled compression ignition (RCCI) and homogeneous charge compression ignition (HCCI). Also, this

approach increases the need to understand both qualitatively and quantitatively how different compound classes behave during autoignition to permit the tailoring of fuel characteristics so that they enable advanced combustion, such as is being considered in the Fuels for Advanced Combustion Engines (FACE) program [4].

As the autoignition phenomenon is essentially dependent on the fuel structures and the temperature and pressure of the combustion environment, studies over the past decade have sought to expand our fundamental understanding of the ignition chemistry of representative structural groups (i.e., linear and branched alkanes, alkenes, cycloalkanes, aromatics and oxygenates), during the low temperature oxidation and the negative temperature coefficient (NTC) regime. More recently, of particular interest is how different compound classes interact with each other, whether synergistically or antagonistically. Thereby, the demand for extensive study of the combustion of fuel-size hydrocarbons in mixtures motivates the examination of binary blends of *n*-heptane and *iso*-octane, the primary reference fuels (PRF) for characterizing anti-knock behavior, and mixtures of other compound classes in PRF fuels. Moreover, recent studies have been more focused on the adoption of ternary or multi-component fuel mixtures in the investigation of the abovementioned advanced combustion modes. The chemical and physical characteristics of well-chosen surrogate mixtures can possess similar autoignition behavior, hydrocarbon functional groups, and low and intermediate temperature oxidation reactivity as the conventional full boiling range fuels. This approach may contribute to reliable predictions of various combustion properties (i.e., ignition behavior, burning velocity, viscosity, vaporization and pollutant emissions) for practical fuels. Although chemical kinetic mechanisms for emerging transportation fuels

have grown rapidly in recent years, investigations of autoignition behavior and validation of their key elementary reactions have seldom been examined under motored engine operating conditions. For this reason, this dissertation contains four different studies, which investigate the impacts of fuel chemical structure and composition on fundamental ignition behavior and autoignition chemistry in a motored engine. Details of current studies in this dissertation are presented as follows.

In **Chapter 4**, the ignition process of ethylcyclohexane and its two isomers were investigated in a modified cooperative fuel research (CFR) octane rating engine. Based on the analysis of the fractions of intermediates species, the favor reaction pathways of major intermediate species for each isomer were suggested. In addition, the reactivity differences in the three isomers were explained through the chemical structure conformation analysis. **Chapter 4** was published in 2015, under the title of “Impact of branched structures on cycloalkane ignition in a motored engine: Detailed product and conformational analysis” in the journal of *Combustion and Flame*.

In **Chapter 5**, the ignition process of C5-paraffinic model isomers such as *n*-pentane, 2-methyl-butane and neo-pentane were also explored in a modified CFR engine. The detailed speciation analysis over a wide range of pressures and temperatures were intended to support and validate the development of the kinetic models for the test fuels. **Chapter 5** was accepted for presentation at *the 36<sup>th</sup> International Combustion on Symposium*, under the title of “Autoignition studies of C5 isomers in a motored engine”.

In **Chapter 6**, the ignition process of diisobutylene, an ideal representative of the hydrocarbon class of highly branched alkene, was investigated with simple hydrocarbons such as *n*-heptane and isooctane in binary blends. Diisobutylene is often used as an

additive to improve antiknock quality in spark ignition engine. This research addressed systematic investigation of binary blends to characterize the nature of the interactions among the fuel constituents, with emphasis on ignition chemistry during low and intermediate temperature reaction in a modified CFR motored engine. **Chapter 6** was published in 2014, under the title of “Combined impact of branching and unsaturation on the autoignition of binary blends in a motored engine” in the journal of *Energy and Fuels*.

In **Chapter 7**, the research presented an experimental validation of recent developments of jet aviation fuel surrogates formulated using a surrogate model-optimizer. The UM surrogates are formulated to emulate a practical Jet-A (POSF 4658) and synthetic alternative jet fuels (S-8 and *iso*-paraffinic kerosene) considering a series of physical and chemical processes in diesel engines. A modified CFR motored engine and an optically accessible constant volume spray combustion chamber are employed to investigate how the chemical and physical properties of jet aviation surrogates affect the fundamental ignition behavior as compared to a real Jet-A. An observation of fundamental ignition characteristics is assessed using a motored engine, while physical and chemical ignition delays are measured using a modified cetane ignition delay (CID) unit under a wide range of air temperatures and oxygen dilution levels. Subsequently, chemical composition effects on autoignition behavior of various practical and synthetic alternative Jet Fuels (18 different fuel/fuel mixtures) were examined in the same combustion systems. **Chapter 7** is prepared for the journal publications under the title of “Experimental investigation of autoignition behaviors of conventional and synthetic alternative jet fuels in a motored engine and an optical constant volume sprayed combustion chamber” and “Experimental study of autoignition characteristics of Jet-A

surrogates and their validation in a motored engine and a constant volume combustion chamber”.

This research not only gives some insights into the autoignition chemistry and combustion behavior of various evolving surrogates comprised of single, binary or multi-component fuels, but also examines impacts of chemical structure and composition on the ignition process in low and intermediate temperature regions, which are important in many advanced combustion engine strategies under consideration. Overall, an understanding of how fuel structure and composition impact the processes in compression ignition engines can offer us long-term solutions to achieve clean and efficient combustion with any fuel and engine combination. In this way, these research efforts aim to address the grand challenge identified by the Clean and Efficient Combustion of 21<sup>st</sup> Century Transportation Fuels workshop: *“The development of a validated, predictive, multi-scale, combustion modeling capability to optimize the design and operation of evolving fuels in advanced engines for transportation application”* [5].

## **Chapter 2**

### **Literature Review**

This chapter includes the research background that is relevant to the studies presented in this dissertation. First, the various methods to ascertain autoignition tendencies of gasoline and diesel relevant fuels are described. Second, since the autoignition process in practical combustion systems relies on hydrocarbon oxidation starting from low temperature, this literature survey includes an overview of hydrocarbon oxidation chemistry followed by general information on experimental approaches for combustion research techniques. Finally, a brief background of the surrogate development is presented. In addition, subsequent chapters include detailed literature references for further understanding as necessary.

#### **2.1 Chain Reactions of Hydrocarbon Oxidation Mechanism**

Chain reactions commonly occur in hydrocarbon oxidation. Semenov [6] was the first to propose the general mechanism for a few carbon atoms, which clarified the processes taking place, as can be seen in Figure 2-1. The chain reaction process contains



chain initiation, chain propagation, chain branching and chain termination. The stable species are first generated by the free radicals, such as  $O\cdot$ ,  $H\cdot$ ,  $\cdot OH$ ,  $HO_2\cdot$  and  $\cdot CH_3$  through the chain initiation reaction. During chain propagation reactions, the number of radicals stays constant; instead, stable species such as  $ROOH$  and  $H_2O_2$  build up.

In contrast to the chain propagation reaction steps, degenerate chain branching reactions increase the number of radical species in a reacting system. Chain branching reactions such as shown in Reaction 2-1 represent one stable species being consumed to form two radicals.



Since rapid growth of the number of radical species is connected to the onset of autoignition in a reacting system, the chain branching reaction steps are considered as the key steps among chain reactions that contribute to the ignition phenomena observed in many combustion systems.

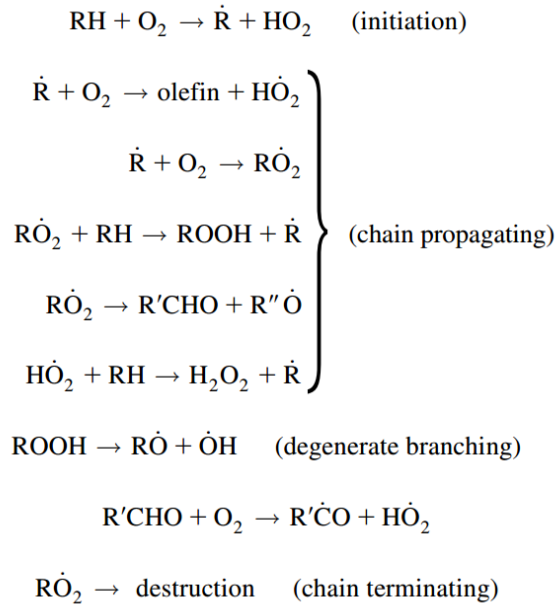


Figure 2-1 Chain reactions of hydrocarbon oxidation proposed by Semenov [6], reproduced from [7]

## 2.2 Temperature Regimes of Hydrocarbon Oxidation

The combustion process occurs in a matter of milliseconds. However, such fast oxidation reaction processes can be classified into three regimes in terms of reaction temperatures, including low temperature, intermediate temperature and high temperature regimes. Each regime has a unique and dominant reaction pathway, resulting in different ignition behaviors, such as cool flame, negative coefficient temperature and autoignition.

As can be seen in Figure 2-2, above the upper line, homolysis of C-C bonds produces the radical pool, which is greatly expanded in the high temperature regime. Reaction 2-2 shows that hydrogen atoms directly released from the hydrocarbon produce two radicals, resulting in a chain branching reaction, leading to the onset of autoignition.



Below the lower lines seen in Figure 2-2, the major reaction step is peroxy radical reactions. In the low temperature regime, the C-H bond in the hydrocarbon is broken with  $O_2$  or radical attack, leading to the formation of peroxy radicals. Since the hydrogen abstraction is largely affected by the size and structure of the carbon backbone of the hydrocarbon, this peroxy radical reaction mainly controls the overall oxidation rate.

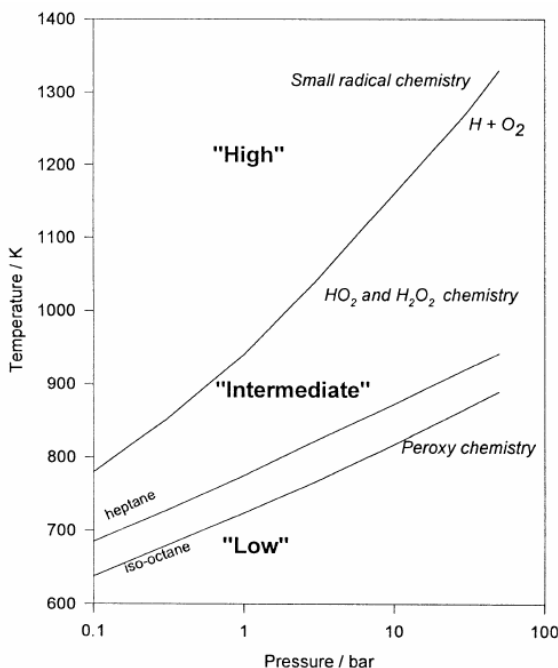


Figure 2-2 Conceptual classification of hydrocarbon oxidation temperature regimes. The lines delineate the main kinetic chain-branching process. The upper line connects points where the overall  $H + O_2$  reaction is neutral: above the line it is net branching; below it is net terminating. The lower lines are where the peroxy chemistry is neutral: above these lines there is net termination and below net branching. The regime between the two lines is the region of negative temperature coefficient. The “low”-, “intermediate”- and “high”-temperature regions are broadly characterized by the types of chemistry included [8].

The regime between the two lines is referred to as the intermediate temperature regime, where hydroperoxy radical ( $HO_2\bullet$ ) accumulates hydroperoxide ( $H_2O_2$ ) via Reaction 2-3a and 2-3b, whereas chain-branching reaction (2-3) becomes less favored.



In other words, the intermediate temperature regime begins with the point where non-chain branching reactions become more favored than chain branching reactions with increasing temperature in the reaction system. This unique phenomenon is called negative coefficient temperature (NTC) behavior. For example, propane oxidation shows that reaction regimes are shifted with constant pressure and increasing temperature, as can be seen in Figure 2-3. This NTC behavior also leads to an interesting behavior of *cool flame*, which increases temperature modestly, by about 100-200 K, with no hot flame arising [7].

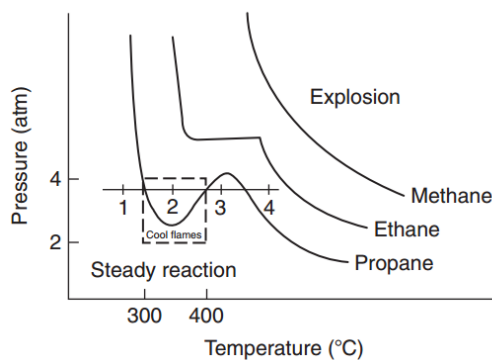


Figure 2-3: Negative temperature coefficient (NTC) and cool flame behaviors in hydrocarbons oxidation [7]

In the intermediate temperature regime, the concentration of  $\text{H}_2\text{O}_2$  keeps building via reactions 2-3a and 2-3b, until the dissociation of  $\text{H}_2\text{O}_2$  takes place, which in general requires a critical temperature, depending on the pressure of a reaction system. Once the system reaches a threshold temperature,  $\text{H}_2\text{O}_2$  is dissociated rapidly into  $\cdot\text{OH}$  radicals, leading to ignition.

It is worth noting that pressure is also a critical factor to determine the combustion regime in a reaction system, which can be seen in Figure 2-2. At a constant temperature, e.g., 850 K, the oxidation can remain in the high temperature regime, if the pressure is lower than 0.1 bar in a vacuum closed vessel reactor. As pressure increases, the oxidation can be either in the intermediate temperature regime if in an atmospheric flow reactor or in the low temperature regime if in a motored engine.

### **2.3 Ignition Behaviors in HCCI Engine**

In a motored engine, typically for homogeneous charge compression ignition (HCCI) mode, the temperature regimes abovementioned can be represented by heat release rate. The heat release rate is an essential property, which indicates the intensity of autoignition. The intensity of autoignition is largely dependent on the temperature and pressure at autoignition, which are in turn determined by initial conditions. Furthermore, the combustion process highly relies on the autoignition chemistry of the fuel. Typically, more reactive fuels exhibit evident two-stage heat release, including low temperature heat release (LTHR) also known as *cool flame*, NTC behavior and high temperature heat release (HTHR), as shown in Figure 2-4. The LTHR occurs at some percentage (0~15%) of total fuel energy released at relatively lower temperatures and pressures. In contrast, less reactive fuels show a single stage heat release, resisting low temperature heat release. This behavior indicates that such fuels tend to avoid active low temperature chemistry and require higher temperatures and pressures to autoignite, resulting in a violent heat release rate.

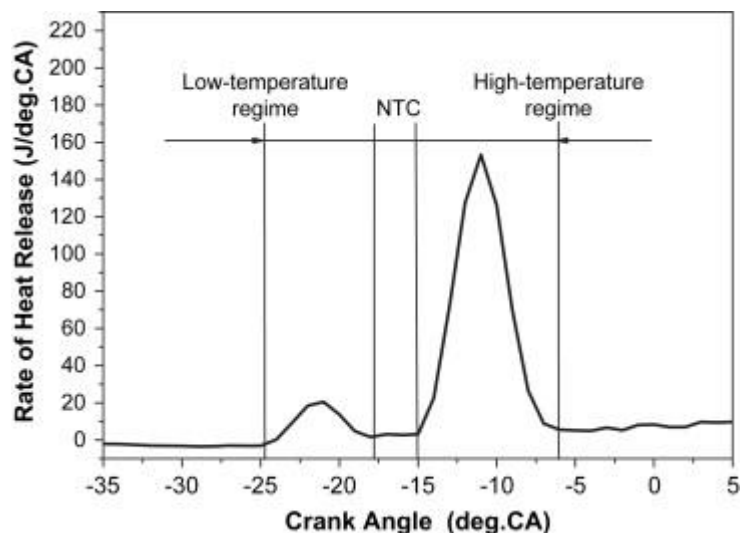


Figure 2-4 Typical two stage heat release curve of HCCI combustion of a reactive fuel such as *n*-heptane [3]

## 2.4 Autoignition Phenomenon

Autoignition often represents a period between the end of low temperature oxidation where  $\text{HO}_2$  and  $\text{H}_2\text{O}_2$  can be successfully accumulated, and the start of high temperature oxidation where  $\text{H}_2\text{O}_2$  readily converts to OH radicals at further elevated temperature. As previously mentioned, the autoignition process in a reaction system largely depends on pressure and temperature history, and hydrocarbon structures. This section briefly introduces the traditional approaches to studying autoignition quality of fuels.

### 2.4.1 Chemical kinetic modeling of autoignition

The aim of the development of comprehensive chemical kinetic models is to predict autoignition quality in relevant chemical reactions. Therefore, Westbrook, Dryer

and colleagues have developed matured chemical mechanisms involving hundreds of species and thousands of reactions for combustion chemistry, starting from the simpler carbon molecules to larger hydrocarbon molecules [9,10]. However, this “comprehensive mechanism” is not perfectly accurate, since the mechanism possesses uncertainties in the reaction rate constants and their temperature and pressure dependence [8,11–13]. As a result, an experimental support is inevitably required to interpolate and extrapolate the chemical reaction mechanisms against autoignition behavior in a reaction system.

The detailed chemical reaction mechanisms applicable to autoignition for internal combustion (IC) engines have been selectively developed for a few pure compounds with lower carbon numbers and simple chemical molecular structures [11,12]. Even though the chemical kinetic mechanism of a pure component is well developed, once it blends with another component such as in olefins or aromatics, matching the initial rate of radical reactions becomes very challenging. Therefore, the lack of understanding of autoignition chemistry for the practical fuels remains an area of significant research interest for internal engine combustion, particularly with regard to autoignition behavior.

#### **2.4.2 Ignition delay**

Ignition delay is a key indicator of the tendency towards autoignition. Many autoignition studies have been conducted using shock tubes and rapid compression machines (RCM), where a fuel/air mixture is rapidly compressed to constant pressure and temperature. The time period ( $\tau$ ) for ignition delay can be measured between the end of compression and autoignition, as marked by heat release. In general, the more reactive fuels possess the shorter time periods ( $\tau$ ) in terms of autoignition.

The ignition delay changes with temperature and pressure. The chemical kinetic models of autoignition are often tuned by the experimental data of ignition delay. In IC engine combustion, pressure and temperature simultaneously increases as the piston starts being compressed from the bottom dead center (BDC). During the cycle, each point will have a different value of ignition delay. Liverwood and Wu first developed the phenomenological models to correlate ignition delay with temperature and pressure as in Equation 2-10 [14], and is commonly used in knock studies [15] as well as HCCI studies [16].

$$\int_{t=0}^{t_i} \frac{d\tau}{\tau} = 1 \quad (2-10)$$

where  $t_i$  is the integral time from time zero to ignition,  $\tau$  is the ignition delay at instantaneous temperature and pressure.

The linear relationship between the logarithm of ignition delay and the reciprocal of temperature is generally observed in the high temperature regime, such as Burcat *et al.* [17]. From this relationship, activation energy and pre-exponential factor can be represented by slope and intercept respectively. Adomit and colleagues showed the undefined slope (activation energy) trends in the low to intermediate temperature regimes in a shock tube, using different types of fuels, even though the linear relationship was still valid, as shown in Figure 2-5 [18,19]. The different slopes from  $\log \tau$  vs.  $1/T$  indicates that the unique combustion chemistries of different type of fuels control their distinct ignition delay in each temperature regime. It should also be noted that increasing pressure in a reaction system leads to a decrease in ignition delay of test fuels. Thus,  $\tau$  can be



expressed as Equation 2-11 and can be also represented by an Arrhenius type expression in Equation 2-12

$$\tau = f(T)P^{-n} \quad (2-11)$$

$$\tau = AP^{-n} \exp\left(\frac{B}{T}\right) \quad (2-12)$$

where A, n and B are fuel-dependent constants. The correlation in equation 2-12 is generally obtained by experimental data for the pressure and temperature history.

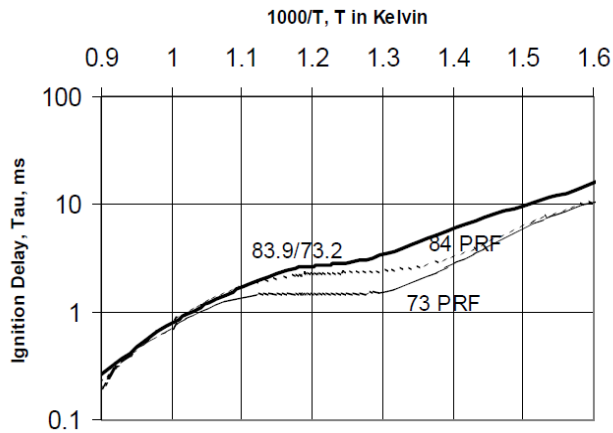


Figure 2-5 Ignition delay time plotted against 1000/T for different fuels at 40 bar [16,19] adapted from [20]

It is not surprising that ignition delay ( $\tau$ ) at one pressure and a wide range of temperature conditions is not reliable to accurately predict engine knock [21]. The test fuels may require the values of  $\tau$  over the entire relevant range of temperature and pressure for IC engines. For this reason, an empirical approach to defining the auto-ignition behavior of practical fuels is inevitable because neither the chemical kinetic modelling approach nor one based on using ignition delay is able to properly describe autoignition in IC engines.

### 2.4.3 Empirical approaches to defining autoignition quality

The research octane number (RON) and motored octane number (MON) are obtained via well-known ASTM methods, D2699 [22] and D2700 [23], which describe indices for auto-ignition, anti-knock or octane quality of fuels for SI engines. The engine used for these tests is a standardized, Cooperative Fuel Research (CFR) engine. Each method has a different distinct test condition in terms of an engine speed and an intake temperature. The research method, RON, is measured at an engine speed at 600 rpm and an intake temperature of 52°C [22], while the motor method, MON, requires an engine speed at 900 rpm and an intake temperature of 149°C [23]. In each test, the fuel-air equivalence ratio can be adjusted to provide the maximum knocking intensity of 50, and the engine compression ratio (CR) increases until the engine just knocks with the maximum intensity. Thus, the fuel that resists autoignition will require higher CR to achieve an engine knock, resulting in higher octane rating. Different proportions of blends of *iso*-octane and *n*-heptane are used as a reference to determine the octane rating of an unknown fuel. Blends of these two primary components are referred to as primary reference fuels (PRF); *n*-heptane and *iso*-octane, where *n*-heptane is given an arbitrary value of 0 octane and *iso*-octane is given the rating of 100, and define the intermediate points in the RON or MON scale. Therefore, an unknown fuel can be rated by comparing its knocking behavior with primary reference fuels in the RON and MON tests. Due to the different test conditions, the values of RON and MON are often different for fuel mixtures. The difference between RON and MON is defined as the fuel octane sensitivity (S) and the value of the sensitivity for practical fuels is typically higher than zero.

Unlike gasoline-like fuels, diesel fuels are significantly reactive, because diesel fuels readily go through autoignition. It should be noted that the RON and MON test methods are not suitable for diesel fuels, because the relatively low intake temperature would not vaporize these low volatility of the fuels, resulting in a lack of homogeneity of the mixtures as it enters the cylinder. As a result, the standard ASTM D613 test method has been adopted to measure the autoignition quality of diesel fuels, which is referred to as cetane number (CN) [24]. As with the measurement of RON and MON, a CFR engine is used to measure the CN for a given fuel by comparing its ignition qualities with reference fuels. The reference fuels are prepared by a binary blend of *n*-hexadecane (*n*-cetane), assigned to have a CN of 100 and heptamethyl nonane (HMN), a highly branched alkane, assigned to have a CN of 15. The cetane number of a blend of *n*-cetane and HMN is determined from the volume percent of each fuel in the blend from the following relationship in Equation 2-13.

$$\text{CN} = x + 0.15(100 - x) \quad (2-13)$$

The CN of an unknown fuel being tested can be determined by a direct comparison to the CN of the reference fuel with the same ignition quality in the cetane engine test.

The autoignition quality of diesel-like fuel can be also measured by commercial instrument based on a constant volume combustion chamber (CVCC) as an alternative method. Two such instruments are AET's Ignition Quality Tester (IQT) and PAC's Cetane Ignition Delay (CID). The autoignition quality of diesel-like fuel is measured under stable initial conditions and obtained by correlating ignition pressure traces to

reference fuels. The value is referred to as derived cetane number (DCN), which correlates with measured ignition delay. These test instruments have been highlighted due to their repeatability and reproducibility and accepted by ASTM methods such as ASTM D6890 and ASTM D7668 [25,26]. It should be noted that ignition delay measured by IQT and CID is different from that measured from the shock tube and RCM, because a different fuel injection method is applied for the CVCC in that a liquid spray injector prevents a perfect pre-mixing of fuel and air.

Kalghatgi demonstrated correlations of the various measurements of autoignition quality, discussed above. Figures 2-6 and 2-7 show strong correlations between measured CN vs RON, and between ID (IQT) vs RON or CN [20]. Those figures account for the same combustion chemistry of the fuel being observed in different empirical measurements of autoignition propensity.

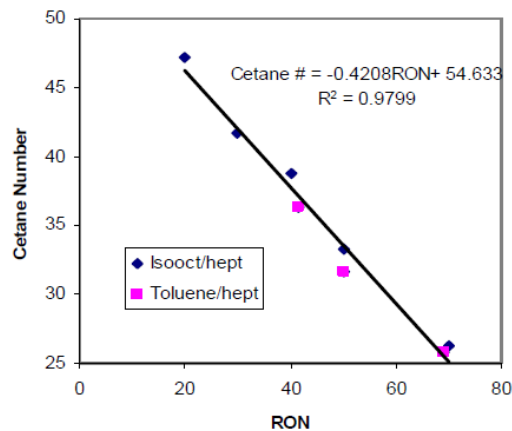


Figure 2-6 A correlation between cetane number measured by ASTM D613 [24] against research octane number measure by [22] for primary reference fuel (PRF) and toluene blended PRF

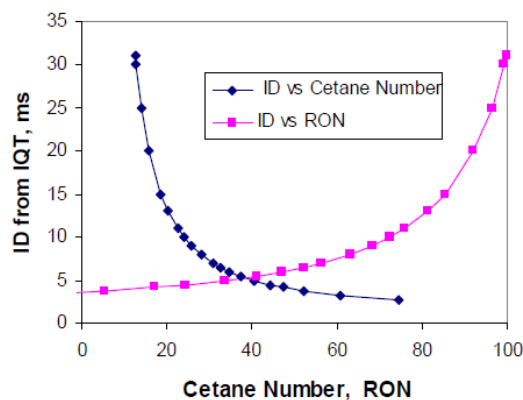


Figure 2-7 Ignition delay (ID) measured by ignition quality tester [25] against cetane number [24] or research octane number [22]

As briefly mentioned above, combustion chemistry is largely dependent on the molecular structure and chemical composition. Therefore, it should be noted that the different fuels exhibit unique key reaction pathways, elementary reaction rates, intermediate products and formation routes, and reaction sensitivity depending on temperature history. Consequently, practical combustion systems show differences in intermediate products, active radicals and their concentrations, pollutant formation and evolution process, and fuel consumption history. These phenomena result in different heat release patterns, burn duration, ignition phasing, pollutant species, and concentrations in the engine combustion system [2,10–13].

For this reason, developing chemical reaction mechanisms for individual hydrocarbon molecules including various *n*-alkanes, *iso*-alkanes, cycloalkanes and aromatics starting from the low temperature becomes more critical in understanding their autoignition behavior. The following section will provide a general description of the major reaction pathways during hydrocarbon oxidation and the reaction sensitivity in each temperature regime.

## 2.5 Overview of Hydrocarbon Oxidation

The phenomenon of low temperature heat release (LTHR), also known as first-stage ignition and cool flame, has been well explained in previous studies of low temperature oxidation of *n*-alkanes [27–30]. Since *n*-alkanes are not only the main component in diesel and jet fuels, but also are the main contributor to LTHR, many fundamental studies of low temperature oxidation of alkanes have been carried out. Among these studies, the noticeable achievements are comprehensive modeling studies of *n*-heptane and *iso*-octane oxidation tested in three different practical reactors over a wide range of experimental conditions [31,32]. Remarkable results were obtained from a large reaction kinetic mechanism including 550 chemical species and 2450 reactions for *n*-heptane and 800 chemical species and 3600 reactions for *iso*-octane. In addition, the corresponding computational results strongly agree with experiment results conducted in flow reactors, shock tubes, and rapid compression machines. As a result, the validated simplified schematic mechanism in Figure 2-8 is proposed for the oxidation of hydrocarbon, based on major reaction pathways in low and high temperature regimes.

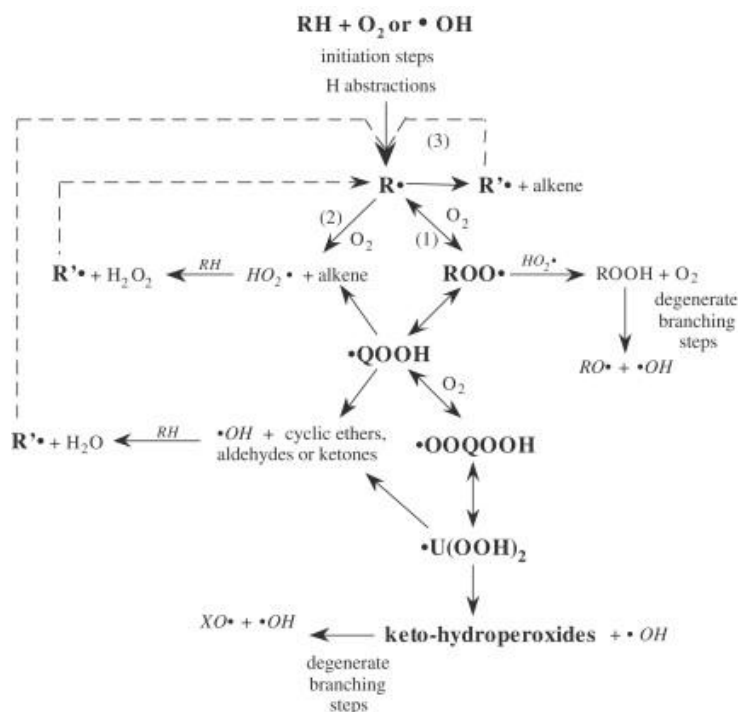


Figure 2-8. Schematic mechanism for low-temperature hydrocarbon oxidation and auto-ignition chemistry [12]

In the beginning of alkane oxidation, the parent fuel molecules lose a hydrogen atom in a C-H bond attacked from oxygen molecules or active radicals, thereby forming a fuel radical. In the low temperature regime, a series of key reaction paths lead to a degenerate branching step. The fuel radicals interact with oxygen to form alkyl-peroxy radicals (ROO•), which then undergo hydrogen shift isomerization to form alkyl-hydroperoxy radicals (•QOOH). A second round of oxygen addition on alkyl-hydroxyperoxide forms •OOQOOH, which again isomerizes via intramolecular hydrogen abstraction, resulting in the formation of ketoalkylhydroperoxide (HOOQ`=O). The formation and decomposition of ketoalkylhydroperoxide generate three active radicals including two •OH, which triggers a degenerate branching reaction in the low temperature regime. This degenerate branching reaction is a precursor to LTHR and cool

flame behavior during hydrocarbon oxidation. In another pathway, the chain propagation reaction from a fuel radical, which forms a HO<sub>2</sub> radical and an alkene, leads to the production of H<sub>2</sub>O<sub>2</sub>, which is structurally stable up to 1100K. The loss of the alkylperoxy radical and emergence of H<sub>2</sub>O<sub>2</sub> result in a relative decrease in reactivity with increasing temperature, leading to the observed negative temperature coefficient (NTC) behavior. In addition, the presence of NTC behavior can account for the occurrence of low temperature heat release (cool flame) at temperature several hundred degrees below the auto-ignition temperature [8]. This competition between two different reaction pathways can determine the reactivity of low temperature oxidation. Further increase of the temperature results in the spontaneous high temperature heat release by the number of radicals formed in the following reaction (2-3c). Alternatively, low temperature oxidation can end prematurely by decomposition of •QOOH, which generates cyclic ethers, aldehydes or ketones.

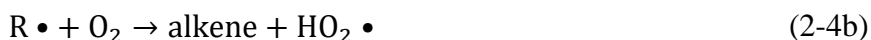
Much simpler and more distinct reaction channels can be found in the high temperature oxidation regime than in the low temperature oxidation regime. The fuel radicals easily experience β-scission in C-C bonds, thereby forming alkenes with a rapid growth of a small alkyl radical pool for further reactions.

The major reaction channels of hydrocarbon oxidation mentioned above are dependent on temperature and fuel molecular structure and size. The following sections describe detailed analysis on reaction sensitivity of major reaction channels with respect to both aspects.



### 2.5.1 Formation of alkylperoxy radicals

The initial step of hydrocarbon oxidation is the formation of alkylperoxy radicals, which is highly dependent on temperature. This reaction channel can be reversible as shown in Reaction 2-4a. The forward reaction proceeds rapidly at low temperatures leading to the formation of  $\text{ROO}\cdot$ , due to zero activation energy required. (i.e., barrierless) [31]. At intermediate temperatures, the reaction shifts toward  $\text{ROO}\cdot$  dissociation, which requires higher activation energy. The reverse reaction for decomposition of  $\text{ROO}\cdot$  is continued until the reaction channel for fuel radical  $\text{R}\cdot$  is again open at high temperatures. As a result of reversible reactions in the intermediate temperature regime, the fuel radical  $\text{R}\cdot$  undergoes an irreversible reaction path (2-4b), building up  $\text{HO}_2\cdot$ , which is a great resource to produce  $\text{H}_2\text{O}_2$  via Reaction 2-3b, as mentioned in the previous section. Therefore, the decomposition of  $\text{ROO}\cdot$  consequently retards the overall oxidation reactivity in the intermediate temperature regime, resulting in NTC behavior.



The temperature at the thermal equilibrium of Reaction 2-4a,  $[\text{ROO}\cdot]/[\text{R}\cdot][\text{O}_2]=1$ , is referred to as the “ceiling temperature. [8]” It should be noted that ceiling temperature is dominated by the pressure of a reaction system. Higher pressure promotes the formation of  $\text{ROO}\cdot$ , increasing low temperature oxidation reactivity and the ceiling temperature. For example, an unreactive fuel, *iso*-octane, which has a single-stage heat

release in a HCCI engine at atmospheric intake condition, shows two-stage heat release under boosted intake conditions.

### 2.5.2 Isomerization in the transition state theory

The key reaction steps in the low temperature regime are those involving intermolecular H atom transfer reactions by forming transition state rings. The selectivity in these internal transfers of a hydrogen atom is based on a free radical isomerization in the transition state theory [33].

According to the transition state theory, elementary reactions are described in the following forms:



where  $C_{\ddagger}$  represents the transition state.

The rate constant of an elementary reaction, such as Reaction 2-5a can in turn be expressed as:

$$k = \frac{k_B}{h} \left(\frac{P^o}{R}\right)^{1-v_1-v_2} \exp\left(\frac{\Delta_{\ddagger} S^o}{R}\right) T^{v_1+v_2} \exp\left(-\frac{\Delta_{\ddagger} H^o}{RT}\right) \quad (2-6)$$

where  $\Delta_{\ddagger} S^o$  is the standard entropy activation and  $\Delta_{\ddagger} H^o$  is the standard enthalpy of activation.

The Equation 2-6 can be rewritten as the Arrhenius-Kooij type;

$$k = AT^b \exp\left(-\frac{E}{RT}\right) \quad (2-7)$$

where  $A = \frac{k_B}{h} \left(\frac{P^o}{R}\right)^{1-v_1-v_2} \exp\left(\frac{\Delta_{\ddagger} S^o}{R}\right) T^{v_1+v_2}$ ,  $b = v_1 + v_2$  and  $E = \Delta_{\ddagger} H^o$

The change of entropy of activation ( $\Delta_{\ddagger} S^{\circ}$ ) is equivalent to the variance between the entropy of the transition state and that of the free radical. The entropy of activation consists of two terms, shown in Equation 2-8.

$$\frac{\Delta_{\ddagger} S^{\circ}}{R} = \ln n_{\text{H}} + 1.75 \Delta_{\ddagger} n_{\text{int.rot}} \quad (2-8)$$

where  $n_{\text{H}}$  is the number of hydrogen atoms concerned by the transfer, and  $\Delta_{\ddagger} n_{\text{int.rot}}$  is the variation of the number of internal rotations.

Figure 2-9 gives an example of the variation of the number of the internal rotors during the isomerization of a 3-peroxyheptyl radical via (1,5) H atom abstraction.

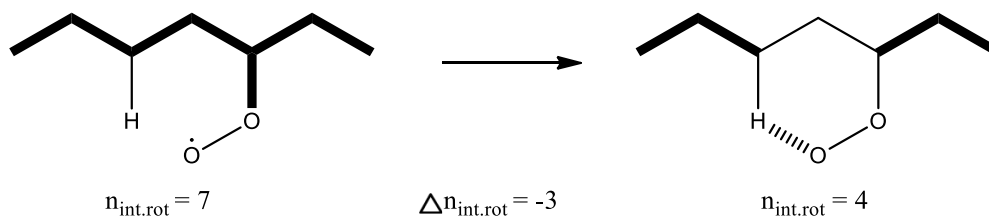


Figure 2-9. Variation of the number of the internal rotors during the isomerization of a 3-peroxyheptyl radical

The change of enthalpy of activation ( $\Delta_{\ddagger} H^{\circ}$ ) from the reactants to the transition state can be represented by the sum of the activation energy of the internal metathesis reaction and the tension energy of the transition state ring.

$$\Delta_{\ddagger} H^{\circ} = E_{\text{me}} + E_{\text{tension}} \quad (2-9)$$

The activation energy of the internal metathesis ( $E_{\text{me}}$ ) is closely related to the type of C-H bond broken, with primary C-H bonds being strongest, secondary C-H bonds next, and tertiary C-H bonds being weakest (i.e.,  $1^{\circ} > 2^{\circ} > 3^{\circ}$ ). The tension energy ( $E_{\text{tension}}$ ) considers the strain energy barriers of the number of atoms participating in

transition state ring. In general, six- and seven membered rings have low strain energy barriers during the isomerization of peroxy radicals [34].

It is concluded that the rate constant for an intramolecular H atom abstraction relies mainly on the type of H atom being abstracted and on the ring size of the transition state. In addition, the A-factor is assumed to be lower with increasing ring size due to the loss of internal rotors.

### **2.5.3 Major chain propagation reaction channels**

After isomerization of alkylperoxy ( $\text{ROO}\cdot$ ) to alkylhydroperoxy radical ( $\cdot\text{QOOH}$ ), two major reaction channels compete according to temperature. If the temperature in a reaction system is sufficiently low, the second round of oxygen addition leads to the low temperature degenerate chain branching reactions. However, the chain propagation reactions of alkylhydroperoxy radical ( $\cdot\text{QOOH}$ ) are not active in the low temperature regime, since the chain branching reaction generally requires higher activation energy. As temperature increases, however, the chain propagation reaction channels become more favored than chain branching reaction channels, as the energy barriers of those reaction channels can be easily overcome. Unlike the chain branching reactions, the chain propagation reactions do not produce significant amounts of active radicals, leading to less fuel consumption than where the reaction system is under chain branching reactions. As a result, the chain propagation reactions play a role in delaying the overall ignition reactivity in a reaction system.

From the chain propagation reactions, the various intermediates can be formed through a decomposition of  $\cdot\text{QOOH}$ . Various aldehydes are generally formed through C-

C  $\beta$ -scission on the carbon backbone. Cyclic ethers can be selectively formed through a five-, six-, and seven-membered transition state (TS) ring as detected reaction intermediates include oxirane, oxetane and tetrahydrofuran structures. Conjugate alkenes can also be produced by intermolecular (1,4) H abstraction reactions. The major reaction pathways to form major intermediate species from the decomposition of 2-hydroperoxy heptyl radicals, are proposed as shown in Figure 2-10.

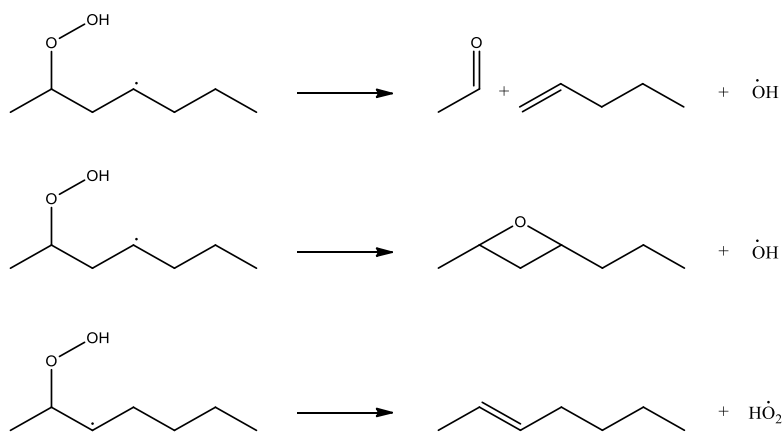


Figure 2-10 Decomposition of 2-hydroperoxyheptyl radicals through chain propagation channels

## 2.6 Reactors for Hydrocarbon Oxidation and Combustion Research

In past decades, chemical kinetic mechanisms of hydrocarbon oxidation have been developed and validated by various practical combustion devices where a wide range of temperatures and pressures applicable for IC engines can be explored [11–13]. Moreover, advanced species analysis techniques (*in situ* method by laser diagnostics and *ex situ* method by gas chromatography) enable a better and deeper understanding of kinetic models as well as chemical and physical behaviors of combustion in a relevant IC engine environment. A brief review of combustion devices and analysis methodology is

given below. Comprehensive reviews on experimental methods for hydrocarbon oxidation can be found in Refs. [8,35]

### **2.6.1 Shock tube**

The shock tube is a well-known device for measuring combustion temperature and ignition delays of many fuels. The gaseous phase mixture of hydrocarbon and oxygen is rapidly compressed by a shock wave, which is normally formed by the rupture of a diaphragm disk. As shown in Figure 2-11, the diaphragm disk divides a tube into two parts, a high pressure driver gas on one side and the sample gas on the other with a low pressure. When the diaphragm is ruptured by helium or hydrogen, such gas creates compression waves that coalesce to create a uniform wave called a shock wave. Then, the shock wave virtually instantaneously elevates a known high temperature and pressure condition over the course of microseconds, and it maintains the condition for a time. (The time available for the reaction is extremely short, which leads to a negligible heat loss against the wall of the tube.) Then, the sample gas can be ignited in an isothermal environment with an expansion wave, which cools the sample rapidly. During this time, the species can be explored by continuous sampling, for example, to a time-of-flight mass spectrometer, or alternatively, sampled at the end of the process for gas chromatography. Ignition delay profiles and temperature can be accurately measured by a pressure sensor and optical devices such as photomultiplier tubes (PMTs). Although accurate, shock tubes are typically limited to ignition delay measurements below 10 milliseconds.

A great amount of ignition, pyrolysis and oxidation studies for various hydrocarbons has been generated in shock tubes by various research groups [17–

19,31,32,36–41]. Furthermore, shock tubes have also been adopted to compare ignition characteristics of surrogate compounds to those of a target fuel [42–48]. The high temperature and high pressure in shock tube make this method less relevant to hydrocarbon LTO of interest in the present study.

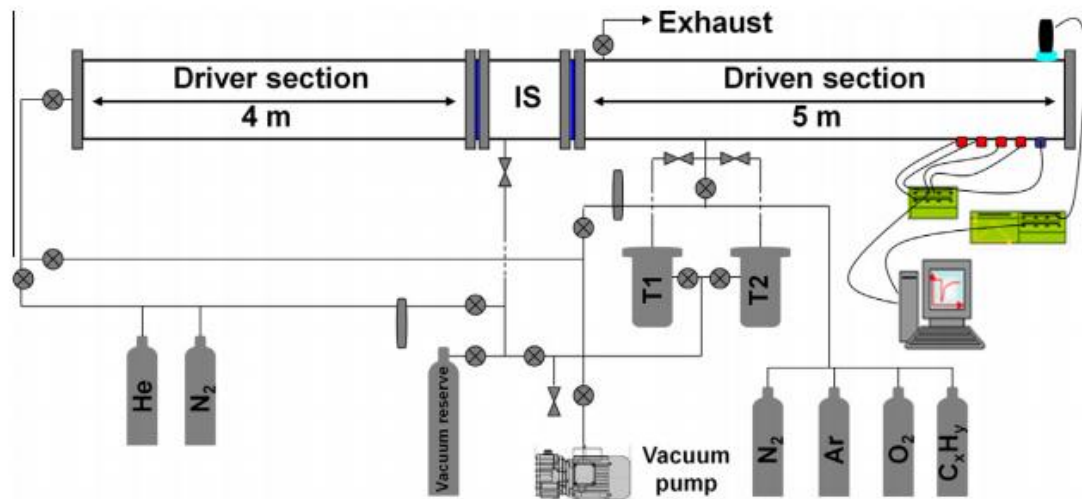


Figure 2-11 Illustration of a single pulse shock tube [49]

## 2.6.2 Rapid compression machine

Like shock tubes, rapid compression machines (RCM) are used as a means to investigate autoignition behavior and ignition delay of many gaseous fuels. The process of a rapid compression machine (RCM) resembles the concept for a piston-cylinder assembly of a reciprocating engine. As shown in Figure 2-12, a standard RCM consists of a driving air tank, driver piston, hydraulic motion control chamber, reactor piston and end reaction chamber. A sample fuel is loaded in the reaction chamber and the other side is filled with compressed air. When a pneumatic piston is released, the pressure difference

creates a rapid heating and pressure increase in a closed cylinder with very little heat loss. Once the piston reaches a pre-determined position, it locks in that position for the remainder of the experiment. After a certain time period, the mixture ignites. This time period between end of compression and start of ignition is defined as the ignition delay, measured by a pressure sensor. Temperature at the end of compression is calculated from the isentropic equation assuming adiabatic compression. The slow compression heating enables the investigation of the oxidation study from a low temperature, but also leads to the undesired errors in measurement. For example, ignition delay for highly reactive fuels tends to be underestimated by the uncounted pre-reactions which start before the end of compression, and tends to be overestimated for unreactive fuels due to the uncounted heat loss after compression. However, many efforts have been also made to eliminate those uncounted effects by supporting the sustained temperature and pressure environment created by the instrument [50]. Although the RCM has been heavily used to study ignition behaviors of fuels by various research groups, the design of RCM from those research groups significantly differs from one device to another. Thus, the results between RCMs are not directly comparable, because the differences in the gas dynamics inside the RCM can have a significant impact on the reaction [51–53].

For this reason, RCMs have been often used to validate autoignition behavior of well formulated surrogate mixtures as compared to that of target practical fuels [44,46–48,54–56]. RCMs may not be an ideal device to study *in-situ* species analysis for hydrocarbon oxidation due to a difficulty in controlling optical diagnostic equipment caused by intensive vibrations that occur during operation [57,58]. However, various



hydrocarbon ignition and oxidation studies with *ex situ* species analysis have been conducted in RCMs to validate detailed chemical mechanisms [31,32,39,59–66].

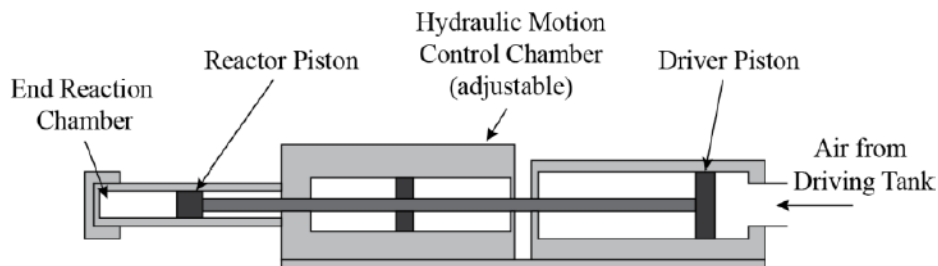


Figure 2-12 Illustration of a basic rapid compression machine (RCM) [66] adapted from [67]

### 2.6.3 Flow reactors

Flow reactors are particularly well suited for the study of the hydrocarbon oxidation processes. Premixed hydrocarbon and oxygen gases continuously flow into the reactor and the products continuously flow out of the reactor with no species accumulation. There are many types of flow reactors, but two types, jet-stirred reactors (JSR) and plug flow reactors (PFR), are commonly used.

The jet-stirred reactor is a type of ideal continuous stirred tank reactor (CSTR). As shown in Figure 2-13, constant pressure and temperature can be maintained, while gas phase reactants flow into the reactors via a nozzle inside of the reactor. The nominal residence time ( $\tau$ ) is determined by the flow rate (i.e., nozzle diameter) and the size of the reactor (i.e., the radius of reactor and the distance from the nozzle). A disadvantage of using other CSTRs is an exponential distribution of residence time of reactant molecules inside the reactor. For this reason, the various designs of JSRs have been extensively developed to overcome issues such as difficulties in mixing reactants well and creating

thermal homogeneity. As a result of continuous efforts on advanced designs of JSRs, many studies of the oxidation and of the pyrolysis of hydrocarbons and oxygenated fuels at atmospheric and high pressures have been successfully conducted, being coupled with various types of *ex situ* analytical techniques [31,32,59,68–72].

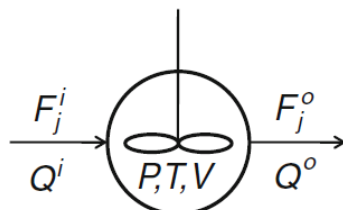


Figure 2-13 Simplified sketch of a jet-stirred reactor of volume  $V$  at constant temperature ( $T$ ) and pressure ( $P$ ).  $F_j^i$  and  $F_j^o$  are the mole flow rates of the species  $j$  at the inlet and at the outlet of the reactor.  $Q^i$  and  $Q^o$  are the volume flow rates of the gas at the inlet and at the outlet of the reactor ( $Q^o$  is symbolized under the conditions of pressure and temperature inside the reactor) [35]

Another flow reactor suitable for gas phase hydrocarbon oxidation studies is a plug flow reactor (PFR), which consists of a cylindrical tube with a fixed diameter, where the reactant mixture flows continuously along the tube, as shown in Figure 2-14. Residence time is translated into a distance along the axial direction of the tube from the point where reactants are introduced to the point of interest. The ideal conditions for plug flow reactors pursue uniform fluid properties (velocity, composition, temperature and pressure) in the radial and axial direction, but those properties are generally disturbed by reaction heat release under plug or laminar flow conditions. To make a fluid property relatively uniform, turbulent flow is usually used, since mixing favors heat transfer and radial temperature uniformity. In addition, dilute conditions generally minimize the axial thermal and flow variation to a negligible level. Under steady state condition, axial profiles of temperature and species can be key factors to determine the reaction progress.

So, the tubular flow reactors are suitable to work with high temperature and pressure conditions, leading to short residence times. Turbulent flow reactors can easily be used with the *ex situ* species analysis using GC and FTIR, and have been extensively used for hydrocarbon oxidation studies [10,31,32,70,73–76] and surrogate validation [44,46–48,56,77,78].

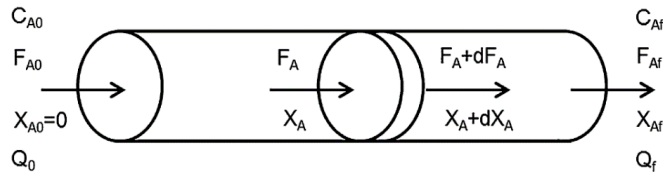


Figure 2-14 Schematic of a basic plug flow reactor [35]

#### 2.6.4 Motored engine

Hydrocarbon oxidation and autoignition can be observed in a motored engine. The motored engine has a continuous reciprocal piston process, but it is different from a firing engine in that the combustion does not necessarily occur. It is different from a spark ignition engine in that the spark plug is disabled and the reaction only relies on piston compression. It is different from a compressed ignition engine in that the fuel and air homogeneously premixed in the intake manifold, before being injected into the engine cylinder. The operating process of the motored engine is essentially the same as that of HCCI, but the reaction can be intentionally controlled for the study of the pre-ignition (oxidation) process.

Unlike the similar RCM process, the motored engine process operates with a dynamic reaction condition, where the pressure, temperature and residence time at each reaction condition are less defined. At each reaction condition, in-cylinder temperature

and reaction heat release generated in the engine cylinder can be calculated from measured in-cylinder pressure and the first law of thermodynamics [15]. However, the estimation of the actual starting in-cylinder temperature at intake valve closing is difficult to implement even if the process assumes an adiabatic compression. For a better prediction, empirical methods calculating the initial in-cylinder temperature for the reaction have been suggested [79].

A noticeable advantage of using this motored engine method is that the reaction takes place under real engine conditions, providing the highly relevant results to the IC engine application. On the other hand, although the designs of combustion devices mentioned above (flow reactors, shock tubes and RCMs) are somewhat limited to the engine relevant conditions, the results of the hydrocarbon oxidation obtained from such combustion devices are often evaluated under an IC engine condition. The *ex-situ* species analysis is generally performed by extracting a gas sample from the exhaust manifold, and sometimes quenched in a liquid solvent for the subsequent gas chromatography analysis. This method is relatively convenient as compared to other practical combustion devices and the repeating engine cycles can provide a sufficient amount of species sample for analysis. Furthermore, a typical Cooperative Fuel Research (CFR) octane rating engine has been used in most cases, providing a common platform for data comparison. This motored engine method has been used for various hydrocarbon oxidation studies such as surrogates for gasoline fuel [80], diesel fuel [30,81,82] and bio-diesel [83–85], and ignition behavior studies for different types of diesel fuels [86,87]. For this reason, in the present work, the motored engine method is employed for the study of hydrocarbon oxidation and ignition characteristics.

### **2.6.5 Constant volume combustion chamber**

Previous research apparatus discussed above have been used for the homogeneous (pre-mixed) gas phase hydrocarbon oxidation studies to develop and validate chemical kinetic mechanisms. Unlike those practical combustion devices, the constant volume combustion chamber (CVCC) has been adopted for heterogeneous fuel and air charge combustion characteristics, which is achieved by a direct liquid fuel spray injection into the chamber. This liquid spray injection method is highly valuable in the validation of computational models for IC engine applications [88].

The liquid spray ignition can occur spontaneously in a secured high temperature and pressure environment created by electrical heaters surrounding a CVCC. Various designs of CVCCs can enable optical access to investigate physical and chemical behavior during the ignition process. For example, Sandia National Laboratory has developed a new design chamber that is accessible for optical diagnostics such as Mie scattering, chemiluminescence, and Schlieren through multiple viewing windows, as shown in Figure 2-15 [89].

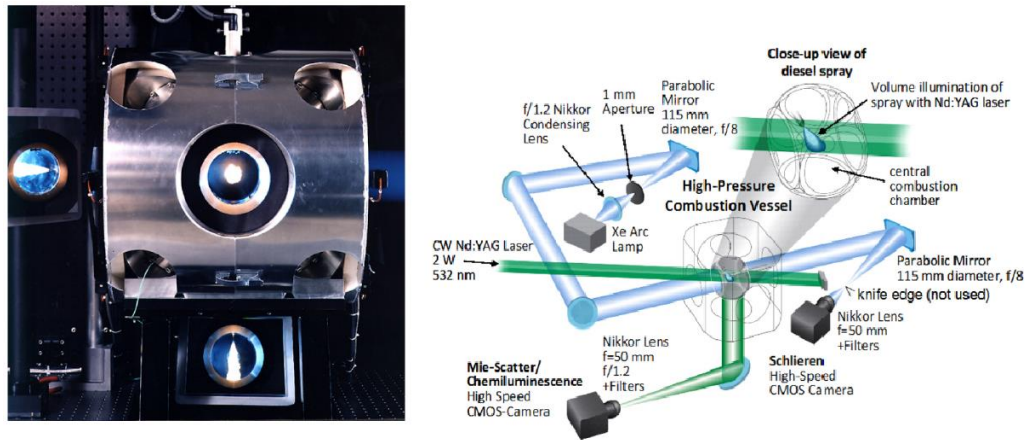


Figure 2-15 Constant volume combustion chamber and design of optical diagnostics at Sandia National Laboratory [89]

As briefly discussed, commercial CVCC instruments including the ignition quality tester (IQT) and cetane ignition delay (CID) were originally targeted to obtain the derived cetane number of diesel-like fuels [25,26]. However, due to the strong repeatability and reliability of these instruments, many experimental ignition studies of diesel-like fuel components have been extensively conducted in the IQT [88,90–93] and CID [94]. Furthermore, CFD combustion models for spray ignition behavior in the IQT’s CVCC have demonstrated excellent agreement with experimental data [88,95]. Another benefit of using commercial CVCCs is that the design and controllability offer a strong platform for optical studies, so comparable studies can be pursued by different research groups.

The current study adopts the CID CVCC to demonstrate spray ignition behavior, by adopting a chemiluminescence detection system with a cooled borescope installed at the bottom of the heated chamber.

## 2.7 Surrogate Development

Detailed chemical kinetic mechanisms have been targeted for the computational design and optimization in practical devices (i.e., internal combustion engines and gas turbines) with an advanced combustion simulation of practical transportation fuels such as gasoline, diesel and jet fuels. However, the fact that practical fuels consist of hundreds of individual chemical compounds presents a barrier to the development of detailed chemical kinetic mechanisms for practical fuels. The kinetic mechanism considering all these compounds would be too huge to be tractable by given current computational ability, and there is a lack of fundamental information (e.g., chemical kinetic rate constants, reaction paths, thermodynamic parameters) for development of such a mechanism. Therefore, in practice, simplified chemical kinetic mechanisms are required based on a handful of pure compounds, which can emulate certain characteristics of the target fuels that contain many compounds. The target properties can be either only chemical or both chemical and physical, based on the target application. The target chemical properties of the fuel may include derived cetane number (DCN), C/H/O content, molecular weight (MW) and sooting tendency, which mainly affect autoignition behavior, gaseous emissions and soot formation. Relevant physical properties of the fuel may include volatility, density, viscosity, surface tension and diffusion coefficient, which mainly affect injection, vaporization and mixing processes that precede ignition in practical devices.

It should be noted that the kinetic mechanisms for each of the pure compounds included in a surrogate fuel formulation must be rigorously developed and then validated

in various combustion devices. As a result, a selection of pure compounds for the surrogate model is limited to a surrogate pallet, as shown in Figure 2-16. The proper fractions of selected compounds need to be identified to best reproduce the properties of the target fuel. Then, the chemical kinetic mechanisms of the individual components will be combined and significant cross-linked reactions between mechanisms will be also recognized. As a means to better formulate the surrogate mixtures for vapor phase combustion, Dryer and co-workers developed an *a priori* methodology, which requires only limited knowledge of the molecular class composition of the specific real fuel [44,46–48]. The method is based on an assumption that a much smaller pool of distinct chemical functionalities can be generated after an initial reaction. The “active radical pool” is mainly responsible for the initial hydrogen abstraction from the original fuel compounds, which is well demonstrated in Figure 2-17 [46]. Also, continuous efforts have improved the development of reduced (simpler) mechanisms, which can facilitate the employment of multi-dimensional computational fluid dynamics (CFD) models for simulating engine combustion. More importantly, accurate computational simulations become valuable only if combustion characteristics of surrogate compounds are experimentally validated in various combustion devices over a wide range of temperatures and pressures pertinent to internal combustion engines as compared to the target fuel.



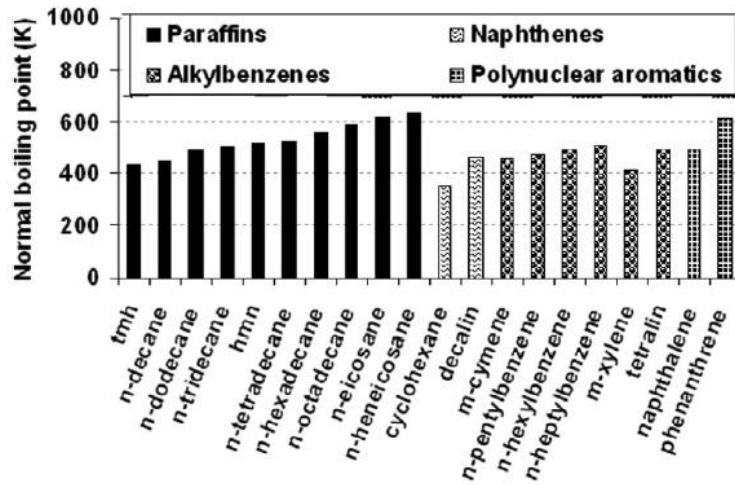


Figure 2-16 Surrogate species pallet used to emulate distillation and physical properties of diesel and jet fuels as originally extracted from [96], regenerated by [97]

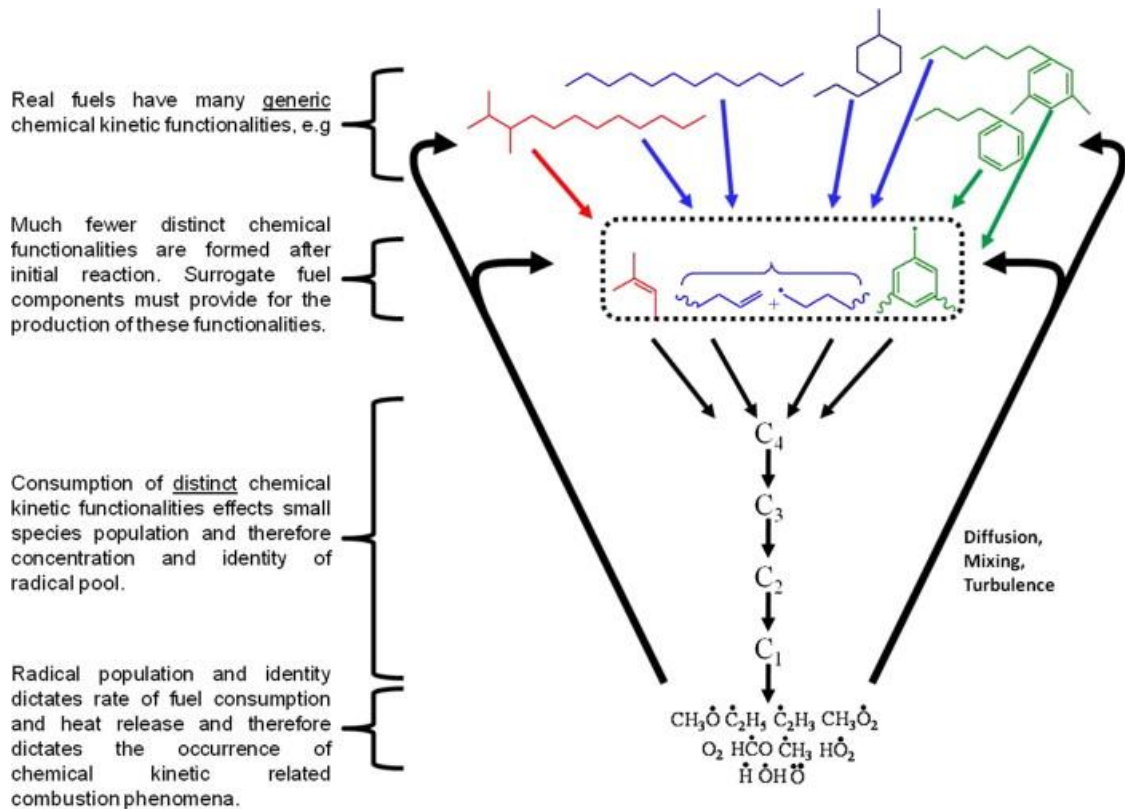


Figure 2-17 Schematic diagram of real fuel oxidation and concept of distinct chemical functionality as it applies to high temperature combustion kinetic phenomena [46].

There are multiple benefits from the development of surrogate fuels. If the known formulation of surrogate fuels can be standardized, this can be reproducible at any time in any experimental device and geographic location. In addition, the surrogate formulations can be easily reassessed and refined under underlying estimations of target properties of the practical fuel. Since surrogate fuels focus mainly on their fuel properties, this would be a good reference for emerging practical transportation fuels through the refinery process. This surrogate development ultimately can lead to improving engine efficiency, cleaner emissions and other critical performance characteristics.

The refining of conventional crude oil produces gasoline, diesel and jet fuels. Figure 2-18 shows the typical distillation range and organic class distribution for gasoline, diesel, and jet fuels, resulting in different chemical and physical properties. For example, gasoline consists of lighter hydrocarbons ( $C_6 - C_{12}$ ), while diesel consists of heavier hydrocarbons ( $C_{12} - C_{20}$ ). Jet fuels have an average carbon number of 12, normally refined between gasoline and diesel. The chemical composition distribution of practical fuels is one of the dominant characteristics for selecting proper individual compounds in surrogate formulations. For instance, a similar carbon number of alkanes to the target fuels is mainly chosen for surrogate formulations, e.g., *iso*-octane ( $C_8$ ) for gasoline, *n*-hexadecane (*n*- $C_{16}$ ) for diesel, and *n*-dodecane (*n*- $C_{12}$ ) for jet fuel. It should also be noted that the detailed chemical kinetic mechanisms for smaller carbon numbers and simpler structures of hydrocarbon molecules are easier to be implemented as compared to those for more complex compounds. This implies that gasoline surrogate models have been more developed due to the mechanism's simplicity than those for

diesel and jet fuel. Earlier studies recognized a lack of detailed kinetic mechanisms for larger and more complex compounds, which rarely exist in the current surrogate pallet.

Many studies have been dedicated to development of advanced and validated surrogate models for gasoline, diesel and jet fuels and an excellent review of recent progress in the development of surrogate fuels can be found in [98] for gasoline, [99] for diesel, and [97] for jet fuel. The current study considers the autoignition characteristics of conventional and synthetic alternative jet fuels and their surrogate mixtures recently developed by Violi and colleagues [100].

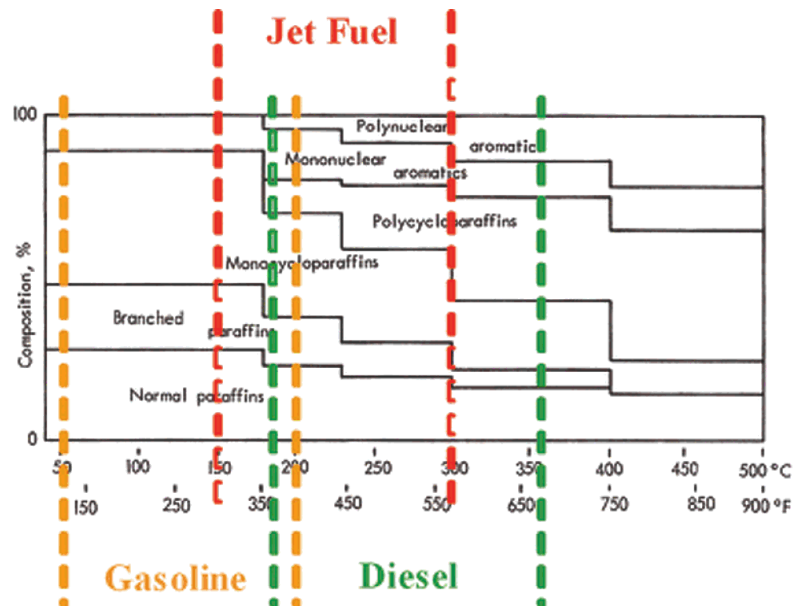


Figure 2-18 Typical distillation range and organic class distribution of species found in gasoline, diesel and jet fuels [101]

## Chapter 3

### Experimental

The work described in this dissertation uses a motored engine to study the oxidation chemistry and the ignition behaviors of various individual hydrocarbons and hydrocarbon mixtures. The engine experiments have been conducted in two different places and additional measurements (fuel flow meter, air boosting system and wall temperature heat flux sensor) were implemented for the purpose of the current study. Furthermore, the parts of this dissertation deal with product analysis using *ex situ* method during pre-ignition in a motored engine, providing quantitative and qualitative information of major intermediate species.

The study discussed in **Chapter 7** additionally adopts an optically accessible constant volume spray combustion chamber to investigate spray ignition behavior of conventional and alternative synthetic jet aviation fuels as compared to their surrogate mixtures.

This chapter describes in the experimental devices, a motored engine and a constant volume combustion chamber, and *ex situ* methods for intermediate species analysis in a motored engine used in this study.

## **3.1 Cooperative Fuel Research (CFR) Motored Engine**

### **3.1.1 Motored engine setup**

The modified motored CFR octane rating engine used in this dissertation was originally developed by Szybist *et al.* [30], and small modifications have been made by previous researchers [82,83] to improve the repeatability of this engine facility. The CFR engine in its present configuration is shown schematically in Figure 3-1. The engine was operated at 600 rpm under steady state condition. Its carbureted fueling system was replaced with a gasoline direct injection (GDI) fuel injector located 1.4 meters above the engine intake valve to provide a premixed fuel-air mixture to the engine cylinder. The intake manifold of the engine includes an electric heater which can heat the intake air and fuel mixture to as high as 260°C. For the study in **Chapter 7**, a supplemental electrical heater was added to preheat the high pressure combustion air, which could be supplied to the engine at pressures up to 3 bar (abs). The original knock meter in this engine used for octane rating was replaced with a Kistler 6052B piezoelectric pressure transducer. For the stabilization of test parameters, the water cooling jacket of the engine cylinder and GDI injector temperatures were maintained at 90°C with an 8L, 1000 W, and a 6L, 1100 W refrigerated/heating circulator, respectively. The CFR engine specifications are shown in Table 1.

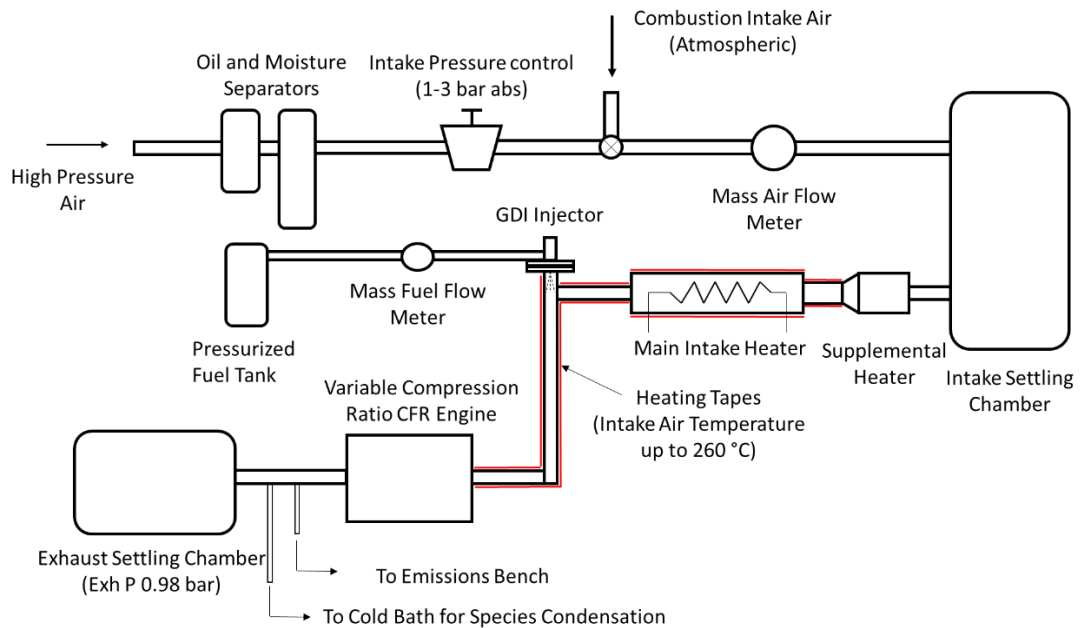


Figure 3-1 Schematic of modified CFR motored engine

Table 1 CFR motored engine specifications

Number of cylinder	1
Bore (cm)	8.26
Stroke (cm)	11.43
Swept volume (cm <sup>3</sup> )	611.7
Compression ratio	4-15.7
Number of overhead valve	2
Engine speed (rpm)	600
Intake valve open (degrees after TDC)	10
Intake valve closes (degrees after BDC)	34
Exhaust valve open (degrees before BDC)	40
Exhaust valve closes (degrees after TDC)	15
Combustion chamber	Pancake piston

### 3.1.2 Method of heat release calculation

The quantitative information on the progress of combustion is often represented by the rate of release of the fuel's chemical energy (often called heat release) or rate of fuel burning, which can be obtained by in-cylinder pressure versus crank angle data over the compression and expansion strokes of the engine operating cycle. The analysis of heat release, which includes the calculation of apparent heat release rate (AHRR) and bulk gas temperature, was based on a zero-dimensional ideal gas combustion using a single zone model [15]. The detailed equations are shown as follows.

The models start with the first law of thermodynamics for an open system, which is quasi static (i.e., uniform in pressure and temperature). The first law for such a system can be represented as Equation 3-1.

$$\frac{dQ}{dt} - p \frac{dV}{dt} + \dot{m}_f h_f = \frac{dU}{dt} \quad (3-1)$$

where  $dQ/dt$  is the heat-transfer rate across the system boundary into the system,  $p(dV/dt)$  is the rate of work transfer done by the system due to system boundary displacement,  $\dot{m}_f$  is the flow rate into the system,  $h_f$  is the enthalpy and  $U$  is the energy of the material contained inside the system boundary.

Calculating this heat release model is very complex, unless several assumptions are made, which are as follows. First, the fuel and air mixture inside of the cylinder is considered to be an ideal gas. Second, the fuel and air mixture is distributed homogeneously, leading to uniform properties across the cylinder. Third, the specific heat of the in-cylinder gas mixture is assumed to be that of air, which is only a function of

temperature. Last, the heat release due to combustion is considered to be heat addition to the cylinder.

If  $U$  and  $h_f$  in Equation 3-1 are taken to be the sensible internal energy of the cylinder contents and the sensible enthalpy of the injected fuel, respectively, then  $\frac{dQ}{dt}$  can be demonstrated as the difference between the heat released from the chemical reaction ( $\frac{dQ_{ch}}{dt}$ ) and the heat transfer to the cylinder wall ( $\frac{dQ_{ht}}{dt}$ ). Since  $h_{s,f} \approx 0$ , Equation 3-1 becomes Equation 3-2.

$$\frac{dQ_{net}}{dt} = \frac{dQ_{ch}}{dt} - \frac{dQ_{ht}}{dt} = p \frac{dV}{dt} + \frac{dU_s}{dt} \quad (3-2)$$

As mentioned in the list of the assumptions, the heat release calculation does not account for the heat losses or heat transfer across the cylinder wall, ( $\frac{dQ_{ht}}{dt} \approx 0$ ), which is called the ‘apparent’ heat release rate (AHRR). It should be noted that  $dU_s = mC_v dT$ . Also, the ideal-gas law,  $\frac{PV}{mR} = T$ , where  $R$  is assumed to be constant, can be applied in Equation 3-2 together with Equation 3-3.

$$dU_s = mC_v dT = C_v d(mT) = C_v d\left(\frac{PV}{R}\right) = C_v P \frac{dV}{R} + C_v V \frac{dP}{R} \quad (3-3)$$

Then, the Equation 3-2 can be demonstrated as Equation 3-4

$$\frac{dQ_{net}}{dt} = \frac{1}{R} P \frac{dV}{dt} + \frac{C_v}{R} P \frac{dV}{dt} + \frac{C_v}{R} V \frac{dP}{dt} \quad (3-4)$$

By substituting  $\frac{C_v}{R} = \frac{1}{(\gamma-1)}$  into Equation 3-4, Equation 3-5 is obtained, which is the commonly used expression for net heat release rate.

$$\frac{dQ_{net}}{dt} = \frac{\gamma}{\gamma-1} P \frac{dV}{dt} + \frac{1}{\gamma-1} V \frac{dP}{dt} \quad (3-5)$$



Cylinder temperature can be estimated via the ideal gas law where PV is known at every point. It is worth noting that residual gas from the previous cycle in an engine cylinder should be theoretically taken into account for the calculation of the mass of the cylinder contents. The contribution of the residual gas to the total mass of cylinder contents can be expected to become increasingly more significant as the engine compression ratio decreases. In the current study, residual gas fraction was estimated using the method proposed by Fox *et al.* [102].

### 3.1.3 Measurement of engine parameters

The fuel was maintained at a pressure of 4.83 MPa (700 psi) upstream of this injector, and injection was carried out at a constant frequency of 10 Hz. The fuel flow rate was controlled by changing the injection pulse using a triggering module. This injector did not account for fuel properties like density and viscosity, and hence, had to be pre-calibrated for the estimated fuel flow range prior to the engine experiment. However, a difficulty in precise calibration for highly volatile liquid fuels has been found. Therefore, in **Chapter 5**, a Max Model 213 piston flow meter was used to measure the mass flow rate of fuel injected for high volatility liquid fuels, *n*-pentane and *iso*-pentane and a Sierra Top-Trak Model 826 was used for a gas phase fuel, neo-pentane. Other than the study reported in **Chapter 5**, pre-calibration of the injector for testing fuels has been adopted as described above.

The air mass fuel rate was measured at the exit of a chiller ( $5\pm 2^\circ\text{C}$ ) by a hot-wire mass airflow (MAF) sensor (Delphi).

Engine speed is measured by a shaft encoder (Accu-Coder), which also provides a clock signal at the resolution of 0.1 crank angle to measure cylinder pressure.

Cylinder wall temperature was obtained by using a MEDTHERM coaxial thermocouple installed on the side of the combustion chamber where the spark plug would normally be placed.

In-cylinder pressure was measured by a Kistler 6052B piezoelectric pressure transducer at a resolution of 0.1 crank angle for 40 consecutive engine cycles at each operating point. The signal from this pressure transducer was amplified using a Kistler 5010 dual mode amplifier and acquired using a LabView based high-speed data acquisition system.

Static pressures are measured at the intake plenum chamber and the exhaust plenum chamber.

### **3.1.4 Descriptions of autoignition characteristics**

The CFR motored engine provides details of the auto-ignition behavior of the test fuels including the ignition limit characteristics such as the critical compression ratio (CCR) and the critical equivalence ratio ( $\phi_{crit}$ ), as well as combustion phasing and the percentage of low temperature heat release (% LTHR) at CCR. These indices are useful for defining the ignition reactivity of the test fuels; for example, comparisons of fuel chemical isomers (**Chapters 4 and 5**), fuel blending effects (**Chapter 6**), and validations of fuel surrogate mixtures against target jet fuels (**Chapter 7**).

Some of the terms used to describe the measurements including CCR, critical  $\phi$  and % LTHR used herein are follows as: First, the concept of CCR was initially

introduced by Curran *et al.*[103], who observed that the autoignition phenomena in a motored engine, where high temperature heat release (HTHR) eventually occurred as the compression ratio was increased at a constant  $\phi$ . In a later work, Szybist *et al.*[30], examined a high CN fuel and demonstrated two-stage ignition process with significant low temperature heat release (LTHR) in the modified CFR motored engine. Second, it is known that localized regions of low  $\phi$  generally occur within the combustion chamber when the fuel is sprayed using diesel injectors. This was recognized as a potential source of unburned hydrocarbon and CO emissions, based on a detailed examination utilizing the concept of critical  $\phi$ , first introduced by Musculus *et al.*[104]. Lilik and Boehman adopted this concept and applied it to the modified CFR motored engine, where localized  $\phi$  in the combustion chamber can be simulated, thus investigating the effects of fuel ignition quality and composition on critical  $\phi$  for autoignition [86,87]. Lastly, the % LTHR is defined as  $[\text{LTHR} / (\text{LTHR} + \text{HTHR})] \times 100 \%$ , thus quantifying the low temperature oxidation reactivity of test fuels. The LTHR and HTHR are often referred to as first and second stage (1<sup>st</sup> and 2<sup>nd</sup>) heat release, respectively [30].

### 3.1.5 Intermediate species analysis methodology

One focus of this dissertation contains intermediate species analysis to gain insight into the oxidation chemistry of individual compounds or compound mixtures. The intermediate species from the oxidation of low volatility of fuels of interest described in **Chapter 4** and **Chapter 6** were captured in the dichloromethane ( $\text{Cl}_2\text{CH}_2$ , DCM) solvent surrounded by a cold bath, leading to a liquid phase sample, but the intermediate species from the oxidation of high volatility of fuels in **Chapter 5** were captured in a tedlar bag,

leading to a gas phase sample. Details of the two different methods of intermediate species analysis are as follows.

For the studies in **Chapter 4** and **Chapter 6**, to identify the intermediate products of oxidation, the exhaust gases were analyzed. A portion was condensed and the other was used to measure the exhaust CO and CO<sub>2</sub> concentration via an AVL CEB II emissions analyzer (NDIR analyzer). The former consists of a custom-made glass condenser, which was connected through braided hoses to the engine's exhaust sample line (190°C), a dry ice/acetone bath (-79°C) and a vacuum pump to move the exhaust gases through the condenser. An exhaust sampling flow rate of 0.944 L/min (2 SCFM) was forced to pass during 10 min through the condenser filled with 25 ml of DCM. This glass condenser system used for collection of GC samples for combustion product analysis has undergone several modifications from the original design [30] in order to maximize the condensation rate, which has been reported to be higher than 70% when the dry ice/acetone bath temperature achieved -79°C [81–85]. After completion of the 10 min sampling time, the vacuum pump was stopped and the condenser was removed from the bath, allowing the DCM solution to reach ambient temperature before quantitative transfer to a 25 mL volumetric flask, completing the volume with additional DCM. The sample collected was transferred to vials for GC analysis. Since most of the condensed intermediates were stable species in a diluted DCM solution, significant changes in the composition were not expected to occur.

Unlike previous studies [81–85], the current study neglected relatively light weight molecules (C<sub>2</sub>-C<sub>4</sub>), which might not be condensed in a cold DCM solvent, although most of the molecules bigger than C<sub>5</sub> were expected to be condensed. The

intermediate products of oxidation in the liquid condensate samples were identified by gas chromatography with mass spectrometry detection (GC-MS) and quantified by gas chromatography with flame ionization detection (GC-FID). GC-MS was performed on a Shimadzu GC-17A equipped with a QP-5000 mass selective detector with an ion source of electron impact at 70 eV. Compounds were identified with the help of the mass spectral library from the National Institute of Standards and Technology (NIST). The quantification was performed on a Varian CP-3800 GC with FID. The column was a Restek Rxi-5MS, 30 m x 0.25 mm i.d. x 0.25  $\mu$ m film thickness. The injector and interface temperatures were 290°C. The oven temperature was programmed to hold at 35°C for 10 min and ramp at 20°C/min to 125°C. The split ratio was set to 30:1. The flow rate of helium carrier gas was 1 mL/min.

The fractions of identified products are quantified in relative terms by normalizing the product yield (FID signal) with the unreacted reactants. Note that different product species may be captured by different condensation rates; thereby causing difficulty in performing quantitative analysis for a wide range of products. However, the compounds with similar chemical structures and boiling points are expected to possess similar condensation rates, therefore the quantitative analysis can be reliable within the compounds possessing similar chemical structures. These relative fractions of product species are critical in understanding the major reaction steps during the low temperature oxidation of branched cycloalkane isomers in **Chapter 4** and diisobutylene blends in *n*-heptane and *iso*-octane in **Chapter 6**.

For the study in **Chapter 5**, quantitative analyses of gaseous emissions were carried out by using a CAI NDIR analyzer for CO and CO<sub>2</sub>, and two gas chromatography

(GC) instruments, each dedicated to a unique set of hydrocarbons. Each GC uses a different capillary column, instrument parameters, and sample preparation techniques. Quantification of oxygenated species was carried out with an Agilent 6890 GC-FID with an HP-5 column (50m x 0.2mm i.d. x 0.33 $\mu$ m film thickness). A vacuum pump was used to draw exhaust samples at 0.944 L/min through a heated exhaust sample line (190°C) into 2L sample bags. Immediately after collection in a bag, each sample was injected into the GC-FID to minimize condensation of exhaust sample in the bag due to temperature drop. The following external standards were used to determine species concentrations: acetaldehyde, propenal, 1-butanal, 1-pentanal and 2-methyltetrahydrofuran. Species identification was performed with an Agilent 6890 GC-MS using the same method and column as the GC-FID used for quantification. To increase species identification accuracy, in a separate test, exhaust gases were bubbled through a 25mL bath of dichloromethane maintained at -79°C using dry ice and acetone at 0.944 L/min for 10 minutes. After 10 minutes the dichloromethane solution was injected into the GC-MS, resulting in larger peaks than were observed from the sample bag. Since most condensed intermediates are stable species in the diluted DCM solution, significant changes in the composition were not expected to occur.

The second GC-FID, a Shimadzu GC-17A with a Restek Rtx-1 column (60m x 0.32mm i.d. x 1 $\mu$ m film thickness) was used to identify non-oxygenated species. The oven temperature was swept from -80 to 238°C to quantify C<sub>1</sub>-C<sub>10</sub> hydrocarbons using a 130 species retention library adapted from [105] and expanded by conducting runs with known hydrocarbon species. Additional instrument parameters are described in [106]. Exhaust gas was captured with the same method mentioned above, but was diluted with

N<sub>2</sub> and 9.3 ppmC<sub>1</sub> propane at 10:1 to avoid water and hydrocarbon condensation, and to provide an internal standard for quantification.

A carbon balance was performed by comparing carbon flow to the engine in the fuel to carbon flow in exhaust CO, CO<sub>2</sub>, oxygenated and non-oxygenated hydrocarbons. For most test points, exhaust carbon agrees to within  $\pm 15\%$  of fuel carbon. Considering the number of exhaust species, this degree of agreement serves as a good verification of instrument performance. Part of the disagreement is likely caused by loss of species by condensation in sample lines and the undiluted sample bag, unmeasured formaldehyde, and for some conditions, a saturated CO measurement (beyond calibration range).

## **3.2 Cetane Ignition Delay (CID) 510 unit**

### **3.2.1 Constant volume combustion chamber modification**

The constant volume combustion chamber (CVCC) is a commercially available Cetane Ignition Delay (CID) 510 instrument manufactured by PAC L.P. This unit is manufactured for measuring the derived cetane number (DCN) of liquid fuels [26]. Three key features of the CID unit are of primary interest for the current study. First, the design of the CID combustion chamber mimics a practical diesel engine combustion chamber. Second, the CID unit utilized a Bosch light-duty diesel injector that delivered fuel at 1000 bar, which is very similar to an automotive common-rail injection system. Finally, the CID unit is user-friendly given that the internal computer of the CID unit has the capability to easily change operating conditions such as chamber temperature, pressure, fuel injection duration and fuel injection pressure.

The constant volume combustion chamber (CVCC) was modified for the purpose of investigating the physical and chemical ignition behavior of liquid fuel by Mayo and Boehman [67], where the details of experimental setup and combustion chamber thermal analysis, and sub-systems installed can be found. Three ports were welded to the bottom of the chamber to provide optical access to the spray during fuel injection. Two sub-systems occupied these ports including a high speed camera system for physical spray characterization and a photomultiplier tube (PMT) system for chemiluminescence detection of excited state chemical intermediate species, details of which are specified in the next section. In the current study, two ports for a high speed camera system were blocked and only the PMT system was utilized. Combustion air was injected into the combustion chamber by using a gas mixer system from Polycontrols (Ontario, Canada), which is installed upstream of the CVCC. In addition, the gas mixer system gave the capability to dilute the air with nitrogen and CO<sub>2</sub> to simulate the exhaust gas recirculation (EGR) commonly utilized in modern diesel engines. Simulated EGR composition (O<sub>2</sub>, CO<sub>2</sub>, and N<sub>2</sub> concentration) were calculated by a method derived by Mueller based on of the chemical reaction formula for complete combustion [107]. Similar to the motored engine heat release analysis, the low-pass filtered pressure trace data collected by the CID's internal computer is used to obtain the apparent heat release rate (AHRR) and the bulk temperature, using the ideal gas law and a similar approach to that explained earlier for the motored engine.



### 3.2.2 Chemiluminescence detection system (CDS)

To observe the presence of known intermediate species throughout ignition delay event, a custom chemiluminescence detection system (CDS) was designed and constructed by Mayo and Boehman [94]. An air-cooled, UV/Vis optical probe designed by SMETec was installed at the bottom of the combustion chamber. The probe was equipped with a 90° wide-angle, quartz lens. The photons emitted from excited state chemical intermediates passed through the optical probe and fiber to the CDS. A collimating lens aligned the light rays in parallel as they exited the fiber tip. This homogeneous beam of light is then directed towards a system of dichroic mirrors, band-pass filters, and three photomultiplier tube (PMT) modules, shown in Figure 3-2. Two dichroic mirrors in series segregated the light at 340 and 460nm. The three resulting channels of light were individually filtered with Edmund Optics band-pass filters. First, the OH\* chemiluminescence signal is measured with a band-pass interference filter centered at 307±5nm. To measure CH\* chemiluminescence, another PMT is used in combination with a band-pass interference filter centered at 430±5nm. Finally, the C\* photon is captured with a band-pass interference filter centered at 515±5nm. In addition, excited state formaldehyde (CH<sub>2</sub>O\*) emissions, which overlapped with the 431nm wavelength of CH\*, were captured during the first stage of the two-stage ignition process. Once photons pass through each filter, a Hamamatsu PMT Module generates an amplified voltage (0-5V) through amplifiers for each excited state chemical intermediate. A National Instruments high-speed data acquisition (DAQ) card simultaneously acquired

40,000 samples at 1MHz from each of the three, amplified PMT signal channels. The acquired data was saved to a test file for further analysis.

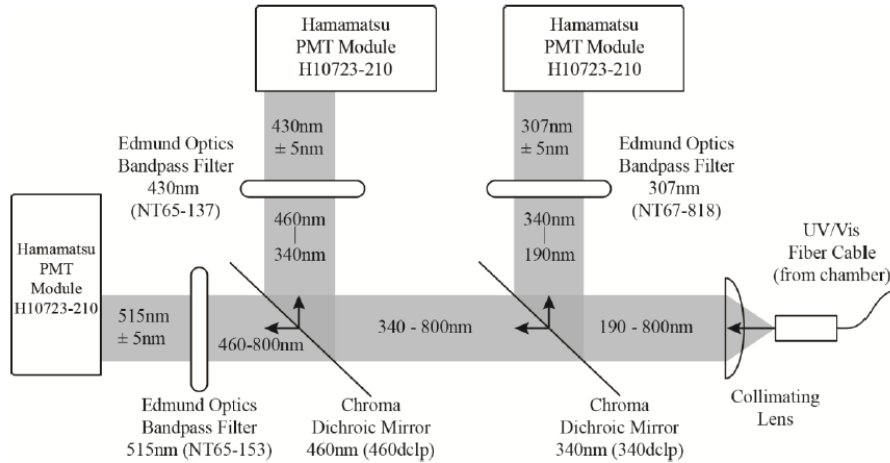
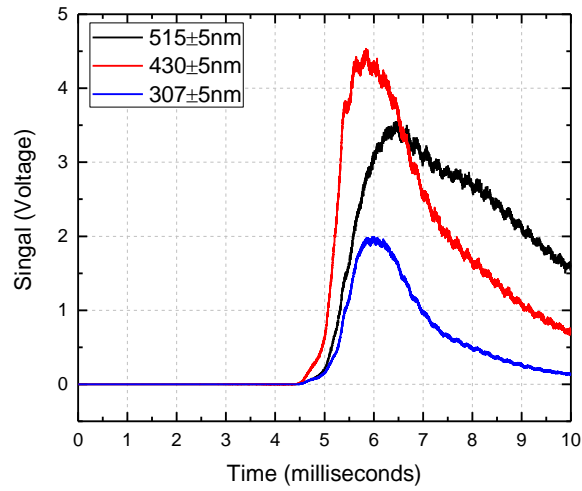


Figure 3-2. Schematic of light pathway in the chemiluminescence detection system (CDS) [67]

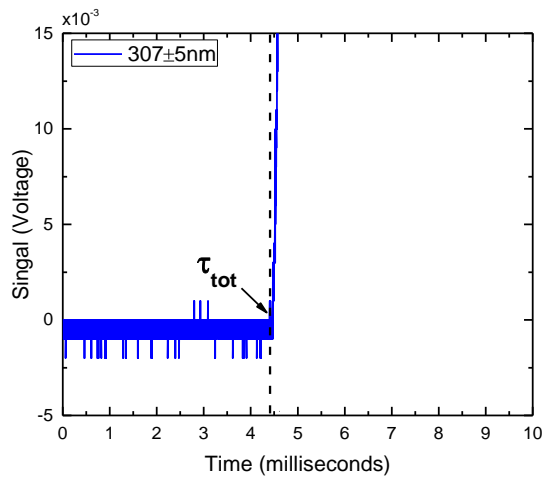
### 3.2.3 Ignition delay from PMT data analysis

The time values at the end of the physical and chemical ignition delay periods were derived from the PMT voltage signals captured by the CDS. Figure 3-3 (a) shows an example of the raw PMT voltage signals captured during POSF 4658 ignition at intake conditions of 600°C, 20 bar without EGR. Millivolt scale signals from the PMTs were used to calculate time values for the ignition delay periods based on the excited state radical species detected, since this could provide better distinction between the low and high temperature ignition regimes. When high temperature ignition occurs, the spontaneous heat release is caused by the active radicals formed in the following reaction,  $\text{H}_2\text{O}_2 \rightarrow 2\text{OH}^*$ . Therefore, the total ignition delay,  $\tau_{\text{tot}}$ , (HTHR, High Temperature Heat Release) was defined as the first significant measurement of  $\text{OH}^*$  chemiluminescence

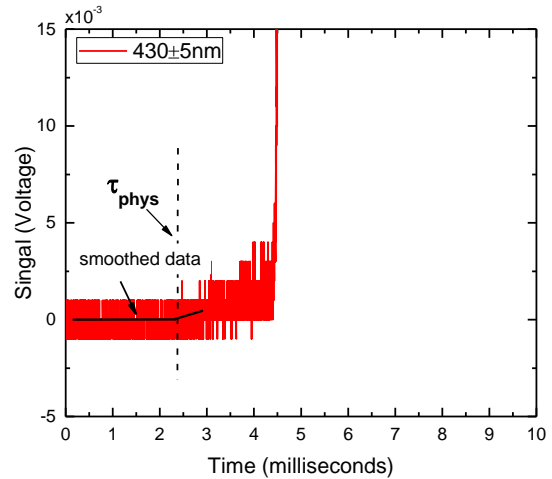
represented by the  $307\pm 5\text{nm}$  PMT signal. The end of physical ignition delay ( $\tau_{\text{physy}}$ ) period occurs at the onset of low temperature combustion chemistry, where formaldehyde is observed. Therefore, the  $\tau_{\text{physy}}$  defines a time period between start of injection and the first observation of excited  $\text{CH}_2\text{O}^*$  chemiluminescence measured by the first significant voltage increase seen in the  $430\pm 5\text{nm}$  PMT signal. These signal analyses were completed by taking the derivative of the smoothed voltage signals (2000 Hz low-pass filter) and analyzing the result to find when the signal began to show a positive rate of increase, as shown in Figure 3-3 (b) and (c). The chemical ignition delay ( $\tau_{\text{chem}}$ ) was calculated by a time difference between  $\tau_{\text{tot}}$  and  $\tau_{\text{physy}}$ .



(a)



(b)



(c)

Figure 3-3. Three PMT signals from one of the fifteen ignitions of POSF 4658 at 600°C and 20 bar; (a) Actual observed raw PMT signals passed for three different wavelength filters observed in LabVIEW house-code; (b) Reduced scale view of raw 307±5nm PMT signal used to derive  $\tau_{tot}$  and (c) Reduced scale view of raw 430±5nm PMT signal used to derive  $\tau_{phys}$

### 3.2.4 Thermodynamic calculations from pressure data

As with the CFR motored engine, apparent heat release rate (AHRR) can be calculated by measured pressure trace data collected by the CID's internal computer. However, the saved pressure trace data often revealed pressure fluctuations near peak combustion pressures, due to the large pressure-rise rate. Thus, this signal noise needed to be eliminated by using a 2,500Hz low-pass filter, thereby calculating an accurate AHRR. The term "apparent" is meant to indicate that the values solely rely on the pressure trace data obtained here and other impacts affecting HRR are ignored. Since the chamber volume is constant, the first term of right-hand-side can be negligible in Equation 3-5, leading to Equation 3-6.

$$\frac{dQ_{net}}{dt} = \frac{1}{\gamma - 1} V \frac{dP}{dt} \quad (3-6)$$

where  $\gamma = \frac{c_p}{c_v}$ , whose value is normally between 1.3 and 1.4 in diesel combustion systems. The ratio of specific heats, gamma ( $\gamma$ ), is often regarded as a constant value, although this fact is rarely true in practical environments. Therefore, a correction of gamma to temperature was adopted to adjust for changes in heat capacity ratio as the phase of air mixture is changed from unburned to burned, as shown in Equation 3-7.

$$\gamma = \frac{1}{1 - \frac{1}{a_1 + a_2 T + a_3 T^2 + a_4 T^3 + a_5 T^4}} \quad (3-7)$$

where,

$$a_1 = 3.6359$$

$$a_2 = -1.33736 \times 10^{-3}$$

$$a_3 = 3.29421 \times 10^4$$

$$a_4 = -1.91142 \times 10^{-9}$$

$$a_5 = 0.275462 \times 10^{-12}$$

The bulk temperature can be calculated via ideal gas law, as shown in Equation 3-7.

$$\frac{PV}{m_{air+fuel}R_{specific}} = T_{bulk} \quad (3-7)$$

where constant volume ( $V$ ) is 0.473 liter,  $R_{specific}$  of air is assumed to be constant value (0.287 kJ/kg-K) and instantaneous chamber pressure  $P$  is measured.

## Chapter 4

### Impact of Branched Structure on Cycloalkane Ignition in a Motored Engine: Detailed Product and Conformational Analyses

#### 4.1 Introduction

In response to the increasing demand for diesel fuel in the United States, recent studies have considered cycloalkanes due to their abundance in many of the “unconventional oil” sources such as oil sands, oil shale and coal derived liquids. Furthermore, cycloalkanes can constitute 40 wt% of commercial diesel and 20 wt% of commercial jet fuels [59,108]. Despite the significance of cycloalkanes, there remains a lack of fundamental understanding of the combustion chemistry of cycloalkanes. Recently, a few studies have focused on the low temperature chemistry of cycloalkanes, which is of great importance for the application of cycloalkanes in next generation engine designs that employ low temperature combustion strategies.

The characteristics of oxidation and autoignition behavior of cycloalkanes are different from those of the acyclic alkanes. For example, observations of ignition delay in

rapid compression machines (RCM) indicate that the oxidation reactivity of cyclohexane in the low temperature regime is significantly less than that of *n*-hexane [27], consistent with the lower cetane number of cyclohexane than *n*-hexane. For low temperature oxidation of cyclohexane, the degenerate chain branching is a main factor that determines the oxidation reactivity and represents the intermolecular (1,5) H-shift of fuel peroxy radical ( $\text{ROO}\cdot \rightarrow \cdot\text{QOOH}$ ). Although this isomerization reaction is similar mechanistically to aliphatic alkanes such as *n*-heptane [31] or *iso*-octane [32], gas-phase cycloalkane oxidation possesses its own kinetic features that cannot be extrapolated from the rate constants of analogous acyclic alkanes with corrections for the ring. In two recent kinetic modeling studies of methylcycloalkane [61] and cyclohexane [70], Pitz *et al.* and Buda *et al.* reached the same conclusion that the cyclic ring plays an important role in determining the activation energy barriers for these isomerization reactions. In addition, Yang *et al.* found that (1,4) H-shift can concurrently occur to form conjugate olefins, i.e., olefins with the same molecular structure as the original fuel compound except for the presence of a double carbon bond, with elimination of  $\text{HO}_2$  during the (1,5) H-shift reaction indicated above [109]. This competition in those two cases during low temperature oxidation of cycloalkanes results in the tradeoff relationship between low temperature reactivity and formation of conjugate olefins [109].

The previous experimental studies of oxidation of alicyclic compounds have focused mostly on cyclohexane (CH) [69,70,110,82] and methylcyclohexane (MCH) [73]. Detailed intermediate and final product analyses for the oxidation of representative cyclic-based fuels including CH, MCH, methylcyclopentane (MCP), tetralin and decalin have been studied in low and intermediate temperature regimes in a motored engine



[81,111]. Yang *et al.* reported that the methyl substituent enhances low temperature reactivity of CH, as confirmed by conformational analysis and quantum calculations using an *ab initio* method [109,112]. Few studies focused on the effect of the presence or the length of alkyl chains on branched cycloalkanes, nor on the effect of the location of the methyl substituents. Ethylcyclohexane was examined in an experimental and modeling study of laminar flame speed in a counter flow configuration and compared with mono-alkylated cyclohexane and cyclohexane [113]. This study found that a mono-alkylated group leads reaction intermediates that lower rates of flame propagation for butyl, propyl, ethyl and methylcyclohexane relative to cyclohexane. The ignition delay for methyl and ethylcyclohexane was measured in a shock tube at conditions of relevance to practical combustion devices in order to investigate the influence of the length of the alkyl side chain on the ignition of alkylcyclohexanes [63]. The very recent study of Husson *et al.* investigated detailed intermediate products during low and intermediate oxidation of ethylcyclohexane in a jet-stirred reactor [71]. In another study, pyrolysis of ethylcyclohexane was performed near supercritical conditions in a batch reactor, providing product analysis and proposed reaction pathways [114].

Recognizing a considerable effect of the length of alkyl substituent in alicyclic compounds on low temperature reactivity, this work considers the effect of a methyl substituent and its location within the chemical structure on ignition behavior. The test fuels are ethylcyclohexane, 1,3-dimethylcyclohexane and 1,2-dimethylcyclohexane. To our knowledge, no previous oxidation studies comparing ethylcyclohexane, 1,3- and 1,2-dimethylcyclohexane have been reported. However, Do *et al.* investigated the ring opening reactions of 1,2- and 1,3-dimethylcyclohexane over Ir catalysts [115]. One

noticeable conclusion from this study is that the presence of a methyl substituent in the reactant molecule has a positive impact on the ring opening of substituted C-C bonds. The C-C bonds between methyl substituents are opened preferentially compared with other C-C bonds, which explains why the position of the methyl substituents on a cycloalkane influences the ignition behavior of branched cycloalkanes.

## **4.2 Research Objectives**


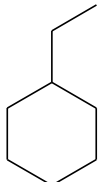
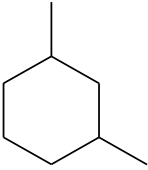
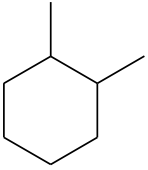
The main goal of the current study is to examine the low temperature reactivity of substituted cycloalkanes through determination of the critical compression ratios (CCR) of three test fuels. Furthermore, this study includes observations of major intermediate species from oxidation of each of the test fuels and proposed reaction pathways during low and intermediate temperature regimes. Lastly, conformation analysis of these three different isomers demonstrates how the alkyl substituents can affect low temperature oxidation reactivity. These results provide new information on the impact of alkyl substituents on ignition behavior during low temperature combustion in a motored engine environment.

## **4.3 Test Fuels**

In the present study, ethylcyclohexane (ECH) and two isomers, 1,3-dimethylcyclohexane (13DMCH) and 1,2-dimethylcyclohexane (12DMCH), were used so as to observe the impact of alkyl substituted cycloalkanes on ignition behavior. The primary reference fuel, *n*-heptane, was also included in order to compare its reactivity

with that of the test fuels. The molecular structures and properties for each fuel are listed in Table 2. A simulated distillation analyzer was used for analyzing mixture compositions for 13DMCH, and 12DMCH and composition was verified by GC-MS. The substituted cycloalkane compounds were obtained from Sigma-Aldrich.

Table 2 Molecular structure of branched cycloalkanes and their properties tested

	<i>n</i> -heptane	ECH	13DMCH <i>cis</i> and <i>trans</i> mixture	12DMCH <i>cis</i> and <i>trans</i> mixture
Formula	C <sub>7</sub> H <sub>16</sub>	C <sub>6</sub> H <sub>11</sub> C <sub>2</sub> H <sub>5</sub>	C <sub>6</sub> H <sub>10</sub> (CH <sub>3</sub> ) <sub>2</sub>	C <sub>6</sub> H <sub>10</sub> (CH <sub>3</sub> ) <sub>2</sub>
Molecule structure				
Boiling point (°C)	98.42	130-132	<i>cis</i> - 121 <i>trans</i> - 126	<i>cis</i> - 124 <i>trans</i> - 132
Density (g/ml) at 25°C	0.684	0.788	0.767	0.778
Molecular weight (kg/kmol)	100.21		112.21	
Composition (wt%)		> 99	<i>cis</i> - > 73.3 <i>trans</i> - > 25.7	<i>cis</i> - >77 <i>trans</i> - >22
Lower Heating Value (kJ/kg)	44925	43485	43357	43429
Cetane number	53-56 [116]	35.8 [116]	30 [115]	22 [115]

## 4.4 Test Conditions

Throughout all the experiments reported in this chapter, the CFR engine was kept constant speed of 600 rpm, and a constant equivalence ratio of 0.5. The intake temperature was fixed at 155°C and the engine is naturally aspirated. The CR was initially set to 3.8 and was gradually increased in a stepwise manner while monitoring the CO, and CO<sub>2</sub> emissions and apparent heat release rate. The final CR was the point where a pronounced high temperature heat release (HTHR) rate, a sharp increase in CO<sub>2</sub> emissions and a decrease in CO emissions (indicating autoignition) were observed.

## 4.5 Results and Discussion

### 4.5.1 Low temperature heat release analysis

Prior to actual ignition, the four test fuels displayed noticeable low temperature heat release (LTHR) at various CRs. The net heat release and in-cylinder temperature at each data point were obtained from the cylinder pressure data. As the CR increases, the magnitude of LTHR gets higher and shifts to an earlier crank angle before top dead center (TDC) for all the test fuels. Figure 4-1(a) shows the heat release rate profiles for the four test fuels at CRs of 4.88 for *n*-heptane and 6 for the cycloalkanes. *n*-Heptane, whose cetane number (52) is roughly in the range of a typical diesel fuel, displayed LTHR at lower CR, compared to the other test fuels, with a noticeable two-stage ignition behavior. The fuel, whose actual ignition (HTHR) is occurred at lower CR where less severe engine cylinder temperature and pressure exists, is generally considered to be a

more reactive fuel. Among the three cycloalkane isomers, ECH shows the strongest LTHR, while 12DMCH shows negligible LTHR at the same CR of 6, indicating that ECH is the most reactive fuel of the three cycloalkanes tested in the low temperature regime. For all the fuels examined here, as CR is further increased, two stage ignition behavior is observed up to their critical compression ratio (CCR) where autoignition is achieved. As shown in Figure 4-1 (b), the CCR is indicated by the compression ratio where the cylinder temperature increases significantly. According to the calculated bulk cylinder temperature, prior to autoignition the cylinder temperatures are roughly between 700K and 900K, indicating that the reactions reside in the low and intermediate temperature regime. As CR is continuously increased after observing a low temperature heat release, the maximum bulk temperatures tend to plateau when HTHR is detected, indicating strong evidence of negative temperature coefficient (NTC) behavior. This observation is in good agreement with previous studies of low temperature oxidation of various cyclic compounds [38,61,75,81,82].

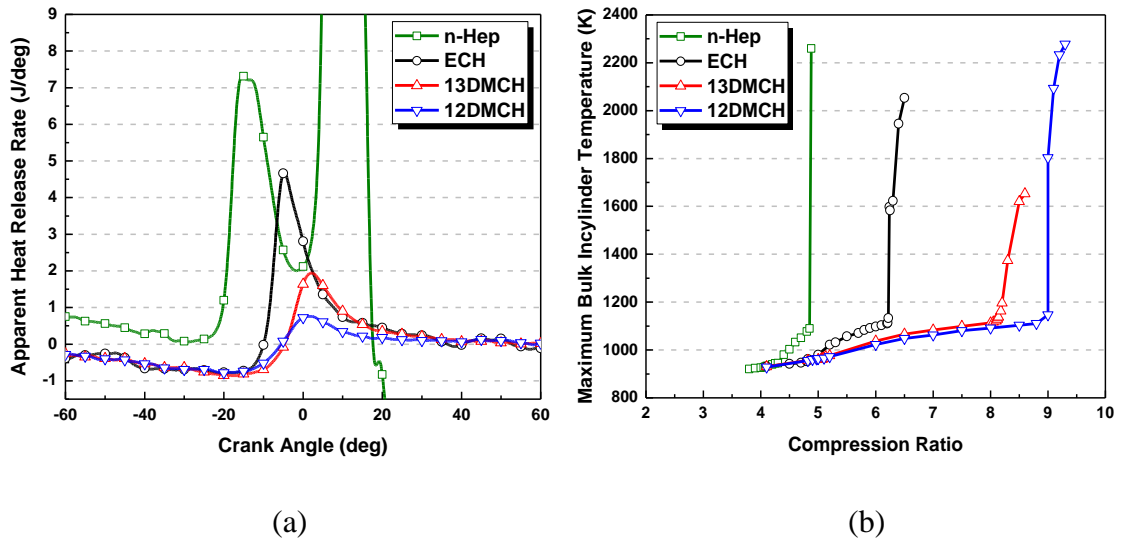


Figure 4-1 Apparent heat release and maximum bulk cylinder temperature for three different substituted cycloalkanes and *n*-heptane: (a) apparent heat release profiles of three different cycloalkanes at a CR of 6 and *n*-heptane at a CR of 4.88 as a function of crank angle. Crank angle 0 deg indicates piston top dead center; (b) Calculated maximum bulk gas in-cylinder temperature profile at various CRs for oxidation of four different pure fuels.

#### 4.5.2 CO and CO<sub>2</sub> emissions from low temperature oxidation

Trends of CO and CO<sub>2</sub> emissions displayed in Figure 4-2 correspond to the global reactivity indicated by the zero-dimensional heat release model. The onset of LTHR is determined by monitoring CO emissions which increase significantly at a particular CR. It is well established that CO is an effective indicator of chemical reactivity in the low temperature regime, since CO is noticeably formed during LTHR and can be accurately measured [77]. However, once the onset of HTHR is detected, the concentration of CO decreases dramatically with further increase of the CR. Formation of CO is a result of decomposition of aldehydes in the low temperature regime. As a result of the sudden change of in-cylinder temperature and pressure at HTHR, CO is rapidly consumed by

hydroxyl radicals. In this way, Figure 4-2 indicates the oxidation reactivity for each fuel. The most reactive fuel, *n*-heptane, has the narrowest NTC region over the range of compression ratios, indicating that as fuel reactivity increases, the range of CRs where NTC behavior takes place is steadily reduced. Conversely, 12DMCH displays the weakest reactivity during low temperature oxidation and shows evident NTC behavior over a wide range of CRs. This observation is also in good agreement with previous cycloalkanes studies, which were performed at similar conditions [81,82]. Benson indicated that this phenomenon is likely to be related to the “ceiling temperature” where the equilibrium constant of the reaction  $R\cdot + O_2 \rightleftharpoons RO_2\cdot$  reaches unity for a given  $O_2$  concentration [117]. Above this ceiling temperature, the peroxy radical is gradually replaced by alkyl radicals with decreasing low temperature reactivity. This is the region where NTC behavior is observed. The more reactive fuels produce a larger magnitude of CO emissions at a given CR prior to the CCR as a larger fraction of the more reactive fuel is being partially oxidized, resulting in higher CO concentrations.

Little  $CO_2$  is formed in the transition from the low temperature region to the high temperature regions. Figure 4-2 indicates that CO oxidizes to  $CO_2$  dramatically during the onset of HTHR. After HTHR, the similar  $CO_2$  formation for each fuel is not connected to their low temperature oxidation reactivity, but is simply an indication of the completeness of combustion at the point when the CCR is detected. Based on the results from the oxidation of the pure fuels shown in Figure 4-2, the CCR for the four different fuels occurs at 4.88 for *n*-heptane, 6.24 for ECH, 8.1 for 13DMCH, and 9 for 12DMCH.

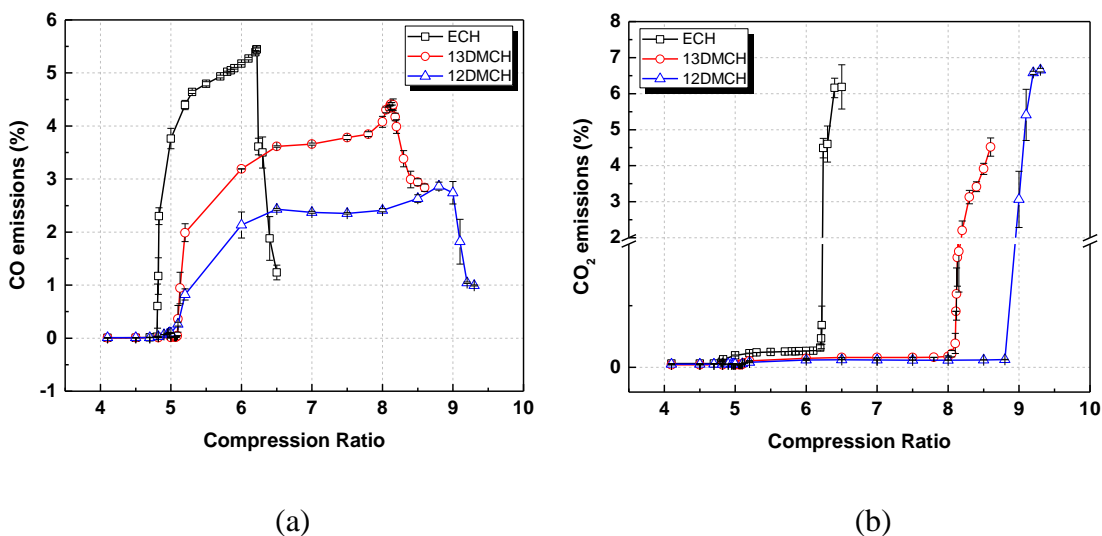


Figure 4-2 Gaseous emissions as functions of compression ratio (CR) from the oxidation of four different neat fuels: (a) mole percent of CO; and (b) mole percent of CO<sub>2</sub>. Error bars indicate the 95% confidence interval

### 4.5.3 Intermediate product analysis

Condensed intermediate species formed during low temperature oxidation of the three cycloalkanes (ECH, 13DMCH, 12DMCH) were analyzed by GC-MS and GC-FID. As can be seen in Table 3, intermediate species are classified into six categories on the basis of different functional groups. The first group contains various C<sub>1</sub>-C<sub>5</sub> olefins. Propene and 2-butene are commonly formed during oxidation of cycloalkanes, while, the evolution of 1-butene, 1,3-butadiene, and 1-pentadiene are influenced by different substituted alkyl branching on three different cyclohexanes. The second group consists of small oxygenated species including aldehydes, ketones, and acids. Acetaldehyde, acrolein, methacrolein, methyl-vinyl-ketone, and acetic acid are major intermediate products formed through C-C β-scission of hydroperoxy alkyl radicals from a radical transfer and subsequent attack from active radicals. These species are commonly formed



from oxidation of the three test fuels, except methacrolein, which is formed only during oxidation of 13DMCH and 12DMCH. The third group includes benzenes and cyclohexenes. Benzene and cyclohexene are likely formed during oxidation of most cycloalkanes, based on their relatively stable molecular structure. In particular, benzene can likely be formed through either successive hydrogen abstraction on a cycloalkene or decomposition of methyl substituents from ortho- and meta-xylene. Toluene and 3-, and 4-methylcyclohexene are the result of decomposition of meta-xylene and 1,3-dimethylcyclohexene respectively. All products in these three groups increase nearly linearly with compression ratio, suggesting that their formation is less affected by NTC behavior. Similar trends for the third group (benzene and cyclohexenes) were also observed in previous experimental studies of the oxidation of cyclic compounds in a motored engine [81,82]. The conjugate olefins, i.e., olefins with the same molecular structure as the original fuel compound except for the presence of a double carbon bond, which in the present context include a double bond on a neat cycloalkane fuel, are collected in the fourth group. The fifth group contains various C<sub>6</sub>-C<sub>8</sub> branched cyclohexanes, mostly formed through establishing a double bond at branched methyl and ethyl substitutions. The last group contains C<sub>6</sub>-C<sub>8</sub> oxygenated species formed through various pathways. The large oxygenated compounds reported herein are classified as key components as a result of their relatively high yields compared to other large oxygenated species, which were difficult to identify due to their small yields and difficulties in peak separation. All reported products were identified by GC techniques and confirmed using the NIST library. The fractions of identified products are quantified in relative terms by

normalizing the product yield (FID signal) with the unreacted reactants and are plotted against the CR.

Table 3 Classified groups of intermediate products from low temperature oxidation of ECH, 13DMCH and 12DMCH

Reactants Groups	ECH	13DMCH	12DMCH
C <sub>1</sub> -C <sub>5</sub> olefins	Propene, 2-butene		
	1,3-butadiene	1,3-pentadiene	1-butene
C <sub>1</sub> -C <sub>5</sub> oxygenated species	Acetaldehyde, Acetic acid, Acrolein, Methyl-vinyl-ketone		
		Methacrolein	
Benzene and Cyclohexenes	Benzene, Cyclohexene		
	Ethylbenzene	Toluene, meta-xylene 3-methylcyclohexene 4-methylcyclohexene	ortho-xylene 1-methylcyclohexene
Conjugate olefins	1-ethylcyclohexene 3-ethylcyclohexene 4-ethylcyclohexene Ethenyl-cyclohexane Ethylene-cyclohexane	1,3-dimethylcyclohexene 1,5-dimethylcyclohexene 3,5-dimethylcyclohexene	1,2-dimethylcyclohexene 1,6-dimethylcyclohexene 1-methyl-2-methylene-cyclohexane
Cyclohexanes	Methylene-cyclohexane		
C <sub>6</sub> -C <sub>8</sub> oxygenated species	Cyclohexanone 2-cyclohexen-1-one Octahydro-benzofuran	3-methyl-2-cyclohexene-1-one 1,5-dimethyl-7-oxabicyclo[4,1,0]heptane 6-methylhept-6-en-2-one	2-methylcyclohexanone Octahydro-2-benzofuran 6-octen-2-one

#### 4.5.3.1 Product analysis of ECH oxidation

Figure 4-3 shows the trends of mole fraction for each species in the unreacted fuel as a function of a range of CR for low temperature oxidation of ECH. Most intermediate products tend to increase from a CR of 4.82, which represents the onset of LTHR for ECH, to a CR of 6.22 right before autoignition occurs. The reactant, ECH, meanwhile, undergoes H-shift isomerization, open rings and fragmentation in low and intermediate temperature regimes. Once CR reaches to 6.24, most of the ECH and intermediate species

are converted into CO<sub>2</sub>. This observation is also in agreement with the trend of CO mole fraction and temperature profiles shown in Figures 4-1 and 4-2. As can be seen in Figure 4-3 (f), even after the complete combustion at CR of 6.5, a considerable amount of cyclohexene still remains, while most of the cyclic compounds shown in Figures 4-3 (c) and (d) dramatically decrease due to oxidation. This may be due to the dehydrogenation of cyclic compounds during the ignition process and also the structural stability of cyclohexene compared to other intermediate products. The cascade dehydrogenation has been also considered as key reaction channels during low temperature oxidation of cyclic compounds, such as decalin and tetralin [82]. The major species including cyclohexene, oxygenated species and most of the conjugate olefins display apparently constant rates of production in the NTC regime. Also, the formation of large oxygenated species and conjugate olefins occurs at lower CR than that of small olefins and small oxygenated species. These observations can be explained by the sequence of the ignition chemistry during low temperature oxidation of hydrocarbons, by which larger molecules can be formed from the isomerization of ECH and then broken down by  $\beta$ -scission on the C-C cyclic ring to convert into small molecules and CO in low temperature regime. Furthermore, this ring opening reaction leads to potential LTHR.

The major products from low temperature oxidation of ECH consist of acetaldehyde, cyclohexene, and conjugate olefins in the NTC regime, based on their concentration in the unreacted fuel. During the low temperature regime, a considerable amount of conjugate olefin is formed through an (1,4) H-shift isomerization with the elimination of HO<sub>2</sub> directly from the peroxy radical ( $R\bullet + O_2 \leftrightarrow$  conjugate olefins + HO<sub>2</sub> $\bullet$ ). The positions at six available carbons in ECH, where active OH radicals can

selectively or unselectively attack, determine the formation of five different conjugate olefins. Based on the relative concentration of these isomers, it is noted that carbons on the cyclic ring are easily attacked by  $O_2$  or active OH more than carbons in the ethyl branch. This major formation of conjugate olefins has also been observed in related studies of low temperature oxidation of cycloalkanes [71,81,82]

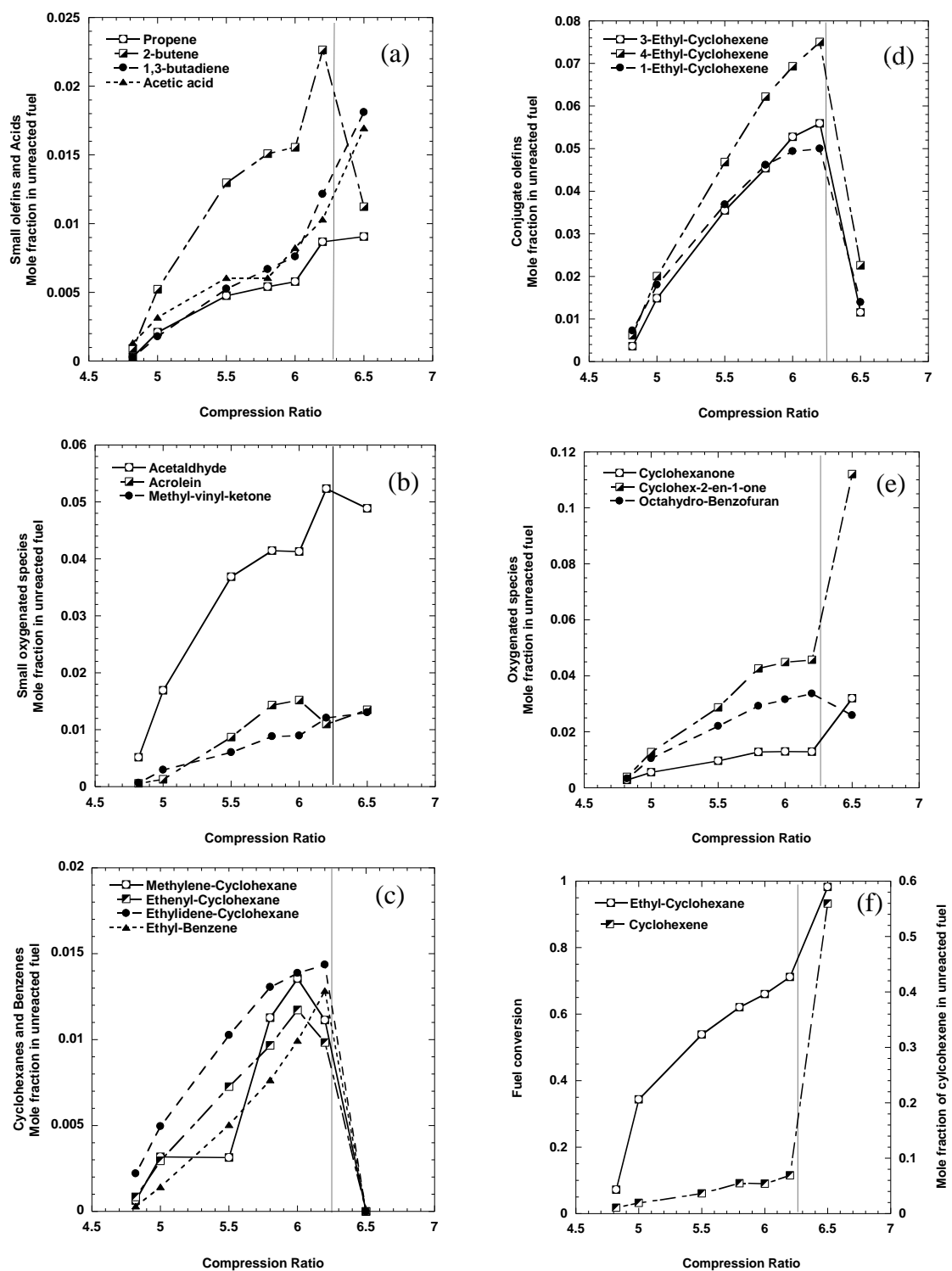


Figure 4-3 Condensed gaseous species from ethylcyclohexane oxidation: (a) small olefins; (b) small oxygenates; (c) cycloalkanes and ethylbenzene; (d) conjugate olefins; (e) oxygenated species; and (f) fuel and cyclohexene. Line represents the onset of autoignition.

Figures 4-4 and 4-5 present the possible reaction pathways of C<sub>6</sub> and C<sub>8</sub> oxygenated species, which also have been found in [71] to be major products during low temperature oxidation of ECH. As seen in Figures 4-4 (a) and (b), the ethylcyclohexylhydroperoxide radicals formed by the (1,6) H-shift isomerization on the  $\alpha$ -carbon position undergo either  $\beta$ -scission to form cyclohexene releasing an HO<sub>2</sub> radical or subsequent dehydroxylation to form the cyclic ether group, resulting in the formation of octahydrobenzofuran. Based on Figures 4-3 (e) and (f), cyclohexene is more abundant than octahydrobenzofuran over the range of CR in the NTC regime. This result indicates that C-C bond  $\beta$ -scission on the ethyl-substituent in the ethyl-cyclohexyl-hydroperoxide radical is a more favored reaction than forming a cyclic ether group after (1,6) H-shift isomerization. However, as seen in Figure 4-4 (c), cyclohexanone can be formed from different positions internal hydrogen abstraction with oxygen addition. After the ROO radical group experiences favored (1,5) H-shift isomerization in ethyl-substituent, ethyl-cyclohexyl-hydroperoxide radical undergoes  $\beta$ -scission on the ethyl-substituent on CH, releasing CH<sub>3</sub> and OH radicals. Figure 4-5 presents a possible reaction pathway of 2-cyclohexen-1-one, which has the same molecule structure of cyclohexanone, except for a double bond in the cyclic ring. Initially, hydrogen abstraction by active radicals occurs at the  $\beta$ -position of a C-H bond and thereafter to O<sub>2</sub> addition, leading to peroxy radicals ROO•. Internal hydrogen isomerization consequently happens by transfer of a tertiary hydrogen atom at the  $\mu$ -position of a C-H bond, which requires a lower activation energy for the same ring strain energy in the bicyclic transition state.

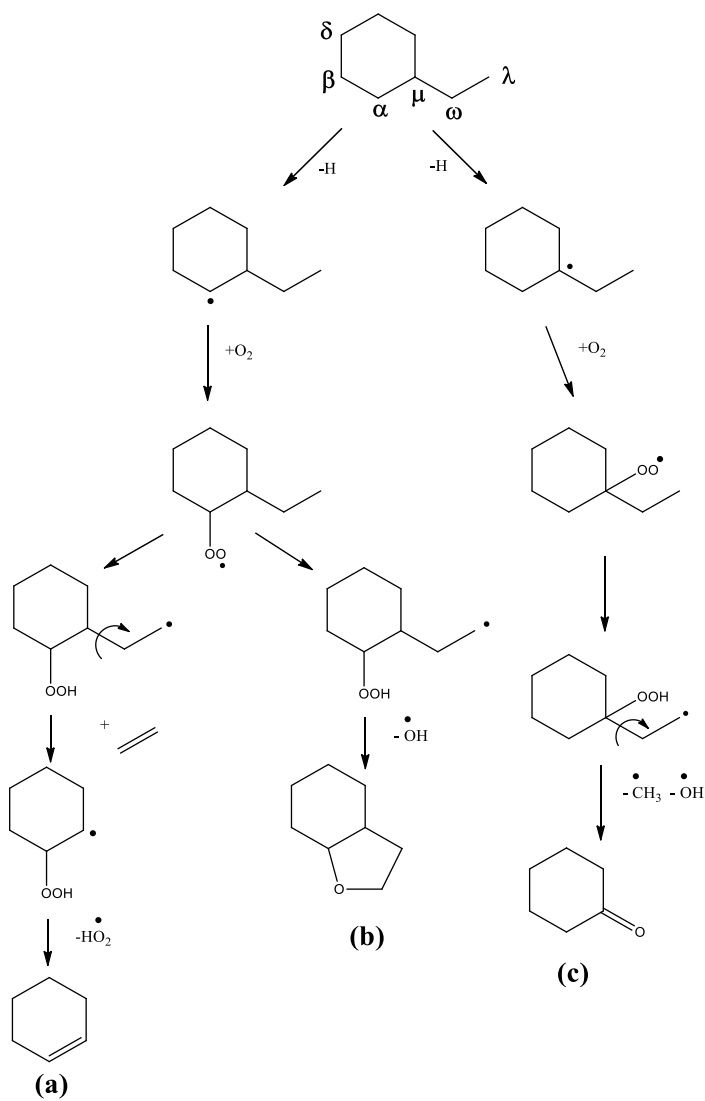


Figure 4-4 Proposed reaction pathways to (A) cyclohexene and oxygenated species: (B) octahydrobenzofuran and (C) cyclohexanone during low temperature oxidation of ethylcyclohexane

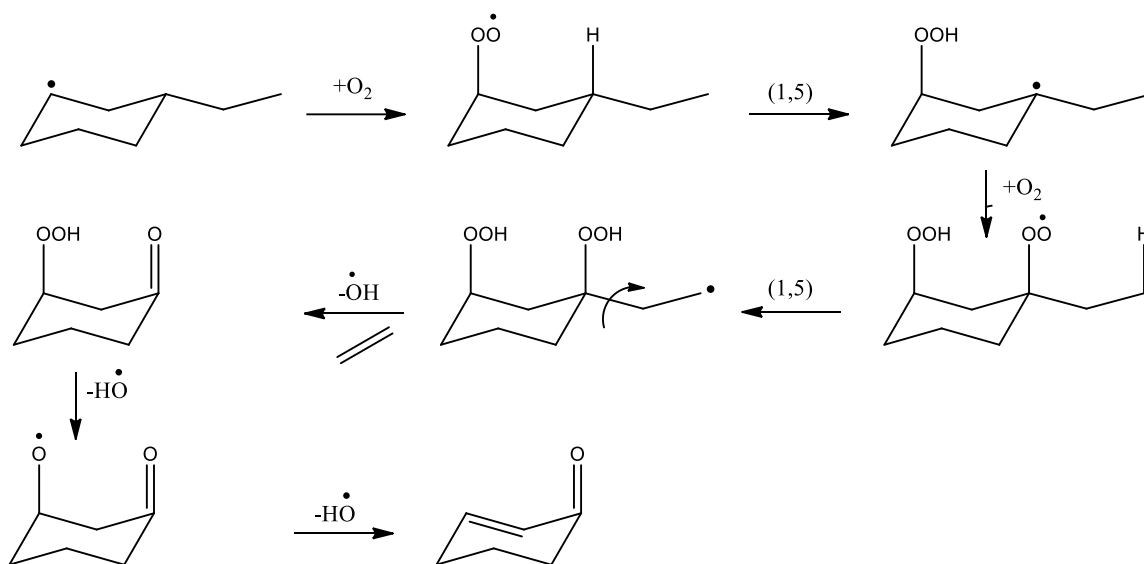


Figure 4-5 A proposed reaction pathway to 2-cyclohexen-1-one during low temperature oxidation of ethylcyclohexane

#### 4.5.3.2 Product analysis for 1,3-dimethylcyclohexane oxidation

The condensed intermediate and complete ignition product species captured from the low temperature oxidation of 13DMCH, one of the isomers of  $C_8H_{16}$ , were analyzed by GC. The products are classified into five groups, including  $C_1$ - $C_5$  olefins and oxygenated products, various cycloalkanes and benzenes, conjugate olefins, and large oxygenated species. The species in the small olefins and oxygenated products are very similar to the species observed for low temperature oxidation of ECH shown in Table. 3. The oxygenated species and conjugate olefins from 13DMCH oxidation, however, are distinguished from those formed from ECH oxidation, since different positions for the two methyl substituents on cyclohexane can affect the formation of conjugate olefins and  $C_6$ - $C_8$  oxygenated species. Figure 4-6 shows the trends of mole fraction for each species as a function of CR. As expected, the trends for most species show evident NTC behavior. A very small amount of conjugate olefins and  $C_6$ - $C_8$  oxygenated species first



are observed at CR of 5.13 at the initiation of the low temperature heat release, which is clearly indicated by CO emissions, shown in Figure 4-2 (a). However, small olefins and C<sub>1</sub>-C<sub>5</sub> oxygenated species are hardly detected at CR of 5.13, but are noticeably formed at CR of 5.5. The formation of small olefins and C<sub>1</sub>-C<sub>5</sub> oxygenated species are derived through subsequent radical attack, favored isomerization, and β-scission on fuel molecule backbones to open up the rings and cleave large molecules into small ones. In addition, the concentrations of most intermediate species gradually increase before the high temperature heat release is detected at the CCR of 8.1. Based on the mole fraction trends shown in Figure 4-6, the dominant reaction is  $R\cdot + O_2 \leftrightarrow \text{conjugate olefins} + HO_2\cdot$  in low temperature regime. Figure 4-6 (d) shows that 1,3-dimethylcyclohexene is the most favored product in the low temperature regime among all the conjugate olefins. However, at the end of the NTC regime, the concentrations of 1,5- and 1,3-dimethylcyclohexene become comparable. Even though conjugate olefins are well known as major intermediate products during low temperature oxidation of cycloalkanes [81,82], an important observation is that comparable amounts of large oxygenated products are also formed during low temperature oxidation of 13DMCH. Furthermore, a lower fuel conversion of 13DMCH into other intermediate species is observed in the low temperature regime, compared to that of ECH. This is due to the higher reactivity of ECH over 13DMCH in the low temperature regime. After high temperature heat release occurs, most of the fuel is converted into CO<sub>2</sub>, but considerable amounts of cyclohexene still remain from 13DMCH, compared to other intermediate species, which indicates that demethylations of conjugate olefins of 13DMCH likely occur via a different reaction path

during high temperature reaction. This result contributes to a sudden increase in the mole fraction of cyclohexene in the unreacted 13DMCH after complete ignition.

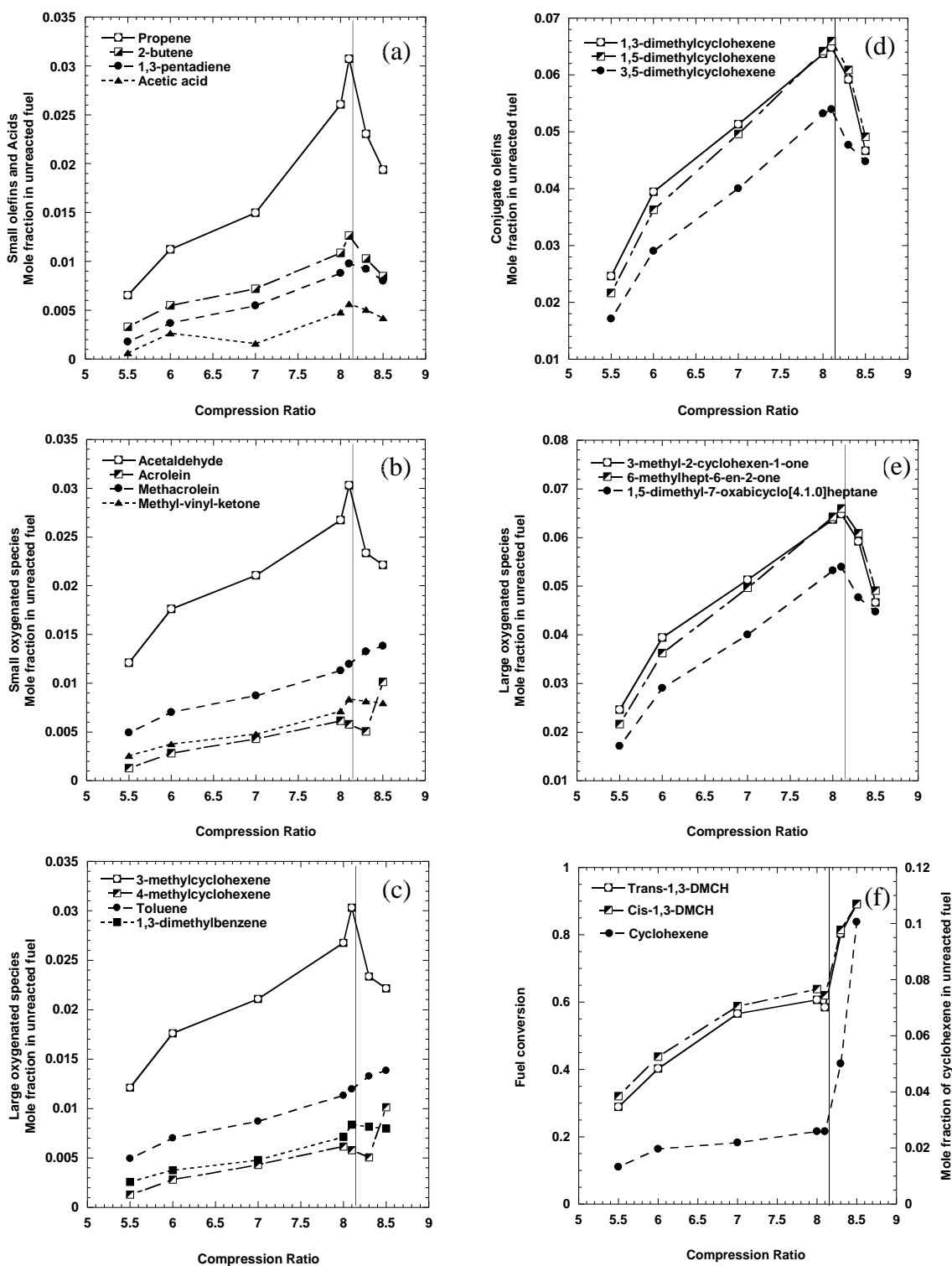


Figure 4-6 Condensed gaseous species from 1,3-dimethylcyclohexane oxidation: (a) Small olefins and acids; (b) Small oxygenated species; (c) Cyclohexenes, benzenes and norbornane; (d) Conjugate olefins; (e) Large oxygenated species; and (f) Fuels and cyclohexene. Line represents the onset of autoignition.

Likewise the reaction pathways for the formation of conjugate olefins from ECH oxidation, formation of conjugate olefins derived from low temperature oxidation of 13DMCH can be formed through the isomerization via (1,4) H-shift taken place at four different sites of  $\alpha$ -,  $\beta$ -,  $\delta$ - and  $\lambda$ -carbons. Each reaction path results in the formation of three different conjugate olefins. For example, the internal hydrogen abstraction from  $\lambda$ -carbon position and subsequent oxygen addition on  $\lambda$ -carbon lead to the alkyl hydroperoxide which undergoes (1,4) H-shift isomerization to form a 1,3-dimethylcyclohexyl-hydroperoxide radical. The decomposition of this hydroperoxide radical releases an OH radical by creating a double bond on a cyclic chain. This is likely to be the most favored pathway in the NTC regime, based on the relative yields of intermediate species observed in Figure 4-6 (d). Note that the considerable yields of 1,3- and 1,5-dimethylcyclohexene provide evidence of hydrogen abstraction by an active radical, which selectively attacks the weakest C-H bond, that of  $\lambda$ -carbon, where the tertiary hydrogen is placed in cyclohexane. Comparable amounts of C<sub>7</sub>-C<sub>8</sub> oxygenated compounds and conjugate olefins were produced over a wide range of CRs during the oxidation of 13DMCH. Figure 4-7 shows a possible reaction pathway for each oxygenated product including 1,5-dimethyl-7-oxabicyclo[4,1,0]heptane, 6-methyl-2-hepten-1-one, and 3-methyl-2-cyclohexenone. As can be seen in Figure 4-7, the place where initial hydrogen abstraction occurs is a very critical step for determining final oxygenated products. For example, initial hydrogen abstraction at the  $\alpha$ -carbon and subsequent oxygen addition lead to the formation of alkylperoxy radicals (ROO•). The tertiary hydrogen atom at the  $\lambda$ -position of the C-H bond is shifted via internal hydrogen shift isomerization and then forms •QOOH, resulting in the formation of cyclic ether and

releasing OH•. Similarly, a reaction pathway for the formation of 6-methyl-6-hepten-2-one starts with hydrogen abstraction on the  $\lambda$ -carbon. ROO radicals formed on the  $\lambda$ -carbon and their (1,5) H shift isomerization leads to the formation of a 1,3-dimethyl-cyclohexyl-hydroperoxide radical. The hydroperoxide radical undergoes  $\beta$ -scission of a C-C bond resulting in ring opening and a double bond is subsequently formed with an adjacent neighbor, leading to a radical formation at the  $\lambda$ -carbon. Finally, O-O dissociation on 6-methyl-hept-6-en-2-yl-hydroperoxide derived from the hydroperoxide occurs, resulting in the release of an OH radical and formation of a ketone. The observation of a relatively higher yield of 6-methyl-6-hepten-2-one derived from ring opening supports the assertion that the ruptured location preferentially occurs between substituted C-C bonds rather than outside the substituted C-C bonds, which was concluded by Do *et al.* [115]. Lastly, a hydrogen abstraction on the  $\omega$ -carbon (methyl substituent) on 13DMCH results in dissociation of one methyl-branch of 13DMCH releasing formaldehyde. The second oxygen addition into the methyl-cyclohexyl radical leads to the formation of ROO•. Then, a tertiary hydrogen atom placed in the other methyl-branch is shifted via internal (1,5) H-shift isomerization, forming •ROOH. Continuous oxygen addition leads to formation of •OOQOOH in the cyclic compound. Subsequent (1,4) H-shift isomerization builds a double bond on adjacent carbons and then a dissociation from branched group of O-OH contributes to the formation of a ketone group, finally resulting in the final product of 3-methyl-2-cyclohexen-1-one. Note that an equivalent yield of 6-methylhept-6-en-2-one was observed as compared to the formation of major conjugate olefins, 1,3-dimethylcyclohexene, and 1,5-dimethylcyclohexene during low temperature oxidation of 13DMCH. This suggests that

the oxidation initiates hydrogen abstraction on the more favored location ( $\lambda$ -carbon position) where the tertiary hydrogen is located. This likely contributes to the formation of major products during low temperature oxidation of 13DMCH.

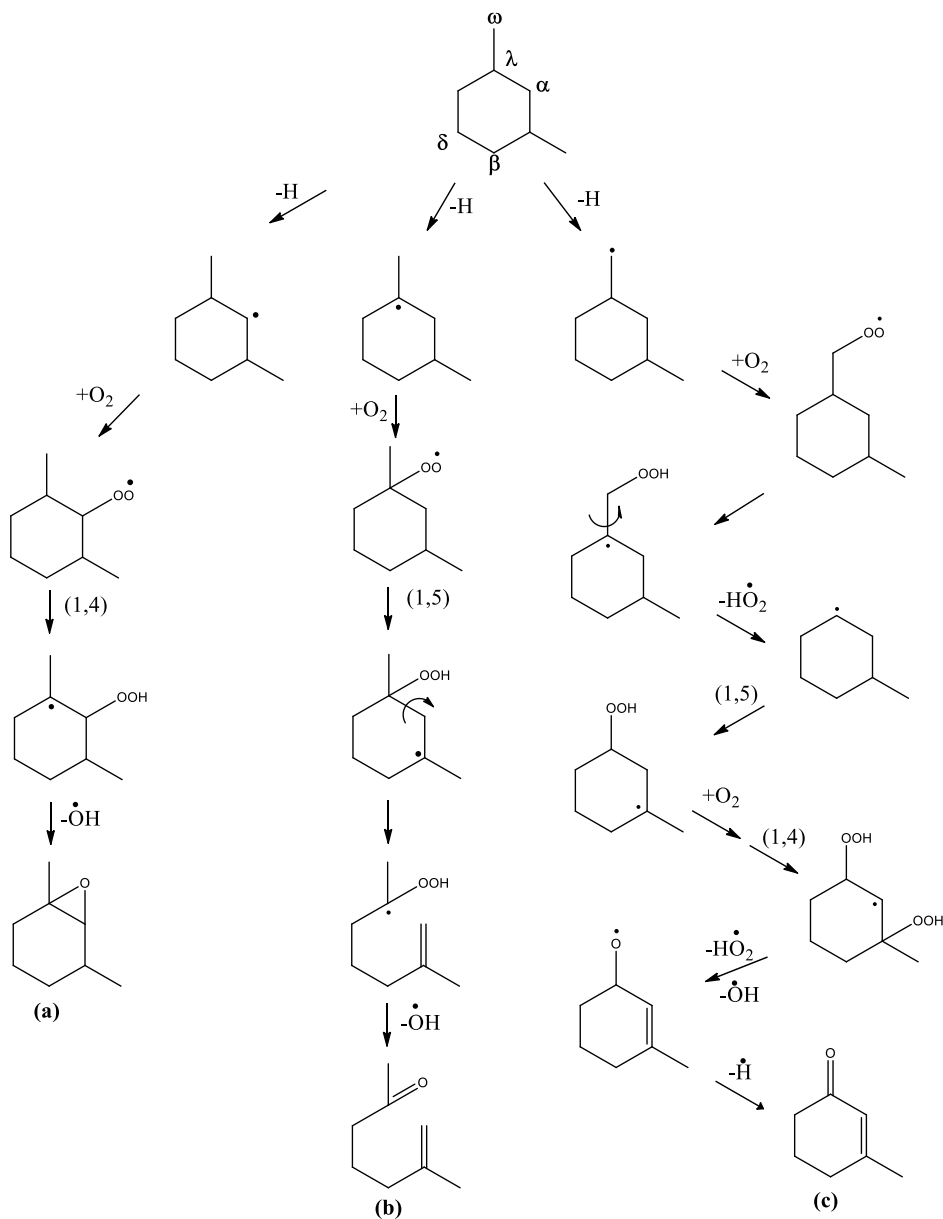


Figure 4-7 A proposed reaction pathway to observed oxygenated species from low temperature oxidation of 1,3-dimethylcyclohexane: (A) 1,5-dimethyl-7-oxabicyclo[4,1,0]heptane; (B) 6-methylhept-6-en-2-one; and (C) 3-methyl-2-cyclohexen-1-one;

#### 4.5.3.3 Product analysis for 1,2-dimethylcyclohexane oxidation

Under the same experimental conditions as discussed earlier for the other test fuels, the low temperature oxidation of 12DMCH was examined. The gaseous products in the exhaust of the engine were captured in a condenser system and were analyzed using GC. The gaseous products are classified into five groups and are shown in Table 3. The small olefins include propene, 2-butene and 1-butene in the first elution group. The formation of 1-butene is unique to 12DMCH and is not observed in the products from the previous two fuels. The C<sub>1</sub>-C<sub>4</sub> oxygenated species comprise the second group and include acetaldehydes, acetic acid, acrolein and methacrolein. The third group contains cycloalkenes and benzenes such as 1-methylcyclohexene, cyclohexene, benzene and 1,2-dimethylbenzene. The conjugate olefins and cycloalkanes, including 1-methyl-2-methylcyclohexane, 1,2-dimethylcyclohexene, and 1,6-dimethylcyclohexene are included in the fourth group. Lastly, three oxygenated species were reported and a number of oxygenated species were not identified with the GC analysis due to the difficulty in controlling retention time for each peak and lack of standards. As expected, most species reported here have very strong NTC behavior, with the onset of LTHR occurring at a CR of 5.20 and terminating at a CR of 9, where the extent of many products dramatically changed, due to the initiation of the HTHR. This phenomenon is consistent with the data for CO mole fraction and low temperature heat release in Figures 4-2 (a) and 4-1 (b), respectively, which show two stage ignition with apparent NTC behavior observed for a wide range of CRs. The C<sub>1</sub>-C<sub>4</sub> small olefins and oxygenated species were hardly detected over the range of CR for LTHR, as compared to conjugate olefins and C<sub>6</sub>-C<sub>8</sub> oxygenated species. As CR increases, however, small olefins and

oxygenated species are noticeably formed. This indicates that small olefins and oxygenated species can be derived from C<sub>6</sub>-C<sub>8</sub> oxygenated species from cleavage of the backbone of the fuel into two small molecules through C-C β-scission after opening the ring.

Another noteworthy observation is that a large amount of unidentified oxygenated species, which are not reported here, were detected as compared to the case of the oxidation of ECH and 13DMCH. The concentrations of oxygenated species are observed at comparable extents to the conjugate olefins. Oxygenated species are major products along with conjugate olefins in the low temperature oxidation of 12DMCH. As can be seen in Figure 4-8 (f), the low fuel conversion indicates a very slow ignition process during the NTC regime and corresponds to slow reactivity during low temperature oxidation, compared to the other test fuels (ECH and 13DMCH). The small conversion of the fuel results in little formation of intermediate species during the NTC regime. However, the fuel is mostly converted into CO<sub>2</sub> once second stage ignition occurs at the CCR.



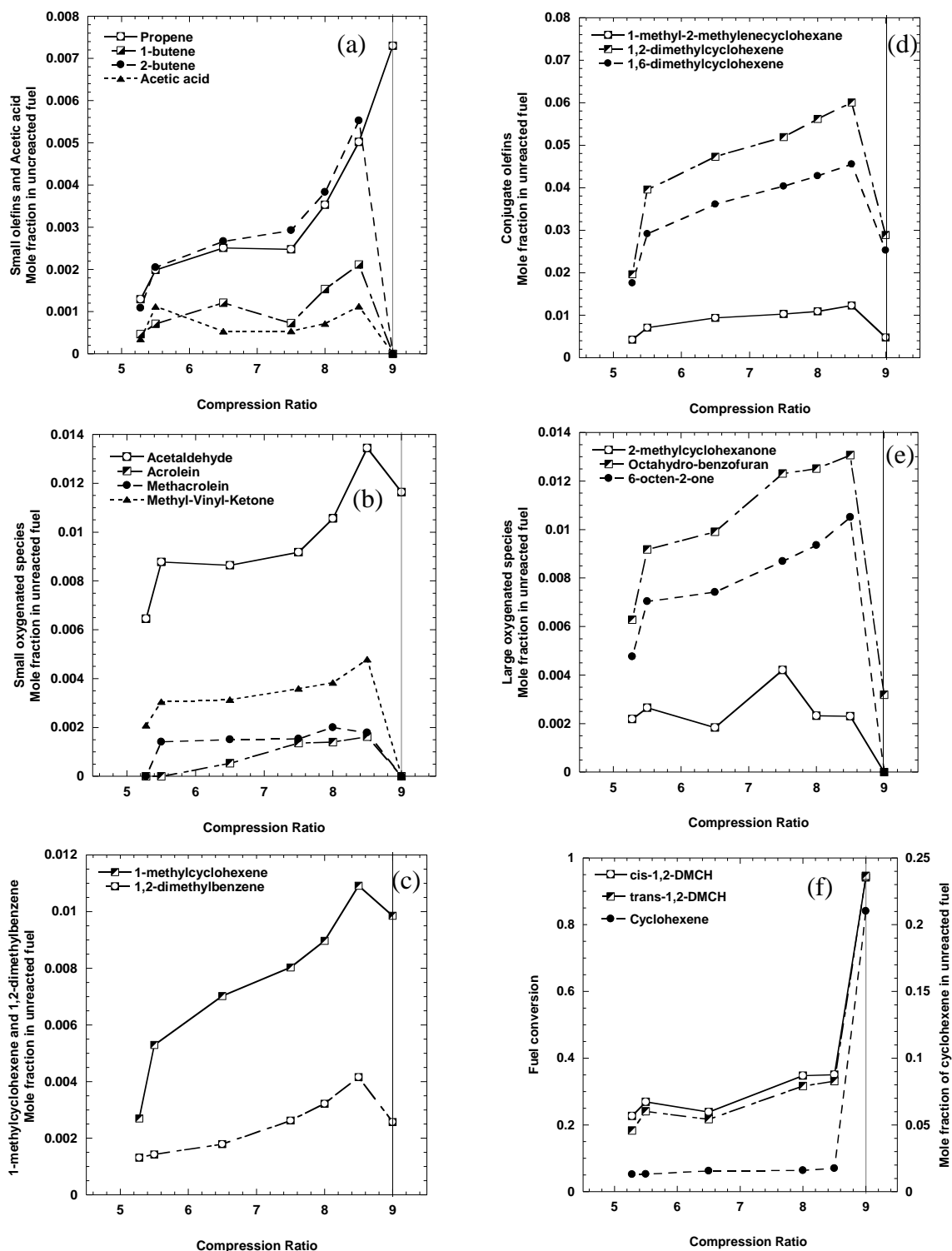


Figure 4-8 Condensed gaseous species from 1,2-dimethylcyclohexane: (a) Small olefins and Acetic acid; (b) Small oxygenated species; (c) 1-methylcyclohexene and 1,2-dimethylbenzene; (d) Conjugate olefins; (e) Large oxygenated species; and (f) Test fuel and cyclohexene. Line represents the onset of autoignition.

As observed with ECH and 13DMCH, the most likely reaction path for formation of conjugate olefins is through (1,4) H-shift isomerization during low temperature oxidation of 12DMCH. The isomerization can take place at  $\alpha$ -,  $\beta$ -, and  $\delta$ -carbons of the ROO radical. The isomerization via a (1,4) H-shift of the radicals leads to the formation of 1,2-dimethyl-cyclohexyl-hydroperoxide. The dimethyl-hydroperoxide radicals can convert into the conjugate olefins releasing an OH radical. The conjugate olefins derived from C-O bond scission are 1,2-dimethylcyclohexene, 1,6-dimethylcyclohexene, and 1-methyl-2-methylenecyclohexane, for which the relative yields of these three conjugate olefins, are approximately 1, 0.4, and 0.3, respectively, normalized by the most abundant species, which indicates that the favored place for the formation of C-C double bonds is between the two methyl substituents on the cycloalkane. The observations of these favored formations of conjugate olefins clearly indicates that the carbon and hydrogen bond in the  $\alpha$ -carbon position, where methyl substituents are attached to the cyclohexane, preferably undergoes a C-H bond cleavage from an active radical attack compared to other carbon locations.

Unlike the products from 1,2-dimethyl-cyclohexyl-hydroperoxide, the isomerization of 3,4-dimethyl-cyclohexyl-hydroperoxide at the  $\delta$ -carbon seems to lead to  $\beta$ -scission without any formation of conjugate olefins, based on the peaks detected by GC. This phenomenon is distinguished from the previous test fuels, which favor the formation of conjugate olefins in the NTC region. Even though the reaction pathways can be proposed so as to show the other expected conjugate olefins such as 3,4-dimethylcyclohexene and 4,5-dimethylcyclohexene, the strongly favored paths through  $\beta$ -scission might restrict the formation of such conjugate olefins. For example, 2,3-dimethyl-

cyclohexyl-hydroperoxide from an isomerization at the  $\beta$ -carbon could undergo  $\beta$ -scission of C-C bonds, providing open ring oxygenated compounds, instead of forming a conjugate olefin. Furthermore, as discussed earlier, the hydrogen abstraction on 1,2-dimethylcyclohexane most likely will occur at the  $\alpha$ -carbon position where an active radical has a preference for attacking the tertiary carbon-hydrogen bond.

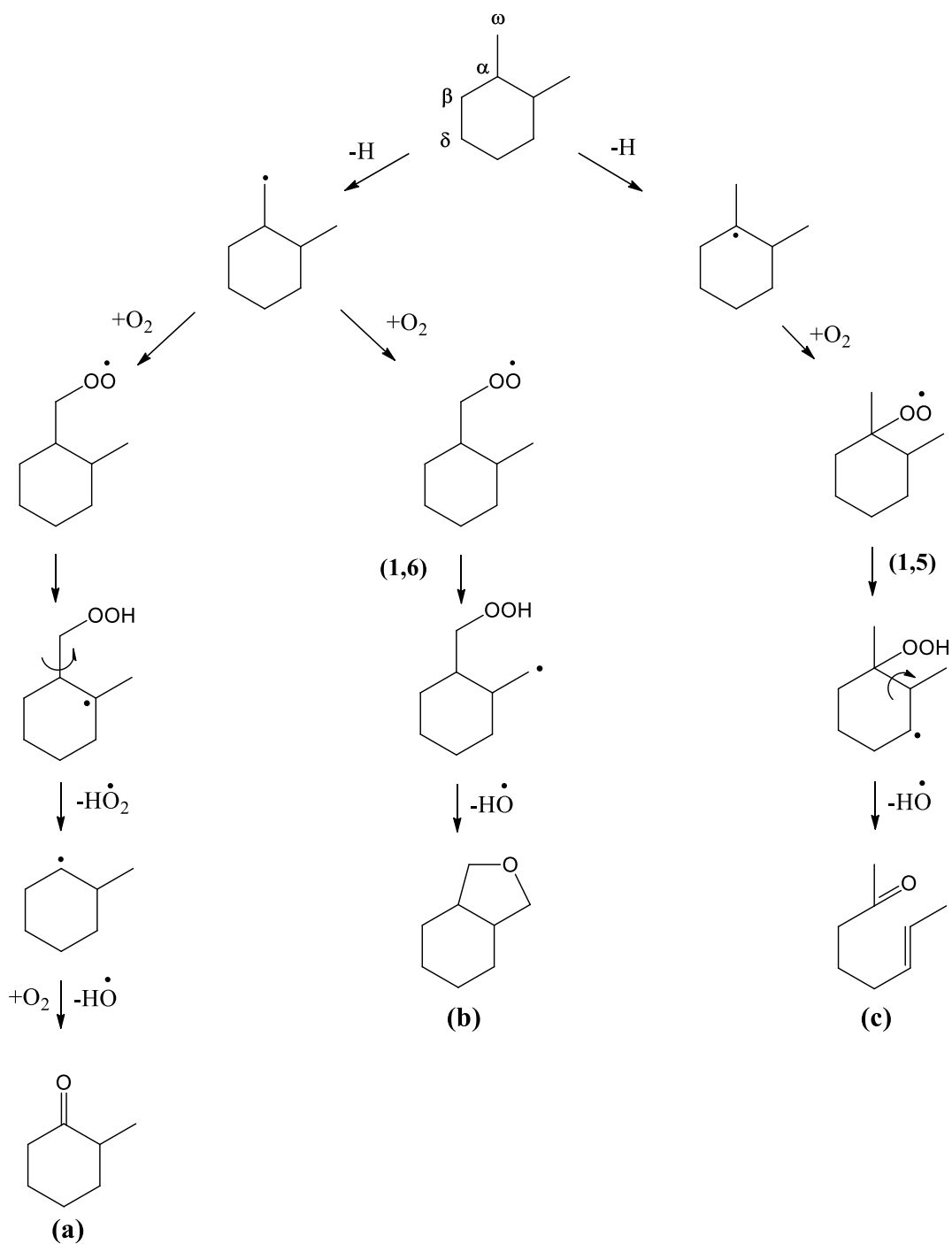


Figure 4-9 Proposed reaction pathways of oxygenated species from the low temperature oxidation of 1,2-dimethylcyclohexane: (A) 2-methylcyclohexanone; (B) octahydro-2-benzofuran ; and (C) 6-octen-2-one;

The reaction pathways for three oxygenated species from low temperature oxidation of 12DMCH are also proposed in Figure 4-9. In the case of not opening the ring of cyclohexane but disbranching one of the methyl substituents, 2-methylcyclohexanone can be formed through transferring one methyl substituent into a ketone group by releasing an OH radical during low temperature oxidation. It is noted that in the low temperature regime, de-methylations (cutting the branched substituent) likely occurs via peroxidation of the methyl or ethyl group with a formation of formaldehyde. This reaction pathway to the formation of a ketone group is also proposed in the low temperature oxidation of ECH and 13DMCH, shown in pathways for cyclohexanone and 3-methyl-2-cyclohexen-1-one, respectively. Also, Figure 4-9 (b) describes how octahydro-2-benzofuran is formed in the low temperature regime. Initial hydrogen abstraction takes place at the  $\omega$ -position carbon. Then subsequent oxygen addition and (1,6) H-shift isomerization contributes to the formation of an ether group on the cyclic compound. As can be seen in Figure 4-9 (c), the isomerization at the  $\alpha$ -carbon builds 1,2-dimethyl-cyclohexyl-hydroperoxide which undergoes  $\beta$ -scission on the position of the C-C bond between the two methyl substituents to open the ring, thereby forming 6-octen-2-one. For the same pathways with different positions of radical transfer, 3- and 7-octen-2-one can be also formed, but these products were not positively identified in this work. Likewise for the ring opening reaction of 6-methylhept-6-en-2-one observed from 13DMCH oxidation, the C-C bond placed between the two methyl substituents is more preferably cleaved than the other C-C bonds of 12DMCH during low temperature oxidation, based on the relatively higher yield of 6-octen-2-one, compared to other oxygenated species.

#### 4.5.4 Conformational analysis

The purpose of this section is to validate the general trend of reactivity observed above by employing the theory from the previous study of Yang *et al.*, where the low temperature oxidation reactivity of various cycloalkanes has been discussed in a phenomenological and qualitative manner [109,112]. As briefly mentioned in the *4.1 Introduction*, the (1,5) H-shift isomerization possesses the lowest energy barrier for forming the alkylhydroperoxy radical ( $\bullet$ QOOH) in the low temperature oxidation of cyclic hydrocarbons. This key reaction path can accelerate the overall low temperature chain branching reaction rate, thereby having a decisive effect on the oxidation reactivity. Therefore, Yang *et al.* counted the total number of hydrogens available for (1,5) H-abstraction of the isomerization of an alkyl peroxy radical ( $\bullet$ ROO) as a factor for anticipating the low temperature reactivity of a particular compound. At the same time, degeneracy of the isomerization of an alkylperoxy radical was considered, counting the number of hydrogens that are available for (1,5) H-abstraction for a given peroxy group, since this number affects the pre-exponential factor in the rate constant [33]. The previous study of Yang *et al.* considered sets of molecular structures such as straight chain molecules (n-hexane) versus cyclic molecules (CH), MCH versus CH, and bicyclic decalin versus CH to explain how the steric cyclic structure affects the low temperature oxidation[81,82]. This study considers isomers of mono-substituted cyclohexane and di-substituted cyclohexanes to characterize the steric cyclic structural impact on low temperature reactivity and to answer the following questions:

- (1) Why is MCH less reactive than ECH and the isomers (13DMCH and 12DMCH)?
- (2) Why is 13DMCH more reactive than 12DMCH?

#### 4.5.4.1 Conformational analyses of mono- and di-substituted cyclohexanes

Cyclic molecules are non-planar (except when they contain three-membered rings), and thereby present important conformational aspects affecting physical and chemical properties. Conformation of cyclic molecules relies on ring size, substitution, number of rings and other factors. Cyclohexane is comprised of a six-membered ring and nearly strainless itself. One conformation of cyclohexane is the well-known chair conformer, which lies in a deep energy valley, showing the enthalpy difference between the chair form and the twist-boat form, which is 4.7-6.2kcal/mol [118]. For an equilibrium mixture of cyclohexane conformers, one can estimate from  $\ln K = -\Delta G/R_u T$  ( $\Delta S \sim 0$  is assumed) that only ~3% of cyclohexane exists in the twist-boat form at 800K. The chair conformer can therefore be regarded as a rigid structure, which indicates that the chair conformations are unlikely change to other conformations, even with a substitution on the ring. For this reason, this study limits consideration to chair forms of mono- and di-substituted cyclohexanes.

In addition, substituted cyclohexane may undergo ring inversion, which switches the substitution groups at equatorial and axial positions. Based on conformation energy ( $\Delta G$ ) measured, the substitution group on MCH and ECH prefers equatorial position, due to the presence of one substitution group [118]. Note that the equatorial preference of substituted cyclohexane helps explain the reactivity disparity compared to cyclohexane. Since a substitution group pre-occupies equatorial position, a peroxy group is forced to

stay in an axial position, which facilitates (1,5) H-shift of the peroxy group and subsequent higher overall reaction rate. This alkylcyclohexyloxy radical (eq-alkyl/ax-peroxy) unlikely undergoes ring inversion, since an alkyl group has the higher conformational energy than a peroxy group. Therefore, this study confines consideration to the methyl- and ethyl-cyclohexyloxy radicals, which isolates an alkyl (methyl and ethyl) group at the equatorial position and a peroxy group at the axial position.

However, the other isomers (13DMCH and 12DMCH) tested in this study are stereoisomers, referred to as *cis-trans* isomers, that have the same molecular formula and sequence of bonded atoms, but that differ only in the three-dimensional orientations of their atoms in space. Therefore, stereo impacts between two methyl substitutions in 1,2- and 1,3-disubstituted cyclohexanes each existing as *cis-* and *trans-* isomers must be taken into account with strain energies generated between hydrogens and substituted methyl groups. Table 4 shows the conformation energy calculated by using the CBS-QB3 for each case of reacting species. The CBS-QB3 performs the quantum mechanical calculations using the complete basis set methodology of Pettersson *et al.* [119]. The results indicate that the eq,eq-13DMCH and the eq,eq-12DMCH conformations are favored over the ax,eq- conformations and ax,ax- conformations, with the former being the highest energy for both 13- and 12-DMCH. Molecular structures for selected conformations of 13DMCH and 12DMCH are shown in Figures 4-11, 4-12, 4-13 and 4-14. The conformation analysis and calculations led to a streamlined set of species for further consideration, those being the most stable structures for each stereoisomer.



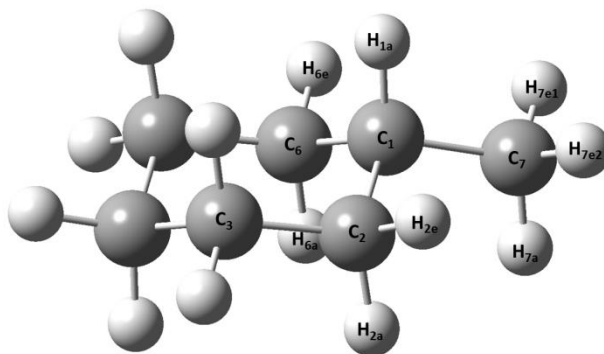
Table 4 Energy barriers of mono- and di-substituted cyclohexane

Molecule	Ax/Eq methyl position(s)	Energy [CBS-QB3 (0K)]	CH (kJ/mol)	Figures
ECH	Eq	-313.806524	0	Fig. 10 (B)
	Ax	-313.803494	7.96	
<i>cis</i> -13DMCH	Eq, Eq	-313.81149	0	Fig. 11
	Ax, Ax	-313.802597	23.35	
<i>trans</i> -13DMCH	Ax, Eq	-313.808389	-	Fig. 12
<i>cis</i> -12DMCH	Ax, Eq	-313.807275	-	Fig. 13
<i>trans</i> -12DMCH	Eq, Eq	-313.810038	0	Fig. 14
	Ax, Ax	-313.805531	11.83	

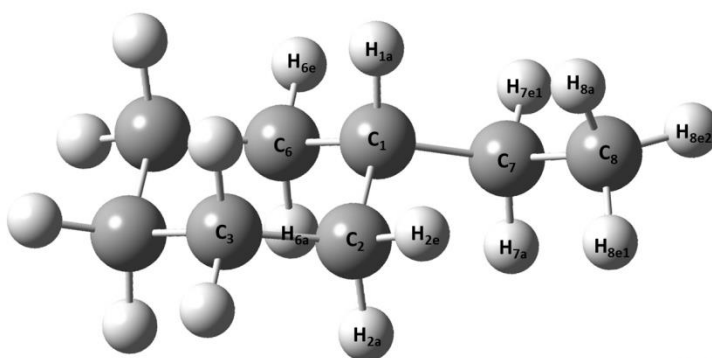
#### 4.5.4.2 Alkyl group size impact on mono-substituted cycloalkanes

In their previous study, of Yang *et al.* discussed the effect of methyl substitution on the low temperature oxidation of cycloalkanes with the adoption of *ab initio* calculations for the (1,5) H-shift for the one step reaction from alkylperoxy to alkylperoxide [109,112]. However, these studies only discussed the impact of the presence of methyl substitution, not the length of alkyl substitution. It is common knowledge that alkyl chain length plays an important role in determining ignition reactivity in the low temperature regime. Also, few studies already showed that longer substitution chain length on cyclic compounds and even on aromatic compounds contributes to stronger reactivity in the low temperature regime [63,64]. However, these studies included little discussion of how and why longer chain length increases the oxidation reactivity in the low temperature regime. To answer this question, MCH was also tested at the same conditions as ECH and resulted in lower reactivity (CCR 9.5) for MCH, compared to ECH (CCR 6.24). This indicates that the greater the carbon number of the straight chain in the alkyl substituent on a cycloalkane, the greater the oxidation

reactivity, by providing more hydrogens that are available for the (1,5) H-shift on the C-C backbones (C-7 and C-8) of the alkyl substituent of ECH, which is shown in Figure 4-10.



(a)



(b)

Figure 4-10 Chair conformation of (a) Methylcyclohexane and (b) Ethylcyclohexane. There are 11 and 16 hydrogens available for (1,5) H-shift of peroxy groups in MCH and ECH, respectively.

Applying the same rationale as in Yang *et al.*, the axial hydrogens on C-6 ( $H_{6a}$ ) and C-2 ( $H_{2a}$ ) are in the corresponding (1,5) position with the “axial” secondary hydrogen on the C-7 ( $H_{7a}$ ). In addition, the equatorial hydrogen on C-6 ( $H_{6e}$ ) is in the corresponding (1,5) position with the “equatorial” secondary hydrogen on the C-7 ( $H_{7e}$ ).

Instead of the other “equatorial” hydrogen on C-7 ( $H_{7e2}$ ) for the case of MCH shown in Figure 4-10 (a), ECH involves the C-8, which possesses one axial hydrogen and two equatorial hydrogens attached to the C-7. As a result, the axial hydrogen on C-8 ( $H_{8a}$ ) corresponds to the (1,5) position with the “axial” tertiary hydrogen on the C-1 ( $H_{1a}$ ). Therefore, the total number of hydrogens available for (1,5) H-shift on ECH is 16, which has greater number than that of MCH (~11). With regard to the degeneracy of the (1,5) H-shift on ECH, it is also the same, except for one peroxy group at the “axial” position on the C-8. However, the only but significant difference between ECH and MCH is the hydrogen distribution, showing that MCH has lower available hydrogens for the (1,5) H-shift of the peroxy groups limited on the C-7. ECH provides more hydrogens attached in the straight substituent (C-7 and C-8) to be shifted to form an alkylhydroperoxy radical, resulting in a faster reaction rate than for MCH. In addition, the secondary hydrogens on the C-7 ( $H_{7a}$  and  $H_{7e}$ ) of ECH are easier to shift than the primary hydrogens on the C-7 of MCH in the isomerization reaction ( $ROO\cdot \longrightarrow \cdot QOOH$ ) in the low temperature regime [34]. This can also explain why ECH has higher oxidation reactivity than MCH, which possesses only primary hydrogens on the methyl substituent in its cyclic structure.

#### 4.5.4.3 Alkyl group position impact on di-substituted cycloalkanes

The reactivity difference between 13DMCH and 12DMCH can be also explained by the above theory as the different position of methyl substitutions makes different numbers of hydrogens available for the (1,5) H-shift. As can be found in Table 2, 13DMCH and 12DMCH tested in this study are comprised of 73.3% of the *cis*-isomer and 25.7% of the *trans*-isomer and of 77 wt % of *cis*- and 22 wt% of *trans*-isomer,

respectively. Therefore, conformation analysis for these four different isomers needs to be considered.

As shown in Figure 4-11, *cis*-13DMCH (with “diequatorial” substituents) in its most stable conformation has eight hydrogens at axial positions for (1,5) H-shift and the “equatorial” hydrogens at C-7 and C-8 ( $H_{7e1}$ ,  $H_{7e2}$ ,  $H_{8e1}$  and  $H_{8e2}$ ) are in corresponding (1,5) H-shift position at C-6 ( $H_{6e}$ ), C-2 ( $H_{2e}$ ), C-2 ( $H_{2e}$ ) and C-4( $H_{4e}$ ), respectively. From the total available hydrogens, the peroxy group for the (1,5) H-shift associated with the hydrogens on the two methyl substituents (C-7 and C-8) is eight. The degeneracy of the (1,5) H-shift is three for the axial peroxy group at C-2. For the peroxy group at the remaining ring axial position, the degeneracy is two. For the peroxy group at the above-mentioned equatorial positions, the degeneracy is one.

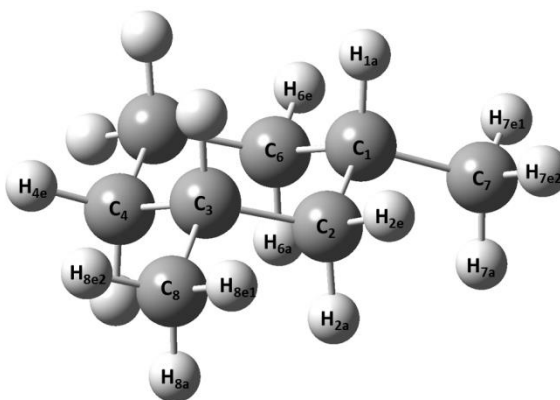


Figure 4-11 Chair conformation of *cis*-1,3-dimethylcyclohexane. The most stable conformation with both equatorial methyl groups is favored over the conformation with both axial methyl groups in the two chair conformations of *cis*-1,3-dimethylcyclohexane.

Roughly 25.7% of 13DMCH tested here is another stereoisomer, *trans*-13DMCH (one equatorial and one axial substituent), shown in Figure 4-12 that is a less stable conformation than *cis*-13DMCH, shown in Figure 4-11. The number of axial position

hydrogens for (1,5) H-shift is six. The “equatorial” hydrogens on C-7 ( $H_{7e1}$  and  $H_{7e2}$ ) and C-8 ( $H_{8e1}$  and  $H_{8e2}$ ) become available for (1,5) H-shift corresponding to “equatorial” hydrogens on C-6 ( $H_{6e}$ ), C-2 ( $H_{2e}$ ), C-2 ( $H_{2e}$ ) and C4 ( $H_{4e}$ ), respectively. Among these available hydrogens, the total number of the peroxy group for (1,5) H-shift associated with the hydrogens on the two methyl substituents (C-7 and C-8) is six. The degeneracy of the (1,5) H-shift for axial peroxy group at C-2 is three. Also, the degeneracy of “axial” peroxy group at C-4, C-6 and C-7 is two and the remaining “axial” peroxy group at C-1 and C-5 is one. The degeneracy for the abovementioned “equatorial” peroxy group is also one.

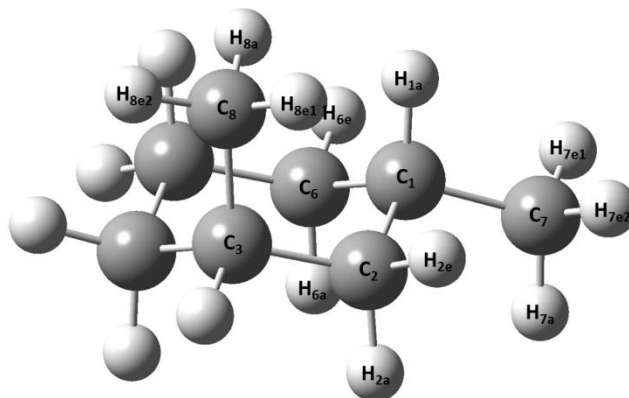


Figure 4-12 Chair conformation of *trans*-1,3-dimethylcyclohexane. The two chair conformations are equal in steric strain energy because each has one axial methyl group and one equatorial methyl group.

As shown in Table 2, 12DMCH used here is likewise a mixture of 77 wt % of *cis*- and 22 wt% of *trans*-stereoisomer. *trans*-12DMCH can exist as two different chair forms (diaxial and diequatorial substituents) with two methyl substituents facing in opposite directions. *trans*-12DMCH (with diequatorial substituents), shown in Figure 4-13, in its most stable conformation, has eight hydrogens at axial positions. Also, two equatorial

hydrogens at C-7 ( $H_{7e2}$ ) and C-8 ( $H_{8e1}$ ) match with equatorial hydrogens at C-6 ( $H_{6e}$ ) and C-3 ( $H_{3e}$ ) in the cyclic ring are available for (1,5) H-shift and the degeneracy of (1,5) H-shift is one. Among the “axial” and the “equatorial” hydrogens, the available peroxy group for (1,5) H-shift associated with the hydrogens on the two methyl substituents (C-7 and C-8) is only six. The degeneracy for the axial peroxy group at C-1, C-2, C-3 and C-6 is three and the degeneracy for the remaining axial peroxy group at C-4, C-5, C-7 and C-8 is two.

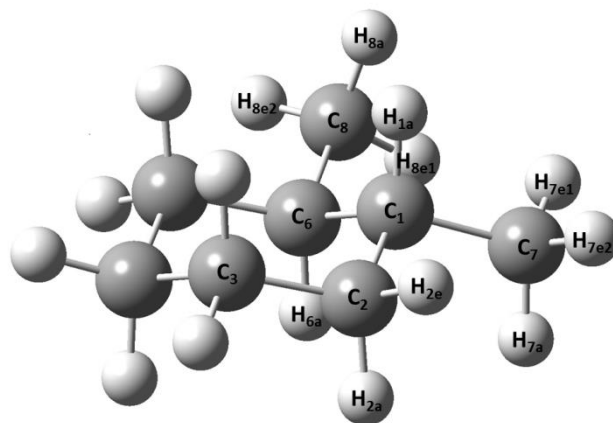


Figure 4-13 Chair conformation of *trans*-1,2-dimethylcyclohexane and the most stable conformation with both equatorial methyl groups is favored over the conformation with both axial methyl groups in the two chair conformations of *trans*-1,2-dimethylcyclohexane.

*cis*-12DMCH (one equatorial and one axial substituents), shown in Figure 4-14, exists in a less stable conformation than the *trans*-isomer and the most abundant isomer in the fuel used in this study was *cis*-12DMCH. As shown below, the number of hydrogens at axial position available for (1,5) H-shift is six. For the available hydrogens on equatorial positions, the hydrogens at C-7 ( $H_{7e1}$ ,  $H_{7e2}$ ) and at C-8 ( $H_{8e1}$ ) in corresponding (1,5) H-shift are the “equatorial” hydrogens at C-6 ( $H_{6e}$ ), C-2 ( $H_{2e}$ ) and C-

3 ( $H_{3e}$ ), respectively. The total number of the peroxy groups for (1,5) H-shift associated with the hydrogens on the two methyl substituents is only four. The degeneracy for the axial peroxy group at C-1, C-3, C-5 and C-6 is 2. For axial and equatorial substituents, the degeneracy for the axial peroxy group is zero and one, respectively. For the remaining axial peroxy groups at C-4 and C-7, the degeneracy is only one. Likewise for the other isomers, the degeneracy of the abovementioned equatorial peroxy group at C-7 and C-8 is one.

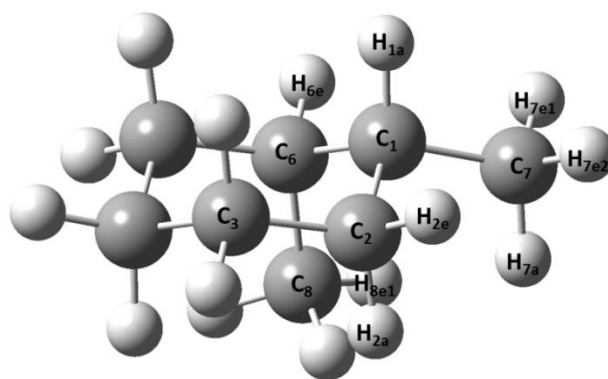


Figure 4-14 Chair conformation of *cis*-1,2-dimethylcyclohexane. The two chair conformations are equal in steric strain energy because each has one axial methyl group and one equatorial methyl group.

As shown in Table 5, the greater number of hydrogens available for (1,5) H-shift can explain the greater low temperature oxidation reactivity of 13DMCH over 12DMCH, which arises from the conformational preference brought by the location of the two methyl substitutions. The more peroxy groups available for (1,5) H-shift in a molecule, the more alkylhydroperoxy radicals can be formed through (1,5) H-shift. The alkylhydroperoxy radical experiences subsequent oxygen addition and internal hydrogen abstraction to form an alkyl dihydroperoxy radical. The alkyl dihydroperoxy decomposes

to an OH radical and an alkyl ketohydroperoxide, which is known to be a degenerate branching agent and produces two active radicals. Therefore, the structural impact on the hydrogen shift of the alkylperoxy radical may affect further decomposition to break the carbon backbone of the reacting hydrocarbon molecules. In the case of the ring opening reaction for 13DMCH and 12DMCH, Do *et al.* explained that the reactivity can be improved by ring opening of cycloalkanes, but only when the C-C bond cleavage occurs at a substituted position [115]. It is observed that C-C bonds between methyl-substituents are preferably cleaved rather than the other locations of the C-C bonds in both test fuels. In this study, the substantial formation of 6-methyl-6-en-2-one, shown in Figure 4-7 (b), and 6-octen-2-one, shown in Figure 4-9 (c), is relatively higher than for other intermediate species, which can be formed by cleaving other locations of C-C cyclic backbones during low temperature oxidation of 13DMCH and 12DMCH, respectively. This relative quantitative analysis agrees well with the study of Do *et al.* [115]. Therefore, C-C bonds in 13DMCH could be more easily ruptured, because of the two C-C bonds between the methyl-substituents, rather than in 12DMCH providing only one C-C bond between the methyl-substituents. This structural impact also explains the disparity in oxidation reactivity between 13DMCH and 12DMCH.



Table 5 Hydrogen availability of cyclic hydrocarbon isomers

	Total # of hydrogens for (1,5) shift	Degeneracy of (1,5) H-shift	Total # of the peroxy group for (1,5) shift associated with the alkyl substituent(s)	Order of LTO reactivity
ECH	16	1-3	7	1
cis-13DMCH	16	1-3	8	2
trans-13DMCH	16	1-3	8	2
cis-12DMCH	12	1-2	4	3
trans-12DMCH	10	1-3	4	3
MCH	10	1-3	3	4

#### 4.6 Conclusions

This study investigates the impacts on ignition characteristic of the position of the alkyl substituent on cycloalkanes, while examining intermediate species from incomplete to complete combustion of the test fuels in a motored engine. Ethylcyclohexane and two of its isomers, 12DMCH and 13DMCH, whose methyl substituents are attached in different positions on methylcyclohexane, were chosen as relevant branched cycloalkanes. The low temperature oxidation of these cycloalkane isomers shows that ECH is the most reactive compound. The high fuel conversion of ECH also indicates stronger reactivity, contributing to higher concentrations of CO and other partial oxidation products in the engine exhaust during the NTC regime. Prior to second stage ignition, most of intermediate species are formed at a constant rate in the low temperature and NTC regimes for all the test fuels. The dominant population of conjugate olefins are likely formed through (1,4) hydrogen shift isomerization, competing with (1,5) H-shift isomerization. An inverse relationship exists between the proportion of conjugate olefins and ignition reactivity among the cycloalkane isomers. The longer chain of the alkyl

substituent in ECH can promote oxidation reactivity, introducing lower energy barrier paths to the (1,5) H-shift of alkylperoxy radical. This indicates that reactivity is more strongly influenced by the alkyl group size of the substituents on a cycloalkane than the number of alkyl chain substituents.

As shown in Table 5, conformation analysis supports the observed disparity in the low temperature oxidation reactivity of these three cycloalkane isomers. From the comparison of MCH and ECH, the longer chain of the alkyl substituent in ECH can promote the oxidation reactivity, introducing more available hydrogens for low energy barrier paths to the (1,5) H-shift on the alkylperoxy radical. For the stereoisomers 13DMCH and 12DMCH, the total number of peroxy groups available for (1,5) H-shift on the two methyl substituents can explain the difference in low temperature oxidation reactivity between them. This reactivity difference during low temperature oxidation results in the formation of different fractions of intermediate species. The fuel with greater reactivity possesses more possible ways to undergo (1,5) H-shift isomerization, and a lower activation barrier. Such isomerization promotes further chain branching reactions producing more active radicals in the low temperature regime. This results in opening the cyclic rings and forming small size of intermediate species. In contrast, the fuel with the weaker reactivity possesses fewer possible ways to undergo (1,5) H-shift isomerization, with a greater activation barrier to form an alkylhydroperoxide radical. Subsequently, alkylhydroperoxide radicals can take various reaction paths, rather than form a ketohydroperoxide. This contributes to formation of oxygenated species rather than small intermediate species. Also, the reversibility of such isomerization of peroxy group can explain the longer NTC duration, resulting in longer ignition delay. Therefore,

it is concluded that the formation and fractions of intermediate species highly relies on the structure of the parent molecule, and the nature of the intermediate species formed during low temperature oxidation correlates with the reactivity of the parent fuel molecules.

## Chapter 5

### Autoignition Studies of C<sub>5</sub> Isomers in a Motored Engine

#### 5.1 Introduction

Even though pentanes are major constituents of gasoline and contribute significantly to the required vapor pressure, the combustion and chemical kinetics of pentanes has not been studied as much as C<sub>1</sub>-C<sub>4</sub> alkanes or C<sub>7</sub> and C<sub>8</sub> primary reference fuels. Furthermore, the development of mature models for straight alkane chain relevant to transportation fuels have been accomplished. However, much less work has been done on branched alkanes, which occupy a large portion of gasoline and diesel fuels.

For this reason, previous ignition and oxidation studies have analyzed pentane isomers, namely *n*-pentane, 2-methylbutane (*iso*-pentane) and 2,2-dimethylpropane (neo-pentane), using a rapid compression machine (RCM), a shock tube and a flow reactor as shown in Table 6. Various experimental studies of oxidation of *n*-pentane have been well established, however experimental data for neo- and *iso*-pentanes are scarcer. In addition,

very few experimental studies have completed a fuel to fuel comparison of pentane isomers in a combustion device [39,60].

Table 6 Previous oxidation and ignition studies of pentane isomers

Compounds	Reactors	$\phi$	T (K)	P (atm)	refs
<i>n</i> -pentane	Shock Tube		1165-1400	8.27-9.46	[40]
		0.5	867-1534	11-530	[36]
	Flow Reactor	Lean	1068-1253	8-10	[72]
		RCM	1	600-900	6.8-9.1
		0.8-1.2	630-920	3-16	[62]
		n/a	640-900	0.5-n/a	[60]
	Shock Tube, RCM	0.3-2.0	643-1555	1-20	[39]
neo-pentane	Flow Reactor	0.3	620-810	8	[74]
	RCM	n/a	640-900	0.5-n/a	[60]
	JSR	0.25-2	800-1230	1-10	[68]
	Shock Tube, RCM	0.3-2.0	663-1675	1-20	[39]
<i>iso</i> -pentane	Shock Tube	0.25-2	1177-2009	1.1-12.58	[41]
	RCM	n/a	640-900	0.5-n/a	[60]
	Shock Tube, RCM	0.3-2.0	651-1718	1-20	[39]

Baldwin *et al.* reviewed studies of C<sub>2</sub>-C<sub>4</sub> hydrocarbons and neo-pentane and assigned rate constants for the four main types of reaction for determining hydrocarbon oxidation products in the oxidation of pentane including: (a) radical attack on the hydrocarbon; (b) alkyl radical decomposition by C-C homolysis; (c) alkyl radical attack

by O<sub>2</sub> to form the conjugate alkene; and (d) alkyl radical reaction by O<sub>2</sub> to form O-heterocycles and other oxygenated products, following the familiar low temperature oxidative reaction pathway [120]. The ignition processes for the three isomers are essentially similar with an observed two stage ignition process at sufficiently low temperatures (and high pressures), with the order of reactivity being *n*-pentane > neo-pentane > *iso*-pentane, with low temperature oxidation taking place via an alkylperoxy radical isomerization. Key differences observed between the three pentane isomers are that while all three molecules follow a similar reaction pathway at low temperatures, H-atom abstraction is inhibited for neo-pentane relative to *n*-pentane and even more so for *iso*-pentane due to limited availability for H-atom shift. Therefore, the C<sub>5</sub> isomers, although relatively small, exhibit significant structural difference, leading to unique oxidation reactivity. Knowing the structural impact on reactivity diversity of C<sub>5</sub> isomers is of importance, especially for typical transportation fuels which contain a large amount of alkanes with various amounts of structural branching. Therefore, better characterization is needed both experimentally and numerically to support qualitative and quantitative analyses of the oxidation processes of C<sub>5</sub> species and of higher hydrocarbons as they oxidize through C<sub>5</sub> species.

The relative lack of studies on pentanes compared to their smaller and larger alkane counterparts motivated a recommendation at the International Workshop on Flame Chemistry at the 2014 International Symposium on Combustion for further investigation of C<sub>5</sub> combustion chemistry as a topic for collaborative research.

## 5.2 Research Objectives

And as part of that effort, this chapter aims to provide autoignition data on these three pentane isomers. The approach here is to conduct a systematic investigation of the autoignition of three C<sub>5</sub> isomers in a motored engine and compare with reference fuels *n*-heptane and *iso*-octane, which can provide useful input for qualitative and semi-quantitative validation of kinetic mechanisms for oxidation of C<sub>5</sub> species. This is a unique approach and represents the first motored engine study of the pentane isomers.

## 5.3 Test Fuels

Three test fuels, *n*-pentane (109-66-0, 99%), *iso*-pentane (78-78-4, 99%) and neo-pentane (463-82-1, 99%), were used. The structures of test pentane isomers are the smallest isomeric set of alkanes containing linear, singly-branched and doubly-branched species, as shown in Fig 5-1. Primary reference fuels, *n*-heptane and *iso*-octane were also included for comparison with the pentane isomers. .

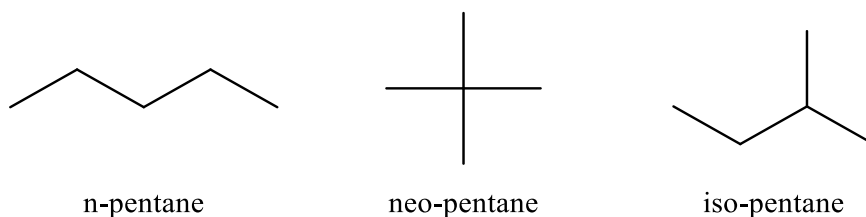


Figure 5-1 Chemical structure of pentane isomers

## 5.4 Test Conditions

Engine speed was kept constant at 600 rpm and equivalence ratios ( $\phi$ ) of 0.25 or 0.5 were maintained during the CCR test. Intake air temperature of 120°C was chosen to promote complete fuel vaporization. Cooling jacket temperature was fixed at 90°C using an external chiller/circulator. For each fuel tested, the compression ratio to obtain the critical compression ratio (CCR) started low enough that no low temperature reaction took place and was then gradually increased in a stepwise manner to increase the extent of reaction.

## 5.5 Results and Discussion

### 5.5.1 Autoignition characteristics of pentane isomers

It is known that carbon monoxide (CO) is largely formed prior to high temperature oxidation (HTO), especially when low temperature reactions are active. For this reason, monitoring raw CO emission in real-time enables observation of global oxidation reactivity and negative temperature coefficient (NTC) behavior during pre-ignition. Figures 5-2 and 5-3 show the unique trend of CO formation and apparent heat release rates of neo-pentane at a lean condition, which represents a wide spectrum of autoignition characteristics, including low temperature oxidation (LTO); (I) and (II), NTC; (III), and HTO; (IV) and (V), as CR increases in a motored engine. Each regime features distinctive behavior in CO formation as follows: (I) no CO formation due to low in-cylinder temperature ( $< 700$  K), which is not high enough to remove hydrogen atoms



consecutively to form CO from formaldehyde ( $\text{CH}_2\text{O}$ ) [7], which is largely formed during LTHR; (II) onset of CO formation where evident low temperature heat release (LTHR) first appears; (III) level CO concentration over a wide range of CR, due to NTC behavior (800-900 K); (IV) rapid growth of CO formation in hot-ignition (thermal-runaway) temperature (900-1100 K) [121], where evident two stage heat release is first observed; (V) a sudden drop of net CO formation mostly due to conversion to  $\text{CO}_2$  ( $>1200$  K), defined as high temperature heat release (HTHR).

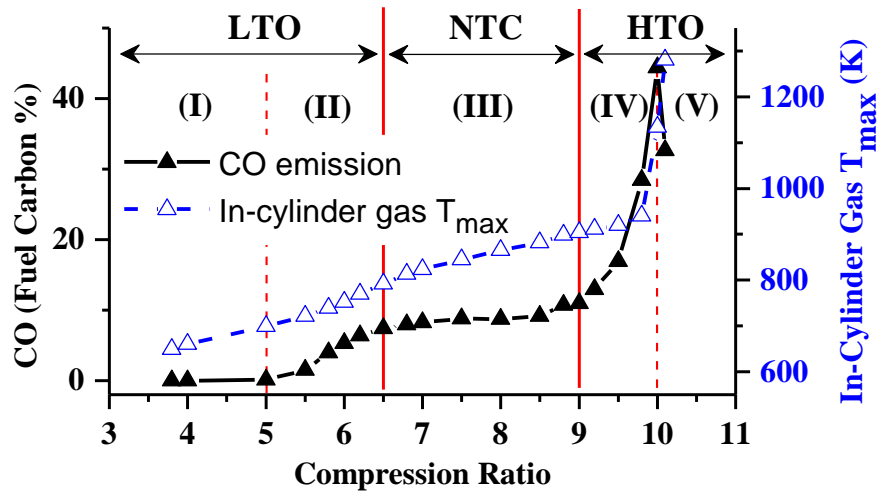


Figure 5-2 Autoignition characteristic of neo-pentane at  $\phi$  of 0.25 in a respect of measured CO formation and calculated in-cylinder gas  $T_{\max}$  (calculated from measured in-cylinder pressure)

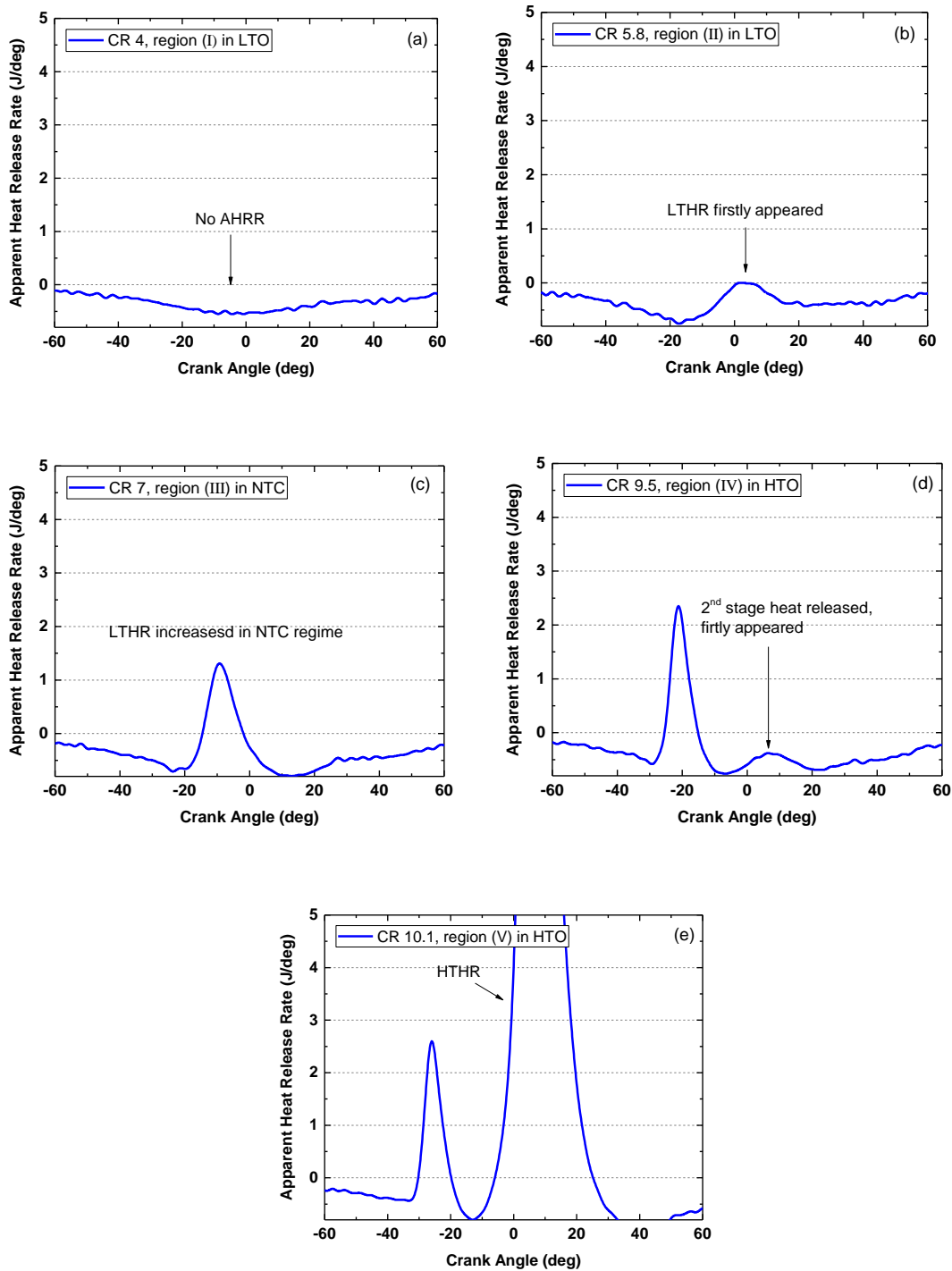


Figure 5-3 Apparent heat release rates (AHRR) in a wide range of CRs of neo-pentane at equivalence ratio of 0.25, as corresponded to Figure 5-2; Apparent heat release rate at (a) CR of 4.0 in region (I), (b) CR of 5.8 in region (II), (c) CR of 7.0 in region (III), (d) CR of 9.5 in region (IV) and (e) CR of 10.1 in region (V)

Overall reaction progress can be studied via fuel conversion and CO formation. Figure 5-4 shows unreacted fractions of pentane isomers, and CO concentrations at two equivalence ratios as a function of CR. Figures 5-4 (b) and (c) show that *n*-pentane, which has research octane number (RON) of 60.0, possesses the strongest oxidation reactivity among the pentane isomers followed by neo-pentane (RON=88.1) and *iso*-pentane (RON=91.4) from the CCR measurements at different equivalence ratios. Figure 5-4 (b) shows that *n*-pentane has earliest onset of CO formation and produces a higher concentration of CO during the low temperature regime, but exhibits less prominent NTC behavior than neo- and *iso*-pentanes, and thus it enters the high temperature regime at the lowest CR. Strong ignition reactivity and weak NTC behavior results in the fast reaction rate and fuel consumption, shown in Figure 5-4 (a). Profiles of fuel consumption also exhibit unique NTC behaviors of pentane isomers, which resemble the profiles of CO formation. The burning rate of *n*-pentane is relatively fast over the whole process of oxidation, however, burning rates of neo- and *iso*-pentane become slow in the NTC regime, and then become rapid once the reaction reaches HTO. The results of global oxidation reactivity of pentane isomers are consistent with recently measured RONs, described above and have a good agreement with ignition behavior of PRFs in that the trends of CO formation lie between those of PRFs (MON=0 and 100). A distinct observation between reactive and less reactive fuels was observed in the relatively richer condition, shown in Figure 5-4. The less reactive HCs (branched-alkanes) still lead to prominent NTC behavior, but the reactive HCs such as *n*-alkanes exhibit a fast oxidation, such that the NTC behavior barely appears. Despite the fact that oxidation reactivity is improved as  $\phi$  increases, the onset of CO formation related to LTHR occurs at similar

CRs regardless of  $\phi$ , indicating that onset of LTHR depends less on the equivalence ratio than in-cylinder temperature and pressure.

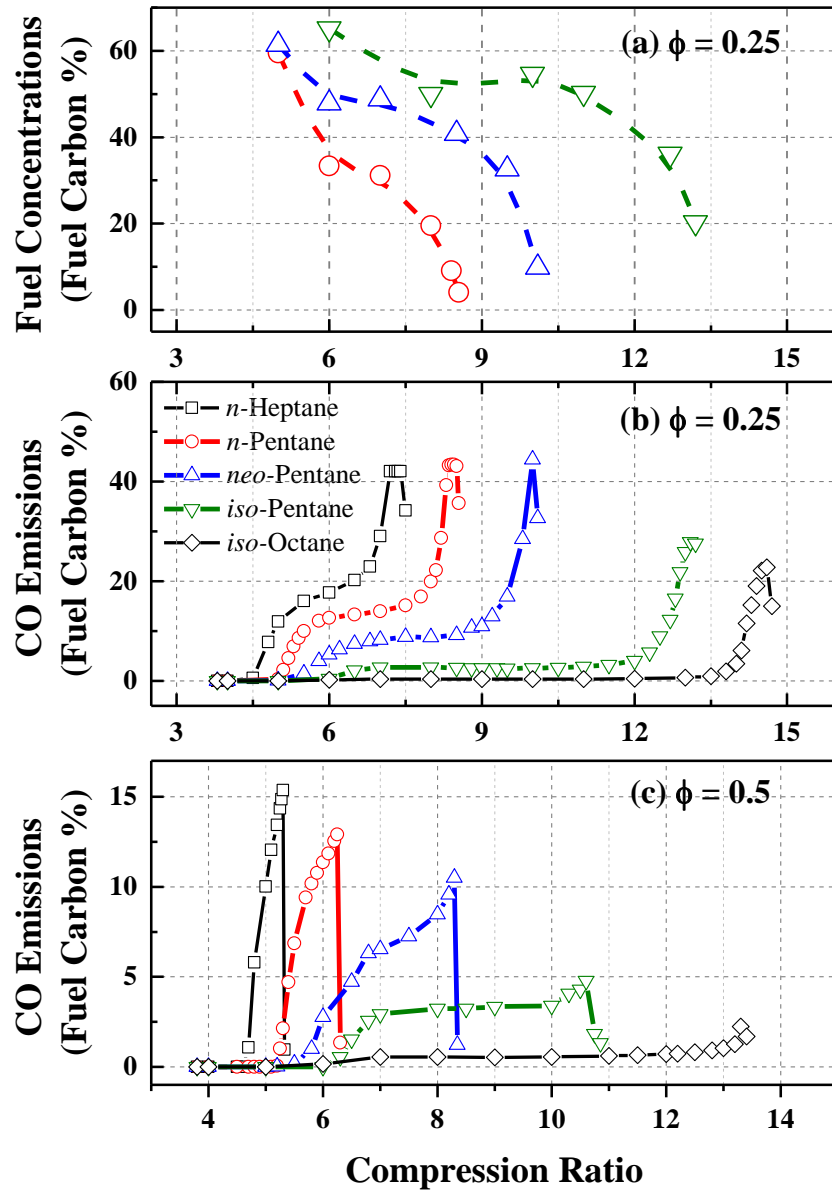


Figure 5-4 Autoignition behaviors of pentane isomers in comparison with primary reference fuels (PRF); (a) Fuel conversions of pentane isomers at equivalence ratio of 0.25; (b) CO emission comparisons at equivalence ratio of 0.25; and (c) CO emission comparisons at equivalence ratio of 0.5

In Figure 5-5 (a), the heat release profiles of pentane isomers are compared at the same CR of 8.5, where clear evidence for the reactivity differences is observed in that *n*-pentane possesses strong two stage ignition behavior, but other isomers exhibit only LTHR to a strong extent for neo-pentane and to a weak extent for *iso*-pentane at the same CR. This indicates that *n*-pentane resides in the HTO regime, but two other isomers remain in the NTC regime at the same CR. The heat release profiles at the CCRs can also indicate ignition reactivity by comparing % LTHR, defined as  $[\text{LTHR} / (\text{LTHR} + \text{HTHR})] \times 100\%$ , thus quantifying the low temperature oxidation reactivity of the test fuels [30]. *n*-Pentane possesses the highest % LTHR at both cases (15.5% at  $\phi$  of 0.25 and 6.47% at  $\phi$  of 0.5), followed by neo-pentane (5.3% and 3.7%) at their respective CCRs, as shown in Figure 5-5 (b) (for the case of  $\phi$  of 0.25). On the other hand, *iso*-pentane exhibits single stage heat release under these experimental conditions at CCR, which ultimately leads to more retarded ignition than for the other isomers. As a result, this study elucidated the impact of molecular structure on the presence of LTHR, which directly relates to the advanced overall reactivity, observed in an engine environment. The critical equivalence ratios of each pentane isomer were also investigated as shown in Figure 5-6 (a). As expected, the higher reactivity fuels required less amount of fuel to be ignited at the same CRs. For example, at the CRs of 8 and 9, *n*-pentane requires  $\phi$ s of 0.3 and 0.24 for the critical threshold, while neo-pentane needs  $\phi$ s of 0.62 and 0.39 for the ignition, respectively. In contrast, at the CRs of 10 and 11, neo-pentane requires  $\phi$  of 0.27 and 0.21 to be ignited, while *iso*-pentane requires  $\phi$  of 0.62 and 0.47, respectively. Furthermore, as can be seen in Figure 5-6 (b), it is found that % LTHR is largely

influenced by  $\phi$ , in that less % LTHR can be found at higher  $\phi$  used for both isomers, which indicates that more complete combustion occurred at higher  $\phi$ , resulting in stronger second stage heat release at CCR.

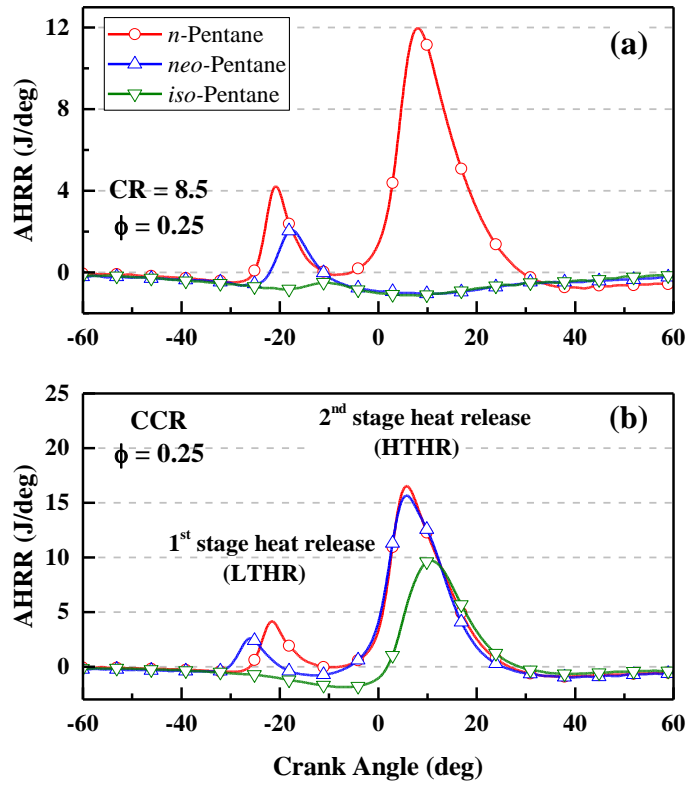


Figure 5-5 Comparisons of apparent heat release rates (AHRR) for pentane isomers in equivalence ratio of 0.25 at (a) compression ratio of 8.5 and at (b) critical compression ratios (CCRs) of 8.5 for *n*-pentane, 10.1 for *neo*-pentane and 13.2 for *iso*-pentane

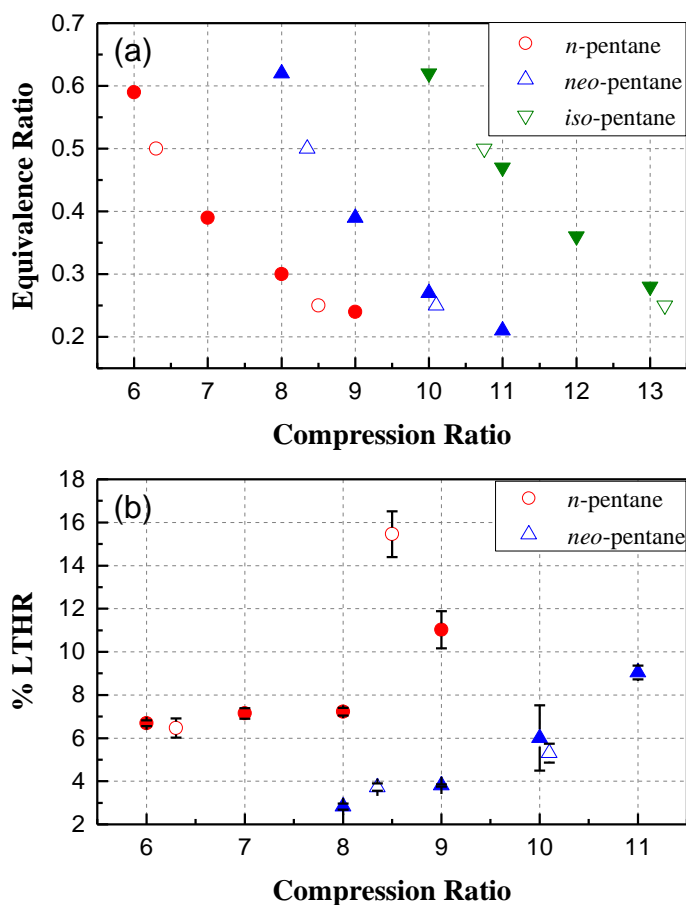


Figure 5-6 Autoignition characteristics of pentane isomers; (a) critical compression ratios (open symbols) and critical equivalence ratios (closed symbols), (b) percentages of low temperature heat release (% LTHR) at high temperature heat releases (open symbols for critical compression ratio and closed symbols for critical equivalence ratio)

### 5.5.2 Intermediate condensed species analysis

To better understand impacts of the pentane isomer structure on their unique ignition reactivity, intermediate species analysis was performed at the leaner condition ( $\phi=0.25$ ) to observe trends of product formation over a wide range of oxidation. Based on the regime classification shown in Figure 5-1, one or two sample points in each regime

were determined. Intermediate species from the oxidation of each isomer are classified into four groups, according to their chemical structural families such as alkenes, aldehydes, ketones and cyclic ethers. The concentration of each species is plotted against compression ratio and the percentage of heat release, which indicates the progress in the autoignition process, and implications for reaction chemistry are discussed.

#### 5.5.2.1 Product analysis of *n*-pentane oxidation

Product analysis for *n*-pentane oxidation was performed at six regimes as follows: CR 5 in LTO, CR 6, 7 and 8 in NTC regimes, and CR 8.4 and CCR 8.55 in HTO. The first group contains methane and various alkenes, including C<sub>2</sub>-C<sub>4</sub> alkenes and conjugate alkenes (C<sub>5</sub>). The second group contains C<sub>2</sub>-C<sub>5</sub> aldehydes. The GC method used did not permit the measurement of formaldehyde. Nonetheless, products observed here provide sufficient insight for the objectives of the study. The third group contains 3-buten-2-one, and 2- and 3-pentanones. The last group contains various cyclic ethers including oxiranes, oxetanes, furans and a pyran. This product composition is fairly consistent with results from rapid compression machine [39,60,62,65] and flow reactor [39,72] studies.

Figure 5-7 shows the variation of major products with compression ratio. As can be seen in Figure 5-7 (a), conjugate alkenes (C<sub>5</sub>) can be formed significantly in LTO and NTC regime as temperature increases (~900 K). This conjugate alkene formation ( $R\cdot + O_2 \rightarrow \text{Alkene} + \cdot HO_2$ ) leads to a reduction of the overall reaction rate and is the main root of the appearance of the NTC regime. With further increase in temperature (~930 K), conjugate alkene formations are inhibited by growing the active radical pool. Similar profiles for oxygenated groups of aldehydes, ketones and cyclic ethers are indicative of the active reaction path in LTO. In the low temperature regime (< 820 K), the reaction



path ( $\text{ROO}\cdot \leftrightarrow \cdot\text{QOOH} \rightarrow \text{RO}$  (oxygenated species) +  $\text{OH}\cdot$ ) tends to inhibit active paths of the low temperature oxidation, producing considerable amounts of  $\text{C}_5$  aldehydes, ketones and cyclic ethers, since this process competes directly with the addition of  $\text{O}_2$  to hydroperoxyalkyl radicals, which leads ultimately to the formation of hydroperoxides. The typical case observed in this study is 2-methyltetrahydrofuran, formed through the least strained six-membered transition state ring, as shown in Figure 5-8. In addition, other  $\text{C}_5$ -cyclic ethers such as 2-proxyoxirane, 2,4-dimethyloxetane and dihydropyran, formed through the transition state ring in other position of hydrogen atom abstraction, also participate in retarding the reaction process. The formation of 2-methyltetrahydrofuran and other  $\text{C}_5$  oxygenated species mentioned above rapidly increases in the LTO regime, but gradually decreases in the NTC regime, as the favored reaction path is gradually shifted to form hydroperoxides, while temperature rises, as shown in Figures 5-7 (c) and (d). The dihydrofuran and 2-methylfuran, which are newly discovered from this study, are likely to be formed through the extra oxygen addition ( $\cdot\text{QOOH} \leftrightarrow \cdot\text{OOQOOH}$ ) and hydrogen isomerization. The group of alkenes and oxygenated species in HTO finally falls off (1100-1200 K), where the reactions  $\text{H}_2\text{O}_2 \rightarrow 2\text{OH}\cdot$  and  $\text{H}\cdot + \text{O}_2 \rightarrow \cdot\text{OH} + \cdot\text{O}\cdot$  are active.

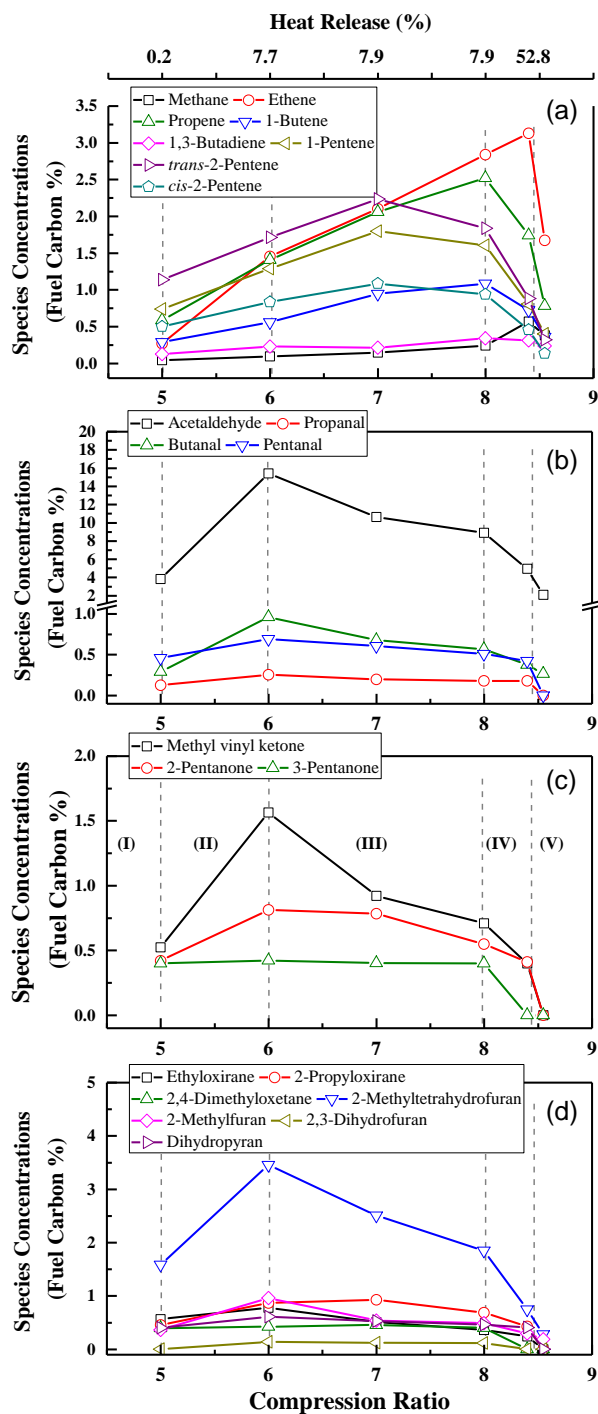


Figure 5-7 Intermediate species of *n*-pentane oxidation (a) alkenes (b) aldehydes (c) ketones and (d) cyclic ethers

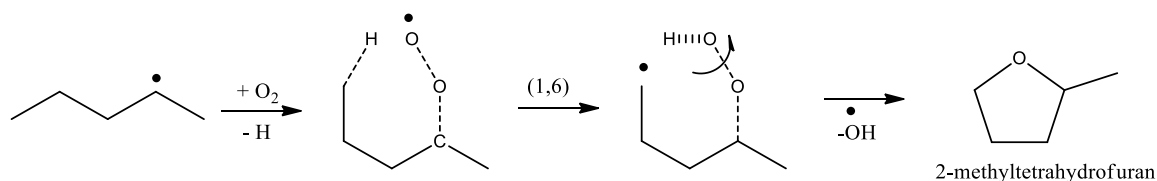


Figure 5-8 A proposed reaction path forming 2-methyltetrahydrofuran in low temperature oxidation of *n*-pentane

### 5.5.2.2 Product analysis of neo-pentane oxidation

Unlike *n*-pentane, neo-pentane is a simple branched alkane, and it has unique molecular structure in that only one parent radical (neo-C<sub>5</sub>H<sub>11</sub>•) can be formed during low temperature oxidation, thus leaving less reaction paths and forming less intermediate species than other isomers. Stable intermediate species formed in the low temperature oxidation of neo-pentane were obtained at various CRs, including CR 5 and 6.5 in LTO, CR 7 and 8.5 in NTC regime, and CR 9.5 and 10.1 in HTO. The first group includes alkenes (C<sub>2</sub>-C<sub>3</sub>), acetylene and *iso*-butene. The second group includes methacrolein, *iso*-butylaldehyde, pivalaldehyde and 2-methyl-2-propen-1-ol. The last group contains acetone, biacetyl and 3,3-dimethyloxetane. Major products mentioned above are also found in previous flow reactor [74] and jet stirred reactor (JSR) [68] studies. The peak for acetaldehyde was not fully separated in GC spectrum, thereby acetaldehyde was unable to be quantified in this study for the neo-pentane experiments. On the other hand, 2-methyl-2-propen-1-ol and biacetyl were newly observed in this study.

Figure 5-9 shows the variation of major products with compression ratio. At the onset of LTHR (~700 K), the main intermediate species formed are 3,3-dimethyloxetane, methacrolein, *iso*-butylaldehyde, acetone and *iso*-butene. Then, in the LTO regime (700-800 K), formation of these oxygenated species becomes favored with significant

increases in their measured concentrations. However, the formation of *iso*-butene tends to be unvarying in this regime as shown in Figure 5-9 (a). This is consistent with the fact that the formation of acetone and *iso*-butene are competitively controlled by the rate of tert-butylperoxy radical isomerization [74]. Acetone and formaldehyde can be formed through the active pathways in low temperature regime. The one of the active pathways forming acetone is shown in Figure 5-9, being formed from  $\beta$ -scission of neo-C<sub>5</sub>H<sub>11</sub>O radical.

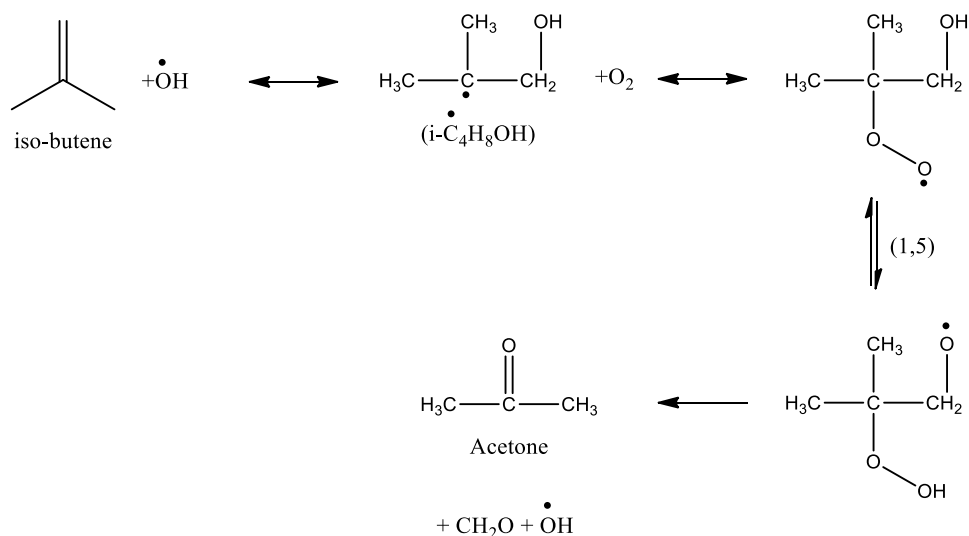


Figure 5-9 Possible reaction pathways of a competitive formation of acetone and *iso*-butene from *i*-C<sub>4</sub>H<sub>8</sub>OH radical in low temperature regime

In the NTC regime (800-900 K), the opposite phenomena in forming major intermediate species are discovered, indicating the reaction path to form *iso*-butene is likely to be dominant in the NTC regime. As can be seen in Figure 5-10, a reaction pathway is proposed to form *iso*-butene. After isomerization of the neopentyl-peroxy radical via internal H-atom transfer to form a hydroperoxy-neopentyl radical, neo-

•C<sub>5</sub>H<sub>10</sub>OOH, the β-scission is conducted to form *iso*-butene and formaldehyde. This reaction path slows the oxidation rate of neo-pentane, and produces its NTC behavior.

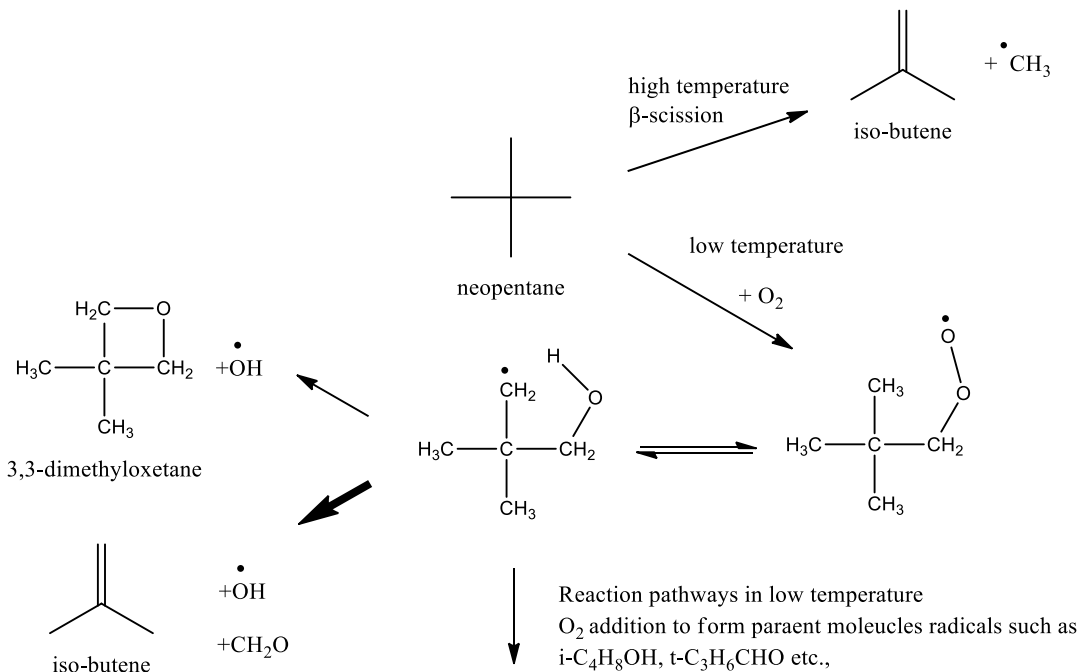


Figure 5-10 Possible reaction pathway forming *iso*-butene and formaldehyde in negative temperature coefficient (NTC) regime during neo-pentane oxidation

Except for the *iso*-butene, formations of other major oxygenated species follows the trend of acetone, whose reaction path is gradually inhibited during the NTC regime. The concentration of major species suddenly rises in the HTO regime, due to the fast burning rate of neo-pentane attacked from the active radicals. Then those species again drop off as HTHR occurred. However, even in HTO regime, *iso*-butene can be formed through the β-scission made directly from parent radical neo-C<sub>5</sub>H<sub>11</sub>•. This pathway contribute to formation of *iso*-butene in HTO regime, as can be seen in Figure 5-10. The concentration profiles of major intermediate species are in agreement with the published

modeling results, accounting for the unique ignition behavior of neo-pentane over a wide range of temperatures.

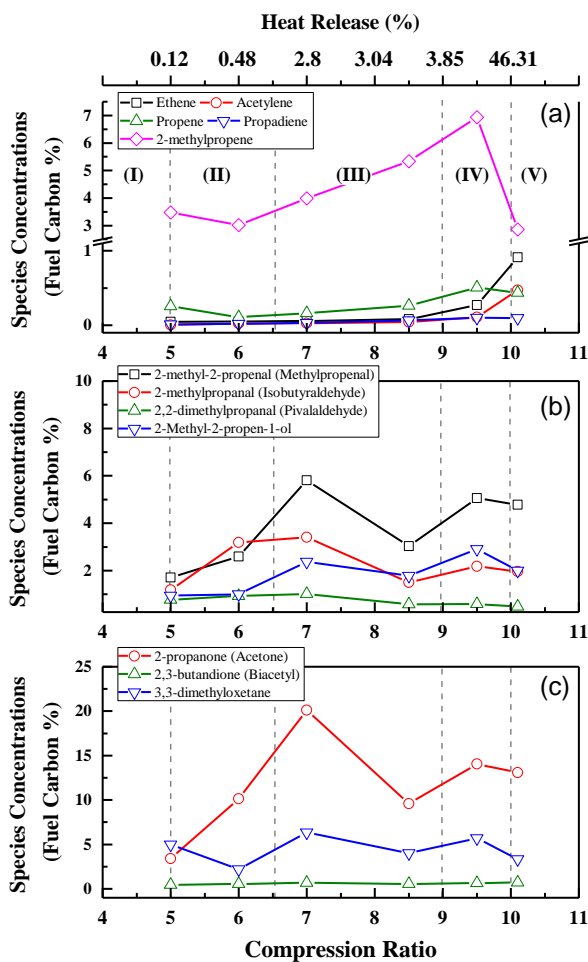


Figure 5-11 Intermediate species of *neo*-pentane oxidation (a) small alkenes (b) aldehydes and 2-methyl-2-propen-ol (c) other oxygenates

### 5.5.2.3 Product analysis of *iso*-pentane oxidation

As discussed earlier, *iso*-pentane has the least reactivity among the pentane isomers, because a methyl substituent on an alkane chain decelerates the oxidation rate by providing fewer hydrogens available for (1,5) H-shift isomerization. The intermediate

species analysis formed from *iso*-pentane oxidation may account for the unique ignition behavior of *iso*-pentane over a wide range of the ignition process, as compared to other isomers. Products analyses of *iso*-pentane oxidation were conducted at different CRs; including CR 6 in LTO, CR 8, 10, 11 in NTC regime and CR 12.5 and 13.1 in HTO. To the author's knowledge, these results represent the first detailed product analysis for *iso*-pentane oxidation.

Variation of major intermediate species with compression ratio is shown in Figure 5-12. The first group involves the various alkenes, which gradually increase as temperature increases. The second group involves conjugate alkenes and isoprene, which are major products in LTO and NTC regime. The third and fourth groups include the oxygenated species, and those profiles are similar. It is also revealed that acetaldehyde is one of the dominant products in entire regime, as shown in Figure 5-12 (c). The active routes for inhibiting overall reaction rate are introduced by the formation of 3-methyltetrahydrofuran and 3-methylbutanone shown in Figure 5-12 (d). It should also be noted that the oxygenated species tend to maintain their yields or even increase during the NTC regime, which behaves differently than the trends observed for *n*-pentane and neopentane. This phenomenon is likely to account for the weaker reactivity for *iso*-pentane, in that the reaction paths to form unreactive species still compete with a reaction path to form peroxide species until the end of NTC regime. In the thermal-runaway regime, the active radicals formed in HTO attack the unburned fuel, resulting in the great amount of intermediate species and CO quickly formed by rapid chain branching reactions and again dropped at HTHR.

The conjugate alkenes, 2-methyl-1-butene, 3-methyl-1-butene and 2-methyl-2-butene, are again dominant products in both the low temperature and the NTC regimes. As reaction enters the NTC regime, formation of conjugate alkenes becomes slower, while the formation of CO and oxygenated species is nearly constant or even decreases. This indicates that relative production of conjugate alkenes is actually promoted in agreement with the conventional explanation of NTC chemistry. As can be seen in Figure 5-12 (b), among the conjugate alkenes formed in the NTC regime, relative yields of 2-methyl-1-butene, 3-methyl-1-butene and 2-methyl-2-butene are around 1, 0.6 and 0.53, respectively, normalized by 2-methyl-1-butene. This can be roughly expected based on the reactivity of primary, secondary, and tertiary hydrogen atoms in the position of methyl substituents on the carbon backbone.



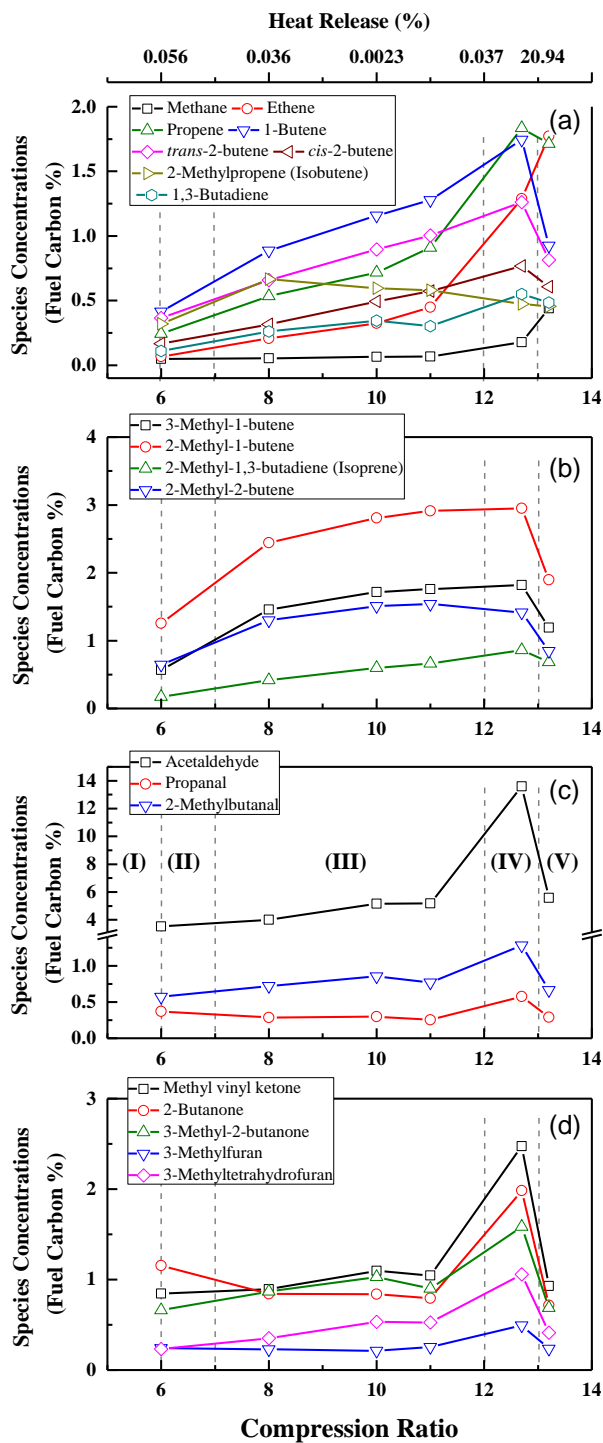


Figure 5-12 Intermediate species from *iso*-pentane oxidation (a) alkenes (b) conjugate alkenes (c) aldehydes (d) ketones and cyclic ethers

## 5.6 Conclusions

This study considers the autoignition of three pentane isomers in a single cylinder CFR motored engine at an intake temperature of 120°C. Products formed from low temperature oxidation of these pentane isomers are investigated over a wide range of compression ratios, and their relationship to the overall oxidation reactivity is suggested. Significant findings are as follows:

1. The unique molecular structures of each pentane isomer lead to different autoignition reactivity. This results in *n*-pentane showing the strongest oxidation reactivity followed by neo- and *iso*-pentanes in terms of the critical compression ratio, with a good agreement in comparable negative temperature coefficient (NTC) behaviors shown in the profiles of CO formation and unburned fuel conversion.

2. The percentage of low temperature heat release (% LTHR) shows a stronger two-stage heat release for *n*-pentane than for neo-pentane at critical ignition conditions. In contrast, single stage heat release is observed for *iso*-pentane, leading to the weakest overall oxidation reactivity of the three isomers.

3. Key reaction paths forming conjugate alkenes and C5 oxygenated species control the autoignition reactivity of *n*-pentane and *iso*-pentane in the low temperature and NTC regimes. However, neo-pentane forms no conjugate alkene due to its unique molecular structure, and instead produces *iso*-butene to retard its overall reaction rate during oxidation.

4. The conjugate alkenes, 2-methyl-1-butene, 3-methyl-1-butene, 2-methyl-2-butene, are formed by the oxidation of *iso*-pentane, with relative yields about 1.0, 0.6 and

0.53, respectively. These relative yields support the reactivity of primary, secondary, and tertiary hydrogen atoms in the position of methyl substituents on the carbon backbone.

## Chapter 6

### Combined Impact of Branched and Unsaturation on the Autoignition of Binary Blends in a Motored Engine

#### 6.1 Introduction

Autoignition phenomena is essentially dependent on the fuel chemical structures and the temperature and pressure of the combustion environment, studies over the past decade have sought to expand the fundamental understanding of the ignition chemistry of representative structural groups (i.e., linear and branched alkane, alkene, cycloalkane and aromatics), during the low temperature oxidation and the negative temperature coefficient (NTC) regime [11–13].

More recently, of particular interest is how different compound classes interact with each other, whether synergistically or antagonistically. Thereby, the demand for extensive study of the combustion of fuel-size hydrocarbons in mixtures motivates the examination of binary mixtures consisting of different classes of hydrocarbons, and mixtures of other compound classes in primary reference fuels (PRF) [21,54,98,66]. The

chemical and physical characteristics of well-chosen surrogate mixtures can possess similar autoignition behavior, hydrocarbon functional groups, and low and intermediate temperature oxidation reactivity as conventional full boiling range fuels [55,99,97]. This approach may contribute to reliable predictions of various combustion properties (i.e., ignition behavior, burning velocity, viscosity, vaporization and emission) of practical fuels.

Therefore, recognizing a lack of the fundamental understanding for ignition characteristics of binary blends mentioned above, the current study focuses on the effects of the degree of unsaturation and branching on the autoignition characteristics of binary mixtures blended with two different hydrocarbon classes under premixed conditions using a modified Cooperative Fuel Research (CFR) octane rating engine. Test fuels were chosen from three different hydrocarbon classes; Diisobutylene (the two common isomers being 2,4,-trimethyl-1-pentene and 2,4,4-trimethyl-2-pentene) was selected as an ideal representative of the hydrocarbon class of highly branched alkenes, possessing a double bond in the carbon skeletal structure of *iso*-octane. *n*-Heptane and *iso*-octane were chosen to represent saturated linear alkanes, often used as diesel surrogates, and saturated branched alkanes, often used as gasoline surrogates, respectively. Figure 6-1 illustrates how the added fuel, diisobutylene, is linked with *n*-heptane and *iso*-octane. Therefore, in this work, different amounts of a highly branched and unsaturated fuel (diisobutylene) were added in the hydrocarbon compounds used in primary reference fuels, *n*-heptane and *iso*-octane, to examine the impact of unsaturation on the autoignition process of two different binary blends. As a supplementary investigation, the effect of branching on

autoignition characteristics also has been examined by using a binary blend of a linear alkane (*n*-heptane) and a branched alkane (*iso*-octane).

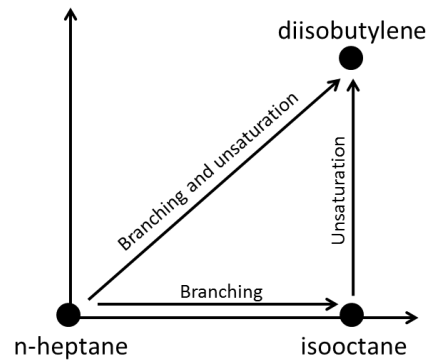


Figure 6-1 Chemical structure parameter of test fuels

Although many ignition studies of blends of primary reference fuels, have been performed under HCCI conditions, only a few previous engine studies have considered diisobutylene neat and in mixtures. Investigations of blends of diisobutylene with *n*-heptane and with *iso*-octane are of great interest, to help understand the ignition characteristics of gasoline surrogates under HCCI conditions. The effect of fuel chemical structures on exhaust hydrocarbons has been examined extensively in spark-ignited (SI) engines. The speciated exhaust emissions from neat diisobutylene are similar to that from neat *iso*-octane, with the exception of significant increases in 2-methyl-1,3-butadiene [122,123]. However, engine out total unburned hydrocarbon (UHC) were much lower from neat diisobutylene than from neat *iso*-octane [122]. Kaiser *et al.* also studied the emissions from a mixture of diisobutylene and gasoline, compared to those of neat diisobutylene and neat gasoline. They found that the UHC emissions from fuel mixtures can be correlated with the known concentration of diisobutylene in the fuel mixture

[123]. Bower *et al.* also reported that the addition of diisobutylene into a fuel mixture caused total UHC to decrease slightly, compared to the total UHC from addition of *iso*-octane [124]. Ninomiya and Golovoy investigated the exhaust hydrocarbons from oxidation of neat diisobutylene and neat *iso*-octane over a wide range of air-fuel ratio [125]. They showed that above fuel rich condition, an olefinic fuel produces less olefinic materials than *iso*-octane fuel, but the reverse is found under a fuel lean condition. Diisobutylene was also used as one of the alkenes in mixtures for gasoline surrogates in order to determine the autoignition quality of practical fuels in SI and HCCI engines [20,126] and also used in order to account for the correlation of low temperature heat release (LTHR) with fuel composition in HCCI engine combustion [28]. Shibata *et al.* observed that different volume additions of a blending fuel in *n*-heptane, compared at the same research octane number, over a range of 75, 80, 85 and 90, can affect LTHR and high temperature heat release (HTHR) behavior in a supercharged four-cylinder engine operated at 1000 rpm. Their study found that increasing volumes of diisobutylene in *n*-heptane can delay CA 50 and HTHR [127], which is confirmed in the present work. However, a binary blend of diisobutylene and *n*-heptane shows less noticeable two-stage ignition, compared to binary blends of *n*-heptane and toluene. Sturgis used a CFR engine to study the knock reactions, with emphasis on the formation of the critical concentrations of stable intermediate species for ignition of *n*-heptane, *iso*-octane and diisobutylene at stoichiometric air fuel ratio [80]. We will make detailed comparisons between Sturgis' and the present work in terms of intermediate species and knock reactivity in the **6.5 Results and Discussion** section.

As mentioned above, the potential use of diisobutylene in surrogate gasoline mixtures has led to research on ignition characteristics of diisobutylene both neat and in multi-component mixtures in practical reactors. Metcalfe *et al.* examined the ignition delay of neat diisobutylene at intermediate temperature and high pressure with fuel lean conditions in a shock tube [37]. They found that the 2-pentene isomer is more ignitable than the 1-pentene isomer and the proportion of each isomer strongly affects ignition delay under shock tube conditions. Fikri *et al.* measured in a shock tube, under various conditions, ignition delay of *quaternary* gasoline surrogate fuels including 10% of diisobutylene, which have octane number comparable to a standard European gasoline of 95 RON at intermediate temperature and three different points of high pressure [43]. Cancino *et al.* and Andrae measured the ignition delay times for *quinary* gasoline surrogate fuels obtained by adding 13% of diisobutylene to the previous quaternary surrogate gasoline mixture in air were measured under stoichiometric conditions behind reflected shock waves [45,55]. In addition, Mittal *et al.* investigated autoignition of 2,4,4-trimethyl-1-pentene (the 1-pentene isomer of diisobutylene) and binary blends with toluene in a rapid compression machine at high pressure and low- and intermediate temperature [66]. They compared ignition delay measurements of neat *iso*-octane, toluene, 2,4,4-trimethyl-1-pentene and their binary blends, and showed that the 1-pentene isomer displays longer ignition delays than *iso*-octane at low temperatures. Also a small amount of 1-pentene isomer added into toluene leads to dramatically faster ignition than neat toluene, whereas addition of toluene to 1-pentene isomer barely affects its ignition delay. Mittal *et al.* also observed that the ignition chemistry of neat or binary fuels at low



temperature experience different ignition chemical reaction paths than at high temperature, resulting in opposite effects on ignition delay.

## 6.2 Research Objectives

Despite the potential of ignition improving characteristics of diisobutylene, few studies have focused on the ignition behavior of diisobutylene and its blends. Furthermore, there are very few reports of the impacts on the ignition behavior and autoignition chemistry of the addition of a branched and unsaturated compound (diisobutylene) in blends with primary reference fuels (*n*-heptane blends and *iso*-octane blends). To address this knowledge gap, the approach in this research is to conduct a systematic investigation of binary blends to characterize the nature of the interactions amongst the fuel constituents, with emphasis on ignition chemistry during low and intermediate temperature reaction in a motored engine environment.

## 6.3 Test Fuels

Three test fuels were studied in this work, *n*-heptane, *iso*-octane (as primary reference fuels), and diisobutylene (as a blend of 67 vol% of 2,4,4-trimethyl-1-pentene and 33 vol% of 2,4,4-trimethyl-2-pentene). Test fuel molecular structures are given in Figure 6-2 and their properties are listed in Table 7. Four blends of diisobutylene and *n*-heptane were prepared by adding 5, 10, 15 and 20% (v/v) of diisobutylene, three blends of diisobutylene and *iso*-octane were prepared by adding 5, 10 and 15% (v/v) of diisobutylene. The 15 vol.% diisobutylene in *iso*-octane blend (referred to as “15DI”) did

not achieve autoignition at any CR, for this reason no higher blends were tested. In addition, four different volume sets of *n*-heptane and *iso*-octane blends were also prepared by adding 5, 10, 15 and 20 % (v/v) of *iso*-octane in *n*-heptane, but they were used only for comparison. As the boiling points of all test fuels were below 120°C, complete vaporization was achieved.

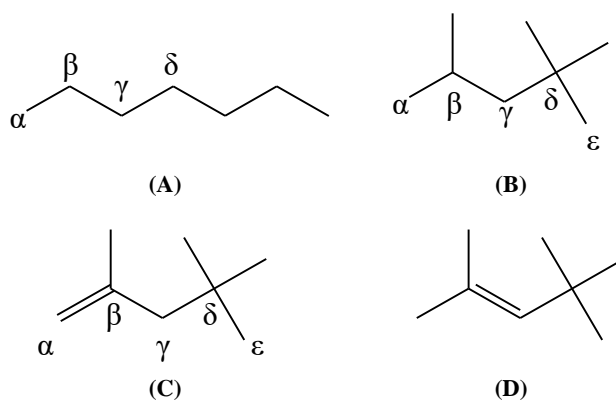


Figure 6-2 Test molecule structures (A) *n*-heptane (B) *iso*-octane (C) 2,4,4-trimethyl-1-pentene, and (D) 2,4,4-trimethyl-2-pentene

Table 7 Properties of pure test fuels

	<i>n</i> -heptane(HEP)	<i>Iso</i> -octane (ISO)	Diisobutylene(DIB)
<b>Formula</b>	C <sub>7</sub> H <sub>16</sub>	C <sub>8</sub> H <sub>18</sub>	C <sub>8</sub> H <sub>16</sub>
<b>Boiling Point (°C)</b>	98.5	99.3	102.5
<b>Vapor pressure (kPa)</b>	5.26 (21°C)	5.34 (21°C)	4.54 (21°C) [128]
<b>Density (kg/m<sup>3</sup>at 25°C)</b>	684	692	712
<b>Molecular density (kg/kmol)</b>	100.2	114.2	112.2
<b>Air/fuel ratio (stoichiometric)</b>	15.18	15.13	14.78
<b>Research octane number</b>	0.53	99.73	158.72 <sup>a</sup>
<b>Motor octane number</b>	0.97	100	148.38 <sup>a</sup>
<b>Cetane number</b>	52.83	18.97	10 [129]

<sup>a</sup> Blending octane numbers, from testing 20% in *n*-heptane blends

## 6.4 Test Conditions

Operating parameters were kept constant during all tests. Experiments for the fourteen fuels were performed with a constant engine speed of 600 rpm and an equivalence ratio of 0.5 because not only would autoignition of *n*-heptane and *iso*-octane occur but this could be a representative condition for homogeneous charge compression ignition (HCCI) combustion. Intake air temperature of 120°C was chosen to guarantee complete fuel vaporization after injection. Cooling jacket temperature was fixed at 90°C. For each fuel tested, the compression ratio (CR) started low enough that no low temperature reaction took place and was then gradually increased in a stepwise manner to increase the extent of reaction. In the cases of *n*-heptane and *iso*-octane, LTHR was

always observed before HTHR took place. Diisobutylene did not achieve HTHR even at the highest CR. The onset of LTHR was determined by observing a sudden increase of CO formation. Testing was repeated once for each fuel. Differences lower than 0.04 in critical compression ratio (CCR) were obtained for all test fuels. In some cases, HTHR was eventually achieved, for this reason the CCR was established here as the CR when the high temperature combustion was sustained. Fuel lines were completely dried and cleaned before operating with each new test fuel.

## **6.5 Results and Discussion**

By monitoring in-cylinder temperature and pressure, and apparent heat release rate, the ignition reactivity of test fuel blends can be determined through ignition behavior such as the percentage of low temperature heat release (% LTHR), which was calculated as in [30];  $\% \text{ LTHR} = \text{LTHR} / (\text{LTHR} + \text{HTHR})$ , and critical compression ratio (CCR). The following sections will discuss the observed ignition behavior while considering impacts of fuel structure for three different binary blends.

### **6.5.1 Heat release analysis**

One way to characterize the ignition behavior of the fuel blends is through heat release analysis. The addition of DIB into the primary reference fuels exerts a strong effect on low temperature oxidation reactivity. As can be seen in Figure 6-3 (a), the

blends of 0, 10 and 20 % v/v DIB in HEP yield a noticeable two stage ignition at the critical compression ratio (CCR) where high temperature ignition is observed. With increasing volume of DIB, the peak of LTHR shifts toward top dead center, reducing NTC behavior and delaying HTHR. In contrast, Figure 6-3 (b) shows that no NTC behavior is observed for 0, 5 and 10% v/v DIB addition in ISO at the CCR, indicating that this blend experiences single stage ignition. The LTHR found in only HEP and DIB blends is mainly due to the presence of sufficient HEP, acting as a radical provider through a hydrogen abstraction at lower temperature. Then, an oxygen addition on the n-heptyl radical can form the heptylperoxy radical, which can initiate growth of the active radical pool of OH through the degenerate branching steps at lower temperature [31]. In contrast, for ISO and DIB blends, initiation by hydrogen abstraction requires a substantially higher activation energy, therefore a more severe combustion environment should be provided to initiate degeneration, which corresponds to the higher CR required to achieve ignition. In Figure 6-3 (c), the compression ratio has been varied to yield similar LTHR profiles, so that the apparent heat release profiles show only low temperature heat release. Neat HEP shows the strongest oxidation reactivity showing the highest LTHR rate at CR of 5.24, which is the lowest CR, compared to the other fuel blends. Increasing amounts of DIB added to HEP results in weaker oxidation reactivity, with a higher CR required for the test mixtures to be ignited, as DIB content increases. Because HEP is a source of active radicals and improves low temperature oxidation reactivity, decreasing amounts of HEP makes for a more radical poor environment in the low temperature regime. In addition, as HEP decreases in binary mixture, less thermal impact can be found from lower gas temperature generated during compression of engine

cylinder, which can delay HTHR. As can be seen in Table 8, the increasing addition of DIB in HEP delays the CCR where HTHR takes place.

Sturgis observed a delayed CR of cool flame duration caused by the addition of 24 v/v % DIB in HEP. The cool flame duration is defined as the difference in CR at the start of cool flame relative to the CR at the start of autoignition. Addition of DIB of 24 v/v% in HEP results in the increase of the cool flame duration (in terms of CR) by 3.9, compared to no addition of DIB [80]. The same inhibitory effect of DIB addition in HEP has been observed in HCCI engine by Shibata *et al.* [127]. The gradual additions of DIB (49, 54, 58 to 62 v/v %) in HEP improve their octane number (ON) by 5 (RON 75, 80, 85 and 90) and results in a gradual delay of CA 50 from TDC (RON 75) to 5 deg ATDC (RON 90). In the same manner, DIB plays a significant role in decreasing the peak of heat release rate as shown in Figure 6-3 (d). At a CR of 14, the peak of heat release decreases with gradual increase of the amount of DIB in ISO. However, no AHRR has been observed at CR of 14 for the cases beyond 10% or more v/v DIB additions. The role of DIB in suppressing reactivity can be explained as a stabilization of the allylic-type radicals formed from HO<sub>2</sub> radical attack on the double bond in DIB [130]. In addition, these observations confirm the expected trend in that low temperature reactivity under premixed conditions in many previous studies [66,131,132] follows the order, HEP >> ISO > DIB, which is consistent with the cetane number of the fuels. However, some early engine studies reached an opposite conclusion in concerning the reactivity difference between DIB and ISO. Bower [124] using an SI engine and Sturgis [80] using a CFR engine both reported greater knock resistance for ISO than for DIB. This represents an interesting dichotomy between the knock resistance of these compounds and their extent

of low temperature oxidative reactivity. The present work focuses on the latter, the extent of LTHR, NTC behavior and transition to HTHR, for the neat compounds and their blends. Knock resistance reported by Sturgis [80] for ISO and DIB is for the neat compounds, and shows that ISO exhibits a higher knock limited compression ratio. But consistent with the present work, Sturgis also saw that DIB exhibits a stronger impact on impeding the autoignition of HEP in blends. Finally, the heat release analysis also indicates that an added fuel whose structure is more branched and unsaturated, can suppress the autoignition reactivity of the fuels, whose structure is relatively simple, when these fuels are mixed.

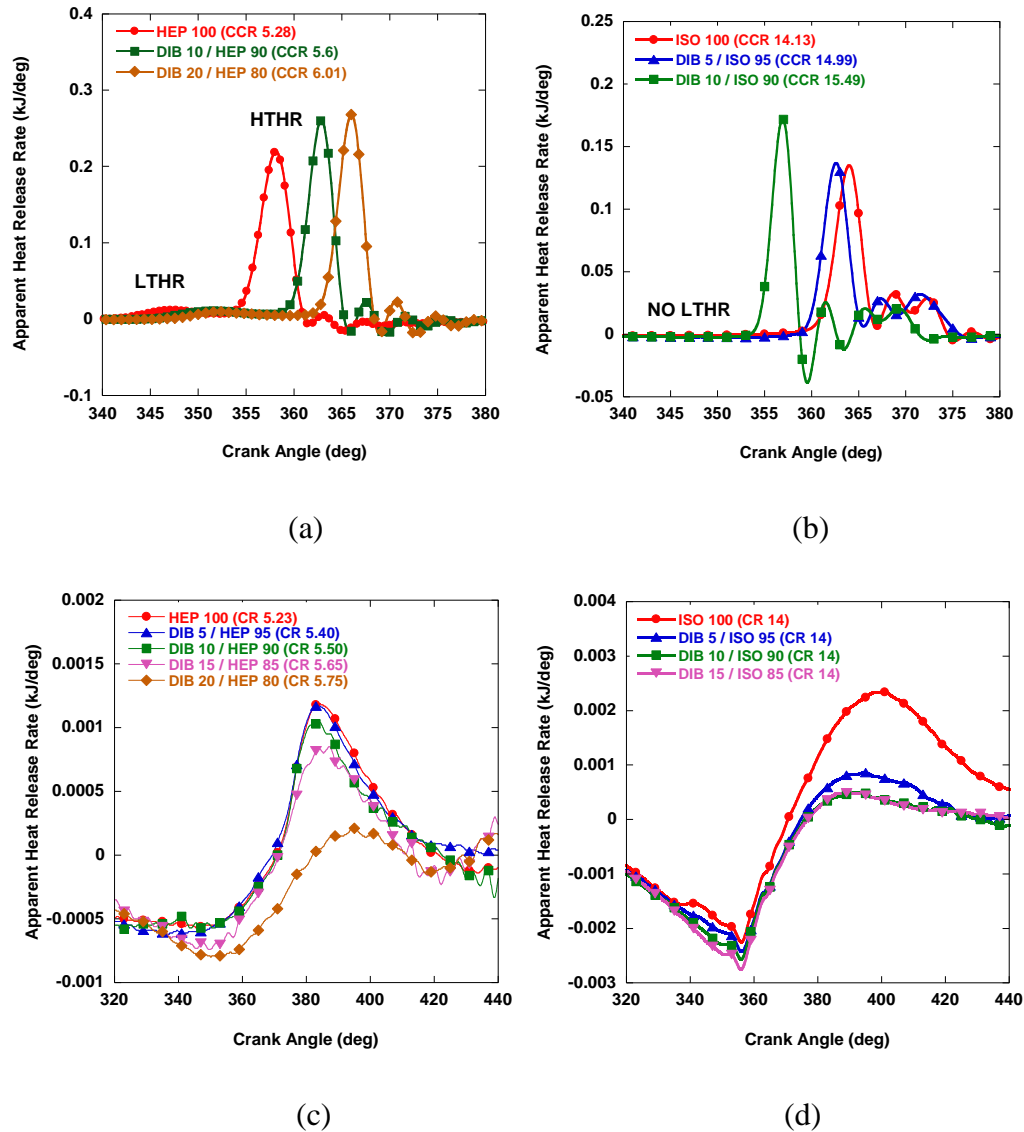


Figure 6-3 High temperature heat release as a function of crank angle for (a) 0, 10 and 20 wt % v/v diisobutylene (DIB) blended in *n*-heptane (HEP) and (b) 0, 5 and 10 wt % v/v diisobutylene (DIB) blended in *iso*-octane (ISO) ; (c) Low temperature heat release for 0, 5, 10, 15 and 20 wt % v/v diisobutylene in *n*-heptane (HEP) at CRs ; (d) Apparent heat release for 0, 5, 10 and 15 wt % v/v diisobutylene in *iso*-octane (ISO) at CR of 14.

The maximum in-cylinder temperatures, just prior to HTHR, for all HEP blends and ISO blends as a function of CR are presented in Figure 6-4. These results clearly indicate the strong two-stage ignition behavior of the HEP blends. Compared to the HEP



blends, however, ISO and its blends display mild NTC behavior at elevated CR and temperature. The HEP blends display a peak temperature increase from about 695K for DIB 5 / HEP 95 (5% of DIB in HEP) to about 758K for DIB 20 / HEP 80. Figure 6-4 (a) shows that increasing the amount of DIB added to HEP provides a broader NTC region and requires higher temperature to initiate chain branching reaction, arising from the comparatively lower oxidation reactivity of DIB. The evident NTC behavior observed in Figure 6-4 (a) is a result of a competition between chain branching and chain propagation reactions. As the temperature increases, chain propagation reactions begin to dominate, resulting in a reduction in the reaction rate. Likewise, in-cylinder temperature for ISO blends increases with increasing addition of DIB. The maximum temperature prior to HTHR during NTC regime is shown to increase from around 820K for DIB 5/ ISO 95 (5% of DIB in ISO) to around 850K for DIB 15 / ISO 85. In all cases shown in Figure 6-4 (b), the NTC region was widely present from CR of 11 to 13.5, supporting the expected observation that the oxidation reactivity of ISO blends is far lower than that of the HEP blends.

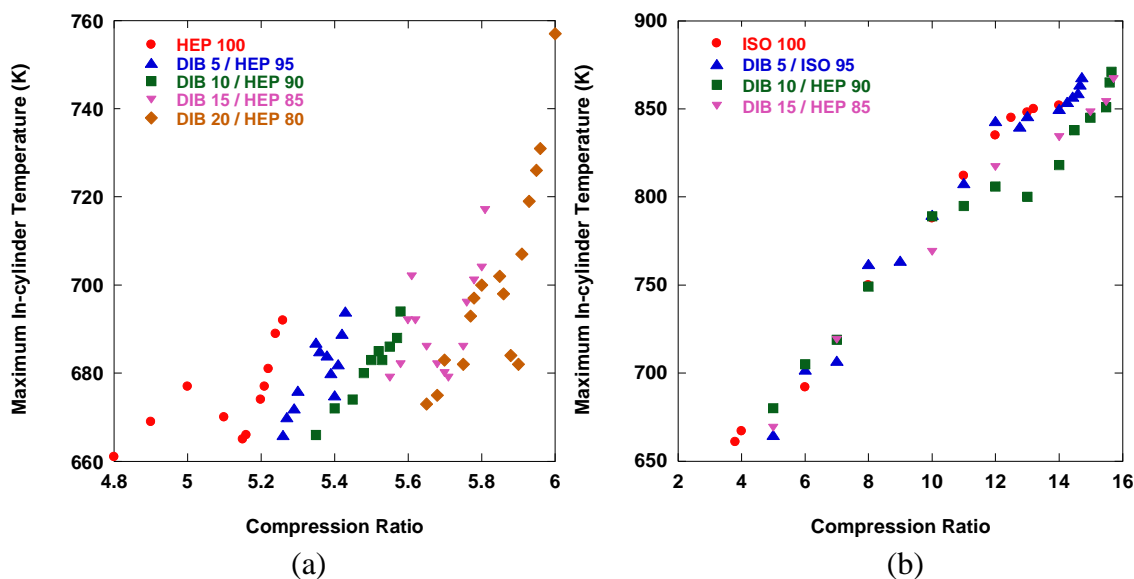


Figure 6-4 Maximum in-cylinder temperature for (a) diisobutylene / *n*-heptane blends and (b) diisobutylene / *iso*-octane blends

### 6.5.2 CO emission analysis

Carbon monoxide emissions as a function of CR presented in Figure 6-5 confirm the retarding effect of DIB on the low temperature oxidation reaction. Shown in Figure 6-5 (a), as DIB was gradually added to HEP, the low temperature oxidation required higher pressure and temperature, corresponding to higher CR, to take place. Noticeable CO emission is initially observed at the onset of LTHR and rapidly increases even with a slight rise of CR. The maximum CO emission is detected at a CR just before full or second stage ignition, referred to as HTHR, and increases with additional DIB in the blend. The CO emission is mostly formed from the aldehydes, which are built from the major intermediate species through C-C  $\beta$ -scission of alkylketohydroperoxide group. Additions of branched and unsaturated structure fuel contribute to building more intermediate species of HEP oxidation in the NTC regime, while delaying the actual

ignition (HTHR). Therefore, CO formation increases with the addition of branched and unsaturated structure fuel in the NTC regime. Figure 6-5 (a) also shows that a small NTC region appears for the DIB 15 / HEP 85 blend and becomes wider for the DIB 20 / HEP 80 blend. As can be seen in Figure 6-5 (b), however, very small amounts of CO emissions are observed from the oxidation of ISO and DIB blends, compared to the HEP and DIB blends. This indicates that the ISO and DIB blends rarely participate via conversion into intermediate species in the low temperature regime. In addition, the decrease in CO emissions as DIB was added to ISO confirms that DIB also depresses the reaction due to the presence of the double bond in DIB. However, the oxidation reaction mechanism is somewhat different from that of the HEP blends, since the NTC behavior observed in the ISO blends tends to disappear as DIB is gradually increased. The addition of DIB provides an increasing presence of double bonds (serving as a radical scavenger), thereby diminishing LTHR and NTC behavior. As a result, a rapid growth of CO emission at the onset of LTHR disappears with addition of the unsaturated component, as shown in Figure 6-5 (b). Finally, in both cases, CO emissions dramatically decrease as CO is rapidly converted to CO<sub>2</sub> when HTHR occurs [76].

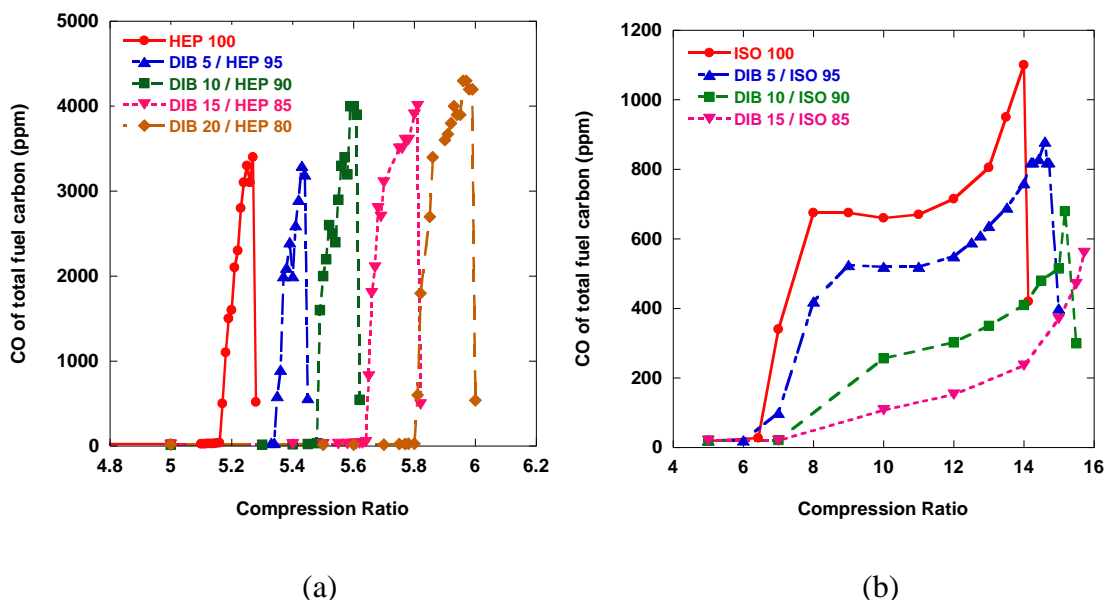


Figure 6-5 CO emissions from the oxidation of (a) *n*-heptane and blends with diisobutylene and (b) *iso*-octane and blends with diisobutylene

### 6.5.3 Structural impact on ignition characteristics

The evidence of structural impact on ignition reactivity of each test blend can be also found through fundamental ignition behaviors such as the determination of CCR, where the actual HTHR occurs, and % LTHR. As can be seen in Figure 6-6 (a), increasing volume amount of unreactive fuel (branching, unsaturation, or branching + unsaturation) added into the pure component showed a linear response to the delayed CCR up to 20% blends. Furthermore, the presence of a double bond in DIB exhibited more suppressing impact on ignition reactivity, resulting in delayed CCR of DIB and HEP blend compared to that of ISO and HEP blend. Figure 6-6 (b) showed the magnitude of the LTHR and % LTHR of binary blends with HEP, once the CCR was achieved. ISO and DIB blend was excluded from the Figure 6-6 (b), due to the absence of LTHR, indicating that the phenomenon of LTHR is likely generated from straight chain

compounds. Increasing volume addition of ISO (branching component) and DIB (branching + unsaturation component) into HEP (straight component) contributes to a decrease in the magnitude of % LTHR on both cases. Structural impact on ignition characteristics of test blends is also found in the magnitude of LTHR, resulting in more suppressing LTHR of DIB and HEP than that of ISO and HEP, which is consistent with the result from the CCR.

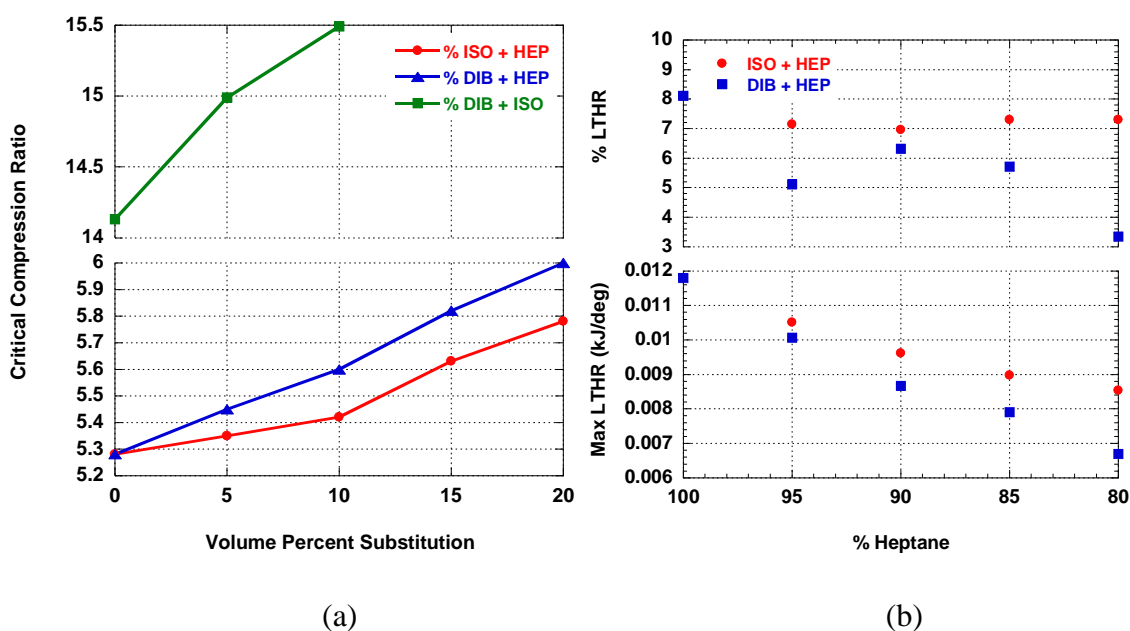


Figure 6-6 Ignition characteristics of the fuel blends, (a) Critical compression ratios of test binary blends at different volume percent substitutions (b) % LTHR and Max LTHR at different % HEP in binary blends. No evidence of LTHR was found in ISO and DIB blend.

#### 6.5.4 Condensed intermediate hydrocarbon species

To gain insight into the impacts of DIB addition on the reaction pathways during low temperature oxidation, major intermediate species are observed by capturing and then analyzing before full or second stage ignition occurs. The goal of this section is to

observe the effects of the addition of DIB (branched and unsaturated structure fuel) into a primary reference fuel (straight and branched structure fuels) on ignition chemistry during low and intermediate temperature oxidation. Therefore, DIB was added from 5% up to 20% v/v into the primary reference fuels. The blends were ignited in the engine cylinder, and then the exhaust was captured at selected CRs. As indicated in Table 8, the intermediate products produced from the oxidation of diisobutylene addition were captured at selected CRs up to just before autoignition occurred (just before the critical compression ratio). Previous motored engine studies of ignition chemistry in the low temperature reaction regime have demonstrated that taking an exhaust sample at selected CR very close to CCR can provide a wide range of large oxygenated intermediate species, including conjugate olefins well known as major products during low temperature oxidation [30,80].

Table 8 Compression ratios (CR) where the intermediates are sampled and analyzed, and critical compression ratios (CCR) where the actual ignition occurred.

	CR of samples captured	Critical CR
HEP (100)	5.2	5.28
HEP (95) -DIB (5)	5.42	5.45
HEP (90) -DIB (10)	5.55	5.6
HEP (85) -DIB (15)	5.7	5.82
HEP (80) -DIB (20)	5.82	6.01
ISO (100)	13	14.13
ISO (95) - DIB (5)	13	14.99
ISO (90) - DIB (10)	14	15.49
ISO (85) - DIB (15)	14	X

As shown in Table 8 and mentioned earlier, the mixtures with 15 and 20 % v/v addition of DIB to ISO were unable to reach the critical compression ratio, indicating that the full ignition was not able to be achieved under these conditions, since the maximum

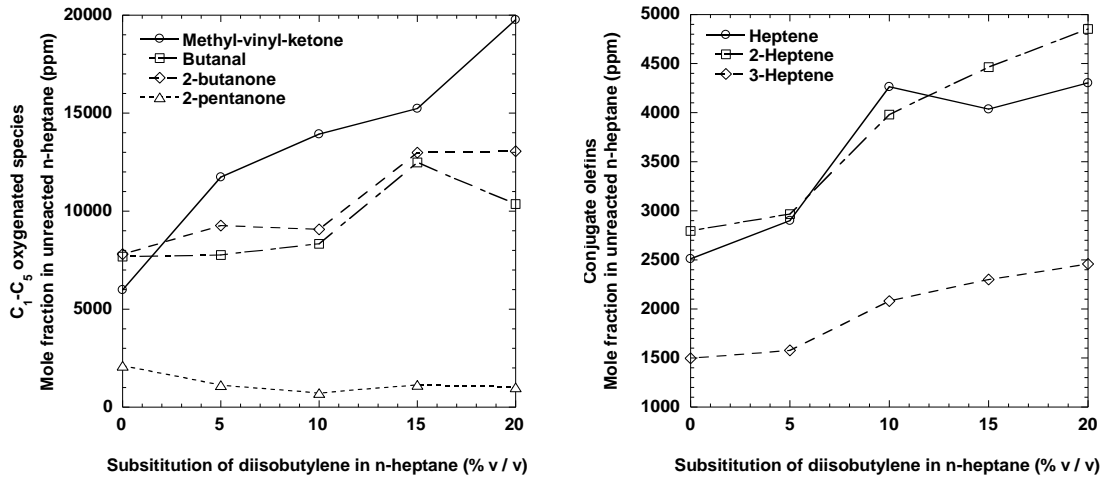
capacity of compression ratio on this CFR engine is 15.7. For this reason, only nine blends were explored including the five different sets of HEP blends and four different sets of ISO blends.

#### 6.5.4.1 *n*-Heptane and diisobutylene blends

The intermediate species produced from the oxidation of HEP and DIB blends can be divided into the following groups; (1) fuel molecules (i.e., *n*-heptane and 2,4,4-trimethyl-1-pentene and 2,4,4-trimethyl-2-pentene), (2) CO and CO<sub>2</sub> (3) olefins (i.e., ethene, propene, 1-heptene, 2-heptene and 3-heptene) (4) aldehydes (i.e., heptanal and butanal) (5) ketones (i.e., 3-buten-2-one, 2-butanone, 2-pentanone, 2-heptanone, 3-heptanone, 4-heptanone and 4,4-dimethyl-2-pentanone) and (6) epoxides (i.e., 2-methyltetrahydropyran, 2-ethyl-3-propyloxirane and 2-butyl-3-methyloxirane).

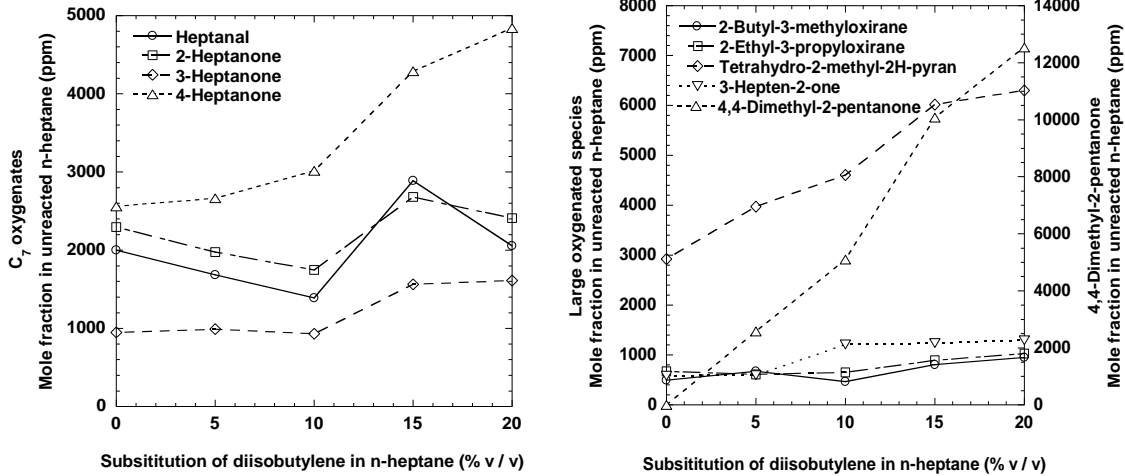
These intermediates are mainly derived from the oxidation of HEP, reflecting the considerable reactivity of HEP in the low temperature regime, which is in stark contrast with the lack of low temperature heat release behavior as well as the lower quantities of CO emissions for blends of ISO and DIB. Figure 6-7 shows that the yields of most intermediates species tend to increase as more DIB is added, although the volume of HEP decreases. The small molecules including butanal, 2-butanone and 3-buten-2-one yielded higher concentrations than the other products. This observation explains that alkylhydroperoxy radical experiences a second oxygen addition and internal hydrogen abstractions to form alkylketohydroperoxide (HOOQOOH), which decomposes into hydroxyl radicals and smaller species from breaking the C-C backbone. In a previous study on knock chemistry of HEP and DIB, Sturgis reported that HEP decomposition favored formation of aldehydes and ketones, and no noticeable intermediate products

from partial oxidation of DIB can be observed until just prior to autoignition [80]. This observation also supports less active participation of DIB during the low temperature reaction of HEP and DIB blends, except the formation of 4,4-dimethyl-2-pentanone.



(a)

(b)



(c)

(d)

Figure 6-7 Mole fractions of intermediates species from the oxidation of blends with *n*-heptane and different volume % of diisobutylene at selected compression ratios at test conditions as per Table 8.



As can be seen in Figure 6-7 (d), a noteworthy observation is that the concentration of 4,4-dimethyl-2-pentanone rapidly increases in proportion to the addition of diisobutylene, indicating that the formation of 4,4-dimethyl-2-pentanone is directly related to the addition of diisobutylene and its highest concentrations can be found at the extreme conditions right before second stage ignition occurs. This indicates that 4,4-dimethyl-2-pentanone is structurally stable in the ignition process. From the mechanism proposed by Stark and Waddington [133], the formation of 4,4-dimethyl-2-pentanone in low temperature regime occurs from the addition of OH radicals to the double bond in 2,4,4-trimethyl-1-pentene. Most OH radicals selectively attacking the double bond can be provided from the propagation reaction of *n*-heptane in lower temperature regime. The subsequent oxygen addition to hydroxyalkyl radicals can form hydroxypentylperoxy radicals, which experience the isomerization, finally leading to the formation of 4,4-dimethyl-2-pentanone with aldehydes and OH radicals, as shown in Figure 6-8. From the one of the characteristics of low temperature oxidation of alkene [12,130], it is noted that the reversibility of the addition to oxygen of hydroxyalkyl radicals during the formation of 4,4-dimethyl-2-pentanone contributes to the existence of a NTC behavior observed in the oxidation of *n*-heptane and diisobutylene blends.

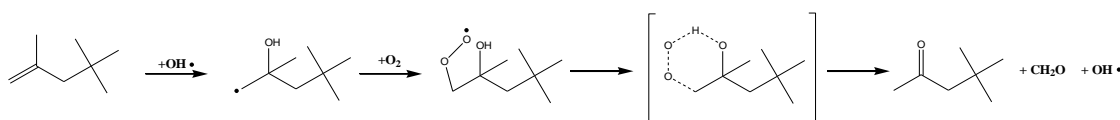


Figure 6-8. A reaction pathway leading to the formation of 4,4-dimethyl-2-pentanone derived from 2,4,4-trimethyl-1-pentene during low temperature oxidation of *n*-heptane blends

Conjugate olefins including 1-heptene, 2-heptene and 3-heptene are formed in different reaction pathways, as shown in Figures 6-9 (D), 6-9 (E) and 6-10 (C). Depending on the location where the initial hydrogen abstraction occurs, the conjugate olefins can be formed through subsequent oxygen addition and (1,4) H-shift isomerization leading to the formation of HO<sub>2</sub> radicals or C-C double bonds at different positions on *n*-heptane. The substantial formation of conjugate olefins mentioned above supports the opportunity for the (1,4) H-shift during the isomerization of the fuel peroxy radicals. Likewise, the ketones including 2-heptanone, 3-heptanone and 4-heptanone, and an aldehyde including 1-heptanal, can be formed depending upon the location where the initial hydrogen abstraction and H-shift isomerization reaction takes place on *n*-heptane. Quantitative analysis of exhaust emissions indicate that these two major groups of conjugate ketones and conjugate olefins are competitively formed during H-shift isomerization, eliminating OH and HO<sub>2</sub> radicals, respectively. As a result of quantitative analysis for different proportions of diisobutylene addition, 4-heptanone and 2-heptene are likely the most favored species to be formed in ketone and olefin groups. In contrast, that 1-heptanal is the least abundant amongst the intermediates is mainly due to the least favored place for primary hydrogen at  $\alpha$ -carbon to be shifted to form alkylhydroperoxy radical [34]. Despite of decreasing participation of *n*-heptane in HEP-DIB oxidation, the formations of these major species tend to increase with gradual addition of diisobutylene in test fuel matrix. As mentioned earlier, this is because increasing volume of diisobutylene likely contributes to prolong NTC behavior, therefore *n*-heptane in blend can participate in forming more intermediate species during the low temperature oxidation of HEP and DIB blend.

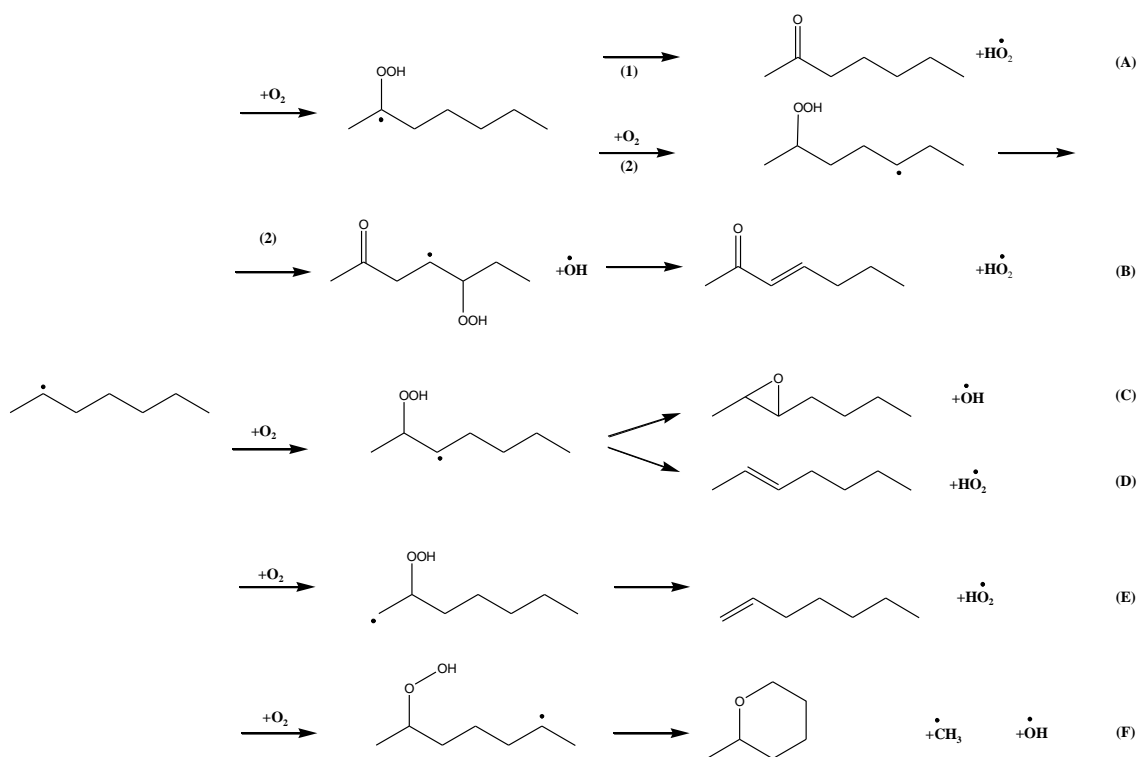


Figure 6-9 Possible reaction pathways leading to the formation of various intermediate species derived from radical attack on beta-carbon of *n*-heptane in low temperature oxidation of *n*-heptane blends: (A) 2-heptanone; (B) 3-hepten-2-one; (C) 2-butyl-3-methyl-oxirane; (D) 2-heptene; (E) 1-heptene; and (F) 2-methyltetrahydropyran

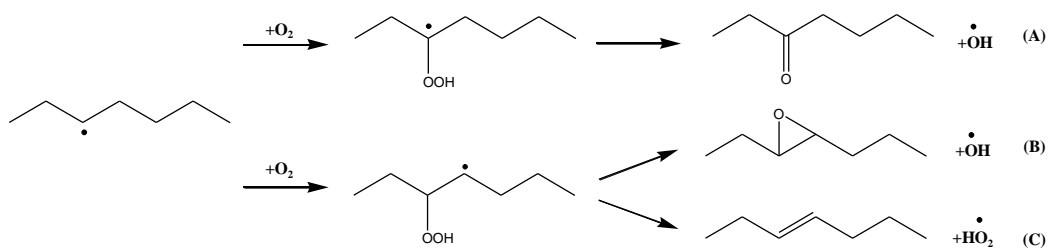


Figure 6-10 Possible reaction pathways leading to the formations of various intermediate species derived from radical attack on gamma-carbon of *n*-heptane in low temperature oxidation of *n*-heptane blends. (A) 3-heptanone; (B) 2-ethyl-3-propyl-oxirane; and (C) 3-heptene

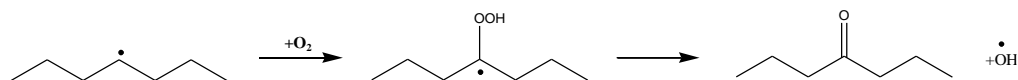


Figure 6-11 A possible reaction pathway leading to the formation of 4-heptanone derived from radical attack on sigma-carbon of *n*-heptane in low temperature oxidation of *n*-heptane blends.

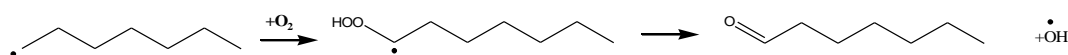


Figure 6-12 A possible reaction pathway leading to the formation of heptanal derived from radical attack on alpha-carbon of *n*-heptane in low temperature oxidation of *n*-heptane blends.

As can be seen in Figures 6-9 (C), 6-9 (F) and 6-10 (B), 2-butyl-3-methyloxirane and 2-ethyl-3-propyl-oxirane are formed through (1,4) H-atom transfer and 2-methyltetrahydropyran is formed through (1,7) H-atom transfer. Comparing the concentrations of 2-methyltetrahydropyran and oxirane, 2-methyltetrahydropyran is more abundant than oxirane, which is mainly due to the lower strain energy barrier for (1,7) H-atom transfer than for (1,4) H-atom transfer. An interesting observation is that no formation of tetrahydrofurans was found in this work, even though the lowest strain energy barrier for H-atom transfer on *n*-heptane is (1,6) H-atom transfer to form tetrahydrofurans, already observed in the study of low temperature oxidation of *n*-heptane and 1-butanol binary blends [85].

### 6.5.4.2 *Iso*-octane and diisobutylene blends

The intermediate species from the low temperature oxidation of *iso*-octane and different volume % addition of diisobutylene were captured at the compression ratios shown in Table 8. These intermediates species can be classified into five groups: (1) Fuels (2,4,4-trimethylpentane and 2,4,4-trimethyl-1-pentene and 2,4,4-trimethyl-2-pentene); (2) CO and CO<sub>2</sub>; (3) Aldehydes (2-methyl-propionaldehyde, 2,2-dimethyl-propionaldehyde and 2-methylpropenal); (4) Conjugate olefins (2,4-dimethyl-pent-1-ene, 4,4-dimethyl-pent-1-ene, 2,4-dimethyl-pent-2-ene and 4,4-dimethyl-pent-2-ene); and (5) Ketones and Epoxide (3-buten-2-one, 4,4-dimethyl-pentan-2-one and 2,2,4,4-tetramethyl-tetrahydro-furan). Figure 6-2 shows the molecular structures of *iso*-octane and diisobutylene, which is comprised of the two isomers 2,4,4-trimethyl-1-pentene and 2,4,4-trimethyl-2-pentene. Small amounts of these two diisobutylene isomers are observed as some of the major intermediate species from the low temperature oxidation of *iso*-octane and their possible formation pathways from *iso*-octane during low temperature oxidation are suggested in Figure 6-13.

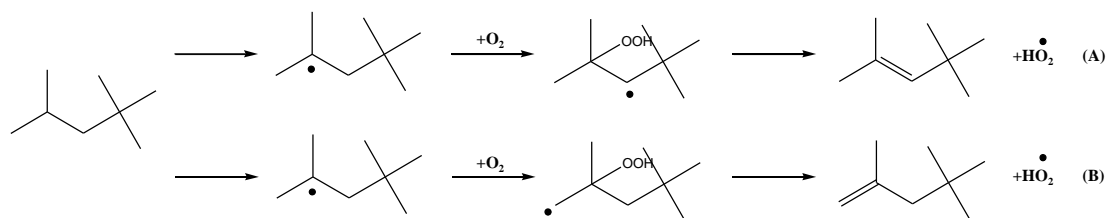
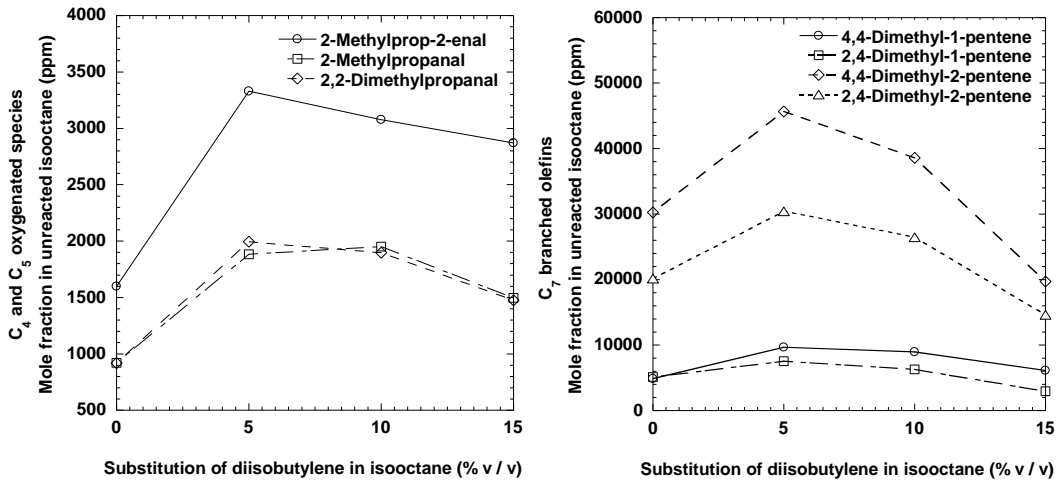


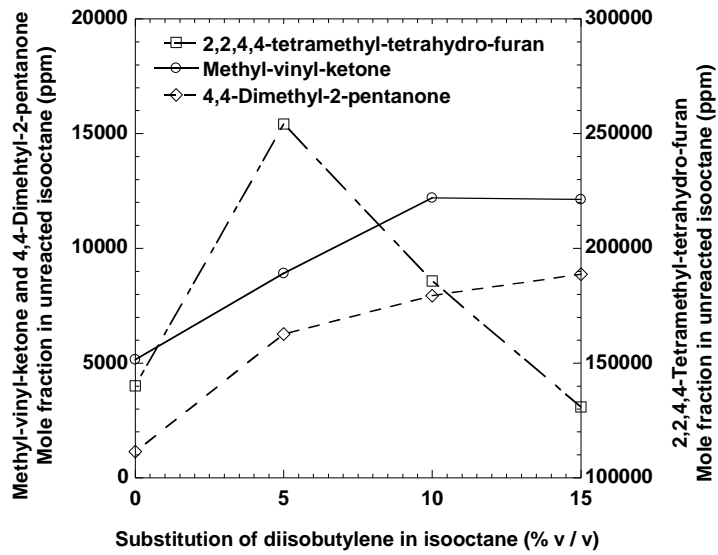
Figure 6-13 Possible reaction pathways leading to the formation of diisobutylene from the low temperature oxidation of 2,4,4-trimethylpentane: (A) 2,4,4-trimethyl-2-pentene; and (B) 2,4,4-trimethyl-1-pentene

Figure 6-14 shows the intermediate species from the low temperature oxidation of *iso*-octane and diisobutylene that were captured at the designated compression ratios identified in Table 8 and the concentrations of intermediate species as a function of diisobutylene addition. The trends look very similar for most intermediate species in that as the volume of diisobutylene increases, the formation of intermediate species from *iso*-octane reaches a relative maximum. In contrast, the ketones group including methyl-vinyl-ketone and 4,4-dimethyl-pentan-2-one increases with increasing addition of diisobutylene. These trends can be explained in that increasing amounts of diisobutylene suppress low temperature reactivity, resulting in decreasing formation of stable intermediates, except 4,4-dimethyl-2-pentanone and methyl-vinyl-ketone. Also, the abundance of aldehydes with respect to increasing addition of diisobutylene shown in Figure 6-14 (A) corresponds to the that of CO formation, shown in Figure 6-5 (b), supporting the observation that the aldehydes are likely the main resource for CO formation [83]. In the present work, as with HEP and DIB blends ISO and DIB blends favored the formation of various olefins shown in Figure 6-14 (b), which has also been reported in a study of knock chemistry at stoichiometric air-fuel ratio during cool flame regime [80]. In contrast, Sturgis also reported that no noticeable amount of olefins was observed in the examination of the knock chemistry of neat DIB. Thus as reported in this work, these various olefins whose formation is favored during low temperature oxidation of blends of ISO and DIB are mostly likely decomposed from ISO.



(a)

(b)



(c)

Figure 6-14 Mole fractions of intermediates species from the oxidation of blends with *iso*-octane and different volume % of diisobutylene at compression ratios before the actual auto-ignition is occurred.

As can be seen in Figure 6-15, the reaction pathways for C<sub>6</sub> branched alkenes can be initiated with a radical attack, providing hydrogen abstraction on β-carbon position of *iso*-octane. Following oxygen addition and its isomerization forms 2,4,4-trimethyl-pent-2-yl-hydroperoxide radical. The radical is formed on γ-carbon of *iso*-octane and subsequent decomposition of the hydroperoxide radical via C-C bond β-scission on two different positions can result in the formation of methyl radical and two different branched groups, including 2,4-dimethyl-C<sub>6</sub>-alkane and 4,4-dimethyl-C<sub>6</sub>-alkane. In terms of the favored location where the following radicals can be formed on branched-C<sub>6</sub>-alkanes, C-C double bond can be formed on C<sub>6</sub>-branched-alkane group, finally forming C<sub>6</sub>-branched-alkene group with HO<sub>2</sub> radical. The noticeable observation can be found in comparisons with the different places where C-C double bonds are formed. The radical position on γ-carbon of C<sub>6</sub>-branched-alkane contributes to form double bond between β- and γ-position carbons, resulting in the formation of 2,4-dimethyl-2-pentene and 4,4-dimethyl-2-pentene. However, the radical being formed on α-carbon of C<sub>6</sub>-branched-alkane leading to formation of C-C double bonds between α- and β-position of carbons, resulting in 2,4-dimethyl-1-pentene and 4,4-dimethyl-1-pentene. Based on the concentrations of intermediate species, the secondary radical formation on the β-carbon position of C<sub>6</sub>-branched-alkane group can be more favored than its formation on the α-carbon position. The more favored formation of dimethyl-2-pentenes than that of dimethyl-1-pentenes have been also discussed from exhaust hydrocarbons analysis with a wide range of equivalence ratio between 0.75 and 1.3 from neat *iso*-octane combustion [125].



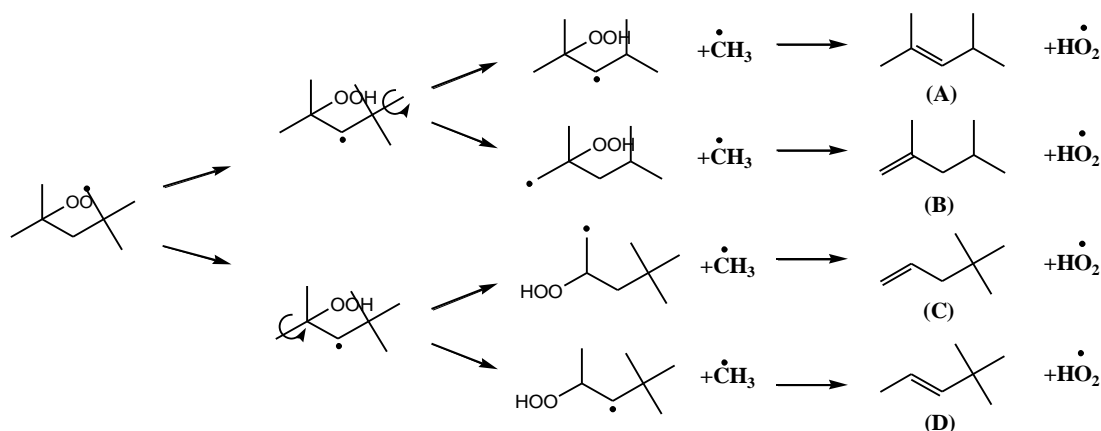


Figure 6-15 Possible reaction pathways leading to the formation of (A) 2,4-dimethyl-2-pentene (B) 2,4-dimethyl-1-pentene (C) 4,4-dimethyl-1-pentene and (D) 4,4-dimethyl-2-pentene in low temperature oxidation of *iso*-octane blends.

The most favored reaction pathways leading to the formation of 2,2,4-trimethylpent-2-yl-hydroperoxide during the low temperature oxidation of *iso*-octane blends are shown in Figures 6-13 and 6-16. As can be seen in Figure 6-16 (A), 2,2,4,4-tetramethyl-tetrahydrofuran is formed through transition state (1,6) H-atom transfer, which is mainly due to the lower strain energy barrier. The formation of 2,2,4,4-tetramethyl-tetrahydrofuran dramatically decreases with reducing volume of *iso*-octane. It indicates that formation of 2,2,4,4-tetramethyl-tetrahydrofuran is directly related to the current existence of *iso*-octane. During the oxidation of *iso*-octane and diisobutylene blends, 4,4-dimethyl-2-pentanone can be formed mainly through the following two channels: (1) The isomerization of alkylhydroperoxy radical to form trimethylalkylperoxide radical leading to the formation of conjugate ketone and a hydroxyl radical shown in Figure 6-16 (B); (2) The isomerization of hydroxypentylperoxy radicals according to the mechanism of Waddington shown in Figure 6-7. The reaction channel (2), however, is more likely

favored than the reaction channel (1), based on the trends of concentrations for 4,4-dimethyl-2-pentanone in Figure 6-14 (C). The very small amount of 4,4-dimethyl-2-pentanone was observed at neat *iso*-octane oxidation. The 5 % volume substitution of diisobutylene in *iso*-octane is likely responsible for a sharp peak of the formation of 4,4-dimethyl-2-pentanone, which increases linearly as increasing the addition of constant volume of diisobutylene.

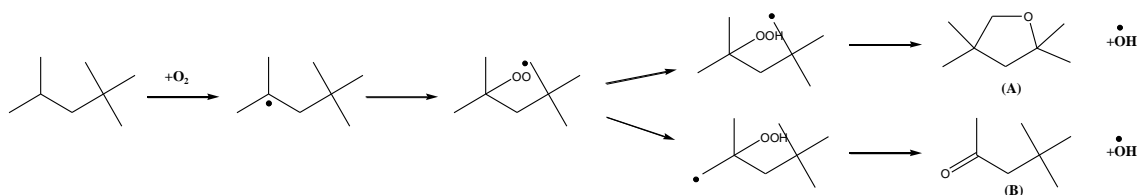


Figure 6-16 Possible reaction pathways leading to the formation of (A) 2,2,4,4-tetramethyl-tetrahydrofuran and (B) 4,4-dimethyl-2-pentanone during the oxidation of the *iso*-octane blends.

Overall, based on the product analyses performed for the low temperature oxidation of *iso*-octane blends in the present study, it can be seen that H-atom abstraction reactions on neat-*iso*-octane through radical attack are primarily occur on the  $\beta$ -carbon position of neat-*iso*-octane shown in Figure 6-13. This is consistent with the activation energy for hydrogen abstraction which follows the order of tertiary C-H abstraction > secondary C-H abstraction > primary C-H abstraction [28,34]. Besides, most intermediate species detected from GC analyses can be mainly formed from neat *iso*-octane. This is mostly due to the higher reactivity of *iso*-octane compared to diisobutylene in the low temperature regime.

## 6.6 Conclusions

A single cylinder CFR motored engine was modified to investigate the effect of the addition of branched and unsaturated structure fuel (diisobutylene) on ignition behavior and autoignition chemistry of binary blends mixed with PRF fuels (*n*-heptane and *iso*-octane). The test binary blends were prepared in sets of different amounts of the diisobutylene addition and were oxidized as a premixed charge of fuel and air at an equivalence ratio ( $\phi$ ) of 0.5 and intake temperature of 120°C. Overall oxidation reactivity and major product analysis are investigated. Significant findings are as follows;

1. Addition of branched and unsaturated fuel structures shows a linear retarding effect on oxidation reactivity, resulting in a longer negative temperature coefficient (NTC) behavior with gradual addition to PRF fuels.
2. Strong evidence of low temperature heat release (LTHR) was found only for *n*-heptane blends. The presence of the double bond in diisobutylene leads to lower % LTHR and higher critical compression ratio (CCR).
3. The more reactive fuel in a binary blend likely governs the ignition reactivity and characteristics, and the major products formed during low temperature oxidation are mostly derived from more reactive fuel.
4. Opposite trends with regard to the formation of major products were observed between *n*-heptane blends and *iso*-octane blends as diisobutylene was added, due to the different degree of ignition reactivity during low temperature oxidation.
5. The active radicals generated from branching step reactions during of cool flame oxidation of *n*-heptane and *iso*-octane in blends, favor attacking the C-C double bond in

diisobutylene, resulting in considerable formation of 4,4-dimethyl-2-pentanone. This reaction contributes to delayed ignition, shown by the increasing mole fraction of 4,4-dimethyl-2-pentanone in the unreacted fuel as the volume of diisobutylene increases in both cases.

## **Chapter 7**

### **Experimental Investigation of Autoignition Behavior of Surrogates for Conventional and Synthetic Alternative Jet Fuels and their Validation in a Motored Engine and a Constant Volume Combustion Chamber**

#### **7.1 Introduction**

In recent years, synthetic liquid fuels produced from the reforming of coal, natural gas and biomass have been drawing the U.S. military's attention as potential alternatives to current petroleum-derived fuels, such as JP-8 for aviation and F-76 for naval applications. Due to the lack of aromatics in these fuels, they are meant to be used as 50/50 blends with conventional jet fuels [134,135]. Fuel specification standards dictate requirements on a variety of chemical and physical properties of such alternative fuels to ensure that the fuels will serve well in their application, for example aviation turbine engines. For aviation turbine fuels, the fuel specification test method, ASTM D7566-14c, ensures that fuels meeting the specification will function effectively in commercial aviation turbine engines [136]. Other tests may be specified beyond the ASTM or

military standards, determining hydrocarbon chemistry, bulk physical and performance properties, electrical properties and ground handling/safety, referred to as ‘fit-for-use’ [137]. Jet fuel specifications are designed to govern their use as fuel for aviation gas turbine engines. However, the U.S Army’s single battlefield fuel policy mandates the use of JP-8 in ground vehicles employing compression ignition engines for the simplification of supply chain logistics [138].

The combustion process in diesel engines is different from gas turbine engines, given that the onset of combustion in a diesel (compression ignition) engine is mostly governed by an ignition delay period between the start of injection (SOI) and the start of combustion (SOC), wherein complex fuel dependent physical and chemical phenomena play a crucial role. Cetane number (CN) is related to the ignition delay period in the diesel engine combustion process under the CN test method (ASTM D613) [24]. The CN variations for petroleum and non-petroleum derived jet fuels may fall below the minimum CN specification for onroad compression ignition engines, leading to difficulties in engine starting and performance [100]. To overcome this critical barrier, the experimental efforts to understand the chemical kinetic behavior of synthetic alternative fuels, for example ignition delay, flame speed and extinction limits, has been made [42,44,46,47,139]; however little work has been performed regarding blends of conventional and alternative fuels [48,140,141]. These results are useful for validation and improvement of chemical kinetic models for use in simulating diesel engine combustion with computational fluid dynamics (CFD) supporting an understanding of how physical and chemical properties of practical jet fuels affect the ignition delay,

However, since practical jet fuels may be comprised of hundreds of hydrocarbon molecules, the development of validated, predictive and multi-scale combustion models is a challenge to implement with the current limited ability to consider detailed reaction chemistry within the scope of engine level CFD applications. Therefore, practical simulation of the diesel engine combustion process requires the use of simplified chemical kinetic models and the consideration of model compounds or mixtures of model compounds, referred to as surrogate fuels [99]. In a diesel engine, liquid fuel is directly injected into the combustion chamber and prepared for ignition by various physical and chemical process. To be useful for capturing combustion behavior within diesel engines, the surrogate fuels for the diesel engine combustion process must successfully emulate the physical properties and gas phase combustion behavior of the target fuel with a limited number of pure components.

In recent decades, much work has addressed the formulation of aviation fuel surrogates and their chemical mechanisms have been reported with experimental validation in simplified combustion chambers such as shock tubes [42,44,46,77,142,143], rapid compression machines (RCM) [44,46,77], pressurized flow reactors (PFR) [44,46,77,143], jet-stirred reactors (JSR) [77,144] and co- and counter flow burners [44,46,56,77,145]. The resultant surrogate developments are important from a point of view of accurate chemical kinetic predictions, as compared to real jet fuels. However, these studies mainly dealt with emulating combustion kinetics of gas phase fuel/oxidizer mixtures, generally matching chemical properties such as derived cetane number (DCN), hydrogen to carbon ratio (H/C), molecular weight (MW) and threshold sooting index (TSI) but no effort was made to match the temperature-dependent physical properties of a

real jet fuel. Meanwhile, Edwards and Maurice stressed the importance of considering the physical properties (e.g., distillation curve, viscosity, density, surface tension, etc.) of surrogates over a wide range of pressures and temperatures [146]. However, replicating the detailed physical properties of a real jet fuel generally requires larger numbers of components of varying molecular weights. For instance, a few previous studies have adopted from 7 to 14 pure components to match the aforementioned physical properties of a practical jet fuel [146,147]. However, the use of a larger number of surrogate components creates challenges to develop tractable gas phase combustion kinetics mechanisms. For this reason, most recent work has favored emulating the fully gas phase global combustion behavior with a small number (from 1 to 4) of surrogate components. It is important to consider both, physical and chemical properties of real fuels, as pointed out by other studies [46,143]. Combined emulation of physical and chemical properties becomes more crucial in development of comprehensive models for the diesel combustion process, where the ignition delay period, the premixed combustion phase, mixing controlled combustion or the diffusion burn phase, and the late combustion phase occur consecutively [15].

Heywood reviewed the significant impacts of surface tension and liquid density on physical processes that affect a diesel spray, while volatility and viscosity play minor roles in ignition delay in a warmed-up engine [15]. Caton *et al.* suggested several ignition delay correlations with respect to physical properties by using various pure component fuels in a single cylinder diesel engine [148]. Figure 7-1 shows a diagram of ignition delay periods, presenting the impacts of physical properties such as liquid density, liquid viscosity, surface tension, and vapor pressure on preparation of liquid fuel after the liquid



fuel jet is injected in the combustion chamber. Once the fuel and air are premixed with a given mixture ratio at suitable temperatures and pressures, there is a chemical delay period where chemical reaction rates promote and ultimately lead to significant chain branching. The rates of fuel decomposition mainly rely on the molecular structure such as chain length, presence of double or triple bonds, degree of branching, cyclic or aromatic structure and substitution of oxygen or other species, as shown in Figure 7-1. During fuel decomposition, an alkyl peroxide isomerization step is considered as the key reaction step for predicting the onset of ignition under low and intermediate temperature regimes usually observed in advanced diesel combustion systems [34]. Furthermore, the molecular weight (MW) affects the liquid/vapor phase diffusive transport of fuel species and the lower heating value (LHV) determines the energy that can be released through the oxidation of the fuel. Finally, the local air/fuel ratio and adiabatic flame temperature are influenced by the H/C ratio during the premixed combustion phase.

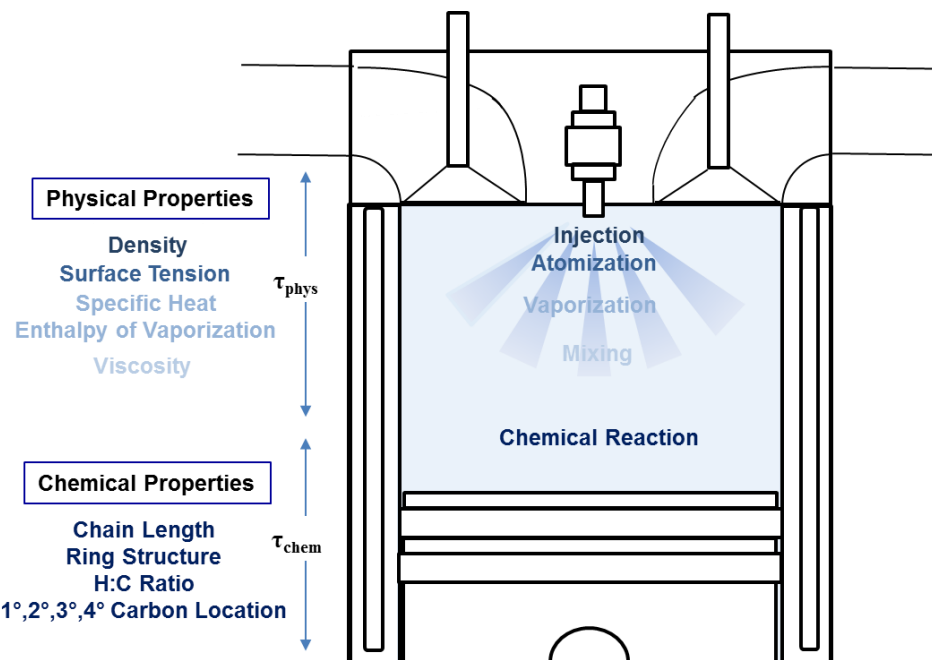


Figure 7-1 Physical and chemical properties affecting diesel engine combustion processes, inspired by [148]

More recently, comprehensive JP-8 surrogates have been developed for CFD applications that are capable of matching both physical and chemical properties during the diesel ignition delay period [100,149]. Shrestha *et al.* from Wayne State University (WSU) formulated six different JP-8 surrogates based on seven properties: DCN, density, volatility, LHV, H/C, MW, and TSI. A Matlab code has been developed and used in conjunction with the ignition quality tester (IQT) and the HYSYS software to formulate optimal surrogates [149]. A similar approach is adopted by Kim *et al.* from the University of Michigan (UM) to develop conventional and synthetic alternative jet fuel surrogates, designated as UM I, UM II for Jet-A, UM S8 for S8 and UM IPK for IPK, by using a model-based optimizer to closely match physical properties such as density, viscosity, surface tension and distillation curve, in addition to DCN, MW, LHV, and H/C

[100,150]. Unlike the WSU surrogates, Kim *et al.* also considered viscosity and surface tension for the surrogate formulations, which has a great impact on spray injection in diesel combustion as mentioned above. In addition, the UM group implemented a thermodynamic model capable of reproducing the distillation curve measured by NIST's Advanced Distillation Curve method [151], which allows the use of experimental data from NIST's most advanced measurement technique within the optimization process. However, the Jet-A surrogates developed by the UM group have not been validated in any practical combustion devices to compare with the practical jet fuel.

## 7.2 Research Objectives

Hence, the work presented here examines the autoignition characteristics of four conventional jet aviation fuels (two Jet-A, POSF 4658 and POSF 10325, JP-5 and JP-8) and five synthetic alternative jet fuels (S-8, synthetic paraffinic kerosene (SPK), *iso*-paraffinic kerosene (IPK), hydro-processed renewable jet (HRJ8) and alcohol to jet (ATJ)) to better understand liquid spray ignition behavior and gas phase combustion process in an engine environment. Furthermore, the combustion characteristics of UM surrogate mixtures, in comparison with their target jet fuels (Jet-A, S8 and IPK) in two unique experimental systems. First, a modified CFR motored engine was used in order to better understand the gas phase combustion characteristics during compression ignition. The main objective of this study with the modified CFR engine is to access ignition limit behavior by looking at critical compression ratio (CCR) and critical equivalence ratio (critical  $\phi$ ), and % low temperature heat release (% LTHR). Secondly, an optically

accessible constant volume spray combustion chamber, originally developed for measuring DCN, was used in this study to verify how well the UM surrogates matched the physical and chemical ignition delays under a wide range of air temperatures and oxygen dilution. The information provided here is intended to offer an intermediate step to validate simulations based upon the surrogate fuel representation of Jet fuels and the kinetic model to describe its combustion.

## **7.3 Test Conditions**

### **7.3.1 Modified CFR engine**

The UM surrogate mixtures are formulated to mimic a series of physical and chemical processes, which occur during the ignition delay period, for a practical jet fuel (POSF 4658) and synthetic alternative jet fuels (S8 and IPK). However, decoupling the physical processes from the chemical processes that occur during the diesel combustion process allows the chemical reaction kinetics of a premixed air-fuel mixture introduced in the engine combustion chamber to govern the ignition process. The modified CFR engine provides direct observation of the homogeneous autoignition behavior of the fuel-air mixture, where ignition occurs under the high temperature and pressure condition produced by the engine cylinder compression. In the present work, in order for test fuels to be fully vaporized and premixed with air, a constant intake manifold temperature was maintained at 260°C (500°F) throughout all test conditions. The equivalence ratios ( $\phi$ ) of 0.25 and 0.5 were used targeting the leaner conditions that are becoming increasingly attractive for achieving reductions in production of harmful emissions. For each test

series, the engine CR is gradually increased from the lowest point (CR = 4) to the point where significant high temperature heat release (HTHR) is observed, so that the progressive change of the ignition behavior of each test fuel with the increase of CR can be observed. Another observation in the experiment involves maintaining a constant CR while varying  $\phi$  from low to high values until ignition is achieved.

### **7.3.2 Constant volume spray combustion chamber**

While the modified CFR engine solely provides a validation of gas phase air/fuel oxidation kinetics and autoignition characteristics under compression ignition in the motored engine, a modified CID 510 derived cetane rating instrument offers a distinct observation of both, physical processes such as liquid to gas phase transition and mixing, and chemical processes in an optically accessible spray injection constant volume combustion chamber. Typically the ignition delay period in a diesel engine can be treated as a contiguous process, however this process can be divided into a physical and a chemical ignition delay. Since the chemical ignition delay solely relies on the chemical reaction kinetics, it can be assumed that the physical ignition delay includes all the other factors that determine the physics of a diesel spray injection process [148]. While some overlap of the physical and chemical processes exists in practice, this simple first order approximation was pursued in this study to validate how the UM surrogates emulated the diesel engine ignition delay in terms of both, physical effect and chemical effect, as compared to the target jet fuels.

The current study also investigates the sensitivity of ignition behavior to air temperature and the amount air dilution by using simulated EGR. The initial chamber

temperature was spanned from 540°C to 640°C. All dilution testing was completed with a sweep of simulated EGR at 0%, 15%, 25%, 40%, 50% and 55%. Other initial test conditions include 20bar chamber pressure, 2.5ms injection duration, and 1000bar injection pressure, which are kept constant throughout all the tests. Combustion air composition was ensured at 20.9% oxygen (by volume), balance nitrogen to assure the consistency of the composition of the intake air.

## **7.4 Conventional and Alternative Synthetic Jet Fuels**

### **7.4.1 Test fuels**

Conventional military aviation fuels used in this study include JP-8 POSF 6169, Jet-A POSF 4658, Shell distilled Jet-A POSF 10325, and Valero distilled JP-5 POSF 10289. Amongst those conventional jet fuels, JP-8 POSF 6169 that is readily available elsewhere is selected as the reference for the comparison toward synthetic jet fuels and as the blending unit mixed with 50 volume percent of synthetic jet fuels. In addition, five synthetic jet fuels derived from different natural resources are being considered in this study as follows; “S-8”(S8) POSF 5018 derived from natural gas by Syntroleum Inc., “synthetic paraffinic kerosene” (SPK) POSF 5729 and “*iso*-paraffinic kerosene” (IPK) POSF 7629 derived from coal in Fischer-Tropsch (FT) process by Shell and Sasol, respectively, “hydro-processed renewable jet” (HRJ) derived from Camelina POSF 11714 and lastly “alcohol-to-jet” (ATJ) POSF 10498 derived from *iso*-butanol by Gevo. The fuels listed above have been prepared and provided from the US Air Force Research Laboratory (AFRL), each identified by specific “POSF” numbers. The specific POSF

number for each fuel, however, can be updated in different years. For example, three POSF numbers (4734, 4820 and 5018) that correspond to S-8 produced in different years, has been processed from the same plant and natural gas feedstock, thus being essentially identical.

Gas chromatography (GC) analysis shows that the conventional jet fuels possess very similar chemical composition, widely distributed between C<sub>8</sub> and C<sub>14</sub>, although JP-5 has a somewhat narrower carbon distribution as compared to other conventional jet fuels, as shown in Figure 7-2. Both F-T process synthetic jet fuels, SPK and IPK, were distilled within noticeably narrow cuts with a lighter end of boiling range. Despite the similar carbon numbers of hydrocarbons for SPK and IPK, the dominant chemical structural family for both fuels is noticeably different, in that SPK contains prominent *n*-alkanes, but a large amount of *iso*-alkanes exists in IPK and almost no *n*-alkanes. In contrast to the F-T process synthetic jet fuels, S8 and HRJ have somewhat wider distillation cuts than the conventional jet fuels, showing evident peaks for C<sub>8</sub> and C<sub>17</sub>, which are the edges of the conventional jet fuels. Also, a significant of “hump” within C<sub>15</sub>-C<sub>17</sub> range observed in HRJ is due to an intentional addition of heavy alkanes to improve the flash point of the fuel to meet the USN MILSPEC requirement. In contrast to conventional and alternative jet fuels tested, ATJ is mainly comprised of highly branched paraffins as identified by total ion chromatogram with mass spectrometry.

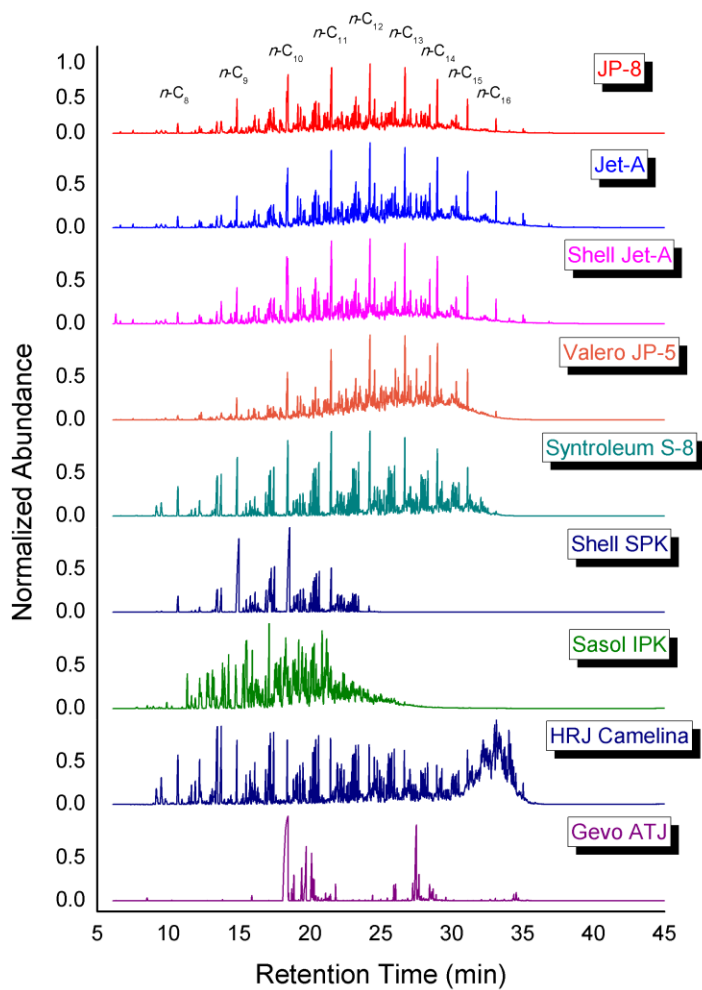


Figure 7-2 Gas chromatography/mass spectrometry scan of conventional and alternative Jet fuels tested



Table 9 Physical and chemical properties of conventional and alternative Jet fuels

Fuel, POSF #	JP-8, 6169	Jet-A, 4658	Shell Jet- A, 10325	Valero JP-5, 10289	Syntroleum S-8, 5018	Shell SPK, 5729	Sasol IPK, 7629	HRJ Camelina, 11714	Gevo ATJ, 11498
Net heat of combustion (MJ/kg)	43.4	43.2	43	43.1	44.1	44.2	44	44.3	44
Flash point (°C)	46	48	48	68	49	44	44	55	49
Density (g/ml)	0.798	0.807	0.803	0.802	0.757	0.737	0.762	0.751	0.757
Freezing point (°C)	-50	-47	-47	-50	-59	-54	-61	-77	
Viscosity (mm <sup>2</sup> /s) at -20 °C	4.2	5.7	4.5	5.39	4.6	2.6	3.6	3.3	1.52
Molecular Formula (C <sub>n</sub> H <sub>m</sub> )	C <sub>10.96</sub> H <sub>22.1</sub>	C <sub>10.17</sub> H <sub>19.91</sub>		C <sub>12</sub> H <sub>22</sub>	C <sub>10.82</sub> H <sub>23.7</sub>	C <sub>9.58</sub> H <sub>21.43</sub>	C <sub>10.5</sub> H <sub>23.02</sub>	C <sub>11.6</sub> H <sub>25.53</sub>	C <sub>12.2</sub> H <sub>26.4</sub>
H/C	2.017	1.957	1.937	1.87	2.14	2.24	2.195	2.202	2.168
MW(g/mol)	153.9±1.4	157.5±2.0	147.6±0.9	156.1±0.8	153.9±0.7	136.7±1.1	149.2±1.0	160.2±1.3	173.0±1.7
<i>n</i> -alkane (%)	21.5	38.6	20	13.9	12.11	41	0.5	45	
<i>Iso</i> -alkane (%)	37.5	29.6	29.4	18.1	86.04	59	89.5	50	>96
Cycloalkane (%)	27	3.3	31.9	47.4	1.85			5	
Aromatic (%)	16.1	28.5	17	20.5				<0.3	

## 7.4.2 Results and discussion

### 7.4.2.1 DCN and sooting tendency

As seen in Table 10, the DCN values for conventional and synthetic alternative jet fuels were obtained by the CID 510 unit based on ASTM D7668 method [26]. It is confirmed that measured DCNs for the conventional and alternative jet fuels are varied, in that Jet-A and JP-8's DCNs are around 47, the DCNs of the alternative jet fuels, including S8, SPK, and HRJ8 are around 60, and other fuels possess their DCNs around 30 for IPK or even below 20 for ATJ. These DCN values mainly rely on the molecular composition of the fuel. As seen in Table 9, higher reactivity fuels such as S8, SPK and HRJ consist of either considerable amounts of *n*-alkanes or blends of *n*-alkanes and less branched alkanes, which greatly promotes the overall ignition reactivity. In contrast, less reactivity fuels such as IPK and ATJ consist of highly branched alkanes and this leads to moderate ignition reactivity. The linear trend can be found in DCN measurements of the alternative fuels blended with JP-8 in that values for highly reactive alternative fuels decrease when blended with JP-8 and *vice versa* for IPK and ATJ.

As briefly mentioned earlier, soot formation during combustion also depends on the chemical composition of the fuels, especially the aromatic content. Therefore, the absence of aromatics in the alternative synthetic jet fuels leads to dramatic reduction of soot, as compared to conventional jet fuels, as seen in Table 10. However, the lack of aromatics in fuels causes leaking problems due to lack of swelling in elastomeric seals [152]. For this reason, blending with conventional fuels is unavoidable to provide

satisfactory aromatic content, but this blending strategy penalizes the sooting tendency as observed by increasing TSI value in blends.

Table 10 Properties of conventional and synthetic alternative jet fuels, and 50 volume percent of JP-8 blended with alternative jet fuels tested in this study

Fuel	POSF#	DCN <sup>a</sup>	MW <sup>c</sup>	H/C <sup>c</sup>	SP (mm)	TSI <sup>b</sup>
JP-8	6169	48.64	153.6	2.017	23.57	15.5
Jet-A	4658	47.01	157.5	1.957	21.18	18.8
Jet-A	10325	48.61	157	1.937	21.81	18
JP-5	10289	43.27	na	1.87	na	na
S8	5018	65.24	154.5	2.14	>45	<4.6
SPK	5729	62.43	138.3	2.24	>45	<3.4
IPK	7629	31.71	148.5	2.195	42.36	4.9
HRJ8	11714	59.77	167.6	2.202	>45	<5.6
ATJ	11498	18.24	173	2.168	35.47	9.7
JP-8/S8		54.53	154	2.1	39.26	6.4
JP-8/SPK	7717	53.87	145.8	2.124	40.63	5.2
JP-8/IPK	7718	39.33	151.1	2.105	32.37	9
JP-8/HRJ8	7721	52.54	160.1	2.104	36.51	8
JP-8/ATJ		33.42	162.5	2.088	30.65	11.2

<sup>a</sup> Derived Cetane Number (DCN) measured in this study by ASTM D7668 [26]

<sup>b</sup> Threshold Sooting Index (TSI) measured in this study by ASTM D1322 [153]

<sup>c</sup> Molecular Weight (MW) and H/C ratio obtained from [48]

#### 7.4.2.2 Comparisons of conventional and alternative fuels in a motored engine

Apparent heat release rates (AHRR), carbon monoxide (CO) emissions, and maximum bulk in-cylinder temperature of conventional and alternative jet fuels and 50 volume percentage blends in JP-8 were observed at selected compression ratios (CR) from the lowest point (CR 3.8) to the critical compression ratio (CCR) at both equivalence ratios at 0.25 and 0.5, shown in Figure 7-3 through Figure 7-7.

As can be seen in Figure 7-3, the four different conventional jet fuels, Jet-A, JP-8 and JP-5 have a similar trend of heat release rates in both equivalence ratios, showing the low temperature heat release (LTHR) from beginning at CR 4. This indicates that *n*-alkane content in these fuels activates the low temperature chain branching reaction path, leading to strong oxidation reactivity in the low temperature regime. The small differences in critical compression ratios observed for the four different conventional jet fuels corresponds well with their different DCN values.

Synthetic alternative jet fuels tested in this study can be classified into two groups; one group includes higher oxidation reactivity fuels, such as S8, SPK and HRJ8, than the conventional jet fuel (JP-8), and the other group includes lower oxidation reactivity fuels, IPK and ATJ, than that of a JP-8.

For the group with higher reactivity alternative jet fuels (S8, SPK and HRJ8) in the case of equivalence ratio ( $\phi$ ) at 0.25, Figures 7-3 (a), (b) and (c) clearly show that strong LTHR can be observed starting at the lowest CR of 4. The intensity of LTHR for these fuels becomes stronger and also shifts to an advanced phase as the CR increases. The onset of evident two-stage heat release is investigated at CR of 5.25 for S8, CR of 5.4 for SPK and CR of 5.8 for HRJ8, where the fuels enter into the high temperature

oxidation regime. The stronger intensity of LTHR and earlier onset of two stage ignition behavior than for JP-8 confirm that the higher reactivity fuels display more intense low temperature heat release, due to active low temperature chain branching reactions induced by higher *n*-alkane and lightly branched alkane content in these fuels as compared to JP-8. This result also can be well demonstrated by CO emission and maximum in-cylinder temperature, shown in Figure 7-6. Higher reactivity synthetic alternative jet fuels show 20-30K higher in-cylinder temperature, resulting in higher CO emission than JP-8 measured at the same CR.

Similar to the case of  $\phi$  at 0.25, the case of  $\phi$  of 0.5 for strong ignition reactivity fuels (JP-8, SPK and HRJ8) shows the same trend of LTHR, except no two-stage heat release is observed during pre-ignition. The two-stage heat release is observed only at the CCR, where the complete ignition takes place. Also, increasing the equivalence ratio to 0.5 leads to higher in-cylinder temperature, greater intensity of LTHR and more advanced CCR, as compared to the leaner condition at  $\phi$  of 0.25. One constraint should be noted that ignition limit behavior of S8 for the case of  $\phi$  of 0.5 was not achieved, since higher oxidation reactivity of the fuel resulted in autoignition even at the lowest CR at the experimental conditions of interest in this study.

Once blended with 50 volume percent of JP-8, the strong reactivity alternative jet fuels become less reactive, mainly due to the aromatics in JP-8, which scavenges the chain propagating radicals and slows down ignition chemistry in the low temperature regime. Blending impact is clearly demonstrated in the trends of heat release rates, CO emissions and maximum in-cylinder temperatures, as compared to the trends for the neat alternative jet fuels. Figures 7-4 and 7-5 show decreased intensity of LTHR and delayed

onset of two-stage ignition behavior, and Figures 7-6 and 7-7 present a blending impact on decreasing in-cylinder temperatures and producing less CO formation, resulting in delayed CCR for both  $\phi$  conditions.

In contrast to high oxidation reactivity fuels, IPK and ATJ, whose chemical compositions mostly consist of highly branched alkanes, show single stage ignition behavior during pre-ignition and even at autoignition for both equivalence ratios investigated, as shown in Figures 7-4 (d) and (e), and 7-5 (d) and (e). The evident heat release rates of IPK and ATJ are first observed at CR 9.5 and CR 10.55, respectively, for the leaner condition ( $\phi=0.25$ ). The relatively richer conditions ( $\phi=0.5$ ) for both fuels have no evident heat release rate until they reached CCR (though, a negligible LTHR of IPK can be observed at  $\phi$  of 0.5). The lack of LTHR and delayed overall ignition reactivity for IPK and ATJ are mainly due to higher amounts of highly branched alkanes. The highly branched *iso*-alkanes tend to impede the stability of ROO adductions and hydrogen isomerization due to the fewer available secondary hydrogen atoms for transfer through isomerization involving energetically preferred 6-membered transition states, which occur during the low temperature chain branching reaction path,  $\text{ROO} \leftrightarrow \text{QOOH}$  [34]. Alternatively, *iso*-alkane molecules tend to proceed via propagation reaction paths creating  $\text{HO}_2$  radicals, which compete with the primary low temperature oxidation paths. The heat release trends of these unreactive fuels contrast sharply with the ignition behavior of JP-8 as shown in Figure 7-3. Maximum in-cylinder temperature measurement supports weak ignition reactivity of IPK and ATJ, in that the in-cylinder temperatures of IPK and ATJ are 50K or 100K (at some CRs) lower than that of JP-8 during pre-ignition. The resultant CO emission of IPK in both equivalence ratios is relatively insignificant

during pre-ignition, as compared to that of JP-8. One noticeable observation from the trends of CO emission for IPK is negative temperature coefficient (NTC) behavior observed under these conditions, shown in Figure 7-6 (i). However, no CO formation for ATJ is observed before the oxidation enters into the high temperature oxidation regime during pre-ignition for both  $\phi$  conditions.

Ignition characteristics of the 50/50 volumetric blends of JP-8 with the less reactive alternative jet fuels, IPK and ATJ, appear to be significantly different from those of neat IPK and ATJ. A high portion of normal alkanes in JP-8 contributes to the occurrence of LTHR prior to autoignition. Those active low temperature chain branching paths result in a rise of in-cylinder temperature and a significant promotion of the overall ignition reactivity in both  $\phi$  conditions. One noticeable observation when blended with JP-8 is that the NTC behavior of neat IPK oxidation disappears in the pre-ignition period, and considerable amount of CO formation is observed.

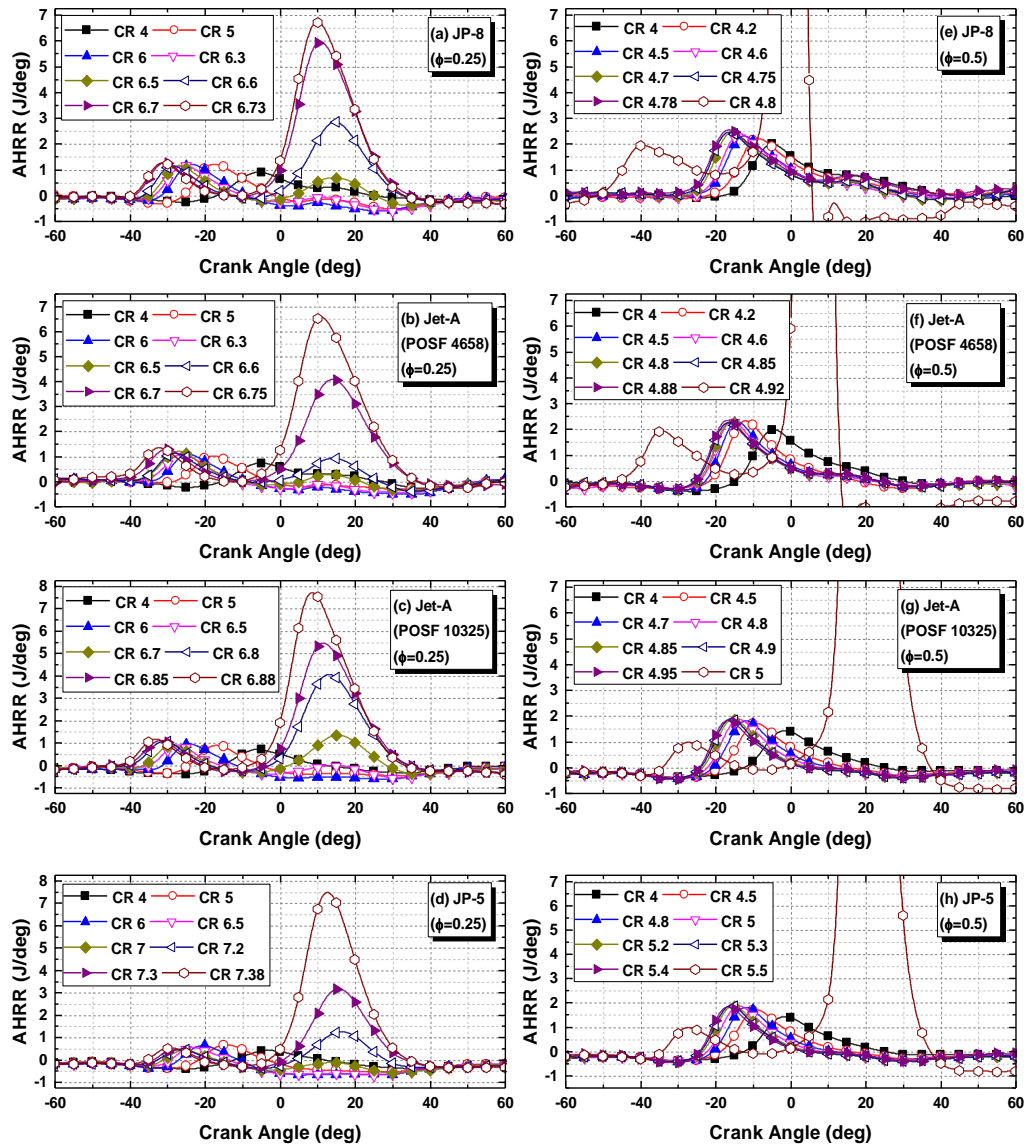


Figure 7-3 Apparent heat release rates (AHRR) of conventional jet fuels of JP-8, Jet-A and JP-5 at equivalence ratios of 0.25 and 0.5



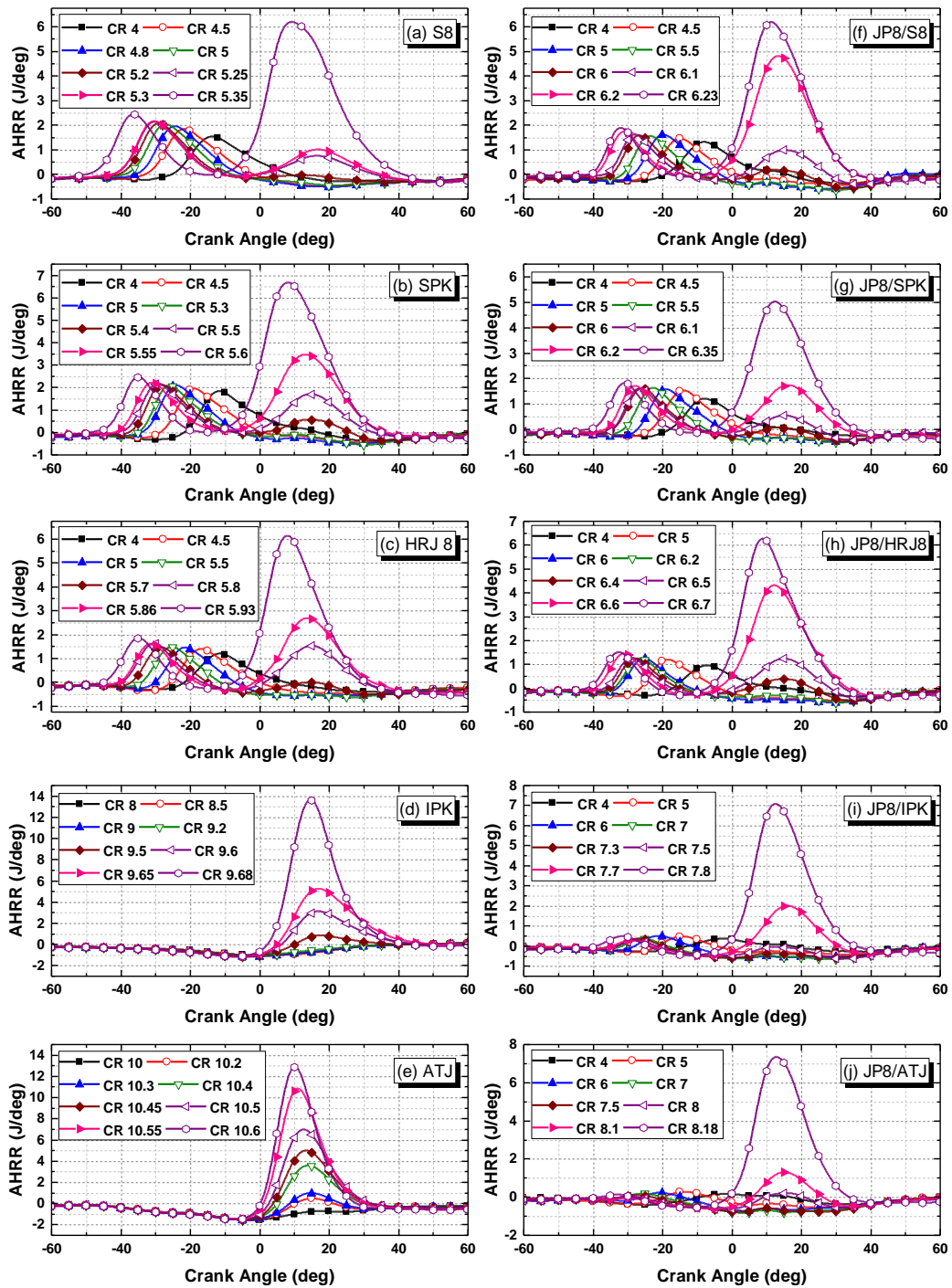


Figure 7-4 Apparent heat release rates (AHRR) of synthetic alternative jet fuels and blends with JP-8 in a wide range of CRs at equivalence ratio of 0.25

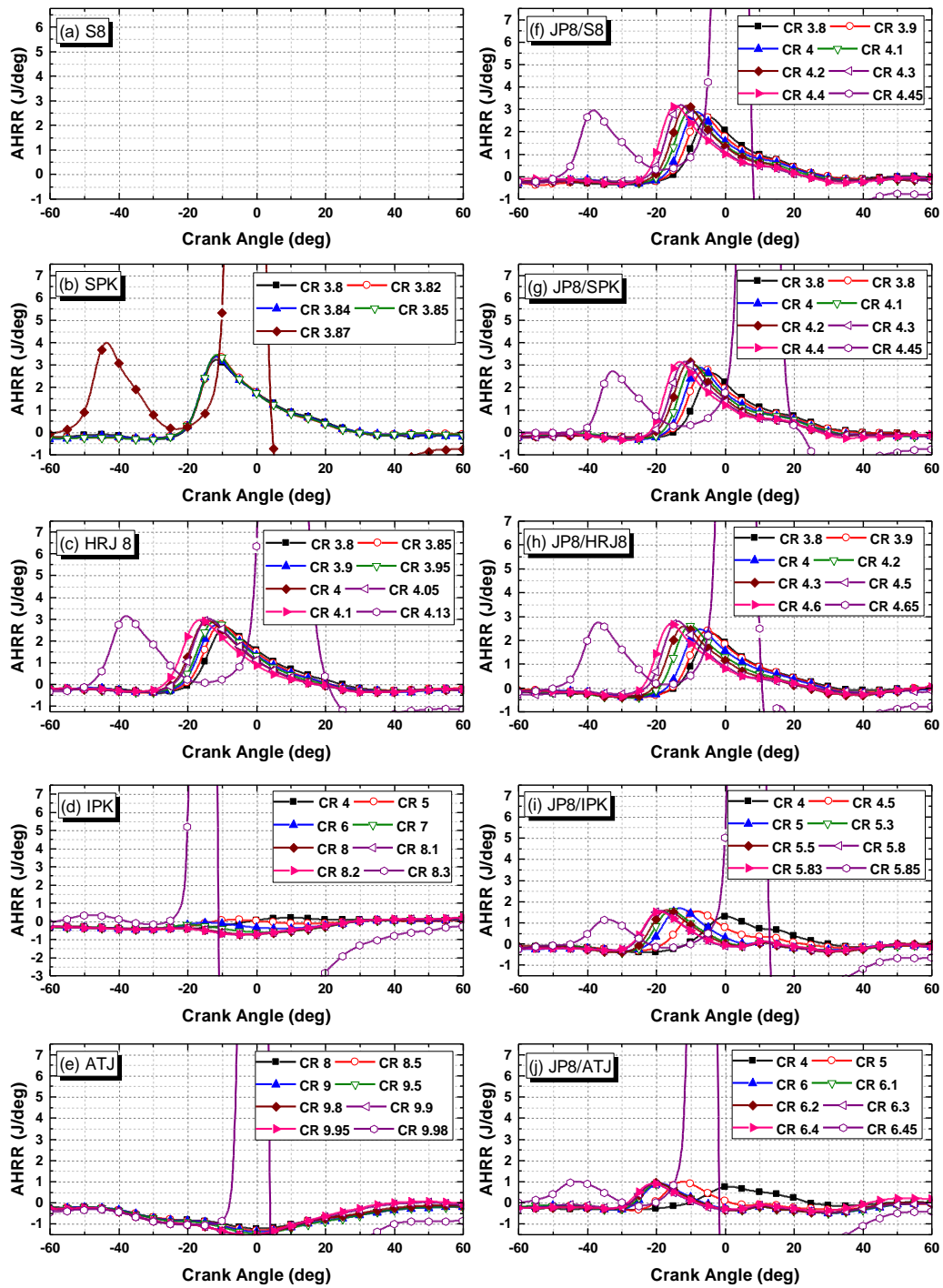


Figure 7-5 Apparent heat release rates (AHRR) of synthetic alternative jet fuels and blends with JP-8 in a wide range of CRs at equivalence ratio of 0.5

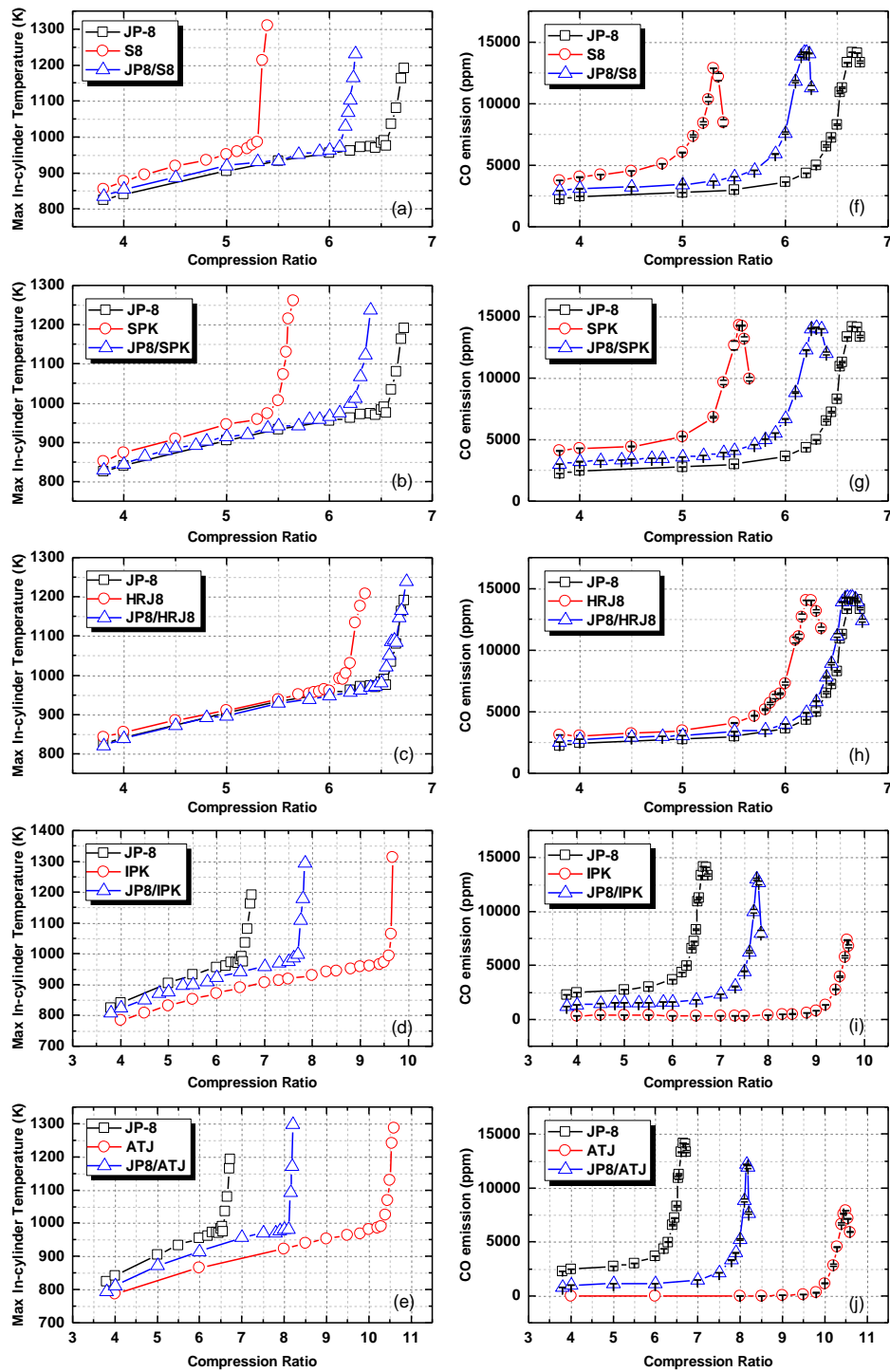


Figure 7-6 (a) – (e); Maximum in-cylinder temperatures and (f) – (j); CO emissions of alternative jet fuels and 50 v/v % of JP-8 in alternative jet fuels in a wide range of compression ratios at equivalence ratio of 0.25

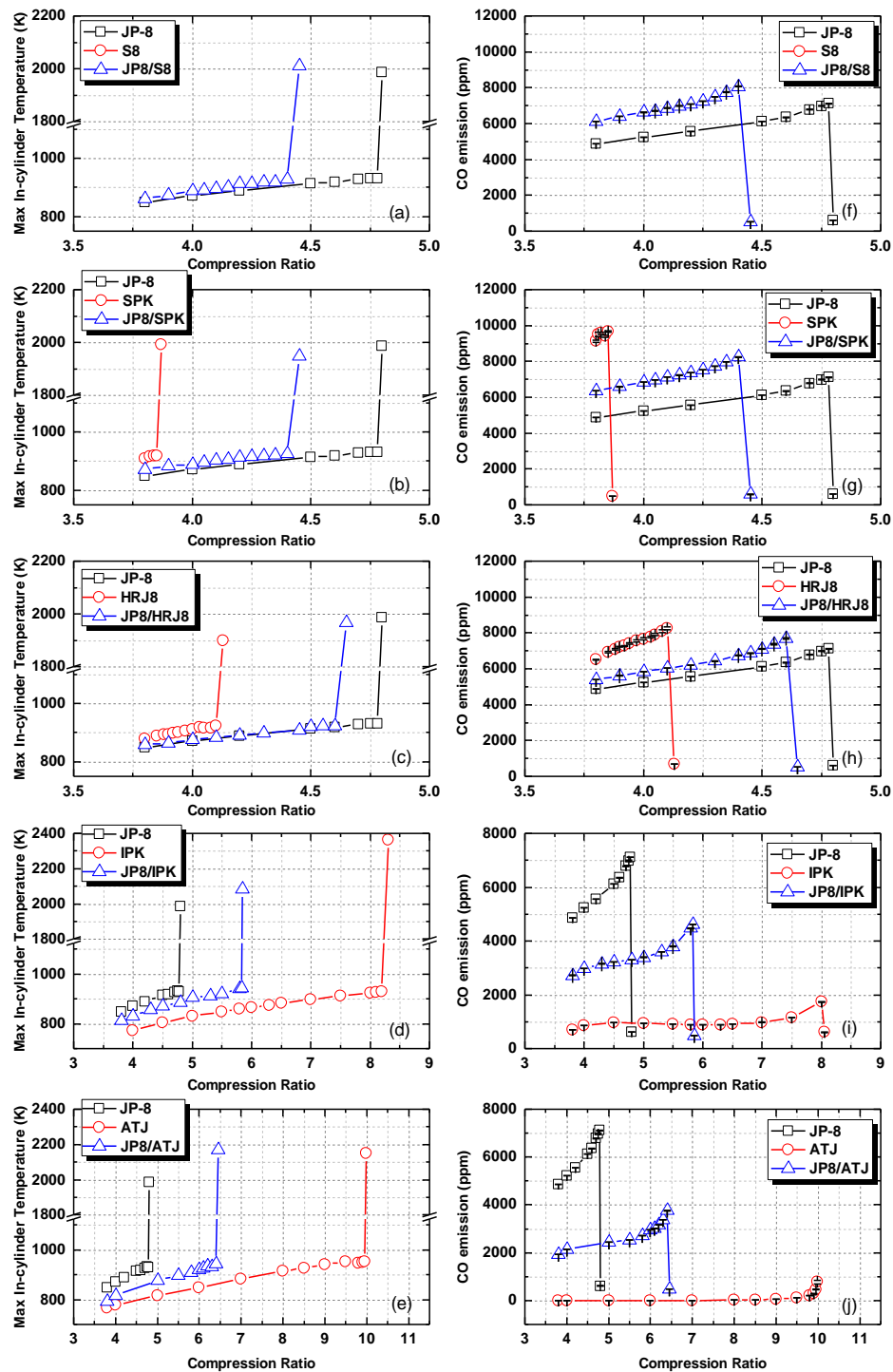


Figure 7-7 (a) – (e); Maximum in-cylinder temperatures and (f) – (j); CO emissions of alternative jet fuels and 50v/v % of JP-8 in alternative jet fuels in a wide range of compression ratios at equivalence ratio of 0.5

The gas phase ignition limit behavior, known as CCR, and the percentage of low temperature heat release (% LTHR) at both intake stoichiometries have a strong linear relationship with their derived cetane number (DCN) shown in Figures 7-8 and 7-9. The alternative jet fuels with higher *n*-alkane contents such as S8, SPK and HRJ8, possess stronger % LTHR than conventional jet fuels for both  $\phi$  cases, while alternative jet fuels with higher *iso*-alkane content such as IPK and ATJ display a lack of 1st stage heat release, due to the lack of *n*-alkanes in these fuels. As expected, once these alternative fuels are blended with JP-8, the ignition behaviors of these fuels promotes % LTHR and decreases CCR or decrease % LTHR and increases CCR, as shown in Figures 7-8 and 7-9.

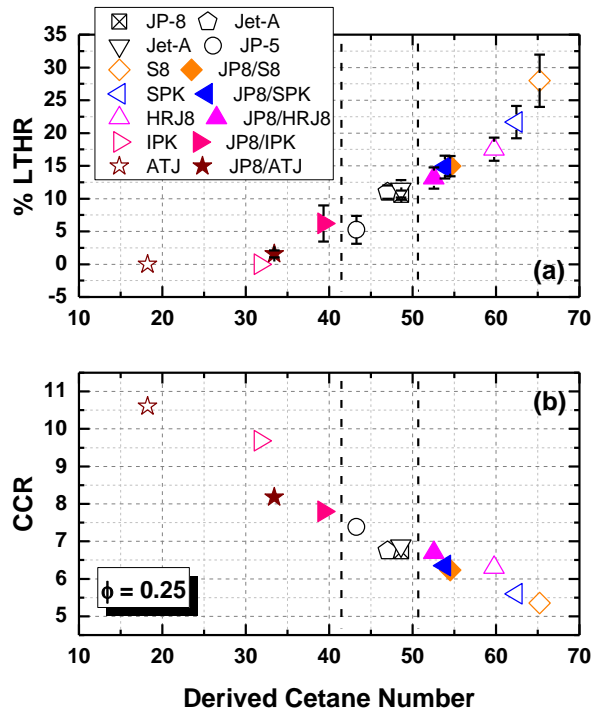


Figure 7-8 The percentage of low temperature heat release (% LTHR) and critical compression ratio (CCR) in respect of derived cetane number (DCN) of jet fuels tested at equivalence ratio of 0.25; Error bar indicates 95 % confidential interval.

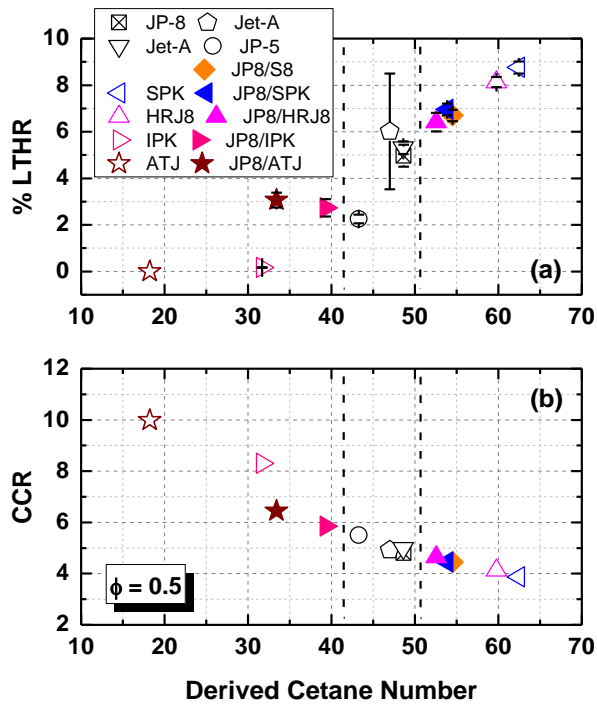


Figure 7-9 The percentage of low temperature heat release (% LTHR) and critical compression ratio (CCR) in respect of derived cetane number (DCN) of jet fuels tested at equivalence ratio of 0.5; Error bar indicates 95 % confidential interval.

Figure 7-10 presents the critical equivalence ratios ( $\phi_{crit}$ ) of conventional and alternative jet fuels and blends with JP-8. As expected, fuel blends aggressively promote ignition reactivity for lower reactivity fuels (IPK and ATJ) with the same amount of fuel injected. One noticeable observation found for higher reactivity fuels (S8, SPK and HRJ) is that the blending impact becomes minimal as  $\phi_{crit}$  becomes leaner, as indicated in the boxes shown in Figure 7-10.

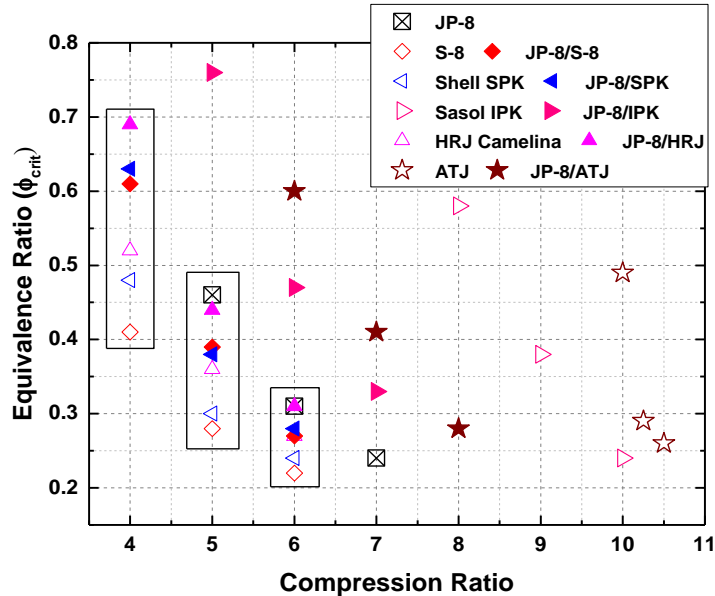


Figure 7-10 Critical equivalence ratio of jet fuels tested at different compression ratios

#### 7.4.2.3 Comparisons of ignition delays between conventional and alternative fuels in constant volume spray combustion chamber

The constant volume spray combustion chamber was used to investigate the distinction between the physical and chemical ignition delays ( $\tau_{phy}$  and  $\tau_{chem}$ ) of a conventional jet fuel (JP-8) and synthetic alternative jet fuels in low to intermediate temperature ranges (540-640°C) at 20 bar, where the low temperature oxidation behavior and the onset of negative coefficient temperature (NTC) can be found. For the better comparisons for each test fuel tested, ignition delays of S8, SPK and HRJ8 are compared with JP-8 and its blends and are shown in Figure 7-11, and ignition delays of IPK and ATJ and its comparisons with JP-8 and its blends are shown in Figure 7-12.

As can be seen in Figure 7-11, the Arrhenius plot revealed a relatively linear dependence of  $\tau_{phy}$  on ambient temperature. Increased ambient air temperature leads to

shorter  $\tau_{\text{phy}}$  across the complete temperature range tested.  $\tau_{\text{phy}}$  values of the synthetic alternative jet fuels are shorter than that of JP-8, mostly likely due to their lower density and viscosity than those of JP-8, leading to faster evaporation and mixing rates, (even though a part of  $\tau_{\text{phy}}$  values is overlapped with a part of  $\tau_{\text{chem}}$ ). The Arrhenius plot of  $\tau_{\text{chem}}$  displays strong negative temperature coefficient (NTC) behavior for S8, SPK and HRJ8 starting from 560°C, while JP-8 has a delayed NTC behavior, observed at a temperature of 580°C. The Arrhenius plots of total ignition delay ( $\tau_{\text{tot}}$ ) for 50/50 blend lies in the middle between JP-8 and the alternative jet fuels. However, plots of  $\tau_{\text{chem}}$  for 50/50 blends of S8 and SPK lean toward those of the neat alternative fuels. This indicates that the active radicals provided by more reactive fuels (neat alternative fuels, here) in low temperature regime can activate the low temperature oxidation pathways, thereby promoting ignition reactivity, when blended with more reactive fuels. Perez *et al.* observed the synergistic and antagonistic behaviors of blending fuels, showing that the ratio of reactive and unreactive components in the fuel highly affects the reactivity of the fuels, and the ignition behavior of these blends has a non-linear trend in respect to the volumetric ratios of these opposite reactivity of the fuels [154]. It should be also noted that the disparities of their reactivity in  $\tau_{\text{chem}}$  is significant in low temperature range, however the gaps in  $\tau_{\text{chem}}$  become negligible, as ambient temperature increases, especially for the fuels in similar DCN values. The results can support the importance of low temperature oxidation chemistry where the ignition characteristics of fuels can be potentially determined.



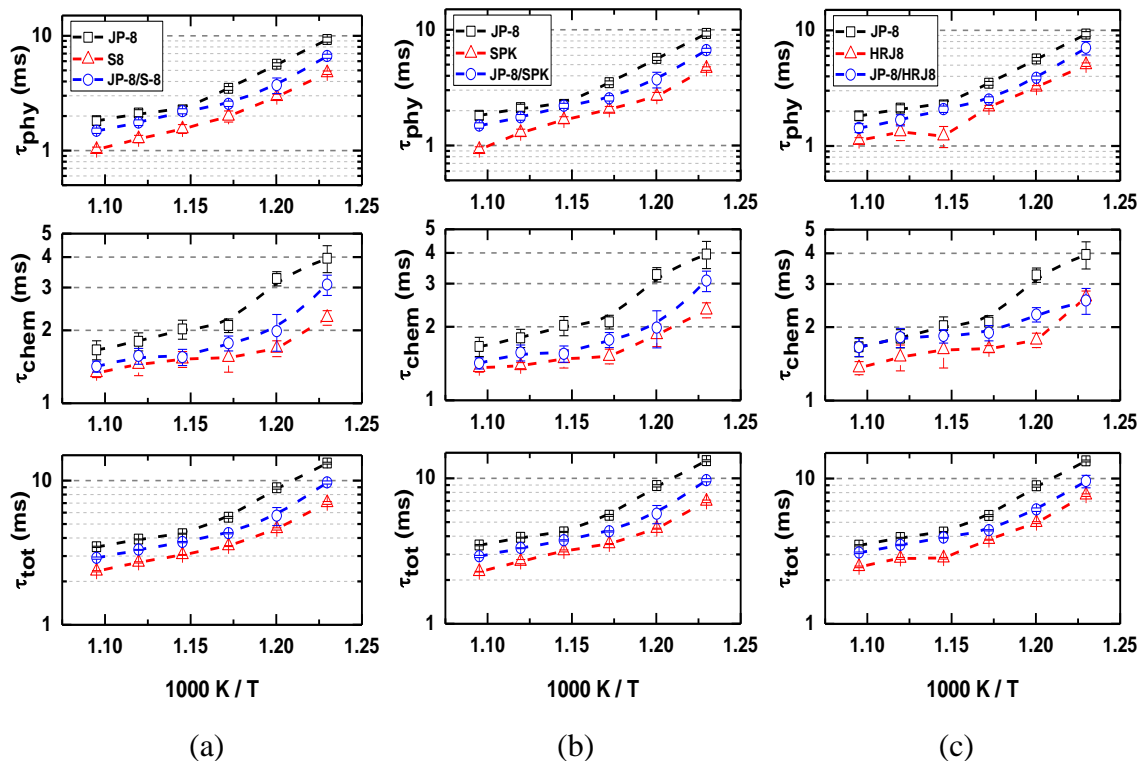


Figure 7-11 Comparisons of physical, chemical and total ignition delays of a conventional jet fuel (JP-8), synthetic alternative jet fuels including (a) S8, (b) SPK and (c) HRJ8, and 50 volume percent of JP-8 in alternative jet fuel blends in a range of temperature (540 to 640°C) at 20 bar in a constant volume spray combustion chamber

Figure 7-12 (a) compares ignition behavior of IPK with JP-8, showing that the onset of NTC behavior for IPK is 20°C higher than that for JP-8. The NTC behavior found in plots of  $\tau_{chem}$  are agree well the ignition reactivity in dedicated by the DCN. It is also found that, when blended with JP-8,  $\tau_{chem}$  of alternative jet fuels is more strongly affected by temperature than  $\tau_{phy}$ , which is dominated by the physical properties of the fuels. Likewise for reactive fuels, such as S8, SPK and HRJ8, the  $\tau_{phy}$  value of IPK linearly decreases as ambient temperature increases. Although density and viscosity of IPK are lower than those of JP-8, an opposite trend is observed for  $\tau_{phy}$  of these fuels,

showing that IPK has longer  $\tau_{\text{phy}}$  than JP-8. This is because the current method using the chemiluminescence detection system (CDS) to classify  $\tau_{\text{phy}}$  and  $\tau_{\text{chem}}$  is an approximation that breaks down in this comparison. The Arrhenius plot of  $\tau_{\text{chem}}$  of 50/50 blend of JP8/IPK exhibits a strong impact of blending of more reactive fuel (JP-8, here) on promoting the ignition reactivity, as discussed in earlier paragraph.

As seen in Figure 7-12 (b), the  $\tau_{\text{phy}}$  of 50/50 blend of JP-8 and ATJ is comparable with that of JP-8. Even though  $\tau_{\text{chem}}$  of these two test fuels are different in test conditions of interest, the onset of NTC behavior for both fuels occurs at the same temperature. The ignition delay of neat ATJ was not accurately determined in this study, due to significantly delayed ignition times observed with ATJ.

With respect to the diesel engine combustion process, the current results indicate that physical properties of the fuel become less important than the chemical properties, as in-cylinder temperature increases. However, both properties must be considered for developing more accurate diesel engine combustion models.

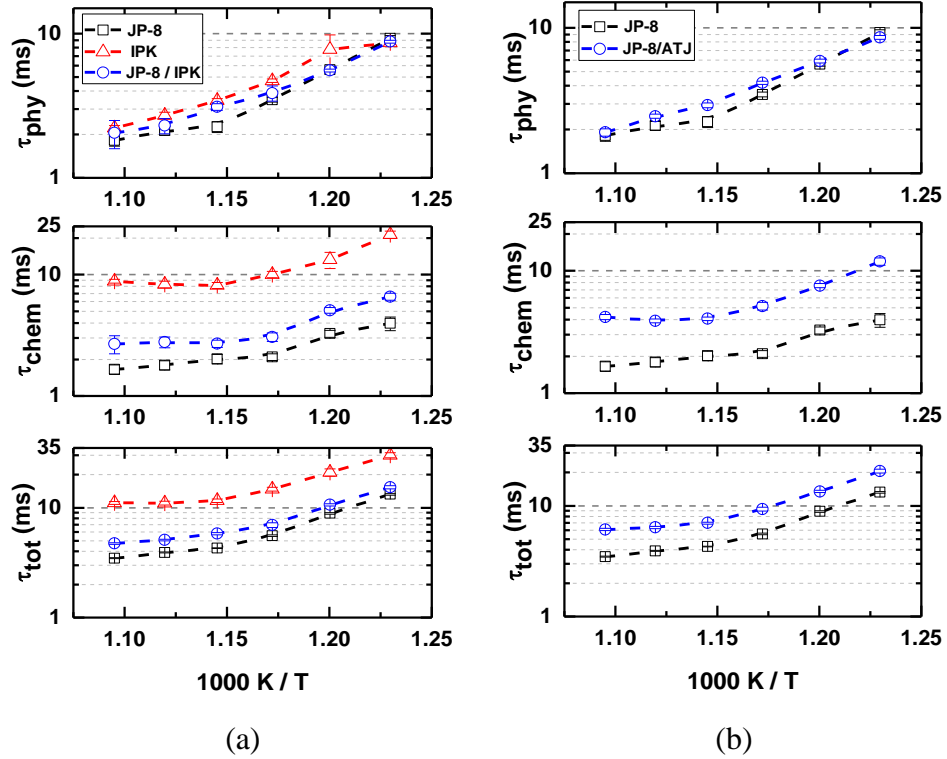


Figure 7-12 Comparisons of physical, chemical and total ignition delays of a conventional jet fuel (JP-8), synthetic alternative jet fuels, IPK and ATJ, and 50 volume percent of JP-8 in alternative jet fuel blends in a range of temperature (540 to 640°C) at 20 bar in a constant volume spray combustion chamber

## 7.5 UM I and UM II Surrogates for Jet-A (POSF 4658)

The following study deals with an experimental validation, presenting fundamental ignition behaviors of surrogate mixtures (UM I and UM II), each comprised of four different hydrocarbon molecules by matching their ignition behaviors with a target Jet-A (POSF 4658) tested in a motored engine and a constant volume spray combustion chamber.

### 7.5.1 Test Fuels

Shafer *et al.* [155] reported that the average composition of a number of Jet-A, Jet-A1, and JP-8 fuels is roughly composed of 60% *n*- and *iso*-alkanes, 20% cycloalkanes, and 20% aromatics. Based on this information Violi and co-workers considered the surrogate components for the surrogate palette based on the following criteria [100]:

- (1) The relevance to the hydrocarbon (HC) molecules in real jet fuels in terms of HC class and molecular size
- (2) The existence of chemical mechanism(s) that are capable of predicting the ignition process of the neat component
- (3) Previous use in other jet fuel surrogate studies or use that has been suggested in the literature

Violi and co-workers selected seven pure HC components from four different HC classes for their surrogate components, based on these criteria listed above [100].

However, the current study selectively considered five surrogate components used in the UM surrogates as shown in Table 11.

Table 11 Properties of individual surrogate components consisting surrogate mixtures formulated by a surrogate optimizer developed by Kim *et al.* [100]

	<i>n</i> -Dodecane	<i>Iso</i> -cetane	MCH <sup>a</sup>	Decalin	Toluene
CN <sup>b</sup>	82.5	15	20.8	46.5	7.4
MW <sup>c</sup>	170.33	226.44	98.19	138.25	92.14
LHV <sup>d</sup>	44.11	44.85	43.36	42.58	40.53
H/C	2.2	2.125	2.0	1.8	1.143

<sup>a</sup>Methylcyclohexane; <sup>b</sup>Average of the reported CNs in Murphy *et al.* [156]; <sup>c</sup>Molecular Weight in g/mol; <sup>d</sup>Lower heating value in MJ/kg from DIPPR [157]

A Jet-A blend, POSF 4658, was chosen as the target fuel, since a wide range of experimental data is readily available for this fuel. Violi and co-workers developed a model-based optimizer to formulate surrogate compositions, capable of emulating the chemical and physical properties of this representative jet fuel [100]. Essentially, two UM surrogates were formulated and were comprised of relevant individual HC components from the four different HC classes as shown in Figure 7-13. The properties of the target fuel, Jet-A (POSF 4658), and two UM surrogates are compared in Table 12. The UM I surrogate was formulated with a much tighter match for temperature-independent properties such as DCN, MW, LHV, and H/C, while the UM II surrogate was better matched to emulate temperature dependent physical properties such as density, kinematic viscosity, volatility, and surface tension, which are known to be important for spray predictions under engine relevant conditions. The DCNs for POSF 4658 and the two UM surrogates were measured by a CID unit which follows the ASTM D7668 standard [26]. The DCN value of a practical Jet-A (POSF 4658) measured by Dooley *et al.* [44] (DCN

47.1) was again confirmed in the current study, showing a very minor difference in both values. Additionally, the DCN value of UM I surrogate estimated by the surrogate optimizer also reasonably agrees with the DCN measurement from CID unit, while the estimated DCN value of UM II is slightly higher than the measured DCN value. In addition, the smoke point (and thereby the threshold sooting index, TSI) for the UM surrogates and the representative Jet-A is also measured following the ASTM D1322 standard [153]. Yang *et al.* were the first to show that TSI not only correlates the sooting tendency of individual hydrocarbons, but the TSI model correlates sooting tendency with fuel hydrocarbon composition over a wide range of fuel samples and that the correlation between TSI and actual combustor soot formation is very good over a broad range of fuel origins, combustor operating conditions, and soot formation parameters [158]. Although the surrogate optimizer took no account of the sooting tendency, soot formation in diesel engine combustion is also a critical issue. The TSI values for the UM surrogates and the target Jet-A showed that the sooting index for both surrogates are very similar but, slightly lower compared to the target Jet-A. This is likely attributed to the higher aromatic content (~ 20 vol%) in the target Jet-A than in both surrogates (13 vol% for UM I and 14 vol% for UM II), as shown in Figure 7-13.

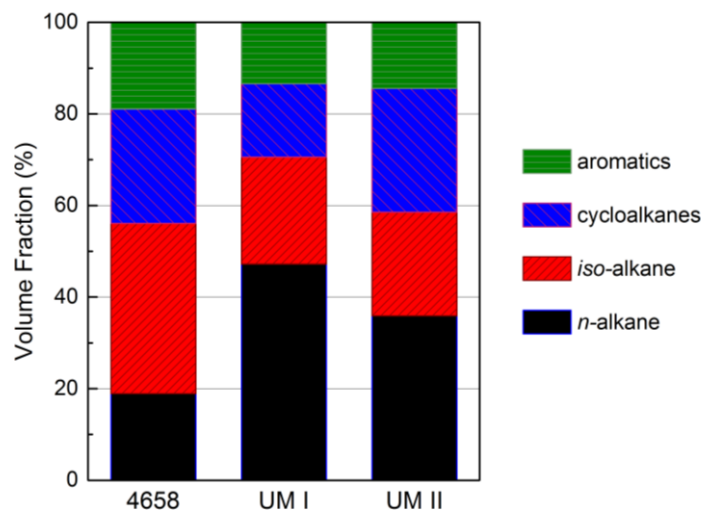


Figure 7-13 Distribution of classes of hydrocarbons as volume fraction for the UM surrogates and POSF 4658 measured in [143];

UM I: *n*-dodecane/*iso*-cetane/MCH/toluene 0.4719/0.2337/0.1608/0.1336

UM II: *n*-dodecane/*iso*-cetane/decalin/toluene 0.3592/0.2265/0.2704/0.1439

Table 12 Properties (except TSI) of a target fuel measured [44] and the UM surrogates mixtures estimated by the surrogate optimizer [100]

	POSF 4658	UM I	UM II
DCN	47.0 <sup>a</sup> /47.1	46.7 <sup>a</sup> /46.8 <sup>b</sup>	45.9 <sup>a</sup> /46.7 <sup>b</sup>
MW	142	143.5	137.2
LHV	43.23	43.62	43.36
H/C	1.967	1.881	2.018
TSI <sup>c</sup>	16.2	11.5	11.8

<sup>a</sup> ASTM D7668 [26], CID measurement of current work

<sup>b</sup> Predicted from surrogate optimizer

<sup>c</sup> ASTM D1322 [153], TSI measurement of current work

## 7.5.2 Result and discussion

### 7.5.2.1 Ignition characteristics of individual surrogate components in a motored engine

To understand the impact of each individual component on the ignition characteristics of the UM surrogate mixtures, the ignition characteristics of each of the individual chemical component must be explored. As shown in Table 10, the UM surrogate mixtures consisted of five representatives of different hydrocarbon classes including straight and branched chain alkanes, cyclic and bicyclic alkanes, and aromatics. This structural difference results in their unique chemical and physical properties, and low temperature oxidation reactivity.

Figures 7-14, 7-15 and 7-16 present the comparisons of low temperature oxidation reactivity of five individual components using different approaches. Figure 7-14 (a) shows the maximum mass-averaged bulk in-cylinder temperature as a function of compression ratio for five individual fuel components. The maximum in-cylinder temperature is obtained from a mass-averaged approximation of the highest global temperature that occurred in the combustion chamber and calculated using the ideal gas law in combination with the direct measurement of in-cylinder pressure. It is commonly observed that each test fuel has a certain CR where the maximum cylinder temperature abruptly increases. This event is referred to as thermal runaway [121]. A dashed linear line shown in Figure 7-14 (a) indicates the thermal runaway for the individual fuel components, where the high temperature heat release begins. Toluene, an aromatic representative, requires relatively high in-cylinder temperature to initiate rapid chain branching reactions and shows evident temperature rise in a narrow range of CRs. In



contrast, for *n*-dodecane, which is a representative of *n*-alkanes, the maximum in-cylinder temperature gradually increases, resulting in less clear transition to the onset of thermal runaway, compared to the other components. Despite operation at constant  $\phi$ , which amounts to approximately the same amount of fuel introduced in the combustion chamber, the maximum in-cylinder temperatures at the same CR exhibits significant disparities among the five test fuels, representing their unique low temperature oxidation reactivity. This is a case of more reactive fuel participating more actively in the low temperature oxidation, leading to higher maximum in-cylinder temperature.

Figure 7-14 (b) displays the apparent heat release rate (AHRR) for individual components obtained at different CRs, which corresponds to their maximum in-cylinder temperatures around 1120 K, marked as a black circle for each fuel in Figure 7-14 (a). Following the ignition characteristics of the test fuels, these compounds can be divided into two groups based on the test condition of interest: those with single-stage ignition and those with two-stage ignition. *n*-Dodecane clearly shows two-stage heat release. In contrast, other components, except toluene with no HRR under the test condition of interest, show a single-stage heat release. It is important to note that this might be suppressed either by fuel and air intake temperatures and/or due to a fuel-lean condition, resulting in the absence of LTHR. It is well documented that before reaching the thermal runaway point for single-stage ignition fuels, the maximum in-cylinder temperature is dominated by intermediate temperature heat release (ITHR) reactions [121,159]. Therefore, the dashed line shown in Figure 7-14 (a) may delineate a range of the maximum temperatures of the five test fuels during ITHR. This agrees well with a study from Hwang *et al.*, revealing the maximum in-cylinder temperature from 950 K to 1170

K during ITHR [121]. Over the dashed line, the maximum in-cylinder temperature is mainly influenced by high temperature heat release (HTHR) reactions. Thus, the HRR for single-stage ignition fuels shown in Figure 7-14 (b) captures the transition from ITHR to HTHR, based on the definition of HTHR used in this study. From the HRR of the single-stage ignition fuels, the oxidation reactivity for individual components can be compared. For example, the magnitude of HRR of decalin is stronger at lower CR than that of methylcyclohexane (MCH), indicating that decalin has higher oxidation reactivity than MCH. In particular, no HRR for toluene was observed even at a CR of 12. As a result, comparing the HRRs of the four compounds follows the trend of  $HRR_{Decalin} > HRR_{MCH} > HRR_{Iso-cetane} > HRR_{Toluene}$  in terms of their reactivity, as observed in this study.

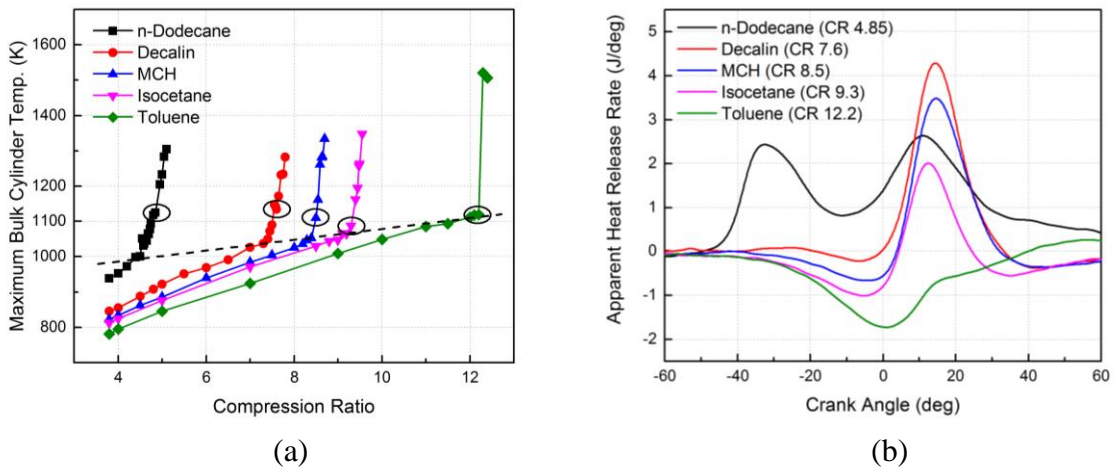


Figure 7-14 Low temperature oxidation reactivity comparisons of five pure individual hydrocarbons at equivalence ratio of 0.25 at intake temperature of 260°C; (a) Maximum bulk in-cylinder temperatures as CR increases; and (b) apparent heat release rates for each individual component at ~1120 K of the maximum bulk in-cylinder temperatures, which are marked as black circles in (a)

Carbon monoxide (CO) is largely formed in localized regions of the combustion chamber in which low temperature reaction pathways are active. For this reason, monitoring raw CO emissions in real time enables observation of the global oxidation reactivity and the negative temperature coefficient (NTC) behavior of the individual components during the CR sweep. CO is mostly formed through a consecutive hydrogen abstraction from formaldehyde (CH<sub>2</sub>O), which is largely formed during LTHR [7]. As can be seen in Figure 7-15 (a), CO emissions of individual test fuels are formed in accordance with the in-cylinder temperatures, shown in Figure 7-14 (a). Furthermore, the global oxidation reactivity of the test fuels can be identified by the CCR where the CO emission begins to decline also resulting in increased CO<sub>2</sub> emission. *n*-Dodecane forms considerable CO, as it exhibits the strongest LTHR behavior among the test fuels. It is well displayed in Figure 7-15 (a) that as global reactivity of the test components decreases, CO reduces and the CCR is delayed. Figure 7-15 (b) shows CO emissions for decalin, MCH, *iso*-cetane and toluene at CRs between 3 and 11. The CO emissions for cycloalkane fuels; decalin and MCH, show NTC behavior in the low temperature regime. MCH, which is a less reactive fuel, shows more prominent NTC behavior than the more reactive fuel, decalin. This is because the ceiling temperature of decalin is lower than that of MCH resulting in earlier shut down of the low temperature pathway. The ceiling temperature represents the temperature at which the equilibrium constant of reaction  $R\cdot + O_2 \leftrightarrow RO_2\cdot$  reaches unity, and thus when a less reactive fuel enters NTC regime, the reactive fuel should be in higher temperature regime where Arrhenius law applies again [8]. One interesting observation is that *iso*-cetane and toluene have virtually no NTC

behavior in the test conditions of interest, while *n*-dodecane could show NTC behavior if it is made accessible to relatively lower in-cylinder temperatures and lower CRs.

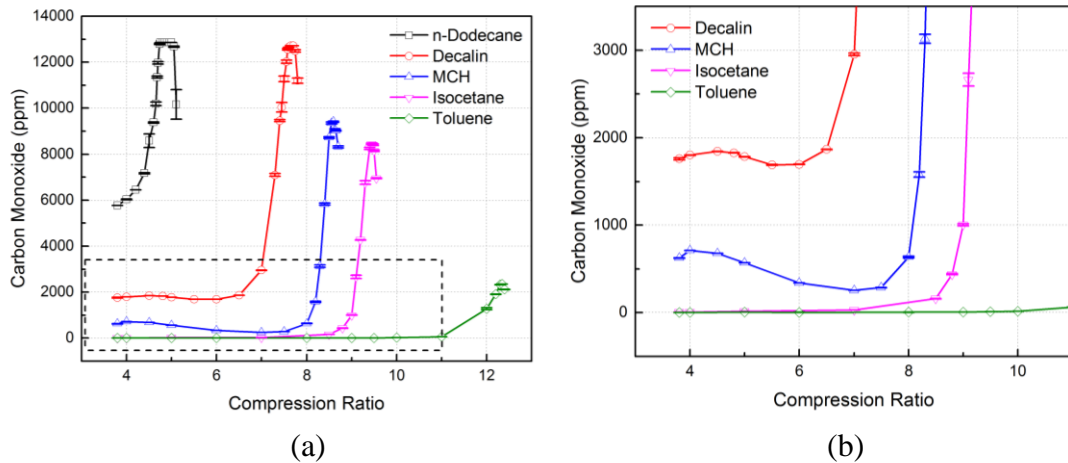


Figure 7-15 Low temperature oxidation reactivity comparisons of five pure individual hydrocarbons at equivalence ratio of 0.25 at intake temperature of 260°C; (a) CO emission for each individual compound in a wide range of compression ratio, representing a good indication of critical compression ratio (CCR) (b) Zoom-in on the dash-square shown in (a). The error bars indicate 95 % confidence interval.

Figure 7-16 shows the critical  $\phi$  of each individual component and the target Jet-A (POSF 4658) at the given CRs. The critical  $\phi$  is determined as the  $\phi$  where the CO emissions begin to decline during a sweep of  $\phi$  beginning at a  $\phi$  of either 0.15 or 0.2. As can be seen in Figure 7-16, the trend of the critical  $\phi$  is distinctly different for each of the test fuels, which possess a wide spectrum in oxidation reactivity. It is found that the relatively lower reactivity fuels, for instance toluene, require higher in-cylinder temperature around 1200 K, corresponding to higher CR, to produce active radicals, regardless of  $\phi$ . After passing the thermal runaway temperature, although  $\phi$  controls the overall reaction rate, the chain branching dominates the overall chemical reaction kinetics, resulting in a rapid autoignition. This can explain why toluene has the narrowest CR range as a function of critical  $\phi$ . In contrast, for the case of reactive fuels, such as *n*-

dodecane and the target Jet-A,  $\phi$  plays a crucial role in the autoignition process. The more the fuel is introduced, the greater is the low temperature chain branching in LTHR, such that the reaction rates can be influenced by the amount of fuel injected into the combustion chamber. The black arrow shown in Figure 7-16 indicates that the low temperature reactivity of the fuels follows the order *n*-dodecane > POSF 4658 > decalin > MCH > *iso*-cetane >> toluene.

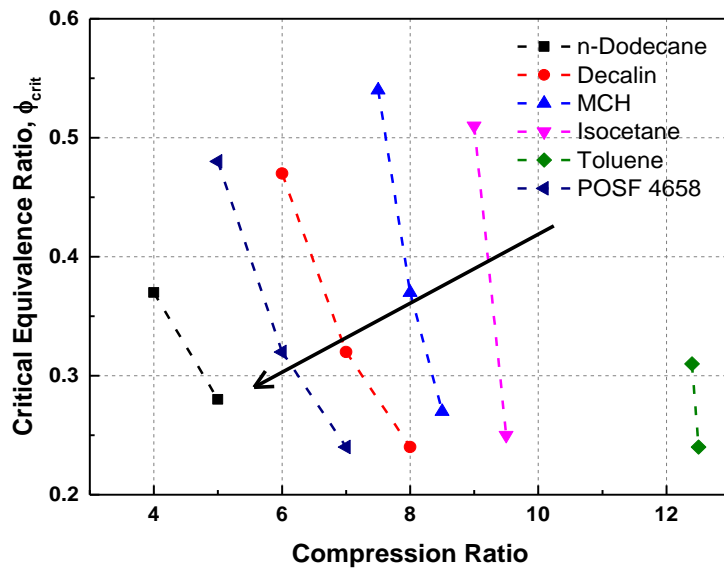


Figure 7-16 Low temperature oxidation reactivity comparison in critical equivalence ratios of each individual component and a target Jet-A over a wide range of compression ratios

#### 7.5.2.2 Ignition characteristics of UM surrogates and a target Jet-A in a motored engine

To properly address the fundamental ignition characteristic comparisons of UM surrogate mixtures (UM I and UM II) and the target Jet-A, two equivalence ratios are considered here (0.25 and 0.5) because the ignition behavior for these conditions can vary significantly. A fuel-lean condition ( $\phi=0.25$ ) can provide a thermal-runaway point with evident two-stage ignition, which is induced by ITHR, shown already in the previous

section. For the higher equivalence ratio condition ( $\phi=0.5$ ), evident low temperature chemistry and HTHR can be clearly observed without the presence of ITHR. Figures 7-17 and 7-18 show the maximum in-cylinder temperatures and CO emissions, which have been used as indicators to determine the ignition limit behavior including CCR and critical  $\phi$ . Here it is observed that the CCR of the target Jet-A and UM II match well, while UM I exhibits advanced CCRs in both cases. For a fuel-lean condition ( $\phi=0.25$ ), as shown in Figure 7-17 (a), the maximum in-cylinder temperature of the UM surrogates in the low temperature regime ( $\sim 950$  K) is well matched with that of POSF 4658. However, as test fuels reach the ITHR regime above a CR of 6.3 corresponding to an in-cylinder temperature of  $\sim 970$  K, the maximum in-cylinder temperature of UM surrogates diverges from that of a target Jet-A. UM I consequently exhibits thermal runaway temperatures at lower CR, corresponding to  $\sim 1036$  K. However, UM II requires a slightly higher CR to meet the thermal runaway temperature ( $\sim 1020$  K), thus eventually satisfying a similar CCR as for the target Jet-A. A similar observation is made for  $\phi$  of 0.5. Although the in-cylinder temperature for the UM surrogates and the target Jet-A during low temperature oxidation lies in almost the same range between 820 K and 900 K, the CCR of 4.75 for the complete combustion of UM I surrogate is advanced, compared to its counterpart. In contrast, the maximum in-cylinder temperature for UM II and the target Jet-A is 20 K higher than for UM I to meet the complete combustion as indicated by a higher CCR of 4.92 for the target Jet-A and a CCR of 4.95 for the UM II surrogate.

Figure 7-18 shows CO emissions for the test fuels over a wide range of CRs, representing how well the overall reaction kinetics of the UM surrogate mixtures are

matched with that of the target Jet-A in the low temperature regime. As can be seen in Figures 7-18 (a) and (b), the overall reaction rates for UM II for both cases are very well matched with the target Jet-A. While the global reactivity is well matched, representing the complex jet fuel mixture exactly, when jet fuels consist of hundreds of compounds, using only four components represents a major challenge. The selection of the fuel components that comprise the surrogate mixture can be done to represent groups or classes of compounds found in the target fuel, but this raises the question of which species one needs to select to represent a class of compounds. The question of species selection can account for two major phenomena, which are, a stronger reactivity of UM I and a discrepancy of CO emission trends. In the low temperature regime, the reactivity is mostly governed by chain branching, especially in both reactions,  $R\cdot + O_2 \leftrightarrow RO_2\cdot \leftrightarrow QOOH$ , where the *n*-alkane group stands out as having the strongest reactivity. Therefore, it is possible that having over 40 volume percent of *n*-dodecane in UM I leads to stronger ignition reactivity during the low temperature regime, compared to the target Jet-A, which contains approximately 20 volume percent of *n*-alkanes. Furthermore, the abundance of *n*-alkanes in the surrogate mixtures results in a discrepancy of CO formation during low temperature oxidation, even though their global reaction kinetics are similar, as shown in Figure 7-18 (b). For this reason, the global reaction rate of the UM I surrogate in both cases somewhat disagrees with that of the target Jet-A. Interestingly, virtually no NTC behavior was observed for all of the test fuels over the range of CRs and  $\phi$ s tested.

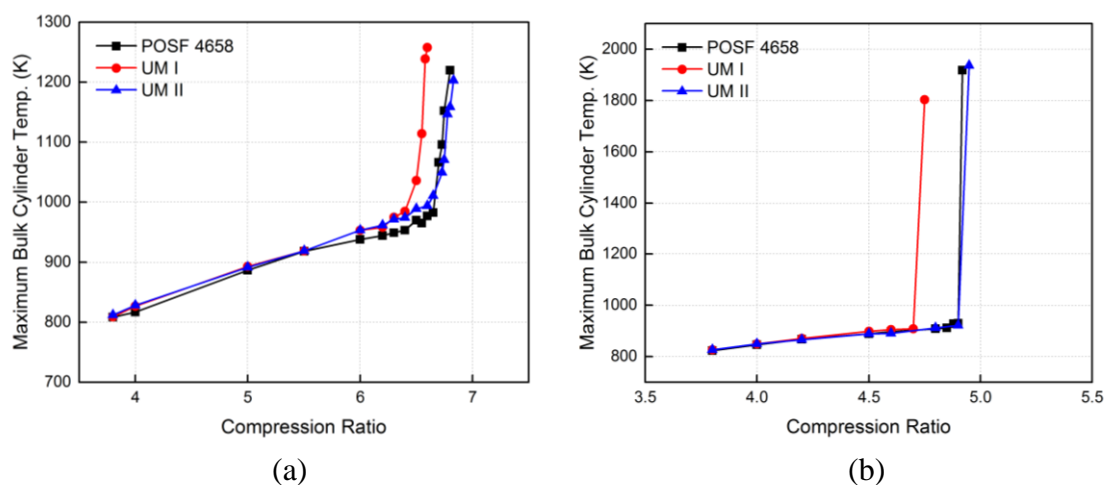


Figure 7-17 The maximum mass-averaged bulk in-cylinder temperature of the target Jet-A (POSF 4658) and the two UM surrogates during a CR sweep; (a)  $\phi=0.25$  (b)  $\phi=0.5$

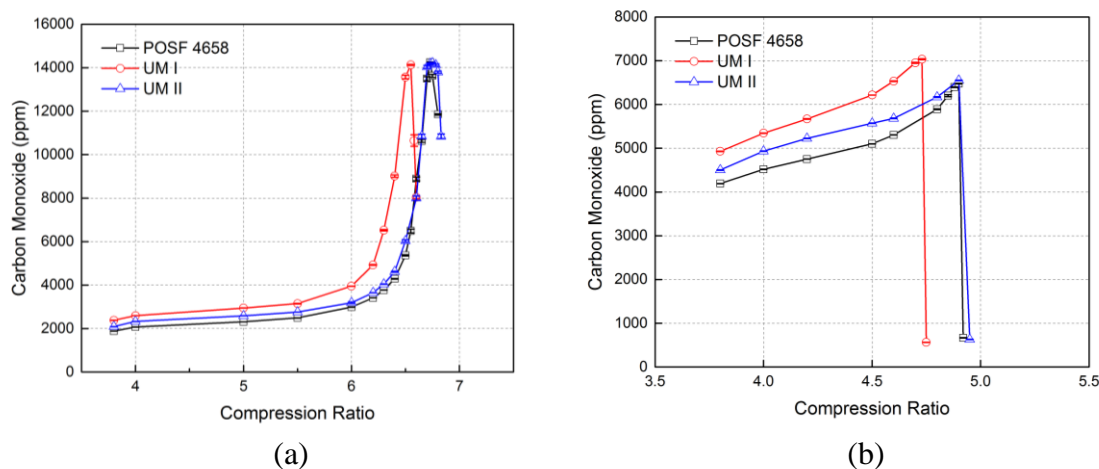


Figure 7-18 CO emissions of the target Jet-A (POSF 4658) and the two UM surrogates in a wide range of CR; (a)  $\phi=0.25$  and (b)  $\phi=0.5$ . The error bar indicates a 95% confidence interval.

Figure 7-19 shows apparent heat release rate for the target Jet-A, and UM surrogates at a condition prior to autoignition where low temperature heat release is observed. In this low temperature regime, two UM surrogates seem to be well matched with the target Jet-A, in terms of their low temperature combustion phasing and magnitude. It is commonly observed for all test fuels of both cases ( $\phi=0.25$  and  $\phi=0.5$ )



that the phasing of LTHR gets advanced as CR increases. The small differences in the magnitude of HRR amongst the test fuels are consistent with the observations made earlier while discussing the reactivity in low temperature regime. For example, in both conditions shown in Figures 7-17 and 7-18, higher CO formation of UM I in low temperature regime results in greater HRR as compared to the other fuels during the CR sweep. In Figure 7-19 (a), it is observed that UM I lies in the middle the transition from ITHR to HTHR at CR of 6.5, while UM II and target Jet-A remain in the initial phase of ITHR at the same CR, which is also confirmed in Figure 7-17 (a). Therefore, strong two-stage ignition behavior is observed for UM I, while UM II and target Jet-A exhibit weak two-stage ignition behavior at the same CR of 6.5.

Figure 7-19 shows the AHRR of the target Jet-A, and the UM surrogates at CCR in both cases ( $\phi=0.25$  and  $\phi=0.5$ ). As already mentioned earlier, the HTHR of UM II in both cases are observed at similar CRs as compared to target Jet-A, while earlier CCR is observed for UM I. The 1<sup>st</sup> and 2<sup>nd</sup> stage combustion phases for the UM surrogates are comparable to that of the representative jet fuel in both cases as shown in Figures 7-19 (a) and (b). Detailed combustion characteristic comparisons between target Jet-A and UM II include calculated % LTHR, and 1<sup>st</sup> and 2<sup>nd</sup> CA 50 (crank angle where 50 percentage of cumulative heat release occurs) observed for an autoignition condition. In the case of low equivalence ratio condition, shown in Figure 7-20 (a), the low temperature reactivity expressed as calculated % LTHR ( $19.133 \pm 3.82$ ) of the UM II is stronger compared to % LTHR ( $14.71 \pm 1.01$ ) of the target Jet-A. However, ignition phasing is very similar with 1<sup>st</sup> CA 50 ( $^{\circ}\text{ATDC}$ ) of UM II ( $-32.22 \pm 1.83$ ) and POSF 4658 ( $-34.16 \pm 0.76$ ) and 2<sup>nd</sup> CA 50 ( $^{\circ}\text{ATDC}$ ) of UM II ( $11.33 \pm 0.22$ ) and POSF 4658 ( $9.91 \pm 0.28$ ). In comparison, a

relatively more fuel rich condition ( $\phi=0.5$ ) is shown in Figure 7-19 (b). Here, % LTHR<sub>s</sub> of UM II ( $7.29 \pm 1.13$ ) and the target Jet-A ( $6.01 \pm 1.35$ ) indicate similar low temperature reactivity. Despite matching the 1<sup>st</sup> CA 50 ( $^{\circ}$ ATDC) for the target Jet-A ( $-33.70 \pm 4.15$ ) and UM II ( $-28.96 \pm 4.20$ ), the 2<sup>nd</sup> CA 50 ( $^{\circ}$ ATDC) there is some discrepancy in matching the combustion phasing, representing a more delayed CA 50 ( $^{\circ}$ ATDC) for UM II ( $-1.4 \pm 1.12$ ) than for the target Jet-A ( $-7.11 \pm 0.97$ ). As discussed in the earlier section, among the five individual components comprising the surrogate mixture, only *n*-dodecane exhibits two-stage ignition behavior at the same experimental condition. Matching the first stage heat release relies on the amount of *n*-alkanes, in this case *n*-dodecane, affecting % LTHR. This also implies that the various *n*-alkanes, which exist in a real Jet-A, control the magnitude and timing of the first stage heat release of the two-stage ignition behavior of the target Jet-A at this experimental condition.

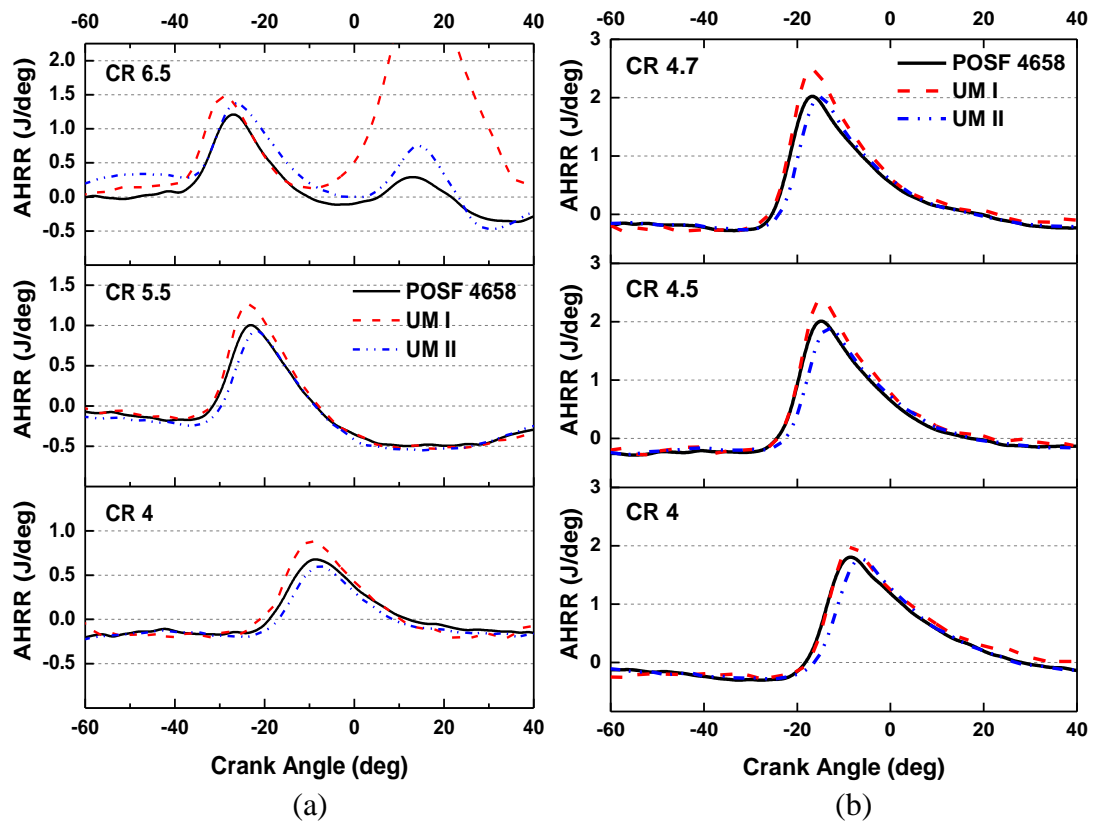


Figure 7-19 Comparisons of LTHR of the practical Jet-A (POSF 4658) and two UM surrogate mixtures; (a)  $\phi=0.25$  and (b)  $\phi=0.5$

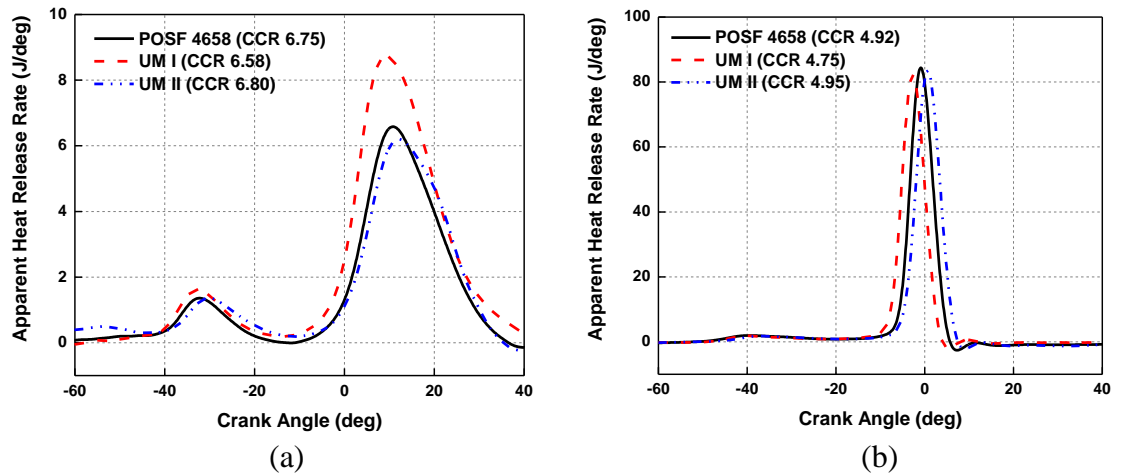


Figure 7-20 Comparisons of HRR of the target Jet-A (POSF4658) and two UM surrogate mixtures; (a)  $\phi=0.25$  and (b)  $\phi=0.5$

The critical  $\phi$  of the UM surrogates and the target Jet-A was assessed by monitoring CO emissions at three different CRs of 5, 6 and 7. The CO emission is used as an indicator to observe critical  $\phi$ , where CO emission is mostly converted to CO<sub>2</sub>. As can be seen in Figure 7-21, higher CR achieves CO conversion at leaner mixtures, but produces more CO emissions along the  $\phi$  sweep. The results of the critical  $\phi$  comparisons show that the UM I and UM II are relatively well matched at higher CR with a leaner mixture. This condition could be the representative of a constant volume combustion chamber where the DCN value of test fuels is measured, because when CR decreases to 5, the disparity of critical  $\phi$  between UM surrogates and a target Jet-A becomes more noticeable, even though DCN values of UM surrogates are reasonably similar as that of a target Jet-A. It should be also noted that the observed amounts of CO emission are different at the same local equivalence ratio for each surrogate and the practical Jet-A. This can be attributed to the different fuel compositions in each test fuel. Lilik *et al.* showed the higher volume fraction of reactive components, such as *n*-alkanes in the fuel composition can significantly reduce unburned products from incomplete combustion, once compared with the similar CN fuels [87]. However, an arguable observation is found that UM I, which has almost twice as much *n*-alkane as in the target Jet-A, produced more CO at the same local equivalence ratio for most of test conditions, especially at CR 5 and 6.

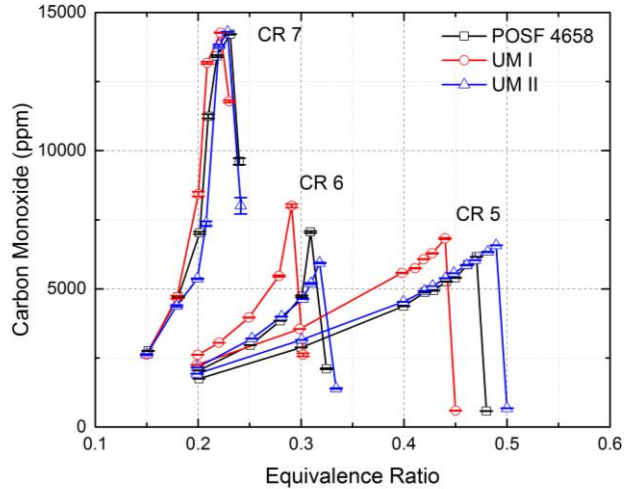


Figure 7-21 Comparisons of critical equivalence ratios of the target Jet-A (POSF4658) and two UM surrogate mixtures at different CRs. The error bar indicates 95% confidence interval.

An intake air boosting system, which enables boosting the intake air pressure up to 3 bar (abs), was employed in the current CFR motored engine. To avoid high pressure rise rates at higher intake pressures, a fuel-lean condition was selected ( $\phi = 0.25$ ). Furthermore, intake pressure higher than 2 bar (abs) was not investigated as the fuels were very reactive at 2 bar (abs) intake pressure, and any increase in intake pressure resulted in autoignition even at the lowest possible compression ratio in this engine. As such, the low temperature combustion characteristics prior to autoignition could not be investigated. As mentioned earlier, the CO emissions were monitored to observe the CCR for the test fuels at which the HTHR is detected at different intake air pressures. Figure 7-22 (a) shows the trends of CCR for the target Jet-A and UM surrogate mixtures at 5 different intake air pressures, including naturally aspirated intake condition and up to 2 bar (abs) in a stepwise manner. It is observed that the global reactivity of UM I surrogate agreed well with that of the target Jet-A at even higher intake air pressures, showing no

noticeable distinction between CCRs of both fuels. This result demonstrates that the selected four individual compounds that comprised of UM II surrogates are well formulated to mimic the global reaction kinetics over a range of intake air pressures. However, a considerable gap between the UM I surrogate and target Jet-A still remains over the higher intake air pressures. Figure 7-22 (b) shows HTHR traces of POSF 4658 and UM surrogates at different intake air pressures. These results indicate that no dramatic change in ignition phasing with intake air boosting system is observed, though the magnitude of HRR noticeably increases with increasing intake air pressure.

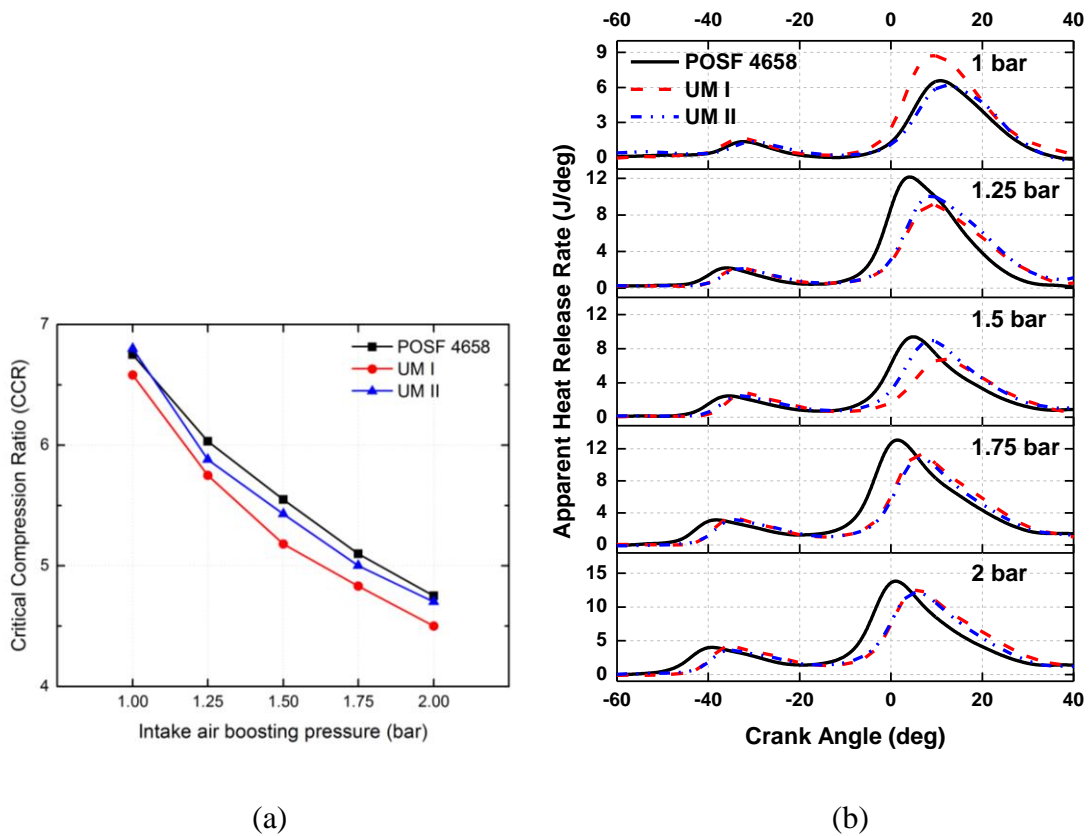


Figure 7-22 Comparisons of critical compression ratios and AHRR of a practical jet fuel and two UM surrogate mixtures with intake air boosting.

### 7.5.2.3 Ignition delay of individual components in a CVCC

Physical and chemical ignition delay values for individual surrogate components and the target Jet-A (POSF 4658) were calculated from the PMT voltage signals as described previously. The results for physical ignition delay ( $\tau_{\text{phys}}$ ) are plotted in Figure 7-23 (a). The Arrhenius plot for test fuels revealed a linear dependence of  $\tau_{\text{phys}}$  on air temperature, except for *n*-dodecane. The trend of  $\tau_{\text{phys}}$  for *n*-dodecane is slightly nonlinear and indicates that the PMT voltage signal is not likely to capture solely  $\tau_{\text{phys}}$ , but includes a phase transition from  $\tau_{\text{phys}}$  to the chemical ignition delay ( $\tau_{\text{chem}}$ ) for the given conditions of interest. Increased air temperature resulted in shorter physical ignition delays across all the temperatures tested. Values for  $\tau_{\text{phys}}$  were ordered from shortest to longest duration as *n*-dodecane < POSF 4658 < decalin < MCH < *iso*-cetane. This result indicates that increasing viscosity and decreasing volatility associated with these fuels results in decreased mixing rates and therefore increases of  $\tau_{\text{phys}}$ , as discussed by Obert [158]. Among the four individual components, decalin possesses the most similar physical properties compared to those of the target Jet-A, thus explaining the well matched value of  $\tau_{\text{phys}}$  for decalin compared to the target Jet-A. A plot of chemical ignition delay ( $\tau_{\text{chem}}$ ) presents a linear trend for *iso*-cetane, but non-linear trends for other test fuels, as shown in Figure 7-23 (b). This result shows the uniqueness of ignition characteristics of each chemical structure and Jet-A over a range of test conditions. Chemical ignition delay ( $\tau_{\text{chem}}$ ) of the target Jet-A displays a linear trend starting from the lowest temperature (813K) up to about 853K. At high temperature, however, the plot diverged in a similar manner to the NTC behavior observed under these pressure conditions in a shock tube [44,139]. This typical NTC behavior is also observed for individual surrogate

components, although this NTC trend appears for a different temperature range, based on the ignition characteristics. The NTC behavior for cycloalkane fuels, MCH and decalin, is observed at 873K, which is higher than the temperature recorded for the target Jet-A. In contrast, the evident NTC trend of *n*-dodecane was found at lower temperature than for the target Jet-A. Over the temperature range used in this study, this ignition behavior of *n*-dodecane agrees well with the work by Vasu *et al* who used a shock tube comparing the ignition delays of Jet-A at similar conditions [42]. Although the relatively narrow scope of our experimental condition limits the comparison of ignition delay over a larger range of temperature, which have been considered by other researchers using various combustion chambers, these observations of chemical ignition delay over a narrow temperature regime remains meaningful, because NTC behavior is observed for some of the fuels. A relatively linear trend of  $\tau_{\text{chem}}$  for *iso*-cetane accounts for the absence of NTC behavior over this temperature range.



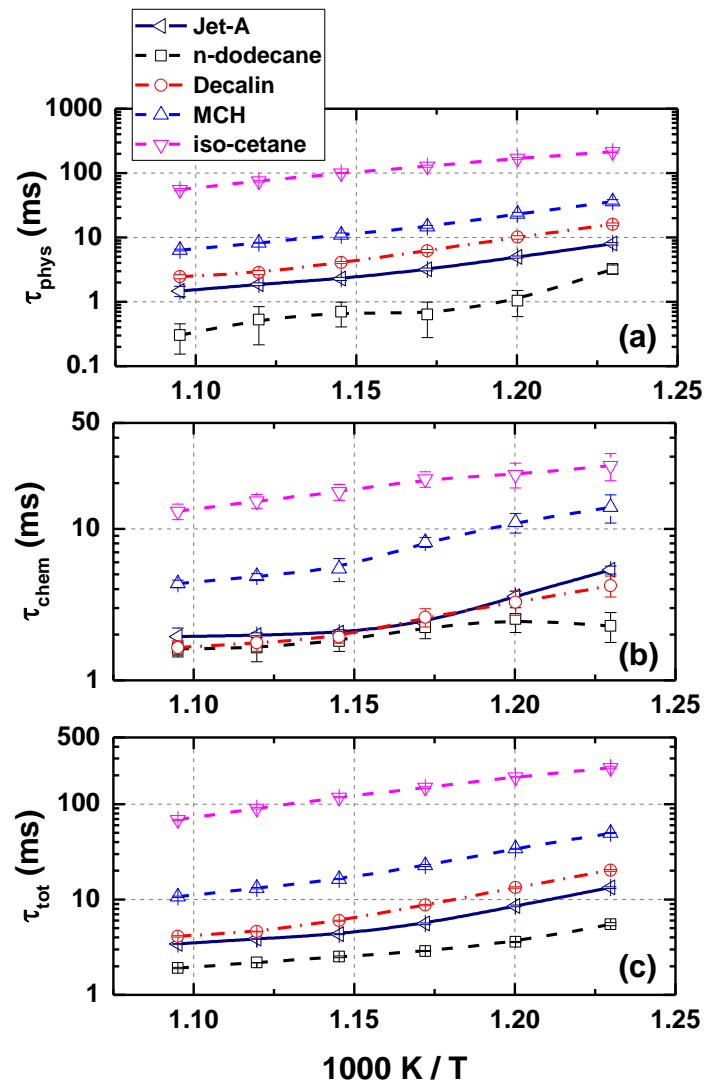


Figure 7-23 Ignition delays against air temperature for individual components and the target Jet-A (POSF 4658); (a) Physical ignition delay (b) Chemical ignition delay and (c) Total ignition delay. The error bar indicates 95% confidence interval.

#### 7.5.2.4 Ignition delay of UM surrogates and the target Jet-A in a CVCC

##### 7.5.2.4.1 Air Temperature Sweep

To validate the UM surrogate mixtures, which are intended to emulate the liquid fuel spray characteristics and gas phase combustion characteristics,  $\tau_{\text{phys}}$  and  $\tau_{\text{chem}}$  for these mixtures are measured by varying the intake air temperature. The results for two UM surrogate mixtures are plotted with target Jet-A for comparison, as shown in Figure 7-24. As with  $\tau_{\text{phys}}$  for the individual components, increasing air temperature shortens  $\tau_{\text{phys}}$  for the test fuels in a linear fashion, shown in Figure 7-24 (a). It is also observed that UM II surrogate mixture emulates the physical properties of the target Jet-A, better than UM I. This result is anticipated as UM II was originally formulated to better match the physical properties of the target Jet-A than UM I by adding a different cycloalkane, decalin, instead of MCH. Decalin possesses an improved matching of physical properties such as higher density, viscosity, and low vapor pressure compared to MCH, resulting in a better representation of mixture density and viscosity, as well as the distillation temperatures. However, as the temperature increases above 893 K, the gap of physical process related to fuel spray break-up and droplet evaporation time between the two UM surrogate mixtures becomes minor. Regardless of the air temperature, it is noted that  $\tau_{\text{phys}}$  for UM surrogates are somewhat different from  $\tau_{\text{phys}}$  of the target Jet-A, indicating that surrogate mixtures with only four individual components might not be able to emulate  $\tau_{\text{phys}}$  of the target jet fuel, which is comprised of hundreds of chemical compounds. Unlike  $\tau_{\text{phys}}$ ,  $\tau_{\text{chem}}$  for the UM surrogate mixtures are relatively well matched with that of target Jet-A, in the range of temperature tested, as shown in Figure 7-24 (b). This result demonstrates that the UM surrogate mixtures emulate the low temperature gas phase

combustion kinetics of the target Jet-A. A small difference in combustion characteristics of UM I compared to other test fuels is revealed at different air temperatures at which NTC behavior for each test fuel is observed. For UM II and the target Jet-A  $\tau_{chem}$  exhibits an almost identical trend as a function of temperature, where NTC behavior of UM I begins about 20K higher temperature (873K) than for the other two test fuels.

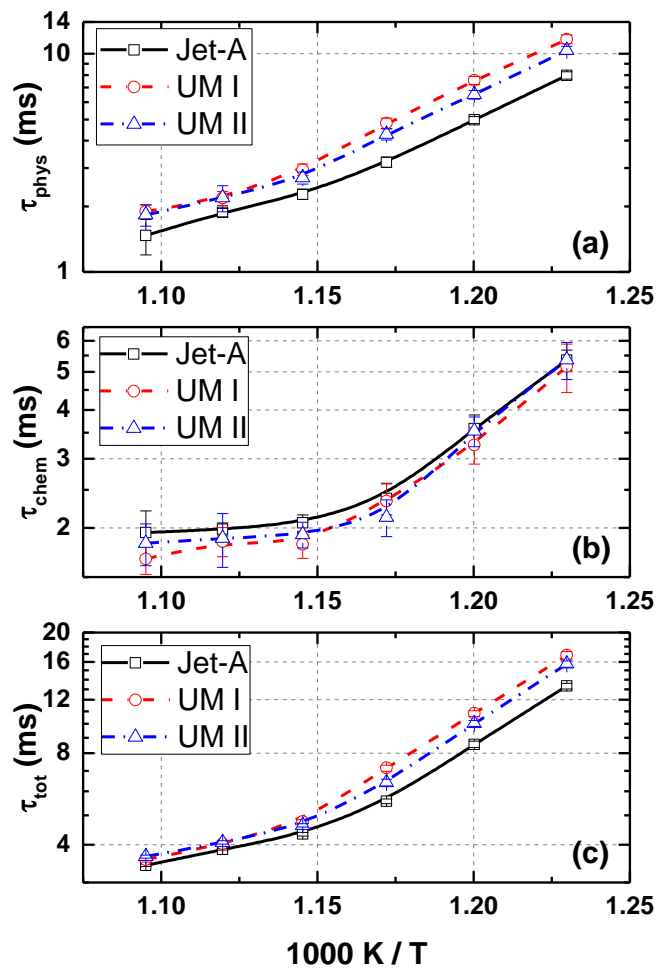


Figure 7-24 Ignition delays against air temperature for UM surrogate mixtures and the target Jet-A (POSF 4658); (a) Physical ignition delay (b) Chemical ignition delay and (c) Total ignition delay. The error bar indicates 95% confidence interval.

Apparent heat release rate (AHRR) was calculated from the combustion chamber pressure trace data captured during these tests. The impact of air temperature is revealed by observing the AHRR profiles for each fuel across the 540-640°C temperature range, as plotted in Figure 7-25, which shows that the target Jet-A is most reactive at all temperatures considered. This observation can be attributed to the total ignition delay ( $\tau_{\text{tot}}$ ) recognized as the time delay between the start of injection (SOI) and the high temperature heat release (HTHR). It is also observed that lower intake air temperatures greatly increase the delay between SOI and the low temperature heat release (LTHR) peak for all test fuels, but the surrogate, UM I, appears to be affected the most. Although  $\tau_{\text{tot}}$  for UM surrogate mixtures disagrees with that of the target fuel at lower air temperature (540-580°C), as the air temperature rises above 600°C,  $\tau_{\text{tot}}$  for both UM surrogate mixtures becomes comparable that of the target Jet-A. Furthermore, two-stage heat release is observed for all the test fuels at all the test conditions, leading to a comparison analysis of % LTHR values, shown in Figure 7-26. The % LTHR for the two UM surrogate mixtures are comparable with that of the target fuel at all of the test conditions. This demonstrates that low temperature chemistry for both UM surrogate mixtures is well emulated, reasonably matching the % LTHR of a target Jet-A, as is also confirmed in the motored engine. It is clearly shown that as the air temperature increases, % LTHR for the test fuels decreases in a linear fashion. High air temperature expedites the ignition rate of the fuel once the fuel spray is injected into the combustion chamber, resulting in short time for air and fuel to mix and consequently resulting in lower % LTHR. Fast and strong ignition rate leads to “sharp” HTHR, whereas slow ignition rate at low air temperatures leads to “slow and wide” HTHR.

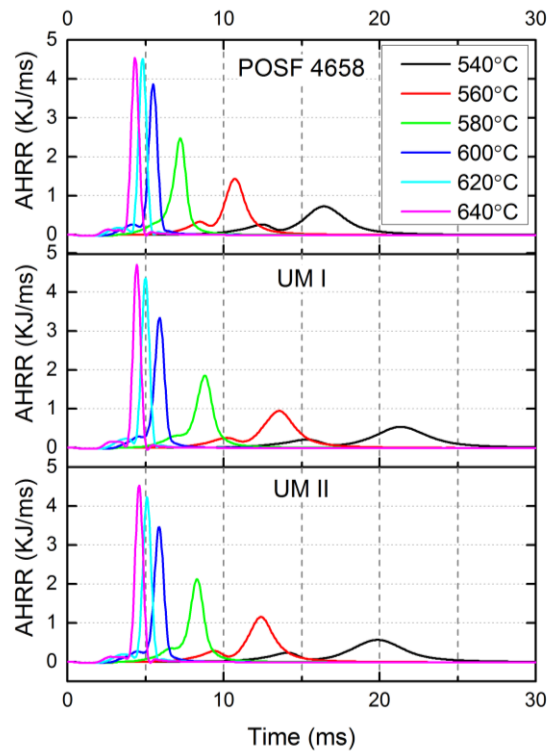


Figure 7-25 Apparent heat release rate profile at various chamber temperatures for the UM surrogate mixtures and the target Jet-A (POSF 4658).

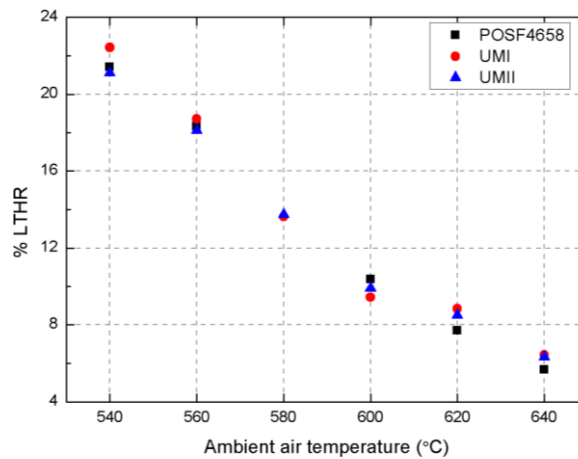


Figure 7-26 The percentage of low temperature heat release in a sweep of chamber temperature for the target Jet-A (POSF 4658) and the UM surrogate mixtures

#### 7.5.2.4.2 Oxygen Dilution by Exhaust Gas Recirculation

Oxygen dilution by using EGR has drawn attention as a means for reducing particular matters (PM) and NO<sub>x</sub>, but it tends to increase unburned hydrocarbon (UHC) and CO emissions in advanced combustion modes. This benefit is provided based on the fact that increased dilution can prolong ignition delay, providing additional time for mixing [1]. The ignition delay values of the physical and chemical processes were measured for the two UM surrogates and the target Jet-A, across the complete EGR dilution range as shown in Figure 7-27. Figure 7-27 (a) shows results for physical ignition delay ( $\tau_{\text{phys}}$ ) of the test fuels, indicating that oxygen dilutions rarely affects the mixing process of the test fuels, resulting in no evident change, regardless of the type of the fuel blend and different types of fuel components. As already discussed, in Figure 7-24 (a),  $\tau_{\text{phys}}$  of UM II is the closest to that of the target fuel for the whole oxygen dilution range, likely recognized to its well emulated physical properties, compared to that of UM I. It was also noted earlier that *n*-dodecane produced the shortest  $\tau_{\text{phys}}$ , likely attributable to its significantly different physical properties such as higher volatility and lower viscosity. However, the non-linear trend for  $\tau_{\text{phys}}$  of *n*-dodecane is difficult to explain, due to significant uncertainty of ignition delay as was observed in a range between 0 to 25% EGR rates, shown in Figure 7-27 (a). In contrast, decalin has an opposite trend in physical properties as that of *n*-dodecane, resulting in relatively longer  $\tau_{\text{phys}}$  along the EGR dilution sweep, compared to other test fuels. Results for chemical ignition delay ( $\tau_{\text{chem}}$ ) values of the two UM surrogate mixtures and a target fuel are shown in Figure 7-27 (b). The  $\tau_{\text{chem}}$  values for two of the pure compounds are also displayed in the same figure for comparative analysis. A non-linear relationship with oxygen dilution is

observed across the all fuel types, except for *n*-dodecane. *n*-Dodecane produced the shortest  $\tau_{chem}$  values and displayed the highest tolerance to EGR dilution. The  $\tau_{chem}$  for the target jet fuel is very similar to the two jet fuel surrogate mixtures and even decalin. This shows that increased dilution will increase ignition delay for fuels tested and which has also been observed in the ignition behavior studies of ULSD, biodiesel blends, and *n*-heptane [94,160].

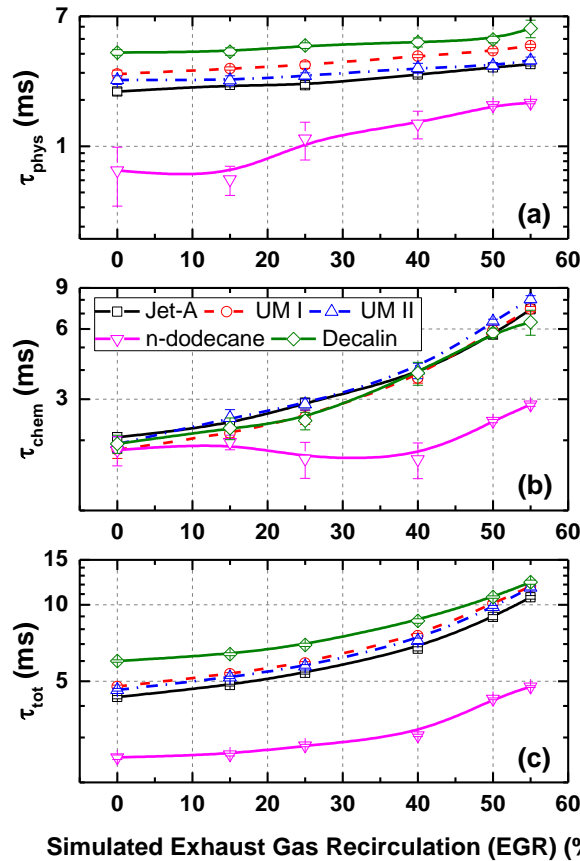


Figure 7-27 Ignition delays against simulated exhaust gas recirculation (EGR) for UM surrogate mixtures, the target Jet-A (POSF 4658), *n*-dodecane and decalin; (a) Physical ignition delay (b) Chemical ignition delay and (c) Total ignition delay. The error bar indicates 95% confidence interval.

## 7.6 UM Surrogates for Alternative Jet Fuels (S8, and IPK)

### 7.6.1 Test Fuels

The UM group have recently developed new surrogates UM S8 and UM IPK for synthetic alternative jet fuels, S8 (POSF 5018) and IPK (POSF 5729), emulating their physical and chemical properties of neat fuels [150]. Their target physical properties include density, viscosity, volatility and specific heat. The specific heat of liquid fuel was chosen as a new key physical property, which provides an impact on spray characteristics and resultant ignition behavior. The target chemical properties include DCN, H/C, MW and LHV. For tighter match to the target alternative jet fuels, a non-linear regression equation correlating the mixture composition to DCN was implemented in the surrogate optimizer.

Figure 7-28 (a) and (b) show mass fractions of UM surrogates for S8 and IPK, as being formulated with four different chemical compounds. As seen in Figure 7-28 (a), the real S8 is comprised of only two chemical structural families, *n*-alkane and *iso*-alkane, therefore, S8 UM surrogate matches its compositional families with four chemical compounds. Most of *iso*-alkanes in neat S8 are considered to be lightly branched alkanes, whose ignition reactivity is strong enough to imitate *n*-alkanes. This allows S8 UM surrogate to increase a fraction of *n*-alkanes to match DCN, as seen in Table 13. It should be noted that the representative of *iso*-alkanes for surrogate composition is currently limited to *iso*-octane and *iso*-cetane in the current surrogate pallet, which are very unreactive; therefore, the group of lightly branched *iso*-alkanes can be often represented



by *n*-alkanes. The real IPK is comprised of three chemical families including a negligible quantity of *n*-alkane, a great portion of *iso*-alkane and small amount of cycloalkanes. The IPK UM surrogate seems to be matched with the fractions of neat IPK, as seen in Figure 7-28 (b). Table 13 shows how UM surrogates for S8 and IPK estimated by the optimizer are well matched with their counterparts.

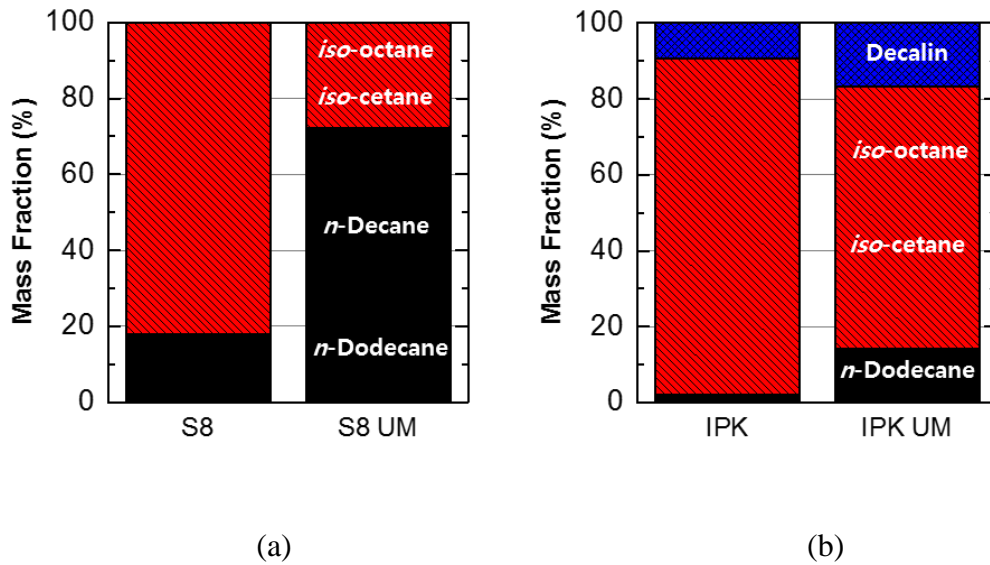


Figure 7-28 Mass fractions of newly developed UM surrogates; (a) S8 and its UM surrogate and (b) IPK and its UM surrogate (black, red and blue colors indicate *n*-alkanes, *iso*-alkanes and cycloalkanes, respectively).

Table 13 Temperature-independent properties of the target fuels and their surrogates  
[150]

	S8		IPK	
	Target	Surrogate	Target	Surrogate
DCN	60.4	60.5/61.1 <sup>a</sup>	30.7	30.7/31.9 <sup>a</sup>
LHV (MJ/kg)	44.1	44.42	44.0	44.21
H/C	2.152	2.173	2.119	2.121
MW (g/mol)	168	163.9	156	149.6

<sup>a</sup> predicted / measured by IQT at Wayne State University

## 7.6.2 Results and Discussion

Gas phase homogeneous combustion behavior of the surrogates and their target fuels were investigated in a modified CFR motored engine. In addition, liquid spray ignition behavior of the UM surrogates and the target fuels are compared in a constant volume combustion chamber.

As can be seen in Figure 7-29 (a), the critical compression ratios (CCR) of S8 UM surrogate and the real S8 are exactly matched at CR of 5.35. The well matched trend of CO formations in a wide range of CRs prior to autoignition indicate the homogeneous fuel air chemical kinetics of S8 UM surrogate well emulate those of real S8 in low- and intermediate temperature regimes. The good agreement between S8 UM surrogate and the real S8 is extended to the measurements of  $\tau_{\text{phy}}$  and  $\tau_{\text{chem}}$  obtained in a constant volume combustion chamber as seen in Figure 7-30 (a).

In contrast to the well matched emulation of the S8 UM surrogate, the IPK UM surrogate is not as well matched with the real IPK, as shown in Figure 7-29 (b) and Figure 7-30 (b). From the motored engine study, as seen in Figure 7-29 (b), the autoignition of IPK UM surrogate occurs at more advanced CR than that of real IPK, indicating that IPK UM surrogate has stronger ignition reactivity than real IPK. The trend of CO formation also indicates the disparity between the IPK UM surrogate and the target IPK fuel. This reactivity disagreement between the IPK UM surrogate and the real IPK is also observed in  $\tau_{\text{chem}}$  in a constant volume combustion chamber as shown in Figure 7-30.  $\tau_{\text{chem}}$  of the two fuels is well matched at lower ambient temperatures until 560°C, but as ambient temperature increases, the trends of  $\tau_{\text{chem}}$  of two fuels diverge greatly at 600°C,

showing different intensities of NTC behaviors. Nevertheless, the physical ignition delay of the UM surrogate and the target fuel show a great match over the range of temperatures of interest, due to a great mimicry of the physical properties by the UM IPK surrogate compared to the real IPK.

It should be noted that decalin, one of the surrogate ingredients in UM IPK surrogate, is a mixture of cis- and trans- isomers. The ignition reactivity of these isomers are quite different, resulting in DCNs, 41.2 for cis-decalin and 32.0 for trans-decalin, due to different thermal stabilities of decalin isomers [90]. Therefore, the decalin mixture purchased by different chemical vendors may have different fractions of these isomers, resulting in a small or large gap in their ignition reactivity of decalin mixture.

From these experimental surrogate validation results, a few observations can be drawn. First, the target fuel, comprised of simpler HC classes, can be easier to be emulated with simple surrogate ingredients. (etc., S8). In addition, matching fractions of HC classes of target fuel may facilitate emulating its chemical ignition behavior. For example, higher portions of *n*-alkane (*n*-C<sub>10</sub> and *n*-C<sub>12</sub> in this study) than a target fuel more likely tend to promote its ignition reactivity, providing active radicals in low temperature regime.

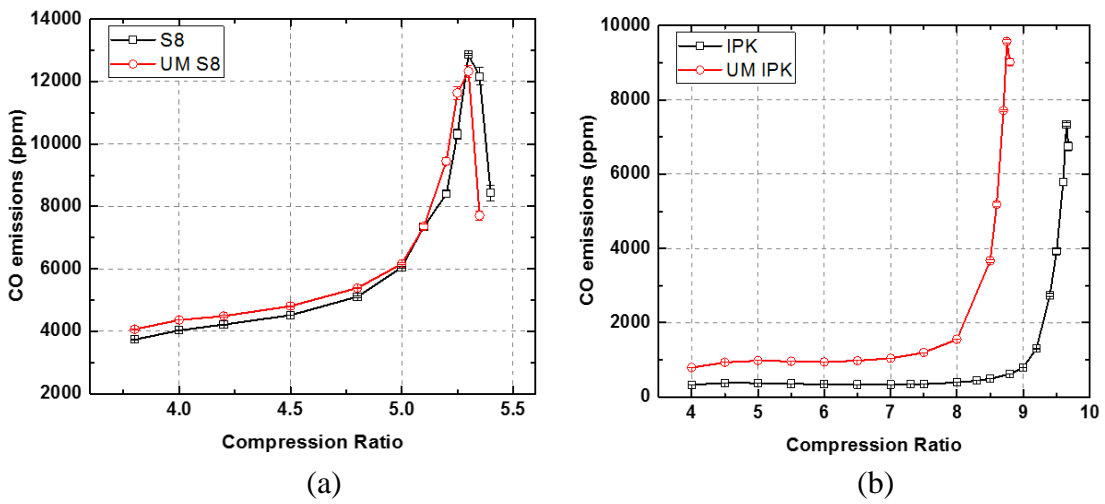


Figure 7-29 CO emissions in a respect of increasing CRs in a modified CFR motored engine at intake temperature of 260°C; (a) S8 and its UM surrogate (b) IPK and its UM surrogate

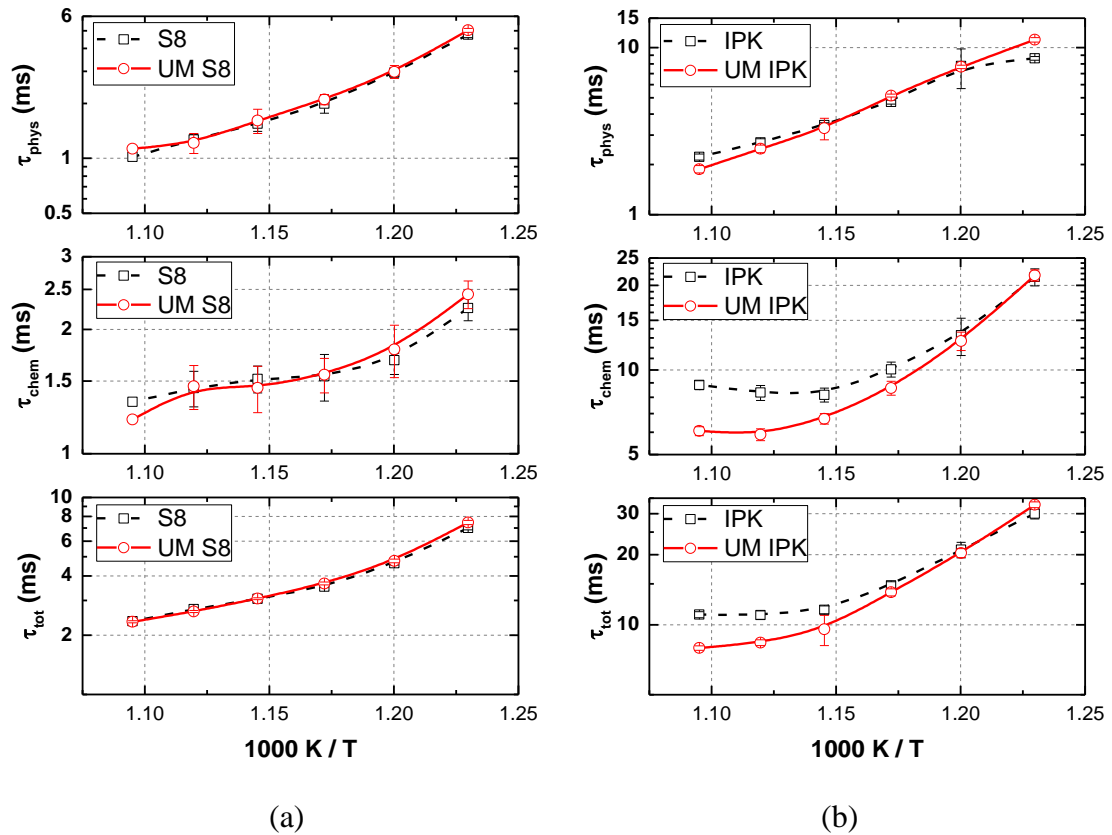


Figure 7-30 Measurements of physical, chemical and total ignition delays in a constant volume combustion chamber in a range of temperature between 540-640°C at 20 bar; (a) S8 and its surrogate and (b) IPK and its surrogate

## 7.7 Summary and Conclusions

The current experimental study was carried out to investigate autoignition behavior of conventional and synthetic alternative jet fuels in a modified cooperative fuels research (CFR) octane rating engine and a constant volume spray combustion chamber. The conventional jet fuels include JP-8, Jet-A (POSF 4658 and POSF 10325) and JP-5, and synthetic alternative jet fuels include “S-8”(S8) derived from natural gas, “synthetic paraffinic kerosene” (SPK) and “*iso*-paraffinic kerosene” (IPK) derived from coal via the Fisher-Tropsch (FT) process, respectively, “hydro-processed renewable jet” (HRJ) derived from Camelina and lastly “alcohol-to-jet” (ATJ) derived from *iso*-butanol. In addition, among conventional jet fuels, JP-8 is selected as the reference for the comparison toward synthetic jet fuels and as the blending unit mixed with 50 volume percent of synthetic jet fuels.

Secondly, the experimental study was conducted to validate recently reported UM surrogates which have been formulated considering the physical and chemical processes occurring in compression ignition engine. The validation has been performed to ensure that the surrogates accurately reproduce fundamental ignition behavior in a variable and a constant volume combustion chamber, compared to their target Jet-A (POSF 4658), S8 and IPK. A modified cooperative fuels research (CFR) octane rating engine was used to determine the ignition behavior of the target and surrogate fuels under premixed compression ignited condition. In addition, an optically accessible constant volume spray combustion chamber allowed the chemical reaction process to be distinguished from the physical process associated from spray injection and ignition.

The conclusions on the fundamental ignition behaviors of conventional and alternative jet fuels, and their blends are described as follows:

1. The lack of aromatics in alternative jet fuels can lead to a dramatic reduction of sooting tendency, however the 50/50 blend takes a disadvantage of increasing sooting tendency, due to aromatics in JP-8.
2. Chemical compositions of alternative jet fuels largely affect the ignition reactivity, showing that S8, SPK and HRJ8, whose compositions are mostly consist of *n*-alkanes and lightly branched alkanes, possess stronger ignition reactivity. In contrast, IPK and ATJ, whose compositions are mostly comprised of highly branched alkanes, possess weaker ignition reactivity, as compared to conventional jet fuels.
3. Measured DCN has a strong linear relationship with % LTHR and CCR in both lean equivalence ratio conditions in a modified CFR motored engine.
4. The distinct onset of NTC behavior can be found in chemical ignition delays measured in a constant volume combustion chamber, based on their ignition reactivity of a conventional jet fuel (JP-8) and alternative jet fuels.

From the experimental validation study of UM surrogates and the target Jet-A (POSF 4658), the following conclusions are derived from the modified CFR octane rating motored engine investigation:

1. The low temperature gas phase oxidation reactivity of five neat compounds comprising the two Jet-A (POSF 4658) surrogate fuel mixtures are compared. The reactivity of the neat test fuels follows the order, *n*-dodecane > POSF 4658 > Decalin > MCH > *Iso*-cetane >> Toluene. Decalin closely matches the ignition behavior of the target fuel. The strongest reactivity fuel, *n*-dodecane, exhibits two-stage ignition

behavior. Cycloalkanes, decalin and MCH, show the classic NTC behavior in the test conditions of interest.

2. According to the derived cetane number (DCN) measured by ASTM D7668, the DCN values of POSF 4658 (47.0) and UM I surrogate (46.7) agreed well, while DCN of UM II surrogate (45.9) was slightly lower than the target fuel. UM I showed advanced critical compression ratio (CCR), relative to the target Jet-A. This change results from the larger UM I *n*-alkane volume fraction, which was approximately twice that of the target-Jet A. In contrast, the CCR, ignition phasing and % LTHR of UM II are reasonably matched with that of a target Jet-A under a boosted intake condition, despite the difficulty in matching the low temperature combustion process of real Jet-A during in-complete combustion.

The following conclusions are derived from the investigation in the modified cetane ignition delay (CID 510) instrument:

3. The Arrhenius plot for individual surrogate component fuels revealed a linear dependence of  $\tau_{\text{phys}}$  on intake air temperature. Among the four individual components, decalin possesses similar physical properties as compared to target Jet-A, resulting in the closest value of  $\tau_{\text{phys}}$  compared to this fuel. The Arrhenius plot of chemical ignition delay ( $\tau_{\text{chem}}$ ) presents a linear trend for *iso*-cetane, but non-linear trends for other test fuels, resulting in the uniqueness of ignition characteristics of each individual component and a target Jet-A under a range of test conditions.

4. The  $\tau_{\text{phys}}$  of the UM II surrogate showed a better match against that of a target Jet-A in the lower temperature region, indicating that the physical properties of the UM II surrogate are better emulated than that of UM I surrogate. However as the intake air



temperature increases, the difference of physical properties for both surrogates become minor. Unlike  $\tau_{\text{phys}}$ ,  $\tau_{\text{chem}}$  and other factors (% LTHR and combustion phasing) for UM surrogate mixtures are relatively well matched with those of a target Jet-A in the range of tested intake temperatures.

5. The oxygen dilution simulated by EGR rate showed a very minor impact on  $\tau_{\text{phys}}$  for UM surrogates and the target Jet-A, while the  $\tau_{\text{chem}}$  is largely affected by increasing oxygen dilution, leading to a substantial increase in  $\tau_{\text{chem}}$  at higher EGR rate. Also, a similar trend is observed for all the test fuels over a wide range of EGR sweep, except for *n*-dodecane.

From the experimental validation study of UM surrogates matching with target alternative jet fuels (S8 and IPK), the conclusions are as follows:

1. Developments of S8 UM surrogate is greatly successful in that the chemical kinetics for a surrogate and a counterpart is perfectly matched in a motored engine and then, spray ignition behaviors of S8 UM surrogate, including physical and chemical ignition delays are identified with the real S8 in test conditions of interest.

2. The physical ignition delay of IPK UM surrogate is well agreed with that of neat IPK in a range of temperatures of interest in a constant volume combustion chamber, however, the trend of chemical ignition delay of IPK UM surrogate is partially matched with that of neat IPK until ambient temperature reaches at 580°C, then the trends of chemical ignition delays lead to diverged NTC behaviors at the relatively high temperature regimes. The advanced onset of NTC behavior of chemical ignition delays of UM IPK surrogate in a constant volume combustion chamber is also verified in a

motored engine, resulting in more advanced critical compression ratio of UM IPK surrogate observed than that of neat IPK.

Finally, the UM surrogates developed using a model-based optimizer show reasonable agreement with the target Jet-A, S8 and IPK with regard to ignition limit behavior and gas phase chemical oxidation kinetics, thus matching ignition processes in an engine like environment. The experimental results reported here suggest that the adoption of decalin as a cycloalkane representative is a better selection than MCH, improving physical properties (viscosity and volatility) of the surrogates relative to the target fuel. However, since decalin is a mixture of cis- and trans-isomers whose reactivity are somewhat distinguished, the fraction of cis- and trans- isomers has to be also considered, when used as a surrogate ingredient.

## Chapter 8

### Conclusions and Recommendations for Future Works

#### 8.1 Conclusions

This first part of this dissertation focused on impacts of chemical structure on their autoignition behaviors and chemistry in a motored engine. The fuel molecules dealt in this dissertation were C8 cycloalkane isomers (**Chapter 4**), C5 alkane isomers (**Chapter 5**) and lastly blends of diisobutylene in primary reference fuels (**Chapter 6**), which are chosen as novel fuel compounds for potential surrogates of gasoline and diesel. Based on heat release analysis and the product speciation measurement performed in this study, the significant findings are shown from 8.1.1 to 8.1.3 for each chapter.

The second part of this dissertation focused on the impacts of chemical composition on the autoignition behaviors by using four conventional jet fuels and five synthetic alternative jet fuels. The autoignition characteristics of these fuels were investigated in a motored engine and a constant volume spray combustion chamber, where gas phase homogeneous combustion characteristics and liquid phase spray ignition

behaviors in considerations of physical and chemical properties of fuels can be investigated.

In addition, the experimental validations of recent developed surrogates proposed by Violi group were included in this study. The target jet fuels are Jet-A (POSF 4658), S-8 (POSF 5018) and *iso*-paraffinic kerosene (POSF 7629). The results can be in turn applicable for the development of high fidelity predictive kinetics models for the optimization of modern engine designs. The conclusions of this study are shown in 8.1.4.

### **8.1.1 Conclusion from Chapter 4; Impact of Branched Structure on Cycloalkane Ignition in a Motored Engine**

The study of low temperature oxidations of C<sub>8</sub> cycloalkane isomers including ethyl-cyclohexane (ECH), 1,3-dimethylcyclohexane (13DMCH) and 1,2-dimethylcyclohexane (12DMCH) was conducted in a motored engine to observe a great impact of the position of the alkyl substituent in cycloalkanes on ignition characteristics. Intermediate species from incomplete to complete combustion of the test fuels were also investigated. Significant findings are as follows:

- ECH is the most reactive compound followed by 13DMCH and 12DMCH. This indicates that reactivity is more strongly influenced by the alkyl group size of the substituents on a cycloalkane than the number of alkyl chain substituents.
- The most dominant intermediate species are conjugate olefins mostly formed through (1,4) H-shift isomerization, competing with (1,5) H-shift isomerization.
- Conformation analysis supports the observed disparity in the low temperature oxidation reactivity of three cycloalkane isomers, as can be seen in Table 5. From the

comparisons between ECH and methylcyclohexane (MCH) and between 13DMCH and 12DMCH, ECH and 13DMCH possess more number of hydrogens available for low energy barrier paths to the (1,5) H-shift on the alkylperoxy radical than MCH and 12DMCH, respectively.

### **8.1.2 Conclusion from Chapter 5; Autoignition Studies of C5 Isomers in a Motored Engine**

This study considered the autoignition of three pentane isomers in a single cylinder CFR motored engine at an intake temperature of 120°C. Products formed from low temperature oxidation of these pentane isomers were investigated over a wide range of compression ratios, and their relationship to the overall oxidation reactivity was suggested. Significant findings are as follows:

- The unique molecular structures of each pentane isomer resulted in n-pentane showing the strongest oxidation reactivity followed by neo- and iso-pentanes in terms of the critical compression ratio, with a good agreement in comparable negative temperature coefficient (NTC) behaviors shown in the profiles of CO formation and unburned fuel conversion.
- The percentage of low temperature heat release (% LTHR) showed a stronger two-stage heat release for n-pentane than for neo-pentane at critical ignition conditions. In contrast, single stage heat release was observed for iso-pentane, leading to the weakest overall oxidation reactivity of the three isomers.
- Key reaction paths forming conjugate alkenes and C5 oxygenated species controlled the autoignition reactivity of n-pentane and iso-pentane in the low temperature

and NTC regimes. However, neo-pentane formed no conjugate alkene due to its unique molecular structure, and instead produced iso-butene to retard its overall reaction rate during oxidation.

### **8.1.3 Conclusion from Chapter 6; Combined Impact of Branching and Unsaturation on the Autoignition of Binary Blends in a Motored Engine**

The effect of the different amount of branched and unsaturated structure fuel (diisobutylene) mixed with primary reference fuels (*n*-heptane and iso-octane) on ignition behavior and autoignition chemistry was investigated in a modified CFR engine. The intermediate product of different sets of test fuel volume mixtures were captured at a compression ratio right before the complete combustion occur and then analyzed. Significant findings are as follows.

- Addition of branched and unsaturated fuel structures showed a linear retarding effect on oxidation reactivity, resulting in a longer negative temperature coefficient (NTC) behavior with gradual addition to PRF fuels.
- Strong evidence of low temperature heat release (LTHR) was found only for *n*-heptane blends. The presence of the double bond in diisobutylene led to lower % LTHR and higher critical compression ratio (CCR).
- The more reactive fuel in a binary blend likely governed the ignition reactivity and characteristics, and the major products formed during low temperature oxidation were mostly derived from more reactive fuel.

- Opposite trends with regard to the formation of major products was observed between n-heptane blends and iso-octane blends as diisobutylene was added, due to the different degree of ignition reactivity during low temperature oxidation.
- The active radicals generated from branching step reactions during of cool flame oxidation of n-heptane and iso-octane in blends, favor to attack C-C double bond in diisobutylene, resulting in considerable formation of 4,4-dimethyl-2-pentanone. This reaction contributed to delayed ignition, shown by the increasing mole fraction of 4,4-dimethyl-2-pentanone in the unreacted fuel as the volume of diisobutylene increases in both cases.

#### **8.1.4 Conclusion from Chapter 7; Experimental Investigation of Autoignition Behaviors of Conventional and Synthetic Alternative Jet Surrogates and their Validation in a Motored Engine and a Constant Volume Combustion Chamber**

Four similar chemical compositions of conventional jet aviation fuels, including JP-8, Jet-As (POSF 4658 and POSF 10325) and JP-5 and distinct chemical compositions of five different synthetic alternative jet fuels, including “S-8”(S8) derived from natural gas, “synthetic paraffinic kerosene” (SPK) and “*iso*-paraffinic kerosene” (IPK) derived from coal via the Fischer-Tropsch (FT) process, “hydro-processed renewable jet” (HRJ8) derived from Camelina and lastly “alcohol-to-jet” (ATJ) derived from *iso*-butanol, were used to investigate the impacts of the chemical composition on autoignition behaviors in a motored engine and liquid spray ignition delays in a constant volume combustion chamber. The ignition characteristics of 50/50 blends with JP-8 and alternative jet fuels

were also investigated and compared with neat JP-8 and alternative jet fuels. Significant findings are as follows:

- Chemical compositions of alternative jet fuels influenced the ignition reactivity greatly, showing that S8, SPK and HRJ8, whose compositions are mostly consist of n-alkanes and lightly branched alkanes, possess stronger ignition reactivity. In contrast, IPK and ATJ, whose compositions are mostly comprised of highly branched alkanes, possessed weaker ignition reactivity, as compared to conventional jet fuels.
- The measured DCNs displayed a strong linear relationship with % LTHR and CCR in both lean equivalence ratio conditions in a modified CFR motored engine.
- The distinct onsets of NTC behavior was found in chemical ignition delays measured in a constant volume combustion chamber, directly connected to their ignition reactivity of a conventional jet fuel (JP-8) and alternative jet fuels.

The UM surrogates for Jet-A, S8 and IPK have been formulated to emulate the diesel engine combustion process of jet fuels in considerations of chemical and physical properties of surrogate fuels. The current experimental study examined gas phase autoignition behavior and liquid spray ignition characteristics of the UM surrogate mixtures and the target fuels, to observe whether proposed UM surrogates well emulate the target jet fuels. Significant findings are described as follows:

- The low temperature oxidation reactivity of the individual surrogate compounds measured in a modified CFR motored engine follows the order, n-dodecane > POSF 4658 > Decalin > MCH > iso-cetane > Toluene.
- The DCN values of Jet-A and UM I surrogate agreed well, while DCN of UM II surrogate was slightly lower than the target fuel. From the modified CFR motored engine,



UM I showed advanced critical compression ratio (CCR), relative to the target Jet-A. In contrast, the ignition characteristics of UM II are reasonably matched with that of a target Jet-A even under a boosted intake condition.

- The physical ignition delay of the UM II surrogate showed a better match against that of a target Jet-A in the lower temperature region, indicating that the physical properties of the UM II surrogate are better emulated than that of UM I surrogate. However as the intake air temperature increases, the difference of physical properties for both surrogates become minor. Unlike the physical ignition delay, the chemical ignition delay and other factors (% LTHR and combustion phasing) for UM surrogate mixtures are relatively well matched with those of a target Jet-A in the range of tested intake temperatures.

- The chemical kinetics for a S8 UM surrogate and a counterpart were perfectly matched in a motored engine and then, spray ignition behaviors of S8 UM surrogate, including physical and chemical ignition delays were also identified with the real S8 in test conditions of interest.

- The physical ignition delay of IPK UM surrogate was well agreed with that of neat IPK in a range of temperature of interest in a constant volume combustion chamber, however, the trend of chemical ignition delay was partially matched with that of neat IPK until ambient temperature reaches 580°C, then the trends of chemical ignition delays led to diverged NTC behaviors in the relatively high temperature regimes. The delayed onset of NTC behavior of chemical ignition delays of UM IPK surrogate in a constant volume combustion chamber was also verified in a motored engine, resulting in more delayed critical compression ratio of UM IPK surrogate than that of neat IPK.

## 8.2 Recommendations for Future Work

The CFR motored engine used in this study is a unique experimental device capable of studying gas phase oxidation of hydrocarbons over a wide range of pressures and temperatures in an engine environment. The current exhaust sampling method of the CFR engine is particularly good for quantitative speciation measurements for the oxidation of small hydrocarbons with low boiling points. However, if the volatility of test fuels gets lower, there would be a chance for the heavy hydrocarbon species to be condensed during exhaust sampling and intermediate species collection, resulting in poor carbon balance. Also, it was challenging to identify formaldehyde in the current gas chromatogram analysis system. To improve the quality of exhaust sampling and species collection, a few methods can be suggested.

First, it is recommended to add diluents (e.g., N<sub>2</sub>) to the engine intake to reduce the partial pressure of fuel molecules in the engine exhaust below their saturated vapor pressure, so that the condensation of heavy hydrocarbons can be prevented.

Secondly, it is recommended to use Fourier Transform Infrared Spectroscopy (FTIR) to better quantify the C<sub>1</sub> and C<sub>2</sub> oxygenated species such as formaldehydes and acetaldehyde, which are key major species in low temperature oxidation of hydrocarbons.

Lastly, it is recommended to implement a gas chromatography mass spectrometry (GC-MS) coupled with a flame ionized detector (FID) directly connected to the exhaust sampling system, thereby preventing any loss of intermediate species during the sample transfer.

With this improvement, it will be of particular interest to extend the present study to the oxidation of novel surrogate fuels for gasoline and diesel, such as highly branched alkanes and aromatic compounds with large alkyl substituents. In addition, it is also be worthwhile to explore the oxidation chemistry of small oxygenated fuel surrogates of biomass pyrolysis oils, such as furans and diols.

Regarding the study of conventional and synthetic alternative jet fuel surrogates, it is recommended to investigate physical spray behavior of a liquid fuel injection described by liquid spray penetration length and cone angle by capturing spray images with a high speed camera, which can be observed in the current constant volume spray combustion chamber manufactured by a cetane ignition delay (CID) 510. Physical spray behaviors of surrogate mixture compared with neat fuel would be a good indicator for validating the successful emulation of the physical properties of surrogate fuels relevant to the diesel engine combustion process.

## **Appendices**

### **Appendix A. Algorithm for Combustion Phase**

Combustion phasing, which is often used to trace the combustion process used in the motored engine, is analyzed from the apparent heat release rate (AHRR) profile. For the CFR engine used in this study, an algorithm was developed by Lilik and Boehman [86], using LabVIEW data acquisition software to calculate the combustion phase parameters, such as first stage combustion (SOC1) for low temperature heat release, start of second stage combustion (SOC2) for high temperature heat release, and end of combustion (EOC). The parameters are necessary to calculate the percent of low temperature heat release (% LTHR), particularly for the strong reactive fuels, e.g., *n*- and neo-pentane and cycloalkane isomers, etc. The steps in the algorithm are described below.

#### **A.1 Filter and Smoothing**

The initial step in analysis of the heat release rate profile is to eliminate high frequency noise that was inherent within the acquisition system, while measuring the in-cylinder pressure. A combination of cubic splines and low pass, and smoothing average

filters was implemented to eliminate the noise without alteration of the features of the pressure trace.

## A.2 Start of Combustion

SOC can be determined at the crank angle where the heat release becomes positive in a simplistic way. However, it was often difficult to make this point clear due to the signal noise and heat loss, which is unaccounted in the calculation of heat release. It is often recognized that CA 5 (crank angle where 5% of the AHRR occurs) is an indicator to determine the SOC in the engine combustion process [161]. However, this study required more robust way to calculate SOC, due to the significance of LTHR and HTHR obtained. Therefore, this study adopted the SOC calculation suggested by Katranik *et al.* [162], as shown in equation A-1.

$$\text{SOC} = \frac{d^3p}{d\theta^3} \quad (\text{A-1})$$

Where P is the crank angle resolved in-cylinder pressure and  $\theta$  is the crank angle. This third derivative of pressure with respect to crank angle indicate SOC as being the inflection point at the beginning of the HRR. The transition between first and second stage heat release is often difficult to distinguish. For example, there is a case where a long duration between the end of first stage combustion and the start of second stage combustion. There is another case where the start of second stage combustion occurs immediately after the peak of the first stage combustion, overlapping each other. However, some criterion must be used to separate the two zones. Therefore, SOC2 is defined as crank angle where the minimum value of the heat release occurs between the peaks of first and second stage combustion.

### **A.3 End of Combustion**

EOC can be defined as the point where the where the HRR becomes negative, crossing zero, in any cases that either the heat release decreases gradually or the heat release ends rapidly. One thing should be noted that even though EOC can be affected by inherent noise in the pressure trace signal, the EOC phasing is a less significant factor affecting the overall combustion and an insignificant difference is expected to the cumulative heat release as the bulk of the combustion has occurred earlier in the cycle.

## Appendix B. Measurements of the CFR Wall Cylinder Temperature

From the study of the oxidation of pentane isomers in **Chapter 5**, the cylinder wall maximum temperatures of pentane isomers and primary reference fuels shown in Figures A-1 (b) and A-2 (b) are measured in a respect of increasing compression ratios at both cases ( $\phi = 0.25$  and  $\phi = 0.5$ ), along with in-cylinder gaseous maximum temperature. This information is intended to support kinetic modeling studies by providing real boundary conditions of combustion chamber, thereby having a fine tuning of kinetic mechanisms of pentane isomers and primary reference fuels in lean conditions of interest, particularly in the aspects of compression ignition engine.

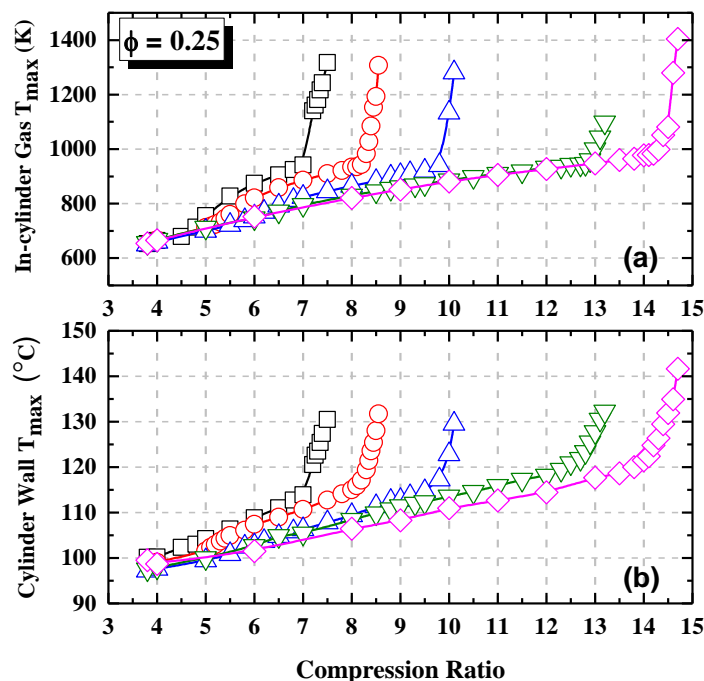


Figure B-1 (a) In-cylinder gas maximum temperatures and (b) cylinder wall maximum temperatures of pentane isomers and primary reference fuels in wide range of compression ratio at  $\phi$  of 0.25 ( $\square$  ; *n*-heptane,  $\circ$  ; *n*-pentane,  $\triangle$  ; neo-pentane,  $\nabla$  ; *iso*-pentane,  $\diamond$  ; *iso*-octane)

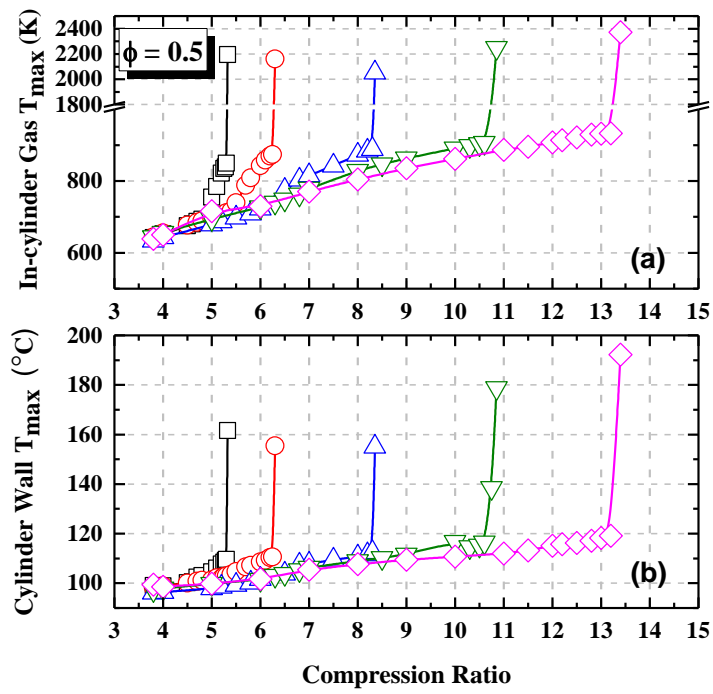


Figure B-2 (a) In-cylinder gas maximum temperatures and (b) cylinder wall maximum temperatures of pentane isomers and primary reference fuels in wide range of compression ratio at  $\phi$  of 0.5 ( $\square$  ; *n*-heptane,  $\circ$  ; *n*-pentane,  $\triangle$  ; neo-pentane,  $\nabla$  ; *iso*-pentane,  $\diamond$  ; *iso*-octane)



## Appendix C. Cross Reference Check for the CFR Motored Engines

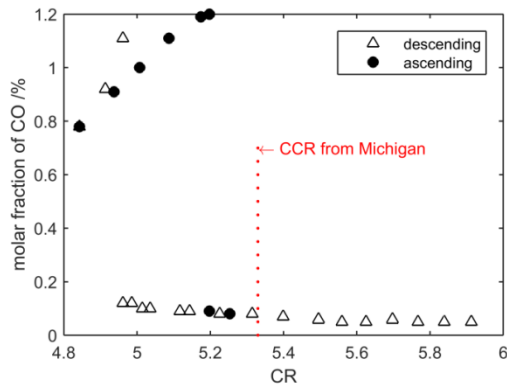
The measurement of critical compression ratio (CCR) of *n*-heptane has been conducted at two different places (the University of Melbourne, Australia and the University of Michigan, United States) for a cross reference check of a common platform of the CFR motored engines. The intake system of CFR motored engine used in this study was modified for the purpose of homogeneous injection of fuel and air mixture as described in **Chapter 3**. The CFR motored engine from Melbourne runs under MON configuration. The *n*-heptane was introduced as liquid, however it is assumed that *n*-heptane is completely vaporized before entering the combustion chamber as the intake temperature is 120°C, which is higher than its boiling point. And for MON configuration, a heater is mounted downstream the fuel injection port, which is held at 120C, this can ensure the fully vaporization of *n*-heptane. Table 14 describes the engine test conditions that both Universities used.

It is found that CCRs of the CFR motored engines are quite close in both equivalence ratio cases, as shown in Figure C-1 and Figure C-2, but the measured CO emission from Melbourne is constantly 0.2% higher than Michigan. This could be due to the different calibration gas for CO measurements. The Horiba emission bench in Melbourne was calibrated at output of 0 using pure N<sub>2</sub> and 0.980 using calibration gas of 1.96 vol% CO in N<sub>2</sub> balance. And the CO emission bench in Michigan was calibrated with 4950 ppm CO in N<sub>2</sub>, which did not cover up to the saturated CO emission observed in experiments, which is around 14000 ppm.

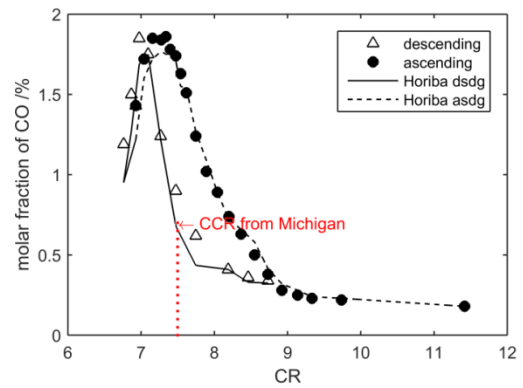
Overall, the CCR agrees excellent, indicating that the data from the two engines are highly comparable.

Table 14. Experimental conditions of the CFR motored engines at two different places

	Phi=0.25 (Melbourne)	Phi=0.25 (Michigan)	Phi=0.5 (Melbourne)	Phi=0.5 (Michigan)
Intake Temp/°C	120	120	120	120
Coolant vapor/°C	47	--	47.3	
Coolant liquid/°C	100	90	100	90
Oil/°C	51.6	--	47.6	
CCR (descending)	7.0	--	4.95	--
CCR (ascending)	7.48	7.5	5.2	5.33

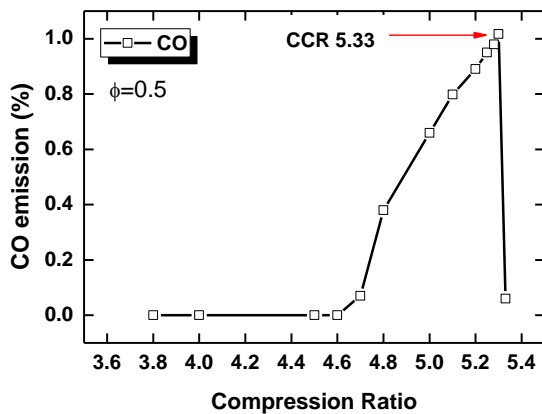


(a)

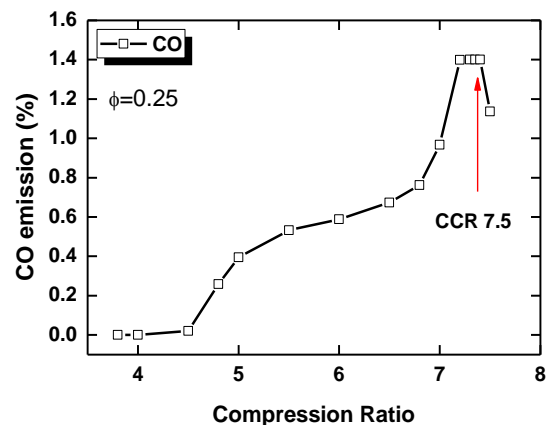


(b)

Figure C-1 CO emissions from the oxidation of *n*-heptane at intake temperature of 120°C and the engine speed of 600 rpm in the CFR motored engine at the University of Melbourne, Australia. (a)  $\phi=0.5$  and (b)  $\phi=0.25$



(a)



(b)

Figure C-2 CO emissions from the oxidation of *n*-heptane at intake temperature of 120°C and the engine speed of 600 rpm in the modified CFR motored engine at the University of Michigan, United States. (a)  $\phi=0.5$  and (b)  $\phi=0.25$

## Appendix D. Product Distribution in the Low Temperature Oxidation of pentane isomers

### D.1 The FID signals of low temperature oxidation of *n*-pentane

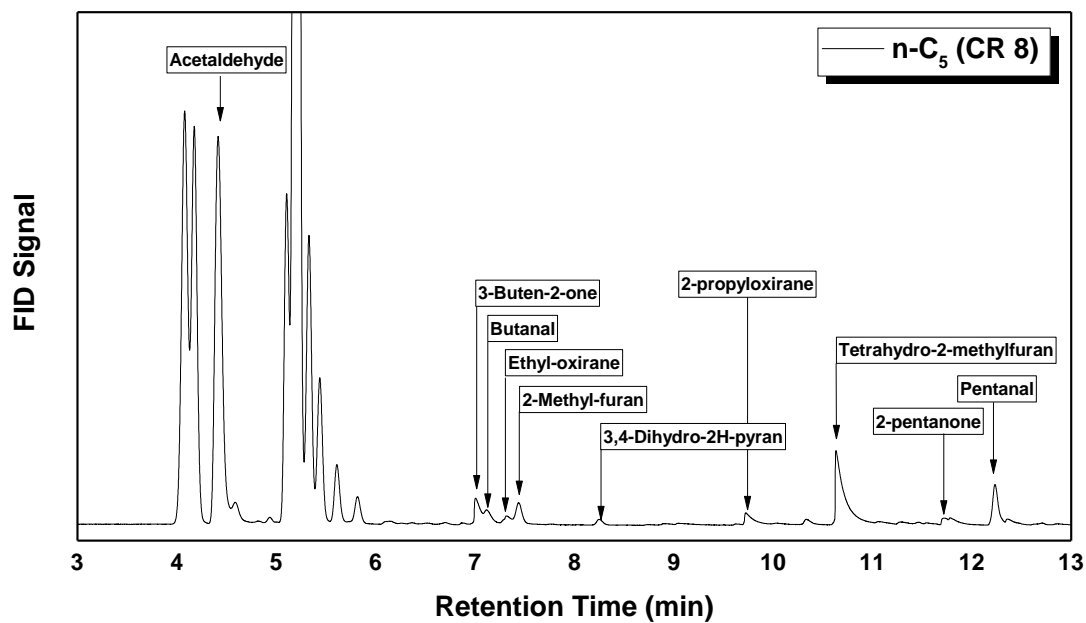


Figure D-1 Product distribution in the oxidation of *n*-pentane at a compression ratio of 8: oxygenated species analyzed in an Agilent 6890 GC-FID with an HP-5 column (50m x 0.2mm i.d. x 0.33 $\mu$ m film thickness)

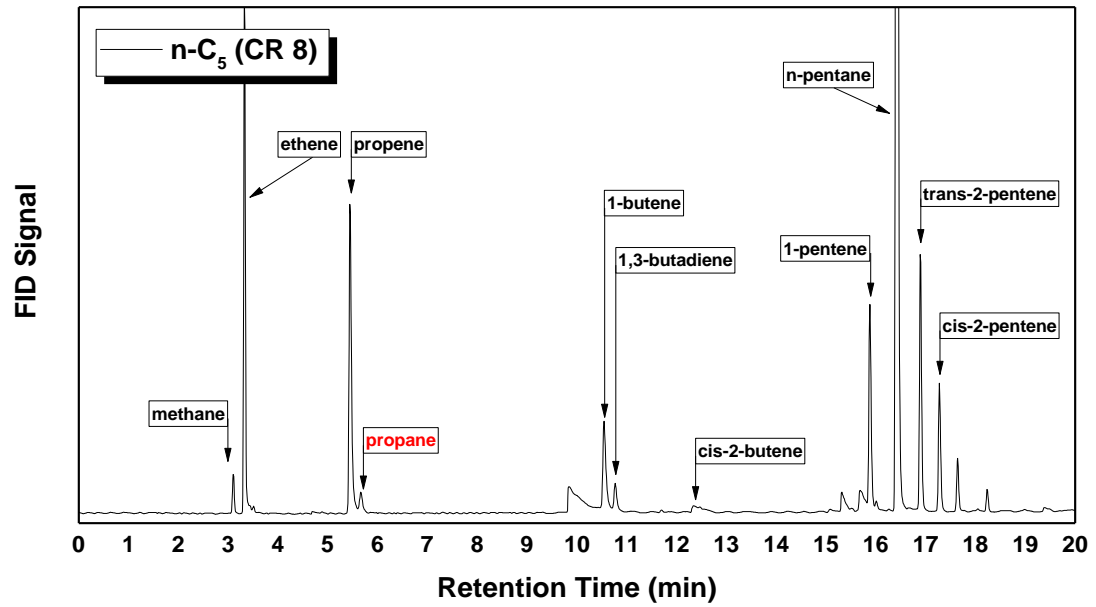


Figure D-2 Product distribution in the oxidation of *n*-pentane at a compression ratio of 8: gas sample was diluted with N<sub>2</sub> and 9.3 ppmC<sub>1</sub> propane (internal standard) at 10:1, and alkanes were analyzed in a Shimadzu GC-17A with a Restek Rtx-1 column (60m x 0.32mm i.d. x 1μm film thickness)

## D.2 The FID signals of low temperature oxidation of neo-pentane

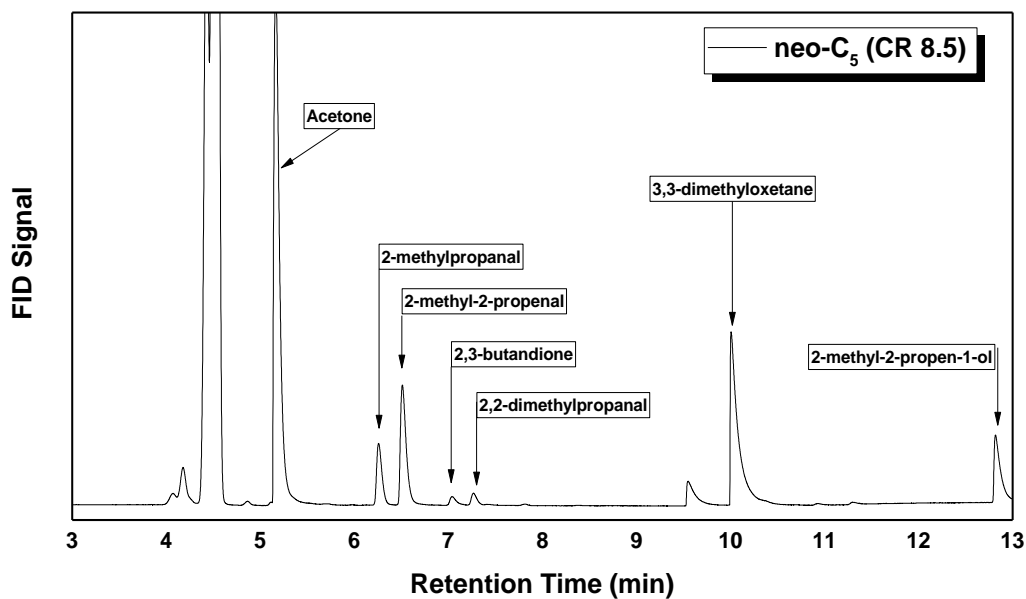


Figure D-3 Product distribution in the oxidation of neo-pentane at a compression ratio of 8.5: oxygenated species analyzed in an Agilent 6890 GC-FID with an HP-5 column (50m x 0.2mm i.d. x 0.33 $\mu$ m film thickness)

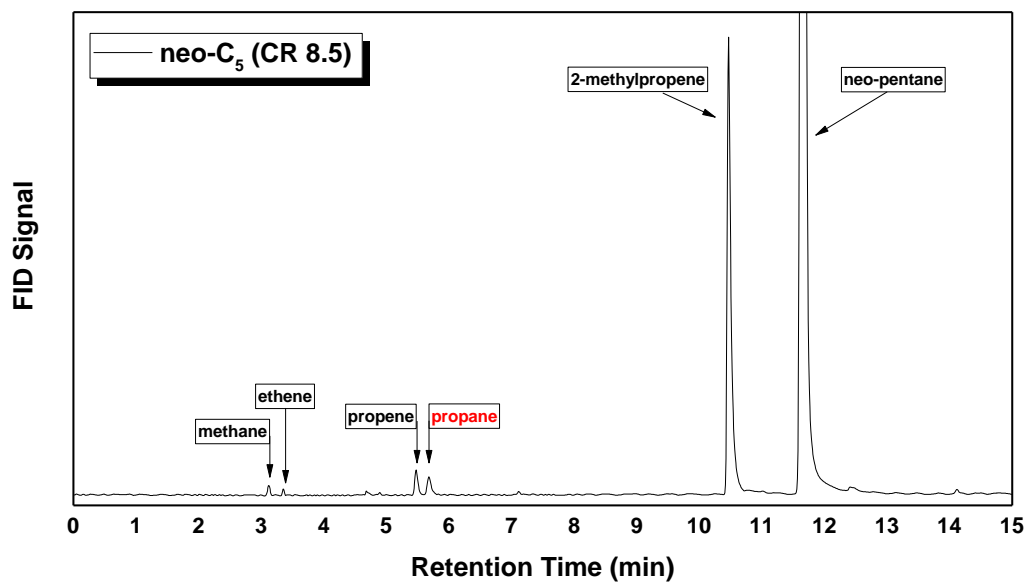


Figure D-4 Product distribution in the oxidation of neo-pentane at a compression ratio of 8.5: gas sample was diluted with N<sub>2</sub> and 9.3 ppmC<sub>1</sub> propane (internal standard) at 10:1, and alkanes were analyzed in a Shimadzu GC-17A with a Restek Rtx-1 column (60m x 0.32mm i.d. x 1 $\mu$ m film thickness)

### D.3 The FID signals of low temperature oxidation of *iso*-pentane

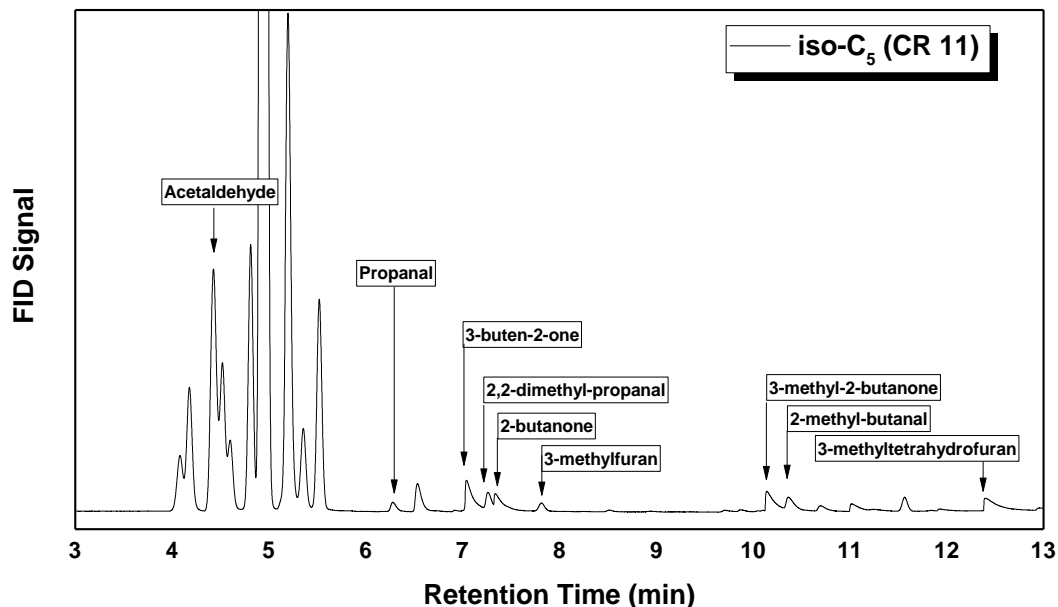


Figure D-5 Product distribution in the oxidation of *iso*-pentane at a compression ratio of 11: oxygenated species analyzed in an Agilent 6890 GC-FID with an HP-5 column (50m x 0.2mm i.d. x 0.33 $\mu$ m film thickness)

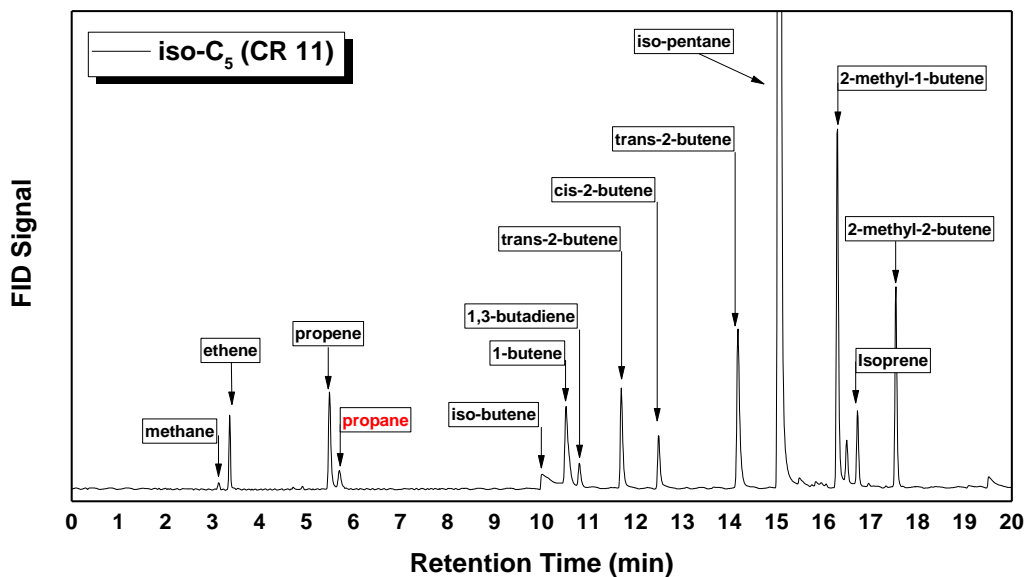


Figure D-6 Product distribution in the oxidation of *iso*-pentane at a compression ratio of 11: gas sample was diluted with N<sub>2</sub> and 9.3 ppmC<sub>1</sub> propane (internal standard) at 10:1, and alkanes were analyzed in a Shimadzu GC-17A with a Restek Rtx-1 column (60m x 0.32mm i.d. x 1 $\mu$ m film thickness)

## Bibliography

- [1] Dec JE. Advanced compression-ignition engines—understanding the in-cylinder processes. *Proc Combust Inst* 2009;32:2727–42.
- [2] Lu X, Han D, Huang Z. Fuel design and management for the control of advanced compression-ignition combustion modes. *Prog Energy Combust Sci* 2011;37:741–83.
- [3] Yao M, Zheng Z, Liu H. Progress and recent trends in homogeneous charge compression ignition (HCCI) engines. *Prog Energy Combust Sci* 2009;35:398–437.
- [4] Kim J, Sluder CS, Wagner RM. Combustion Studies with FACE Diesel Fuels: A Literature Review. *SAE Int J Engines* 2012;5:1648–60.
- [5] McIlroy A, McRae G, Sick V, Siebers DL, Westbrook CK, Smith PJ, et al. Basic Research Needs for Clean and Efficient Combustion of 21st Century Transportation Fuels. 2006.
- [6] Semenov NN, Bradley JES. Some problems in chemical kinetics and reactivity. Princeton University Press. Princeton, NJ: 1959.
- [7] Glassman I, Yetter RA. Combustion. 4th ed. Amsterdam ; Boston: Academic Press; 2008.
- [8] Pilling MJ, editor. Low-temperature combustion and autoignition. Amsterdam ; New York: Elsevier; 1997.
- [9] Warnatz J. Twentieth Symposium (International) on Combustion Chemistry of high temperature combustion of alkanes up to octane. *Symp Int Combust* 1985;20:845–56.
- [10] Westbrook CK, Dryer FL. Chemical kinetic modeling of hydrocarbon combustion. *Prog Energy Combust Sci* 1984;10:1–57.
- [11] Simmie JM. Detailed chemical kinetic models for the combustion of hydrocarbon fuels. *Prog Energy Combust Sci* 2003;29:599–634.
- [12] Battin-Leclerc F. Detailed chemical kinetic models for the low-temperature combustion of hydrocarbons with application to gasoline and diesel fuel surrogates. *Prog Energy Combust Sci* 2008;34:440–98.
- [13] Zádor J, Taatjes CA, Fernandes RX. Kinetics of elementary reactions in low-temperature autoignition chemistry. *Prog Energy Combust Sci* 2011;37:371–421.
- [14] Livengood JC, Wu PC. Correlation of autoignition phenomena in internal combustion engines and rapid compression machines. *Symp Int Combust* 1955;5:347–56. [15] Heywood JB. Internal combustion engine fundamentals. New York: McGraw-Hill; 1988.



- [16] Bradley D, Morley C, Walmsley HL. Relevance of Research and Motor Octane Numbers to the Prediction of Engine Autoignition. SAE Tech Pap 2004;2004-01-1970.
- [17] Burcat A, Scheller K, Lifshitz A. Shock-tube investigation of comparative ignition delay times for C1-C5 alkanes. Combust Flame 1971;16:29–33.
- [18] Ciezki HK, Adomeit G. Shock-tube investigation of self-ignition of n-heptane-air mixtures under engine relevant conditions. Combust Flame 1993;93:421–33.
- [19] Fieweger K, Blumenthal R, Adomeit G. Self-ignition of S.I. engine model fuels: A shock tube investigation at high pressure. Combust Flame 1997;109:599–619.
- [20] Kalghatgi GT. Auto-Ignition Quality of Practical Fuels and Implications for Fuel Requirements of Future SI and HCCI Engines. SAE Tech Pap 2005;2005-01-0239.
- [21] Griffiths JF, Halford-Maw PA, Mohamed C. Spontaneous ignition delays as a diagnostic of the propensity of alkanes to cause engine knock. Combust Flame 1997;111:327–37.
- [22] ASTM D2699-15a. Standard Test Method for Research Octane Number of Spark-Ignition Engine Fuel. ASTM International, West Conshohocken, PA, 2015; [www.astm.org](http://www.astm.org).
- [23] ASTM D2700-16a. Standard Test Method for Motor Octane Number of Spark-Ignition Engine Fuel. ASTM International, West Conshohocken, PA, 2016; [www.astm.org](http://www.astm.org).
- [24] ASTM D613-15a. Standard Test Method for Cetane Number of Diesel Fuel Oil. ASTM International, West Conshohocken, PA, 2015; [www.astm.org](http://www.astm.org).
- [25] ASTM D6890-15b. Standard Test Method for Determination of Ignition Delay and Derived Cetane Number (DCN) of Diesel Fuel Oils by Combustion in a Constant Volume Chamber. ASTM International, West Conshohocken, PA, 2015; [www.astm.org](http://www.astm.org).
- [26] ASTM D7668-14a. Standard Test Method for Determination of Derived Cetane Number (DCN) of Diesel Fuel Oils—Ignition Delay and Combustion Delay Using a Constant Volume Combustion Chamber Method. ASTM International, West Conshohocken, PA 2014; [www.astm.org](http://www.astm.org).
- [27] Tanaka S, Ayala F, Keck JC, Heywood JB. Two-stage ignition in HCCI combustion and HCCI control by fuels and additives. Combust Flame 2003;132:219–39.
- [28] Shibata G, Oyama K, Urushihara T, Nakano T. Correlation of Low Temperature Heat Release With Fuel Composition and HCCI Engine Combustion. SAE Tech Pap 2005;2005-01-0138.
- [29] Sjöberg M, Dec JE. Smoothing HCCI Heat-Release Rates Using Partial Fuel Stratification with Two-Stage Ignition Fuels. SAE Tech Pap 2006;2006-01-0629..
- [30] Szybist JP, Boehman AL, Haworth DC, Koga H. Premixed ignition behavior of alternative diesel fuel-relevant compounds in a motored engine experiment. Combust Flame 2007;149:112–28.
- [31] Curran HJ, Gaffuri P, Pitz WJ, Westbrook CK. A comprehensive modeling study of n-heptane oxidation. Combust Flame 1998;114:149–77.
- [32] Curran HJ, Gaffuri P, Pitz WJ, Westbrook CK. A comprehensive modeling study of *iso*-octane oxidation. Combust Flame 2002;129:253–80.

- [33] Côme G-M. Gas-Phase Thermal Reactions Chemical Engineering Kinetics. Dordrecht: Springer Netherlands; 2001.
- [34] Westbrook CK. Chemical kinetics of hydrocarbon ignition in practical combustion systems. *Proc Combust Inst* 2000;28:1563–77.
- [35] Battin-Leclerc F, Simmie JM, Blurock E, editors. Cleaner combustion: developing detailed chemical kinetic models. London: Springer; 2013.
- [36] Zhukov VP, Sechenov VA, Starikovskii AY. Self-ignition of a lean mixture of n-pentane and air over a wide range of pressures. *Combust Flame* 2005;140:196–203.
- [37] Metcalfe WK, Pitz WJ, Curran HJ, Simmie JM, Westbrook CK. The development of a detailed chemical kinetic mechanism for diisobutylene and comparison to shock tube ignition times. *Proc Combust Inst* 2007;31:377–84.
- [38] Daley SM, Berkowitz AM, Oehlschlaeger MA. A shock tube study of cyclopentane and cyclohexane ignition at elevated pressures. *Int J Chem Kinet* 2008;40:624–34.
- [39] Bugler J, Marks B, Mathieu O, Archuleta R, Camou A, Grégoire C, et al. An ignition delay time and chemical kinetic modeling study of the pentane isomers. *Combust Flame* 2016;163:138–56.
- [40] Burcat A, Scheller K, Lifshitz A. Shock-tube investigation of comparative ignition delay times for C1-C5 alkanes. *Combust Flame* 1971;16:29–33.
- [41] Oehlschlaeger MA, Davidson DF, Herbon JT, Hanson RK. Shock tube measurements of branched alkane ignition times and OH concentration time histories. *Int J Chem Kinet* 2004;36:67–78.
- [42] Vasu SS, Davidson DF, Hanson RK. Jet fuel ignition delay times: Shock tube experiments over wide conditions and surrogate model predictions. *Combust Flame* 2008;152:125–43.
- [43] Fikri M, Herzler J, Starke R, Schulz C, Roth P, Kalghatgi GT. Autoignition of gasoline surrogate mixtures at intermediate temperatures and high pressures. *Combust Flame* 2008;152:276–81.
- [44] Dooley S, Won SH, Chaos M, Heyne J, Ju Y, Dryer FL, et al. A jet fuel surrogate formulated by real fuel properties. *Combust Flame* 2010;157:2333–9.
- [45] Cancino LR, Fikri M, Oliveira AAM, Schulz C. Ignition delay times of ethanol-containing multi-component gasoline surrogates: Shock-tube experiments and detailed modeling. *Fuel* 2011;90:1238–44.
- [46] Dooley S, Won SH, Heyne J, Farouk TI, Ju Y, Dryer FL, et al. The experimental evaluation of a methodology for surrogate fuel formulation to emulate gas phase combustion kinetic phenomena. *Combust Flame* 2012;159:1444–66.
- [47] Dryer FL, Jahangirian S, Dooley S, Won SH, Heyne J, Iyer VR, et al. Emulating the combustion behavior of real jet aviation fuels by surrogate mixtures of hydrocarbon fluid blends: implications for science and engineering. *Energy Fuels* 2014;28:3474–85.
- [48] Won SH, Veloo PS, Dooley S, Santner J, Haas FM, Ju Y, et al. Predicting the global combustion behaviors of petroleum-derived and alternative jet fuels by simple fuel property measurements. *Fuel* 2016;168:34–46.
- [49] El Merhubi H, Kéromnès A, Catalano G, Lefort B, Le Moyne L. A high pressure experimental and numerical study of methane ignition. *Fuel* 2016;177:164–72.

- [50] Donovan MT, He X, Zigler BT, Palmer TR, Wooldridge MS, Atreya A. Demonstration of a free-piston rapid compression facility for the study of high temperature combustion phenomena. *Combust Flame* 2004;137:351–65.
- [51] Lee D, Hochgreb S. Rapid Compression Machines: Heat Transfer and Suppression of Corner Vortex. *Combust Flame* 1998;114:531–45.
- [52] Würmel J, Simmie JM. CFD studies of a twin-piston rapid compression machine. *Combust Flame* 2005;141:417–30.
- [53] Mittal G, Sung C-J. Aerodynamics inside a rapid compression machine. *Combust Flame* 2006;145:160–80.
- [54] Vanhove G, Petit G, Minetti R. Experimental study of the kinetic interactions in the low-temperature autoignition of hydrocarbon binary mixtures and a surrogate fuel. *Combust Flame* 2006;145:521–32.
- [55] Andrae JCG. Development of a detailed kinetic model for gasoline surrogate fuels. *Fuel* 2008;87:2013–22.
- [56] Honnet S, Seshadri K, Niemann U, Peters N. A surrogate fuel for kerosene. *Proc Combust Inst* 2009;32:485–92.
- [57] Akiyama H, Nishimura H, Ibaraki Y, Iida N. Study of diesel spray combustion and ignition using high-pressure fuel injection and a micro-hole nozzle with a rapid compression machine: improvement of combustion using low cetane number fuel. *JSAE Rev* 1998;19:319–27.
- [58] Baert RSG, Frijters PJM, Somers B, Luijten CCM, de Boer W. Design and Operation of a High Pressure, High Temperature Cell for HD Diesel Spray Diagnostics: Guidelines and Results. *SAE Tech Pap* 2009;2009-01-0649.
- [59] Silke EJ, Pitz WJ, Westbrook CK, Ribaucour M. Detailed Chemical Kinetic Modeling of Cyclohexane Oxidation†. *J Phys Chem A* 2007;111:3761–75.
- [60] Ribaucour M, Minetti R, Sochet LR, Curran HJ, Pitz WJ, Westbrook CK. Ignition of isomers of pentane: An experimental and kinetic modeling study. *Proc Combust Inst* 2000;28:1671–8.
- [61] Pitz WJ, Naik CV, Mhaoldúin TN, Westbrook CK, Curran HJ, Orme JP, et al. Modeling and experimental investigation of methylcyclohexane ignition in a rapid compression machine. *Proc Combust Inst* 2007;31:267–75.
- [62] Minetti R, Ribaucour M, Carlier M, Sochet LR. Autoignition Delays of a Series of Linear and Branched Chain Alkanes in the Intermediate Range of Temperature. *Combust Sci Technol* 1996;113:179–92.
- [63] Vanderover J, Oehlschlaeger MA. Ignition time measurements for methylcyclohexane- and ethylcyclohexane-air mixtures at elevated pressures. *Int J Chem Kinet* 2009;41:82–91.
- [64] Roubaud A, Minetti R, Sochet LR. Oxidation and combustion of low alkylbenzenes at high pressure: comparative reactivity and auto-ignition. *Combust Flame* 2000;121:535–41.
- [65] Minetti R, Roubaud A, Therssen E, Ribaucour M, Sochet LR. The chemistry of pre-ignition of n-pentane and 1-pentene. *Combust Flame* 1999;118:213–20.
- [66] Mittal G, Sung C-J. Homogeneous charge compression ignition of binary fuel blends. *Combust Flame* 2008;155:431–9.

- [67] Mayo MP, Boehman AL, Rioux RM. Effects of air temperature and oxygen dilution on the ignition behavior of liquid fuels in an optical spray chamber. [University Park, Pa.]: Pennsylvania State University; 2014.
- [68] Dagaut P, Cathonnet M. Oxidation of neopentane in a jet-stirred reactor from 1 to 10 atm: an experimental and detailed kinetic modeling study. *Combust Flame* 1999;118:191–203.
- [69] El Bakali A, Braun-Unkloff M, Dagaut P, Frank P, Cathonnet M. Detailed kinetic reaction mechanism for cyclohexane oxidation at pressure up to ten atmospheres. *Proc Combust Inst* 2000;28:1631–8.
- [70] Buda F, Heyberger B, Fournet R, Glaude P-A, Warth V, Battin-Leclerc F. Modeling of the Gas-Phase Oxidation of Cyclohexane. *Energy Fuels* 2006;20:1450–9.
- [71] Husson B, Herbinet O, Glaude PA, Ahmed SS, Battin-Leclerc F. Detailed Product Analysis during Low- and Intermediate-Temperature Oxidation of Ethylcyclohexane. *J Phys Chem A* 2012;116:5100–11.
- [72] Westbrook CK, Pitz WJ, Thornton MM, Malte PC. A kinetic modeling study of n-pentane oxidation in a well-stirred reactor. *Combust Flame* 1988;72:45–62.
- [73] Zeppieri S, Brezinsky K, Glassman I. Pyrolysis studies of methylcyclohexane and oxidation studies of methylcyclohexane and methylcyclohexane/toluene blends. *Combust Flame* 1997;108:266–86.
- [74] Wang S, Miller DL, Cernansky NP, Curran HJ, Pitz WJ, Westbrook CK. A flow reactor study of neopentane oxidation at 8 atmospheres: experiments and modeling. *Combust Flame* 1999;118:415–30.
- [75] Natelson RH, Kurman MS, Cernansky NP, Miller DL. Low temperature oxidation of *n*-butylcyclohexane. *Combust Flame* 2011;158:2325–37.
- [76] Koert DN, Miller DL, Cernansky NP. Experimental studies of propane oxidation through the negative temperature coefficient region at 10 and 15 atmospheres. *Combust Flame* 1994;96:34–49.
- [77] Agosta A, Cernansky NP, Miller DL, Faravelli T, Ranzi E. Reference components of jet fuels: kinetic modeling and experimental results. *Exp Therm Fluid Sci* 2004;28:701–8.
- [78] Diévert P, Kim HH, Won SH, Ju Y, Dryer FL, Dooley S, et al. The combustion properties of 1,3,5-trimethylbenzene and a kinetic model. *Fuel* 2013;109:125–36.
- [79] Sjöberg M, Dec JE. An Investigation of the Relationship Between Measured Intake Temperature, BDC Temperature, and Combustion Phasing for Premixed and DI HCCI Engines 2004.
- [80] Sturgis BM. Some Concepts of Knock and Antiknock Action. SAE Tech Pap 1955;550249.
- [81] Yang Y, Boehman AL. Oxidation chemistry of cyclic hydrocarbons in a motored engine: Methylcyclopentane, tetralin, and decalin. *Combust Flame* 2010;157:495–505.
- [82] Yang Y, Boehman AL. Experimental study of cyclohexane and methylcyclohexane oxidation at low to intermediate temperature in a motored engine. *Proc Combust Inst* 2009;32:419–26.
- [83] Zhang Y, Yang Y, Boehman AL. Premixed ignition behavior of C9 fatty acid esters: A motored engine study. *Combust Flame* 2009;156:1202–13.

- [84] Zhang Y, Boehman AL. Experimental study of the autoignition of C<sub>8</sub>H<sub>16</sub>O<sub>2</sub> ethyl and methyl esters in a motored engine. *Combust Flame* 2010;157:546–55.
- [85] Zhang Y, Boehman AL. Oxidation of 1-butanol and a mixture of *n*-heptane/1-butanol in a motored engine. *Combust Flame* 2010;157:1816–24.
- [86] Lilik GK, Boehman AL. Effects of fuel ignition quality on critical equivalence ratio for autoignition. *Energy Fuels* 2013;27:1586–600.
- [87] Lilik GK, Boehman AL. Effects of fuel composition on critical equivalence ratio for autoignition. *Energy Fuels* 2013;27:1601–12.
- [88] Bogin G, Dean AM, Ratcliff MA, Luecke J, Zigler BT. Expanding the Experimental Capabilities of the Ignition Quality Tester for Autoigniting Fuels. *SAE Int J Fuels Lubr* 2010;3:353–67.
- [89] Pickett LM, Genzale CL, Bruneaux G, Malbec L-M, Hermant L, Christiansen C, et al. Comparison of Diesel Spray Combustion in Different High-Temperature, High-Pressure Facilities. *SAE Int J Engines* 2010;3:156–81.
- [90] Heyne JS, Boehman AL, Kirby S. Autoignition Studies of trans- and cis-Decalin in an Ignition Quality Tester (IQT) and the Development of a High Thermal Stability Unifuel/Single Battlefield Fuel. *Energy Fuels* 2009;23:5879–85.
- [91] Perez PL, Boehman AL. Experimental Investigation of the Autoignition Behavior of Surrogate Gasoline Fuels in a Constant-Volume Combustion Bomb Apparatus and Its Relevance to HCCI Combustion. *Energy Fuels* 2012;26:6106–17.
- [92] Bogin GE, Osecky E, Ratcliff MA, Luecke J, He X, Zigler BT, et al. Ignition Quality Tester (IQT) Investigation of the Negative Temperature Coefficient Region of Alkane Autoignition. *Energy Fuels* 2013;27:1632–42.
- [93] Zheng Z, Badawy T, Henein N, Sattler E. Investigation of Physical and Chemical Delay Periods of Different Fuels in the Ignition Quality Tester. *J Eng Gas Turbines Power* 2013;135:061501–061501.
- [94] Mayo MP, Boehman AL. Ignition behavior of biodiesel and diesel under reduced oxygen atmospheres. *Energy Fuels* 2015;29:6793–803.
- [95] Bogin GE, De Filippo A, Chen JY, Chin G, Luecke J, Ratcliff MA, et al. Modeling the Fuel Spray and Combustion Process of the Ignition Quality Tester with KIVA-3V. National Renewable Energy Laboratory Golden, CO 2010.
- [96] Krishnasamy A, Reitz RD, Willems W, Kurtz E. Surrogate Diesel Fuel Models for Low Temperature Combustion. *SAE Tech Pap* 2013;2013-01-1092.
- [97] Dryer FL. Chemical kinetic and combustion characteristics of transportation fuels. *Proc Combust Inst* 2015;35:117–44.
- [98] Mehl M, Pitz WJ, Westbrook CK, Curran HJ. Kinetic modeling of gasoline surrogate components and mixtures under engine conditions. *Proc Combust Inst* 2011;33:193–200.
- [99] Pitz WJ, Mueller CJ. Recent progress in the development of diesel surrogate fuels. *Prog Energy Combust Sci* 2011;37:330–50.
- [100] Kim D, Martz J, Violi A. A surrogate for emulating the physical and chemical properties of conventional jet fuel. *Combust Flame* 2014;161:1489–98.
- [101] Zhang HR, Eddings EG, Sarofim AE, Mayne CE, Yang Z, Pugmire RJ. Selection of surrogates for jet fuels. *Combust. Gener. Fine Carbonaceous Part. Proc. Int. Workshop Held Villa Orlandi Anacapri May 13-16 2007, KIT Scientific Publishing; 2009, p. 137.*

- [102] Fox JW, Cheng WK, Heywood JB. A Model for Predicting Residual Gas Fraction in Spark-Ignition Engines. SAE Tech Pap 1993;931025.
- [103] Curran HJ, Gaffuri P, Pitz WJ, Westbrook CK, Leppard WR. Autoignition chemistry in a motored engine: An experimental and kinetic modeling study. Symp Int Combust 1996;26:2669–77.
- [104] Musculus MPB, Lachaux T, Pickett LM, Idicheria CA. End-of-injection over-mixing and unburned hydrocarbon emissions in low-temperature-combustion diesel engines. SAE Tech Pap 2007;2007-01-0907.
- [105] Jensen TE, Siegl WO, Richert JFO, Lipari F, Loo JF, Probst A, et al. Advanced Emission Speciation Methodologies for the Auto/Oil Air Quality Improvement Research Program - I. Hydrocarbons and Ethers. SAE Tech Pap 1992;920320.
- [106] Bohac SV, Han M, Jacobs TJ, López AJ, Assanis DN, Szymkowitz PG. Speciated Hydrocarbon Emissions from an Automotive Diesel Engine and DOC Utilizing Conventional and PCI Combustion. SAE Tech Pap 2006;2006-01-0201.
- [107] Mueller M. General air fuel ratio and EGR definitions and their calculation from emissions. SAE Tech Pap 2010;2010-01-1285.
- [108] Briker Y, Ring Z, Iacchelli A, McLean N, Rahimi PM, Fairbridge C, et al. Diesel Fuel Analysis by GC–FIMS: Aromatics, *n*-Paraffins, and Isoparaffins. Energy Fuels 2001;15:23–37.
- [109] Yang Y, Boehman AL, Simmie JM. Effects of molecular structure on oxidation reactivity of cyclic hydrocarbons: Experimental observations and conformational analysis. Combust Flame 2010;157:2369–79.
- [110] Gulati SK, Walker RW. Addition of cyclohexane to slowly reacting H<sub>2</sub>–O<sub>2</sub> mixtures at 480 °C. J Chem Soc Faraday Trans 2 Mol Chem Phys 1989;85:1799–812.
- [111] Yang Y, Boehman AL. Experimental study of cyclohexane and methylcyclohexane oxidation at low to intermediate temperature in a motored engine. Proc Combust Inst 2009;32:419–26.
- [112] Yang Y, Boehman AL, Simmie JM. Uniqueness in the low temperature oxidation of cycloalkanes. Combust Flame 2010;157:2357–68.
- [113] Ji C, Dames E, Sirjean B, Wang H, Egolfopoulos FN. An experimental and modeling study of the propagation of cyclohexane and mono-alkylated cyclohexane flames. Proc Combust Inst 2011;33:971–8.
- [114] Lai W-C, Song C. Pyrolysis of alkylcyclohexanes in or near the supercritical phase. Product distribution and reaction pathways. Fuel Process Technol 1996;48:1–27. doi:10.1016/0378-3820(96)01030-2.
- [115] Do PT, Alvarez WE, Resasco DE. Ring opening of 1,2- and 1,3-dimethylcyclohexane on iridium catalysts. J Catal 2006;238:477–88.
- [116] Yanowitz J, Ratcliff MA, McCormick RL, Taylor JD, Murphy MJ. Compendium of experimental cetane numbers. NREL Report: NREL/TP-5400-61693: 2014.
- [117] Benson SW. Effects of Resonance and Structure on the Thermochemistry of Organic Peroxy Radicals and the Kinetics of Combustion Reactions I. J Am Chem Soc 1965;87:972–9.
- [118] Eliel EL, Wilen SH, Doyle MP. Basic organic stereochemistry. New York: Wiley-Interscience; 2001.

- [119] Jr JAM, Frisch MJ, Ochterski JW, Petersson GA. A complete basis set model chemistry. VII. Use of the minimum population localization method. *J Chem Phys* 2000;112:6532–42.
- [120] Baldwin RR, Bennett MJ, Walker RW. Rate constants for elementary steps in hydrocarbon oxidation. *Symp Int Combust* 1977;16:1041–51.
- [121] Hwang W, Dec J, Sjöberg M. Spectroscopic and chemical-kinetic analysis of the phases of HCCI autoignition and combustion for single- and two-stage ignition fuels. *Combust Flame* 2008;154:387–409.
- [122] Shore PR, Humphries DT, Haddad O. Speciated Hydrocarbon Emissions from Aromatic, Olefinic, and Paraffinic Model Fuels. SAE Tech Pap 1993;930373.
- [123] Kaiser EW, Siegl WO, Cotton DF, Anderson RW. Effect of fuel structure on emissions from a spark-ignited engine. 3. Olefinic fuels. *Environ Sci Technol* 1993;27:1440–7.
- [124] Bower SL, Litzinger TA, Frottier V. The Effect of Fuel Composition and Engine Deposits on Emissions from a Spark Ignition Engine. SAE Tech Pap 1993;932707.
- [125] Ninomiya JS, Golovoy A. Effects of Air-Fuel Ratio on Composition of Hydrocarbon Exhaust from Isooctane, Diisobutylene, Toluene, and Toluene-*n*-Heptane Mixture. SAE Tech Pap 1969;690504.
- [126] Risberg P, Kalghatgi G, Ångström H-E. Auto-ignition Quality of Gasoline-Like Fuels in HCCI Engines. SAE Tech Pap 2003;2003-01-3215.
- [127] Shibata G, Urushihara T. Dual Phase High Temperature Heat Release Combustion. *SAE Int J Engines* 2008;1:1–12.
- [128] Dykij J, Svoboda J. *Vapor Pressure of Chemicals*. Springer; 1999.
- [129] Rose JW, Spiers HM, Cooper JR. Technical data on fuel. British National Committee, World Energy Conference; 1977.
- [130] Baldwin RR, Walker RW. Eighteenth Symposium (International) on Combustion Elementary reactions in the oxidation of alkenes. *Symp Int Combust* 1981;18:819–29.
- [131] Kelly-Zion PL, Dec JE. A computational study of the effect of fuel type on ignition time in homogenous charge compression ignition engines. *Proc Combust Inst* 2000;28:1187–94.
- [132] Touchard S, Fournet R, Glaude PA, Warth V, Battin-Leclerc F, Vanhove G, et al. Modeling of the oxidation of large alkenes at low temperature. *Proc Combust Inst* 2005;30:1073–81.
- [133] Stark MS, Waddington DJ. Oxidation of propene in the gas phase. *Int J Chem Kinet* 1995;27:123–51.
- [134] AIR FORCE ENERGY PLAN, <http://www.safie.hq.af.mil/shared/media/document/AFD-091208-027.pdf>. 2010.
- [135] Department of the Navy's ENERGY PROGRAM for Security and Independence, [http://greenfleet.dodlive.mil/files/2010/04/Naval\\_Energy\\_Strategic\\_Roadmap\\_100710.pdf](http://greenfleet.dodlive.mil/files/2010/04/Naval_Energy_Strategic_Roadmap_100710.pdf). 2010.
- [136] ASTM D7566-14c. Standard Specification for Aviation Turbine Fuel Containing Synthesized Hydrocarbons. ASTM International, West Conshohocken, PA, 2014; [www.astm.org](http://www.astm.org).

- [137] Edwards T, Moses C, Dryer F. Evaluation of combustion performance of alternative aviation fuels. 46th AIAAASMEASAEASEE Jt Propuls Conf Exhib 2010;AIAA 2010-7155.
- [138] U.S. Department of Defense. DoD Management Policy for Energy Commodities and Related Services, Directive 4140.25, <http://www.dtic.mil/whs/directives/corres/pdf/414025p.pdf>. 2004.
- [139] Wang H, Oehlschlaeger MA. Autoignition studies of conventional and Fischer–Tropsch jet fuels. *Fuel* 2012;98:249–58.
- [140] Zhu Y, Li S, Davidson DF, Hanson RK. Ignition delay times of conventional and alternative fuels behind reflected shock waves. *Proc Combust Inst* 2015;35:241–8.
- [141] Valco D, Gentz G, Allen C, Colket M, Edwards T, Gowdagiri S, et al. Autoignition behavior of synthetic alternative jet fuels: An examination of chemical composition effects on ignition delays at low to intermediate temperatures. *Proc Combust Inst* 2015;35:2983–91.
- [142] Dean AJ, Penyazkov OG, Sevruck KL, Varatharajan B. Autoignition of surrogate fuels at elevated temperatures and pressures. *Proc Combust Inst* 2007;31:2481–8.
- [143] Dryer FL, Jahangirian S, Dooley S, Won SH, Heyne J, Iyer VR, et al. Emulating the Combustion Behavior of Real Jet Aviation Fuels by Surrogate Mixtures of Hydrocarbon Fluid Blends: Implications for Science and Engineering. *Energy Fuels* 2014;28:3474–85.
- [144] Dagaut P, El Bakali A, Ristori A. The combustion of kerosene: Experimental results and kinetic modelling using 1- to 3-component surrogate model fuels. *Fuel* 2006;85:944–56.
- [145] Humer S, Frassoldati A, Granata S, Faravelli T, Ranzi E, Seiser R, et al. Experimental and kinetic modeling study of combustion of JP-8, its surrogates and reference components in laminar nonpremixed flows. *Proc Combust Inst* 2007;31:393–400.
- [146] Edwards T, Maurice LQ. Surrogate mixtures to represent complex aviation and rocket fuels. *J Propuls Power* 2001;17:461–6.
- [147] Violi A, Yan S, Eddings EG, Sarofim AF, Granata S, Faravelli T, et al. Experimental formulation and kinetic model for JP-8 surrogate mixtures. *Combust Sci Technol* 2002;174:399–417.
- [148] Caton PA, Hamilton LJ, Cowart JS. Understanding ignition delay effects with pure component fuels in a single-cylinder diesel engine. *J Eng Gas Turbines Power* 2010;133:032803–032803.
- [149] Shrestha A, Zheng Z, Badawy T, Henein N, Schihl P. Development of JP-8 surrogates and their validation using ignition quality tester. *SAE Int J Fuels Lubr* 2014;7:337–51.
- [150] Kim D. Conventional and Alternative Jet Fuels for Diesel Combustion: Surrogate Development and Insights into the Effect of Fuel Properties on Ignition. University of Michigan, 2016.
- [151] Bruno TJ. Improvements in the measurement of distillation curves. 1. A composition-explicit approach. *Ind Eng Chem Res* 2006;45:4371–80.
- [152] DeWitt MJ, Corporan E, Graham J, Minus D. Effects of Aromatic Type and Concentration in Fischer–Tropsch Fuel on Emissions Production and Material Compatibility. *Energy Fuels* 2008;22:2411–8.



- [153] ASTM D1322-14a. Standard Test Method for Smoke Point of Kerosine and Aviation Turbine Fuel. ASTM International, West Conshohocken, PA, 2014; [www.astm.org](http://www.astm.org).
- [154] Perez PL, Boehman AL. Effects of the chemical structure and composition of surrogate gasoline fuels on homogeneous charge compression ignition combustion in a single-cylinder engine. *Energy Fuels* 2014;28:3377–90.
- [155] Shafer L, Striebich R, Gomach J, Edwards T. Chemical class composition of commercial jet fuels and other specialty kerosene fuels. 14th AIAAAHI Space Planes Hypersonic Syst Technol Conf 2006;AIAA 2006-7972.
- [156] Joshua D. Taylor Michael J. Murphy. Compendium of Experimental Cetane Number Data 2004..
- [157] Design Institute for Physical Properties. DIPPR Project 801 - Full Version. AIChE 2016.
- [158] Yang Y, Boehman AL, Santoro RJ. A study of jet fuel sooting tendency using the threshold sooting index (TSI) model. *Combust Flame* 2007;149:191–205.
- [159] Sjöberg M, Dec JE. Comparing late-cycle autoignition stability for single- and two-stage ignition fuels in HCCI engines. *Proc Combust Inst* 2007;31:2895–902.
- [160] Zheng M, Reader GT, Hawley JG. Diesel engine exhaust gas recirculation—a review on advanced and novel concepts. *Energy Convers Manag* 2004;45:883–900.
- [161] Cho K, Han M, Sluder CS, Wagner RM, Lilik GK. Experimental Investigation of the Effects of Fuel Characteristics on High Efficiency Clean Combustion in a Light-Duty Diesel Engine. SAE Tech. Pap., SAE International; 2009.
- [162] Kutrašnik T, Trenc F, Oprešnik SR. A New Criterion to Determine the Start of Combustion in Diesel Engines. *J Eng Gas Turbines Power* 2005;128:928–33.